Model development and simulation of membrane separation systems for the recovery of intracellular protein products from crude biological feedstocks

A thesis submitted to the University of London

for the degree of

DOCTOR OF PHILOSOPHY

by

Roy Emmanuel Peter Okec MEng (Hons)

August 1998

Advanced Centre for Biochemical Engineering

Department of Biochemical Engineering

University College London

Torrington Place

London WC1E 7JE

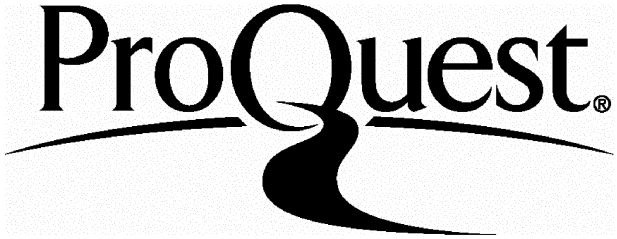

ABSTRACT

The definition of a microfiltration operation for the recovery of protein products from complex biological feedstocks requires an understanding of a large number of operating variables including the permeate flux rate and transmission characteristics of the membrane. This thesis examines the use of computer-based simulation techniques, accompanied with experimental studies, for the rapid design and evaluation of crossflow microfiltration systems for use in the bioprocess industries.

The thesis sets out to test the hypothesis that single laboratory tests of permeate flux rate and transmission, accompanied by selected laboratory-scale characterisations, may be used to define the operating characteristics of a membrane separation process and hence allow the evaluation of the effect of a range of operating variables including the recirculation rate and the concentration factor on process performance. The results of single microfiltration experiments have been used to establish a relationship between the rejection of soluble species as a function of their molecular weight and the membrane operating conditions. Verification trials have been conducted to test the accuracy of the model predictions.

Microfiltration experiments have also been conducted on biological systems including polyethleneimine flocculated yeast homogenate and *Escherichia coli* cell lysate. The results of experiments indicate that the use of physical property characterisations as a generic basis for the prediction of membrane performance is limited by the highly specific nature of biological feed-streams and their interaction with the membrane.

Simulations studies were conducted on a 3-stage filtration process for the recovery of alcohol dehydrogenase from yeast homogenate. The studies assessed the impact of the recirculation rate, the membrane module length, the starting cell concentration and diafiltration volumes on the product yield and product purity. The benefits of simulation were further illustrated through a realistic case study where the objective was to specify the design and operating conditions for a membrane separation process leading to the lowest overall cost for a fermentation-based product manufactured to a specified level.

The work highlighted the high degree of specific interactions between membranes and typical bioprocess feed-streams making statistical modelling approaches most appropriate for describing membrane filtration. The importance of simulation as an efficient tool to aid process development work was also illustrated.

ACKNOWLEDGEMENTS

I would like to thank my supervisor Dr. Nigel Titchener-Hooker and my advisor Professor Mike Hoare for their support and guidance throughout the preparation of this thesis.

I would also like to thank Dr. John Levesley for his helpful advise.

The financial support provided by the ORS Award scheme and the UCL Graduate School is gratefully acknowledged.

Special thanks to Billy Doyle, Chris Seaton and Alison Clayton for their assistance in the UCL pilot plant.

'BIG UP' to the '1st floor POSSE', the 'GYM POSSE' and the 'FOOTBALL CREW'.

Raf, Kamran, Edwin and Srini, thanks for the curries.

To my parents, Apost and Mama, none of this would have been possible without your support. Thank-you.

To my brothers and sisters, being around you guys is a privilege.

TABLE OF CONTENTS

LIST OF FIGURES

LIST OF TABLES

ABBREVIATIONS

ADH	alcohol dehydrogenase
CFD	computational fluid dynamics
FPLC	fast protein liquid chromatography
GPC	gel permeation chromatography
G-6-P	glucose-6-phosphate
G-6-PDH	glucose-6-phosphate dehydrogenase
HIC	hydrophobic interaction chromatography
HPLC	high performance liquid chromatography
MDH	malate dehydrogenase
NAD^+	nicotinamide-adenine dinucleotide
$NADP^+$	nicotinamide-adenine dinucleotide phosphate
NADPH	nicotinamide-adenine dinucleotide phosphate (reduced form)
PEI	polyethyleneimine
PSD	particle size distribution
β-NADH	nicotinamide-adenine dinucleotide (reduced form)

1 INTRODUCTION

Membrane filtration has been used in the bioprocess industries for a range of applications including media sterilisation, cell harvesting, removal of cellular debris and protein concentration. The success of such operations depends on a range of factors including the membrane material characteristics, the membrane configuration and the operating regimes selected. The development of effective and economical bioseparation processes often requires the bioprocess engineer to make rational decisions based on limited information. This thesis examines the use of computer-based simulation techniques, accompanied with experimental studies, for the systematic design and evaluation of crossflow microfiltration systems for use in the bioprocess industries. It explores the hypothesis that single laboratory tests of flux and transmission may be used to define the operating characteristics of a membrane separation process. Such a capacity has significant potential for reducing the time taken to investigate such separations making for accelerated process development.

1.1 Downstrean processing of biological materials

Downstream processing of biological materials is defined as the recovery of a protein product from source to a desired purity, quantity and biological activity (Varga, 1997). The purification of biological materials from microbial fermentations usually involves biomass removal, product recovery, product concentration and product purification (Kelly *et al*, 1991). The goal of downstream processing is to attain high product purity and high yields but at minimum cost. However, the purification protocol is complicated by low product concentrations and the presence of contaminating species such as lipids, nucleic acids and colloidal material. The choice of recovery methods will depend on the physical, chemical and biological properties of the bioprocess feed-stream including particle size distributions and rheological properties and the properties of the protein product including the product molecular weight, solubility characteristics and sensitivity to pH, heat and shear. Extensive reviews of downstream operations for protein production are available in the literature (Atkinson *et al.*, 1987, Belter *et al.*, 1988, Ogez *et al.*, 1989, Liddell, 1994). In following three sections, the most common steps for product recovery and purification are presented.

1.1.1 Biomass removal and cell disruption

The production of therapeutic and diagnostic protein products using cloning technology is often performed in large scale fermentation vessels. The fermented broth contains the host organism and the protein of interest may be present in the extracellular medium, inside the cells or in the periplasmic compartment of the cells. Biomass removal and/or the recovery of extracellular protein products from microbial fermentations can be achieved using crossflow membrane filtration (Gabler, 1985) or centrifugation (Axelsson, 1985). Crossflow membrane filtration is often performed using flat sheet and tubular modules. A number of different centrifugation configurations are available including tubular bowl, multichamber, disk stack and decanter centrifuges.

If the protein of interest is not secreted, physical or chemical methods of cell disruption are employed to release the protein product (Engler, 1985). Physical disruption of cells is often achieved using a high pressure homogeniser. Chemical disruption of cells include osmotic shock, detergent addition, alkali treatment or enzymatic methods (Kelly *et al.*, 1991). The resulting mixture contains cell debris and other contaminating intracellular species which often complicate subsequent product recovery operations.

The recovery of intracellular protein products from cell wall fragments can be accomplished using crossflow membrane filtration or centrifugation (Varga, 1997). This operation is more complicated than biomass removal and/or extracellular product recovery. The release of intracellular components increases the viscosity and density of the liquid phase (Mosqueira *et al.*, 1981). There is also an accompanying reduction in the particle size distribution during cell disruption (Shamlou *et al.*, 1995). Both conditions reduce the efficiency of typical downstream operations and a balance between cell disruption conditions and the subsequent ease of debris removal is important and has been demonstrated by Zhou *et al.* (1997).

1.1.2 Product concentration

The processing of large liquid volumes often has adverse economic effects on bioprocesses (Datar, 1986). Since products are often present in very dilute concentrations, the recovered volume after biomass removal and/or cell disruption is large and membrane

ultrafiltration may be used to reduce the product volume prior to further processing. This has the additional benefit of achieving some degree of polishing by removing low molecular weight components from the product concentrate. Membrane ultrafiltration is also used for buffer exchange to provide a stable product environment (Tutunjian, 1985) and/or facilitate the use of subsequent purification steps such as ion exchange.

1.1.3 Product purification

Initial purification steps may involve fractionation by ultrafiltration, flocculation of certain feed components such as lipids, nucleic acids and colloidal material or precipitation of the protein product by addition of inorganic salts or organic solvents. These steps remove broad classes of contaminating species (Ersson *et al.*, 1990). The basis of fractionation by ultrafiltration is the removal of contaminating species on either side of the molecular weight of the protein of interest. Selective flocculation of certain feed components will reduce the amount of contaminating soluble components. However, altering the composition of the bioprocess feed-stream with respect to solids volume fraction and chemical constituents may have adverse effects on recovery operations. Milburn *et al.* (1990) used polyethyleneimine (PEI) to selectively flocculate lipids, nucleic acids and colloidal proteins from a yeast homogenate process stream but concluded that the processing of flocculated material at high concentrations would be inefficient because of the high solids content. Hall (1996) filtered the supernatant of PEI treated yeast homogenate and observed higher fouling characteristics probably due to the interaction of excess PEI with the polymeric membrane. Precipitation techniques utilise the differences in protein solubility behaviour as a basis for separation. An extensive review of various precipitation methods is given by Scopes (1988).

High resolution techniques are used to attain acceptable protein purification levels. Chromatographic methods are employed for the final polishing steps which often involve reversible adsorption of the protein of interest to an immobilised ligand attached to an insoluble matrix. Various types of chromatography are possible including ion exchange chromatography, hydrophobic interaction chromatography (HIC), affinity chromatography and high performance liquid chromatography (HPLC). Purification factors for chromatographic processes are generally

very high. Gel filtration methods may be employed to obtain very pure products in an essentially monomeric form. Electrophoresis may also be applied as a high resolution technique. The operation is based on the acceleration of charged proteins in an electric field and separation is achieved as a result of proteins having different net charges (Stryer, 1995). However, the use of electrophoresis is limited to small scale operations due to scale-up difficulties as a result of product heating (Liddell, 1994).

Finishing operations are conducted to stabilise the product and preserve activity. Crystallisation is often used when a dry product is required. Crystallisation involves the formation of solid particles of protein of defined shape and size in a supersaturated solution (Jacobsen, 1998). Filtration or centrifugation operations may be used to recover the solid protein crystals followed by a drying stage. Several drying processes are possible including spray drying, freeze drying, fluid bed drying and vacuum drying (Liddell, 1994). Where the final product is required in liquid form, filtration operations may be used to concentrate the product in the liquid phase and exchange buffer to stabilise the product. Product sterility is also achieved during filtration operations.

1.2 Accelerated design of bioprocesses

Developments in the area of bioscience have resulted in new opportunities in medicine, nutrition, agriculture and the environment (Dunnill, 1994). In recent years, the growth of biotechnology companies exploiting these new discoveries has been rapid. To achieve commercial scale and regulatory approval as quickly as possible so as to maximise returns on research and development work, the design of efficient and economic bioprocesses using limited information is critical. The research group at UCL has adopted two approaches to speed up bioprocess development. The first approach uses scale-down systems to mimic large scale operations and allow better prediction of bioprocess performance (Maybury, 1998). Scale-down systems are important during initial process development because the limited availability of research material often constrains the researcher to using small laboratory processes. However, product development and characterisation at the bench-scale could lead to sub-optimal processes at full-scale if scale-down studies are not conducted properly. The second approach uses computer-

based simulation techniques to develop downstream processing routes for biological products. In the development of a bioprocess simulator, the research group use information and data to develop models which describe individual unit operations and processes, which are solved using numerical techniques and simulation tools (Gritis *et al.*, 1989).

1.2.1 Bioprocess simulation

Computer-assisted process modelling is a representation of the physical, chemical and biological phenomena occurring in unit operations by mathematical expressions and equations. Process flowsheet simulation is the calculation of material and energy balances for a particular process via a linked series of unit operation models which are solved using numerical methods to yield performance data for whole processes (Bhattacharya, 1993). The benefits of process simulation are numerous and include reducing process development time, reducing manufacturing costs through improved resource utilisation, quicker evaluation of alternative processing schemes and compliance with environmental and regulatory standards (Evans *et al.*, 1989, Petrides *et al.*, 1989, Bhattacharya, 1993, Narodoslawsky *et al.*, 1993). Process simulation has been used for the improvement of chemical processes for several years. However, its use in the bioprocess industries has been restricted for a variety of reasons. These include a general lack of physical property data of biological systems, poorly understood unit operations, a high degree of process interactions between upstream and downstream operations and the heavy employment of batch and/or semi-continuous processes (Cooney *et al.*, 1988, Clarkson, 1994).

The model equations within a process simulator are solved using two main techniques. The sequential-modular approach solves unit operation models sequentially, with the calculation sequence mirroring the flow of material in the actual process (Biegler, 1989). The modular structure allows alteration of unit operation models with minimum change to the process flowsheet. However, incorporation of recycle streams and optimisation calculations are difficult to perform on such simulators. Equation-oriented simulators lump all unit operation equations and solve them simultaneously. Thus, flowsheets containing recycle streams and optimisation routines are performed readily. However, equation-oriented simulators are limited by the capabilities of the equation solver (Biegler, 1989). Most commercial steady-state simulators such

as ASPEN (Evans *et al.*, 1979), PROCESS (Biegler, 1989) and DESIGN-II (Biegler, 1989) utilise the sequential-modular approach and can only describe processes at steady-state conditions. Dynamic simulators such as SPEEDUP (Sargent *et al.*, 1964), QUASILIN (Smith *et al.*, 1988) and gPROMS (Pantelides *et al.*, 1993) employ the equation-oriented approach. Such simulators can describe the transient behaviour encountered in batch and semi-batch operations. Varga (1997) gives an extensive review of existing process simulators, the pros and cons of sequential-modular and equation-oriented simulators and their application to bioprocesses.

In the development of a bioprocess simulator, two alternative routes have been proposed (Gritis *et al.*, 1989). The first approach is to adapt and modify an existing chemical process simulator by including new unit operation models and specific physical property data. Cooney *et al.* (1988) used this approach to develop BioProcess Simulator (BPS, AspenTech Ltd., Massachusetts, U.S.A.), by adapting the chemical process simulator ASPEN-Plus (AspenTech Ltd., Massachusetts, U.S.A.). The resulting package was unsuitable for dealing with many bioprocesses because it retained several chemical engineering characteristics. These included maintaining a sequential-modular structure which was unsuitable for dealing with batch processes, limited predictive capability of unit operation models and physical property prediction not applicable to bioprocesses. The second approach has been adopted by the research group at UCL and involves the development of mathematical models for common downstream unit operations using research data. The models are solved using simulation tools. Existing simulators suitable for this approach include SPEEDUP (AspenTech Ltd., Massachusetts, U.S.A.) and gPROMS (Imperial College, London, U.K.).

Most publications of bioprocess simulation have focused on the use of BPS applied to conventional bioprocesses where the technology is similar to that employed in chemical processes. Cooney *et al.* (1989) used BPS to simulate the recovery of Penicillin G from a fermentation broth using a single centrifugal extractor. They examined the impact of penicillin concentration in the fermentation broth on the cost of recovery and also the effect of using an alternative solvent for extraction. They also examined the merits of using a second counter-current extractor and whole broth extraction versus filtered broth extraction. Petrides *et al.* (1989) simulated the manufacturing of porcine growth hormone (pGH) from recombinant *Escherichia coli* using BPS.

Their main focus was on the conceptual design and economics of the downstream recovery process. pGH is an intracellular product in the form of inclusion bodies, and the process flowsheet included cell disruption, solubilisation of inclusion bodies, and protein refolding. The performance characteristics of each unit operation was drawn from laboratory and pilot plant data. The output from the simulation gave final product purity and quantity. These results were then used to examine the economic feasibility of the process. Petrides (1994) also used BioDesigner (Intelligen Inc., New Jersey, U.S.A.), similar to BPS in its architecture, to simulate the production of beta-galactosidase from *Escherichia coli*. Beta-galactosidase is an intracellular product, and the focus of the simulation was on the recovery and economic feasibility of the proposed processing route. An additional feature, production scheduling, was included. Using the second approach, Zhou *et al.* (1997) used simulations to explore the nature and impact of interactions that exist in a typical bioprocess for the recovery of an intracellular protein. The work was done using LABVIEW (National Instruments, U.S.A.). The trade-offs between product recovery and the extent of cell debris removal for a range of operating conditions were represented through a series of windows of operation (Woodley and Titchener-Hooker, 1996). Clarkson (1994) used SPEEDUP (AspenTech Ltd., Massachusetts, U.S.A.), to model and experimentally verify centrifugation and precipitation operations for the recovery of alcohol dehydrogenase from yeast homogenate. Varga (1997) extended the models to a recombinant yeast strain and simulated centrifugation and precipitation operations using MATLAB (The MathWorks Inc, Massachusetts, U.S.A.). Siddiqi *et al.* (1991) identified and modelled the process interactions between a high pressure homogeniser and the subsequent centrifugation step for cell debris removal in a typical downstream process for the recovery of an intracellular product. Bogle *et al.* (1993) simulated the production and recovery of porcine somatotropin inclusion bodies from *Escherichia coli*. Lu *et al.* (1994) used gPROMS (Imperial College, London, U.K.) to simulate typical downstream operations for the production of intracellular enzymes. Samsalti and Shah (1996) presented a two stage approach to dynamically optimise the operation and scheduling of a typical intracellular enzyme recovery process.

The implementation of simulation techniques to the bioprocess industries will allow rapid and systematic development and evaluation of possible bioprocess flowsheets. The added

advantage of using computer technology to produce optimal downstream bioprocessing routes is the possibility of continuous process monitoring, on-line measurements and automatic control which improve productivity, process control, safety and validation issues and lower operating costs (Varga, 1997). In the following section, the application of microfiltration in the bioprocess industries is presented and a review of the most common modelling techniques.

1.3 Microfiltration and its application in bioprocesses

Solid-liquid separations using microfiltration are achieved via a selective permeable membrane barrier in the presence of a pressure driven force. The basis for separation is the physical size of the molecules and particles being processed. In the bioprocess industries, microfiltration is suitable for cell broth harvesting, cell washing to remove extracellular products or contaminants as well as cell debris removal and product recovery. Microfiltration provides an attractive means of achieving solid-liquid separations because it provides high levels of separation in contained and sterile environments. Separation performance is affected by the chemical and physical interactions between the materials passing through the membrane and the membrane itself, and their interaction with the solvent (Le *et al.*, 1985). The permeation rate through the membrane and the rejection of soluble products and contaminants provide the key performance variables describing microfiltration. The interaction between process feed components and the membrane leading to fouling and the effect of key process parameters such as the recirculation rate and the concentration of suspended species often have a significant effect on the performance of microfiltration. These will be discussed in more depth in the next section.

1.3.1 Factors affecting microfiltration performance

In this section, the key process parameters that influence the dynamics of membrane systems during filtration are considered.

1.3.1.1 Transmembrane pressure

The definition of microfiltration implies that increasing the pressure should be beneficial with respect to permeate flux rates. This is true at low transmembrane pressures until a critical

pressure is reached. The critical pressure is the transmembrane pressure at which further increases in the pressure result in a much reduced rate of increase of the permeate flux rate, no further increases in the permeate flux rate or a reduction in the permeate flux rate. The value of the critical pressure is a function of the recirculation rate, the pore size and the cell concentration (Howell *et al.*, 1991). Typical values for biological systems range from 40 to 100 kPa. Beyond the critical pressure, the effect of increasing the transmembrane pressure is offset by increases in the degree of fouling. Ofsthun *et al.* (1987) showed that the thickness of the cell layer adjacent to the membrane surface increased with increasing pressure. Several workers (Reismeier *et al.*, 1987, Attia *et al.*, 1991, Haarstrick *et al.*, 1991, Field *et al.*, 1995) have demonstrated that the transmembrane pressure at start-up of a membrane process has a significant effect on the long term performance. They showed that increasing the transmembrane pressure increased the initial permeate flux rate but flux decline was more rapid due to the formation of more compact cakes resulting in lower quasi steady-state permeate flux rates.

1.3.1.2 Recirculation rate

Increasing the recirculation rate reduces the degree of concentration polarisation of retained species on the membrane surface. This in turn promotes permeate flux rates, and several workers have demonstrated the above hypothesis (Le *et al.*, 1985, Patel *et al.*, 1987, Forman *et al.*, 1989). The flux increases proportionally to the recirculation rate raised to a power. The recirculation rate exponent varies from 0.4 to 1.1 in the literature. There appears to be no upper limit for the recirculation rate across membranes but three factors will often limit this. The first results from the increased pumping costs which will result in an economic upper limit. The second is an operational problem involving pressure drops. Higher recirculation rates are accompanied by higher pressure drops across the membrane module. Thus, increases in the recirculation rate will result in increased fouling rates due to increases in the pressure driving force, reversing the benefits of higher recirculation rates. Gabler *et al.* (1985) and Datar (1984) found there was an upper limit of recirculation rate above which there was no improvement in membrane performance. The third factor is important with regard to the processing of biological

materials which are sensitive to shear damage. The stresses imposed on such materials as a result of the velocity flow field may limit the upper value of the recirculation rate.

1.3.1.3 Viscosity

Viscosity changes will occur as a result of changes to cell broth concentration and the temperature of the broth. Increases in the cell broth concentration will lead to higher viscosities resulting in a decrease in permeate flux rates. Increases in temperature have the reverse effect by decreasing the viscosity of the broth.

1.3.1.4 Surface chemistry effects

Several workers (Kroner *et al.*, 1984, Fane *et al.*, 1987, Van der Berg *et al.*, 1988, Lokjine *et al.*, 1992) recommend the use of hydrophilic membranes to reduce protein adsorption. Pre-treatment methods may be used to alter the membrane surface chemistry, but such methods may lead to a loss in membrane performance. The chemical environment can also influence the flux and transmission properties of the membrane separation process. Le *et al.* (1985) found that the ionic strength and the pH affected the permeate flux rate and the level of enzyme transmission when filtering whole cells. Bowen *et al.* (1992) found that the quantity of enzyme adsorbed to the membrane increased as the solution pH approached the isoelectric point of the enzyme.

1.3.1.5 Particle size and pore size

The effect of particle size and pore size is poorly understood. The particle size to the membrane pore size ratio will determine the predominant nature of filtration, i.e. screen filtration for small membrane pore sizes and depth filtration for small particle sizes. Kawakatsu *et al.* (1993) concluded that during the filtration of compressible particles, steady-state permeate flux rates reached a minimum when the particle-to-pore size ratio was equivalent to 10. This observation is not consistent with other studies conducted on compressible systems. Several researchers have investigated the recovery of protein products from microbial broths using microfiltration membranes since a large membrane pore size should confer the free passage of macromolecules and achieve high permeate flux rates at low transmembrane pressures. In reality,

microfiltration membranes are rapidly fouled by proteins and solid material until permeate flux rates are equal to or even worse than those for ultrafiltration membranes. McDonogh *et al.* (1992) filtered solutions containing proteins and proteins with cells using microporous membranes with pore sizes ranging from 0.01 μm to 1.0 μm and found that the differences in operating behaviour in the long term were not so great across the range of membranes. Patel *et al.* (1987) investigated the feasibility of harvesting yeast cells using synthetic microfilters and an ultrafilter and found that the permeate flux rate of the ultrafilter was comparable to or better than that of the microfilters. Stratton *et al.* (1994) studied the effect of membrane pore size on the crossflow microfiltration of *Escherichia coli* whole cells and *Saccharomyces cerevisiae* whole cells and concluded that ultrafiltration membranes were better suited for harvesting *Escherichia coli* cells, while microporous membranes were better suited for *Saccharomyces cerevisiae* cells. Le *et al.* (1985) observed better permeate flux rates when filtering whole cells through 0.45 μm pores than for either 0.2 μm pores or 0.6 μm pores. Bailey *et al.* (1997) studied the effect of viscosity and particle size on the processing of recombinant *Escherichia coli* cell lysates using crossflow microfiltration. Their results showed no significant effect of the particle size on membrane performance.

The performance of microfiltration membranes used for bioprocess recovery operations tends to be highly system specific. In the next section, design considerations that need to be addressed when using membranes for bioprocessing will be presented.

1.3.2 Membrane design considerations for bioprocessing

The success of membrane separation processes used for bioprocessing will depend on the membrane material characteristics, the membrane module design and the influence of process parameters on separation performance (Hilderbrant, 1993). This section considers design factors critical for improved separation performance and compatibility when processing biological products.

1.3.2.1 Membrane type

New polymeric microfiltration membranes and inorganic microfiltration membranes are available that can operate in harsh environments including extremes of pH and temperature. Biological feeds are often complex in nature and highly fouling. As a direct consequence, the manufacture of bioproducts usually involves the repeated cleaning of membranes. Cleaning procedures often subject the membrane to very harsh environments including hot aqueous sodium hydroxide, inorganic acids such as sodium hypochlorite and hydrogen peroxide, various detergents, enzymes and even high sterilisation temperatures. Most polymeric membranes used in bioprocessing including polysulphone, polyethersulphone, polyvinylidene diflouride, cellulose acetate, polyamide, polyolefin and polyacrylonitrile have limited chemical tolerance and pH compatibility (Hilderbrant, 1993). Inorganic membranes, however, exhibit physical and chemical properties that are highly compatible with bioprocessing. They can operate at very high temperatures, have better structural stability and can withstand very harsh chemical environments (Mikulàšek *et al.*, 1994). They are not subject to microbial attack.

1.3.2.2 Membrane configuration

Commercial membranes for bioprocessing are supplied in four main configurations including hollow fibre, tubular, flat plate and spiral wound configurations. Hollow fibre membranes are bundles of small tubular membranes of internal diameter ranging from 0.2 to a few mm sealed in a tube. Feed flow is down the centre of the each fibre and the permeate is collected in the exterior of the fibres. The advantages of using hollow fibres include large membrane area per unit volume of retentate and operation in turbulent flow. Devereux *et al.* (1986) used PM50 hollow fibre ultrafiltration membranes to recover protein precipitates from clarified soya protein extracts. Other workers (Tutunjian, 1983, Le *et al.*, 1985, Warren *et al.*, 1991) used hollow fibre membranes to concentrate whole cell suspensions of *Saccharomyces cerevisiae* and *Escherichia coli*. However, the narrow capillaries are often blocked by particulate material and hollow fibre membranes tend to be unsuitable for processing streams containing a high proportion of solid material. Tubular membranes, in comparison to hollow fibre membranes, have internal diameters of ~ 5 - 25 mm. Often the membrane is cast on the inside of a porous

cylindrical support housed in a stainless steel pipe (Hall, 1996). They are widely used in bioprocessing because they can operate in turbulent regimes without blockage by particulate species (Baker *et al.*, 1985, Patel *et al.*, 1987, Redkar *et al.*, 1993, Piron *et al.*, 1995, Field *et al.*, 1995). They are also very easily cleaned. However, a low membrane area per unit volume of retentate and high hold-up volumes make tubular membranes expensive and bulky to handle. Flat sheet membranes used in process operations are either supplied as flat plate or spiral wound membranes. Flat plate membranes consist of sheets of membranes stacked in parallel with spacers separating the membranes. The spacers contain either the flow channels for the retentate stream or the permeate stream. Flat plate membranes are suitable for processing streams containing a high level of particulate material (Le *et al.*, 1984 & 1985, Patel *et al.*, 1987, Taddei *et al.*, 1990, Stratton *et al.*, 1994, Foley *et al.*, 1995). They are also easy to scale-up because of their modular construction. Spiral wound membranes are of similar construction to flat plate membranes except that the membrane and spacers are rolled around a perforated tube resulting in a cylindrical module. The feed enters one end of the module, and the permeate collects at the centre of the tube. Prádanos *et al.* (1995) used polysuphone spiral wound membranes to determine the permeate flux rate and retention characteristics of model protein solutions during crossflow ultrafiltration. Porter (1972) and Gabler (1983) also used spiral wound membranes for ultrafiltration experiments conducted on plasma and *Streptomyces* bacteria respectively. Although spiral wound membranes have a large membrane area per unit volume of filtrate, they are prone to blockage by streams containing particulates. They are also difficult to clean.

Currently, crossflow devices employing flat sheets are commonplace in the bioprocess industries. However, tubular devices, which are prevalent in food and beverage applications, are increasingly being used.

1.3.2.3 Membrane pore size

Most bioprocess operations require the absolute retention of submicron particles with concomitant passage of soluble macromolecules. A tight pore size distribution is important for achieving complete retention of suspended species. Brown *et al.* (1987) observed a reduction in membrane performance with increases in the spread of the pore size distribution. They attributed

the loss in performance to increased pore plugging as a result of the overlap between the pore size and particle size distributions. Developments in polymer technology have enabled the production of membranes with narrow pore size distributions, but it is generally accepted that ceramic membranes have tighter distributions than their polymeric counterparts (Glimenius, 1985).

The development of new membrane compositions for bioprocessing is fuelled by the need for more durable membranes with low protein binding tendencies leading to increased processing rates and an extended usable membrane life. In the next section, a review of the most common approaches to modelling of membrane separation processes is presented.

1.3.3 Microfiltration models

Most microfiltration models have their origins in ultrafiltration theory (Fischer, 1996). Some workers (Bowen *et al.*, 1996, Song *et al.*, 1995) have used fundamental approaches to model microfiltration. These approaches often make assumptions such as spherical and non-interacting particles and often require detailed knowledge of the thermodynamic properties of the system, which are difficult to measure. In reality, a description of typical biological systems using fundamental thermodynamics is difficult and often invalid in many practical applications.

Most modelling of filtration is based on the concentration polarisation model or the resistance model and these will now be considered. Models describing the time dependent nature of filtration, the sieving mechanism of filtration and mass transfer in membrane modules will also be considered.

1.3.3.1 Concentration polarisation model

The concentration polarisation model assumes a thin boundary layer of retained solutes and/or solids between the bulk solution and the membrane surface which limits membrane permeability. At steady-state, the permeate flux rate and the boundary layer thickness remain constant with time. Thus, the convection of retained species towards the membrane surface by the filtrate flux is balanced by the back diffusive transport away from the membrane surface as a result of the concentration gradient. Polarisation will always occur when the membrane is selective to certain feed components.

Porter (1972) outlined the theory of polarisation during the ultrafiltration of protein solutions. The gel layer concentration of protein, the concentration at which there is no further increase in protein concentration in the boundary layer, was estimated from a linear plot of the permeate flux rate and the log (protein concentration) as the x-axis intercept. Different workers have obtained different values for the protein gel concentration ranging from ~ 20-30 wt %. The polarisation model is extended to microfiltration by estimating the diffusivity of suspended particles and macromolecules. This can be done using the Stokes-Einstein relationship (Porter, 1972) or empirical correlations. However, the standard polarisation model is inadequate for modelling filtration of suspensions containing deformable solids such as those found in bioprocesses. The maximum packing concentration of rigid spheres can be calculated from the geometry of close packed structures. However, as biological suspensions are often constituted of deformable particles, the maximum packing structure becomes a function of the operating pressure. The second problem arises from the under-prediction of the back diffusive transport of suspended species into the velocity flow field using the Stokes-Einstein equation. Several possible theories have been proposed to explain the discrepancy between the predictions and the observed permeate flux rates. Most of the proposed theories fall into two main categories, inertial lift and shear induced diffusion theories, which account for increased back transport of particles from the membrane surface.

Inertial lift theories estimate the hydrodynamic forces acting on an individual particle in a shear field. Segré *et al.* (1962) found that neutrally buoyant spheres in Poiseuille flow migrated away from the walls of the tube in which they were flowing. They called this effect the tubular pinch effect, and produced an empirical formula to correlate their results. Several workers (Forstrom *et al.*, 1974, Green *et al.*, 1980, Altena *et al.*, 1983) have later examined the effects of lift forces on filtration. However, the solutions are valid only for laminar flow and very dilute suspensions as they ignore interactions between particles.

Eckstein *et al.* (1977) used a Couette flow device to measure the particle diffusivity due to particle interactions in a shear field. They obtained an empirical correlation for the particle diffusivity as a function of the particle radius. Zydney *et al.* (1986) suggested that particles will rotate, collide and overtake neighbouring particles travelling along slower streamlines in a

suspension. These particle interactions will result in a net lateral migration of particles which can be modelled by an effective diffusive coefficient. They used the expression developed by Eckstein *et al.* (1977) for the particle diffusivity to model plasmapheresis using a polarisation model and obtained good agreement between the predictions and observed data. Davis *et al.* (1987) proposed that shear induced diffusion resulted in flowing cakes due to solids resuspension, and the cake layer was balanced by axial convection out of the filter. Romero *et al.* (1988) produced a global filtration model predicting the axial variation of permeate flux and cake layer thickness. The model was extended to include time dependent effects, and experimental verification of the model was provided. The drawback of the models developed is the assumption that flow is laminar.

Fane *et al.* (1982) proposed a scour model to correlate results of ultrafiltration experiments of an activated sludge liquor. The relationship between the permeate flux rate and the bulk concentration of solid particles was essentially an empirical relationship with no theoretical basis.

1.3.3.2 Resistance model

A resistance model assumes that the permeate flux rate is directly proportional to the transmembrane pressure but inversely proportional to the viscosity of the permeating fluid. The permeability of the membrane is limited by the resistance due to the membrane, the cake layer or boundary layer and irreversible fouling.

The resistance of the membrane can be determined from water flux measurements or Pousielle flow for membranes with cylindrical pores of uniform radius. The membrane resistance depends on the membrane thickness, the membrane pore size and other morphological features such as the porosity and the pore size distribution.

For incompressible and spherical particles, the specific cake resistance may be estimated using the Carman-Kozeny equation (Carman, 1937). The mean specific resistance of compressible suspensions may be evaluated from steady-state permeate flux rates. Biological materials are compressible and show a decrease in the void fraction and an increase in the specific resistance as the transmembrane pressure is increased. These effects are often accounted for by assuming a power law relationship between the imposed pressure and the specific

resistance (Nakanishi *et al.*, 1987). Nakanishi *et al.* (1987) also determined that the specific resistance was a function of the size and shape of microorganisms.

The resistance due to irreversible fouling is difficult to measure and is often intrinsically incorporated into the cake resistance. Membrane fouling is the irreversible adsorption and/or deposition of protein material and other contaminating species on the membrane surface. This type of fouling can only be removed by chemical cleaning agents and/or harsh physical methods. Protein adsorption is defined as the partitioning of a solute between a solution and a surface (Hall, 1996). Thus protein adsorption refers to the monolayer of solutes in contact with the membrane. Several types of interactions between the solvent and solute are responsible for adsorption including London-van der Waals forces, electrostatic interactions and entropic forces (Bowen *et al.*, 1996 & 1998). Protein deposition often accounts for the majority of retained solutes. Fane *et al.* (1983) found that the amount of protein deposited on an ultrafiltration membrane corresponded to 100-400 layers of protein. Deposition of protein material is thought to occur as a result of intermolecular bonding and hydrophobic interactions.

Other workers (Blake *et al.*, 1992, Stamatakis *et al.*, 1993, Elzo *et al.*, 1996) have used force balance models to predict the probability of particle adhesion to the membrane and/or cake surface. The basic principle of force balance models is a determination of the probability of particle deposition by comparing the net axial forces to the net radial forces in the vicinity of the suspension-cake interface. Incorporation of particle adhesion probability with existing cake filtration models then forms the basis of the permeate flux prediction. This is achieved by satisfying the equilibrium condition stated above which results in an adhesion criterion defined as the minimum particle diameter required for deposition, the minimum medium protrusion height necessary to stop particles in motion and the minimum angle of contact needed to deposit particles colliding with the cake (Piron *et al.*, 1995). The adhesion criterion allows calculation of the cake height and thus the prediction of the permeate flux rate. Force balance models are little used because the inter-particle forces and drag forces are difficult to measure or estimate (Lojkine *et al.*, 1992).

1.3.3.3 Fouling models

Models describing the time dependent nature of filtration are largely empirical and mainly developed for dead-end filtration. During quasi steady-state operation, dead-end and crossflow membrane filtration systems exhibit a decline in the permeate flux rate under constant operating conditions. This decline is caused by membrane fouling. Membrane fouling is the irreversible process caused when the feed components adsorb onto the membrane surface, blocking and narrowing membrane pores. Hermia (1982) developed models for dead-end filtration describing the mechanisms of membrane fouling. These included the complete blocking filtration law, the intermediate blocking filtration law, the standard blocking filtration law and the cake filtration model. The essential format of the equations were exponential or power law expressions of the permeate flux rate as a function of the processing time. Several modifiers are available describing crossflow filtration which often include a back diffusive term. Patel *et al.* (1987) used a power law relationship to describe the crossflow microfiltration of whole cells. Foley *et al.* (1995) developed a model for crossflow filtration systems that included a back diffusive term. Such models are useful for process design and scale-up studies but deliver little insight into the fouling process (Russotti *et al.*, 1995).

1.3.3.4 Sieving mechanism of filtration processes

The ability of a membrane to stop or transmit molecules/particles will depend on their relative sizes. Ferry (1936) used simple steric considerations to determine the membrane sieving coefficient for isoporous membranes filtering monodisperse systems. The membrane sieving coefficient was defined in terms of the instantaneous permeate concentration and the corresponding bulk concentration and was evaluated with respect to the effective membrane pore size. The effective membrane pore size was defined as the smallest molecular/particulate species that absolutely failed to penetrate the membrane. Particles migrating towards a pore will have a probability of penetration which is a function of the particle size and position near the pore. Ferry used simple hydrodynamic considerations to evaluate this probability. The resulting model was sigmoidal in nature. Cherkasov (1990) revealed inadequacies in the sieving model by testing the theory on empirical data obtained from ultrafiltration and microfiltration experiments of model

protein solutions. The results of his experiments revealed a sigmoidal relationship between the retention coefficient and the particle-to-pore size ratio, but this relationship was characterised by a sharp fall in membrane permeability at a critical particle-to-pore size ratio. The differences between the model predictions and experimental data were attributed to the effects of concentration polarisation, which are not accounted for in the sieving model.

1.3.3.5 Mass transfer in membrane modules

Mass transfer in membrane modules is often solved by simulating the solute mass transfer balance through the convective-diffusion equation (Belfort *et al.*, 1994). Several simplifying assumptions render the solutions impractical for predictive purposes, but many workers believe that the results have provided valuable insight. Belfort *et al.* (1985) provide a summary of the governing equations and methods of solution. These methods involve using the continuity equation, the Navier-Stokes equation, and the initial and boundary conditions are solved for a given membrane geometry. A more practical approach is to use experimental measurements to determine the mass transfer coefficients. Aimar *et al.* (1991) provide two approaches to estimate the mass transfer coefficient from experimental measurements. Both methods assume a boundary layer of even thickness along the membrane resulting in an average value for the mass transfer coefficient and the wall concentration. The constant gradient model assumes the concentration profile is linear across the polarisation layer. The second approach assumes an exponential profile. The mass transfer coefficient is obtained by solving the mass balance equation across the polarisation layer. Porter (1972) provides correlations for estimating the mass transfer coefficient using analogous solutions for heat transfer. These include the Lévêque solution for laminar flow and the Dittus-Boelter solution for turbulent flow.

Models developed for filtration processes tend to be empirical in nature and thus system specific. The more rigorous models make numerous assumptions which render their predictions inaccurate. Certain physical property characterisations of the membrane and the bioprocess feed-stream including particle and pore size distributions and rheological measurements often aid model development. In the next section, a review of the most common characterisation techniques for bioprocess feed-streams is presented.

1.4 Characterisation techniques

The characterisation of process feed-streams and the membrane itself play an important role in making the right membrane choices. In this section, a description of the most common characterisation techniques of process feed-streams including particle size distributions, rheological measurements, solids volume fraction determination and protein concentration measurements and their relevance to membrane bioprocessing will be outlined. Membrane characterisation techniques to estimate pore size distributions, interfacial area, void fractions, tortuosity and surface charges will not be reviewed and readers are advised to refer to Rõcek *et al.* (1994) who reviewed and evaluated selected methods for the characterisation of ceramic membranes which are used in this study.

Particle size distributions of biological process feed-streams, which contain a high degree of heterogeneity, are often measured using light scattering techniques and/or an electrical sensing zone method. When a monochromatic beam of light is incident on particles in a cell, the beam is diffracted and the stationary diffraction pattern produced represents the size distribution of the particles. Light scattering techniques use this principle of diffraction to obtain particle size distributions. Measurements using the electrical sensing zone method are obtained by forcing material suspended in an electrolyte solution to flow through a small orifice as a result of a negative pressure applied across the orifice. The change in electrical resistance across the orifice is monitored by means of immersed electrodes on either side of the tube wall. The resistance is converted into a voltage pulse and the number of pulses represents the number of particles passing through the orifice and the height of a voltage pulse is proportional to the volume of the particle. The choice of particle sizer largely depends on the size range of the particles to be measured. The diameter of the smallest particulate species often determines the upper limit of the membrane pore size.

Rheological studies are conducted on process feed-streams to determine the degree of non-Newtonian behaviour and also determine viscosities of feed-streams as a function of the solids volume fraction and protein concentration levels. These measurements are conducted on rheometers and they improve the predictive capabilities of polarisation models.

The solids volume fraction of process feed-streams is often determined using dry weight measurements. Dry weights are determined by drying known volumes of sample in pre-weighed containers at temperatures in excess of 100°C to a constant weight before re-weighing. Protein concentration levels are often determined using simple and precise assay techniques such as the BIO-RAD protein assay (Bradford, 1971).

Characterising a solution's filtration properties will aid model development and also allow scale-up calculations to be performed. A brief overview of scale-up issues concerning membrane processes is presented in the next section.

1.5 Scale-up of membrane processes

Commercial membrane manufacturers supply their kit in modular formats. This makes the scale-up of the membrane separation area appear straightforward. Brose *et al.* (1995) proposed a method for scaling from laboratory-scale to process-scale systems. Their approach was based on characterising a solution's filtration properties with specific ultrafiltration or microfiltration membranes in laboratory-scale devices. Based on the experimental results at laboratory-scale, the performance of process-scale systems were estimated using correlations based on the gel polarisation theory and mass transfer coefficient correlations. Complex rheological properties of biological feed-streams may however complicate such scale-up calculations. An example of such a scenario will result when filtering a non-Newtonian feed-stream. Ensuring that feed flow conditions mimic those at the laboratory-scale will be very difficult. Another consequence of scaling up to process level is a change in the amount of foulant material per unit area. This could alter fouling characteristics and change performance of the membrane system. When scale-up issues are complex, tests at process-scale may be conducted. Such tests are expensive and only a limited number of variables can be studied economically.

Typically, scale-up of membrane systems is achieved by adding new modules in series or parallel. This makes scale-up issues relatively easy. However, when the geometry of the modules are changed or when dealing with non-Newtonian systems, scale-up issues become more complicated.

1.6 Product inactivation during membrane processing

The inactivation of proteins during downstream processing could result in significant reduced recovery levels. The bioprocess engineer needs to account for such potential product losses. Inactivation of protein products will often occur when there are conformational changes to the structure of the protein molecule. Such changes will occur as a result of physical, chemical and biological effects.

1.6.1 Physical effects

The exposure of protein products to shear fields during downstream processing is a potential cause of protein denaturation and enzyme inactivation. Membrane processing involves retentate recycling at high flowrates, mixing, flow through narrow channels and high pumping rates which result in high shear fields. Charm *et al.* (1970) showed that partial enzyme inactivation occurred when certain enzymes were exposed to shear fields. Other workers (Thomas *et al.*, 1979, Virkar *et al.*, 1981) observed little or no inactivation of proteins exposed to high shear fields in the absence of air. They concluded that shear induced inactivation of proteins required an air-liquid interface where deformed molecules could aggregate. Protein inactivation can be reduced by the addition of surfactants, which prevent protein molecules from reaching the air-liquid interface (Fischer, 1996). Lee *et al.* (1989) observed a reduction in the rate of denaturation of a lipase on addition of polypropylene glycol.

Heat denaturation effects are another potential source of protein inactivation. Proteins are sensitive to heat, and prolonged exposure often leads to irreversible inactivation (Campbell *et al.*, 1993).

1.6.2 Chemical effects

The side chains of individual amino acids that constitute a protein molecule are susceptible to alteration when the solution environment changes. The solution environment can be altered by changing the pH and the ionic strength. Such changes will alter the ionisation state of the protein molecule resulting in electrostatic interactions which may result in product inactivation (Weijers *et al.*, 1992).

Most industrially important enzymes are metalloenzymes. Metalloenzymes have metal atoms as part of their integral structure, and these metal atoms are necessary for enzyme activity. The presence of metal ions in enzyme solution can result in inactivation by substitution of the integral metal atom.

1.6.3 Biological effects

Proteolytic action by proteases will lead to product inactivation (Weijers *et al.*, 1992). Proteases, which are an integral part of biological cells, break down protein material but their actions can be minimised by operation at low temperatures or at elevated temperatures. The former option slows down the rate of proteolytic action, the latter option inactivates proteases but is only applicable to thermostable products. Protease inhibitors may be added to product streams to limit proteolytic action. The use of protease inhibitors will though increase purification costs and quantities used should be minimised as inhibitors are often hazardous to health (Fischer, 1996).

1.7 Choice of protein for experimental study

Yeast alcohol dehydrogenases (ADH) have been chosen as a suitable vehicle for bioprocess modelling and verification trials in the research centre at UCL. ADH are multimeric intracellular soluble isoenzymes located in the cytoplasm and mitochondria of yeast cells with an approximate molecular weight of 150 kDa (Magonet *et al.*, 1992). ADH consist of four identical sub-units, each containing a zinc atom at its catalytic site necessary for enzyme activity (Jörnvall *et al.*, 1978). The isoelectric point of the enzymatically active form of ADH (ADH I) is 5.4 and ADH I is unstable outside the pH range of 6.0-9.0 (Hall, 1996). The diameter of discrete ADH molecules has been estimated as 7.6 nm by Bowen *et al.*, (1995). However, the molecular state and the degree of aggregation of ADH will depend on the solution conditions. Hall (1996) has shown that the pH and the ionic environment significantly affect the size distribution of ADH. Studies on the effect of shear on ADH have been conducted by Thomas *et al.* (1979), Virkar *et al.* (1979) and Narendranathan *et al.* (1982). The studies showed that shear-induced structural damage to ADH in solution was not significant when applied in Couette flow, stirred reactors or

pumps. However, Charm *et al.* (1970) and Korus *et al.* (1977) observed damage to protein products during laboratory-scale ultrafiltration and enzyme reactor operations. Narendranathan *et al.* (1982) concluded that globular proteins such as ADH are not damaged by ultrafiltration involving high shear fields. However, structural damage to proteins due to adsorption and interfacial effects will occur in the vicinity of solid-liquid and gas-liquid interfaces. Thus, damage to proteins during ultrafiltration will be observed as a result of the entrainment of air into such systems.

The research group at UCL have used ADH for the development of a bioprocess simulator. There are several reasons for the choice including

- packed baker's yeast as the starting material which is a cheap and reliable source material
- low-risk biosafety studies
- a substantial amount of information for ADH production and purification at UCL allowing the examination of a wide range of process sequence alternatives and the influence of process interactions on the overall design
- comparative studies on genetically modified yeast systems

Hetherington *et al.* (1971) developed an empirical model describing the release of soluble protein from baker's yeast during high pressure homogenisation. Siddiqi (1998) simulated the changes in cell debris particle size distribution of both packed and fermented baker's yeast during high pressure homogenisation. Mannweiler (1989) developed a grade efficiency model to describe particle separation in a disc stack centrifuge and Clarkson (1994) verified the grade efficiency approach by simulating cell harvesting, cell debris removal and the precipitation separation stages in a process for the recovery of ADH from baker's yeast. Zhou *et al.* (1997) examined the impact of high pressure homogenisation on subsequent debris removal by a disc stack centrifuge on the recovery of ADH from baker's yeast. Habib (1998) examined the benefits of pre-treatment using PEI prior to disk stack centrifugation of yeast homogenate on the recovery of ADH from baker's yeast. Levesley *et al.* (1996) examined the effect of rapid backflushing of ceramic membranes on the performance of membrane systems using ADH from baker's yeast as a test system. Maybury (1998) studied the scale-down of unit operations used in the downstream processing of ADH from baker's yeast. Varga (1997) conducted comparative studies on a recombinant yeast strain

(Creaser *et al.*, 1990) overexpressing ADH and used the approach of Mannweiler to simulate the recovery operations in the process flowsheet.

1.8 Aims of research

The primary aim of this project is to generate models predicting permeate flux rate and soluble product transmission during crossflow microfiltration of typical biological feed-streams and demonstrate its application in a bioprocess simulation environment. Such demonstration will involve selected laboratory-scale characterisations. ADH from baker's yeast will be used as the test system. Other aims of the project are to

- compare two alternative approaches to modelling filtration systems including a statistical approach and a polarisation approach
- develop predictive models using single laboratory measurements of permeate flux rate and transmission of soluble components
- examine the generic nature of the models developed by conducting single microfiltration experiments on alternative biological systems including PEI treated yeast homogenate and *Escherichia coli* cell lysate
- examine the possibility of using physical property measurements to predict membrane performance
- use simulation-based studies to develop a systematic approach to the design of membrane separation bioprocesses
- explore the use of simulation-based studies as a teaching module

The development of unit operation models is an essential component of any simulator. In Chapter 4, the examination of two alternative approaches to modelling is presented. The first is based on a statistical approach. The second uses a polarisation model. Microfiltration experiments have been conducted on yeast whole cells to demonstrate the relative merits and demerits of the two approaches. In Chapter 5, the results of single microfiltration experiments conducted on yeast homogenate have been used to develop a polarisation model describing permeate flux properties and a sigmoidal model describing the rejection of soluble species as a

function of their molecular weight and the membrane operating conditions. Verification trials have been conducted to test the accuracy of the model predictions.

In Chapter 6, the application of simulation based studies for the systematic design of membrane separation processes is demonstrated. The models used in the simulations have been obtained from Chapter 5 and literature reviews. The work was carried out on SPEEDUP (AspenTech Ltd., Massachusetts, U.S.A.). The effect of processing variables such as the recirculation rate, the concentration factor, the diafiltration volume, and the membrane area on the product yield, product volume and the product concentration in the permeate have been examined.

Microfiltration experiments have also been conducted on other biological systems including PEI treated yeast homogenate and *Escherichia coli* cell lysate. The results are presented in Chapters 7 and 8 and include model development work. A comparative study of the membrane processing of different biological systems is addressed in the appropriate sections. Recommendations for the prediction of the performance of process-scale membrane systems are provided in the concluding chapter.

2 MICROFILTRATION MODELS

2.1 Introduction

Solid-liquid separations using microfiltration are achieved via a selective permeable barrier in the presence of a pressure driven force. Several researchers have proposed models describing the microfiltration of suspensions which are useful for design and optimisation of such unit operations. This chapter reviews the most commonly used filtration models.

2.2 Fouling models

The accumulation of rejected feed components on the membrane surface as a result of convective flow under an applied pressure gradient, often termed concentration polarisation, is thought to be responsible for the initial sharp decline in permeate flux rates during crossflow microfiltration. The build up of rejected material and the associated boundary layer on the membrane surface is limited by the back diffusion of feed components into the main velocity stream, which runs parallel to the membrane surface. At steady state, the rate of convection of material to the membrane surface equals the diffusion of material from the boundary layer to the main flow path. However, crossflow microfiltration systems exhibit a decline in the permeate flux rate with time under constant operating conditions. This phenomenon can be attributed to a process often termed membrane fouling. Membrane fouling is an irreversible and time-dependent process caused when a membrane adsorbs or its pores are plugged by some feed components (Patel *et al.*, 1987). The narrowing or blocking of pores results in a lowering of the permeate flux rate.

Several models have been developed to describe time dependent nature of filtration processes. Many of these models have been developed for dead-end filtration but modified versions for use in crossflow filtration by including terms that account for back transport are available. Patel *et al.* (1987) used a power law relationship to describe their data obtained from crossflow microfiltration experiments.

$$J_t = J_1 t^{-b} \qquad (2.1)$$

where J_t is the permeate flux rate at time t

b is the experimentally determined fouling index

The fouling index (b) is indicative of the rate of fouling. Higher values indicate higher rates of fouling. The value of b ranges from ~0.1 to ~0.8 for yeast whole cells and yeast homogenate.

Hermia (1982) developed several models to describe the mechanisms of membrane fouling during dead-end filtration. The complete blocking filtration law assumes that each particle reaching the membrane participates in the blocking phenomenon by pore sealing. Thus, particles are not superimposed upon the other, and the portion of the membrane surface area blocked is proportional to the filtered volume. The resulting flux-time relationship is described by equation 2.2.

$$J_t = J_0 e^{-kt} \qquad (2.2)$$

where k is a constant

The intermediate blocking law also assumes that a particle reaching an open pore will seal it but evaluates the probability of a particle reaching an open pore. Assuming a homogenous suspension, the increment in blocked area due to particles reaching an open pore is proportional to the ratio of unblocked and blocked surface area since the likelihood of a second particle layer settling on an existing layer or on free surface is equal. Equation 2.3 describes the intermediate blocking filtration law.

$$J_t = J_0 e^{-kV} \qquad (2.3)$$

where V is the filtrate volume

The standard blocking filtration law assumes that the pore volume decreases proportionally to the filtrate volume by particle deposition on the pore walls. Assuming the membrane consists of a set of pores of constant diameter and length, and using Poiseuille's equation, Hermia derived an expression for the flux as a function of the time of filtration.

$$J_t = \frac{J_0}{(1 + kJ_0 t)^2} \qquad (2.4)$$

The cake filtration model assumes the resistance to filtrate flow is composed of a membrane resistance and a cake resistance. The resulting flux-time relationship is described by equation 2.5.

$$J_t = \frac{J_0}{(1 + kJ_0^2 t)^{0.5}} \qquad (2.5)$$

Foley *et al.* (1995) presented a deposition model developed for crossflow filtration systems that included a back diffusion term. In this model, the net accumulation of matter on the pore walls was expressed as a difference between the rate of deposition and the rate of removal.

$$\frac{dh}{dt} = \nu_D - k_f h \qquad (2.6)$$

where h is the fouling layer thickness at time t

ν_D is the rate of increase of the deposit layer thickness

k_f is the foulant removal rate constant

The fouling layer thickness is the difference in pore radii of fouled and unfouled membrane.

$$h = r_0 - r \qquad (2.7)$$

where r_0 is the unfouled pore radius

r is the fouled pore radius

Integrating equation 2.6 gives an expression for the fouled pore radius as a function of the filtration time.

$$\frac{r}{r_0} = 1 - \frac{v_D}{k_f r_0}(1 - e^{-k_f t}) \qquad (2.8)$$

Most models consider one aspect of the fouling phenomenon. In reality, a combination of effects i.e. increased hydraulic resistance due to concentration polarisation and fouling, pore blocking and osmotic pressure effects will occur simultaneously.

2.3 Flux models

The performance of microfiltration systems is dependent on a number of process parameters including the membrane pore size, the broth concentration, the recirculation rate and the transmembrane pressure. Most modelling of filtration systems is based on the concentration polarisation model or a resistance model.

2.3.1 Concentration polarisation model

The concentration polarisation model assumes that the limiting resistance to flow is provided by a dynamically formed thin layer of retained solutes or solids between the bulk solution and the membrane surface. The dynamic layer is assumed to have a fixed concentration of solutes or solids but varying thickness or porosity. In such a scenario, the permeate flux rate is independent of the pressure driving force or the membrane permeability since the dynamic boundary layer resistance to permeate flow will adjust itself until the convective transport of retained species to the membrane surface equals the back diffusive transport to the bulk stream (Porter, 1972). This balance within the layer is described by equation 2.9.

$$JC = D\frac{dC}{dy} \qquad (2.9)$$

where J is the permeate flux rate

C is the concentration of retained species

D is the diffusion coefficient of retained species

y is the distance from the membrane surface

$\frac{dC}{dy}$ is the concentration gradient

Integration across the boundary layer gives an expression of the permeate flux rate as a function of the wall and bulk concentrations and the mass transfer coefficient.

$$J = k_m \ln\left(\frac{C_w}{C_b}\right) \tag{2.10}$$

where k_m is the mass transfer coefficient

C_w is the wall concentration of retained species

C_b is the bulk concentration of retained species

The mass transfer coefficient and the wall concentration are unknown and need to be estimated. The wall concentration can be estimated by assuming that the boundary layer resembles a layer of closed-packed spheres having 65-75% solids by volume (Porter, 1972). The mass transfer coefficient can be estimated using analogous solutions for heat transfer (Taylor *et al.*, 1994) such as the Dittus-Boelter correlation for fully developed turbulent flow.

$$k_m = K\, U^{0.8}\, D^{0.67}\, d_m^{-0.2}\, \nu^{-0.47} \tag{2.11}$$

where K is the proportionality constant

U is the recirculation rate

d_m is the inner membrane diameter

ν is the kinematic viscosity

Porter (1972) has shown with measurements of fluid velocity as a function of the pressure drop that a definite transition from laminar to fully developed turbulent flow occurs at a Reynolds number of ~2,000. The recirculation rate and the inner membrane diameter are easily determined. The diffusion coefficients of suspended species can be estimated using the Stokes-Einstein relationship.

$$D = \frac{k_b T}{6\pi\mu_s r_p} \tag{2.12}$$

where k_b is the Boltzman constant

T is the absolute temperature

μ_s is the viscosity of the suspension

r_p is the radius of the diffusing particle

Correlations to estimate the diffusivity of spherical molecules and macromolecules are available in the literature as given by Porter (1972) and Kawakatsu *et al.* (1993).

2.3.2 Resistance model

A resistance model assumes the permeate flux rate is directly proportional to the transmembrane pressure but inversely proportional to the viscosity of the permeating fluid. The pressure driven flux is described by equation 2.13.

$$J = \frac{\Delta P}{\mu R_{total}} \tag{2.13}$$

where ΔP is the transmembrane pressure

μ is the viscosity of the permeate

R_{total} is the total resistance to permeate flow

The total resistance to permeate flow usually comprises the membrane resistance, the cake resistance and resistance due to fouling.

$$R_{total} = R_{membrane} + R_{cake} + R_{fouling} \tag{2.14}$$

The membrane resistance depends on the membrane thickness, its pore size and other features such as the porosity and the pore size distribution. For cylindrical pores of uniform radius perpendicular to the membrane, the membrane resistance can be obtained from Pouseuille flow (Davis, 1992).

$$R_{membrane} = \frac{8\delta_{membrane}}{\pi n r^4} \qquad (2.15)$$

where $\delta_{membrane}$ is the membrane thickness

n_p is the number of pores

r is the pore radius

For incompressible and spherical particles, the specific cake resistance per unit thickness may be estimated using the Carman-Kozeny equation (Carman, 1937).

$$R_{cake} = \frac{180(1-\varepsilon)^2 \delta_{cake}}{d_p \varepsilon^3} \qquad (2.16)$$

where ε is the cake void fraction

δ_{cake} is the cake thickness

d_p is the particle diameter

Biological materials, such as microbial cells, tend to be compressible and show a decrease in the void fraction and an increase in the specific resistance as the pressure is increased. This makes estimation of the cake resistance difficult. The resistance due to irreversible fouling can only be estimated from experimental data.

2.4 Sieving mechanism of filtration processes

Ferry (1936) proposed that membranes can be considered as sieves which pass or stop molecules or particles according to their size. The membrane sieving coefficient is defined by equation 2.17.

$$\chi = \frac{C_p}{C_b} \qquad (2.17)$$

where χ is the membrane sieving coefficient

C_p is the instantaneous permeate concentration

C_b is the corresponding bulk concentration

Ferry used simple steric considerations to describe the sieving characteristics of perfectly isoporous membranes for monodisperse systems. The sieving characteristics are evaluated in terms of the effective pore size defined as the diameter of the smallest molecular or particulate species which absolutely fails to penetrate the membrane. The difference between the average pore diameter and the effective pore diameter is attributed to adsorption effects. The membrane structure is assumed to consist of parallel cylindrical capillaries of circular cross-section. Ferry also assumed that the solution remained homogenous throughout filtration.

The filtering solution follows uniformly distributed streamlines in the bulk phase but these streamlines become concentrated near pore openings. According to Poiseuille flow, the velocity distribution at the centre of any pore to the walls of the pore is given by equation 2.18.

$$u(r) = u_0\left(1 - \frac{r^2}{R^2}\right) \tag{2.18}$$

where $u(r)$ is the velocity at a distance r from the centre of the pore

u_0 is the velocity at the centre of the pore

R is the effective pore radius

The volumetric flowrate is given by equation 2.19

$$Q = \frac{dV_p}{dt} = \int_0^R 2\pi r u(r) dr = \frac{\pi u_0 R^2}{2} \tag{2.19}$$

where Q is the volumetric flowrate

V_p is the volume of material entering a pore

Particles migrating towards a pore, as a result of the suspension flow, will have a probability of penetrating the pore. This probability is equal to unity for particles whose centres fall within a concentric circle having a radius equal to $(R - r_p)$, where r_p is the particle radius, otherwise there is no penetration. This steric limitation introduces a statistical sieving coefficient.

Thus, neglecting Brownian motion, the number of particles entering a pore is equivalent to the number of particles whose velocities exceed the hydrodynamic velocity corresponding to that at the limiting probability radius.

$$\frac{dn}{dt} = C_b \int_0^{R-r_p} 2\pi r u(r) dr = C_b \pi u_0 \left[(R - r_p)^2 - \frac{(R - r_p)^4}{2R^2} \right] \qquad (2.20)$$

where n is the number of particles entering a pore

The concentration in the permeate is given by equation 2.21.

$$C_p = \frac{dn}{dV} = C_b \left[2\left(\frac{R - r_p}{R} \right)^2 - \left(\frac{R - r_p}{R} \right)^4 \right] \qquad (2.21)$$

Thus, the sieving model is described by equation 2.22.

$$\chi = 2\left(1 - \frac{r_p}{R} \right)^2 - \left(1 - \frac{r_p}{R} \right)^4 \qquad (2.22)$$

The retention coefficient curve can be estimated from equation 2.22.

$$\sigma = 1 - \chi = [1 - (1 - \lambda)^2]^2 \qquad (2.23)$$

where σ is the retention coefficient

λ is the particle-to-pore size ratio

Several factors have been ignored in the derivation of the sieving model. These include the influence of operating conditions and the effect of concentration polarisation on membrane performance and the changes in selective behaviour of the membrane with processing time. Also, the criterion for particle penetration may be too restricting. Cherkasov (1990) revealed inadequacies in the sieving model by testing the theory on empirical data obtained from ultrafiltration and microfiltration experiments. The results of his experiments showed a

dependence of the retention coefficient on the particle-to-pore size ratio, but this relationship was sigmoidal with a critical relationship.

$$\lambda_{cr} = 0.3 \pm 0.2 \qquad (2.24)$$

λ_{cr} represents the particle-to-pore size ratio at which there is a sharp fall in membrane permeability.

2.5 Experimental determination of the mass transfer coefficient of proteins in the boundary layer

Aimar *et al.* (1991) have developed two approaches to estimate the mass transfer coefficient of solute molecules during filtration of protein solutions. Both methods assume a boundary layer of even thickness along the membrane resulting in an average value for the mass transfer coefficient and the wall concentration. The first approach assumes a linear concentration profile in the boundary layer. The second assumes an exponential profile.

2.5.1 Constant gradient model

The constant gradient-constant boundary layer model assumes that the concentration profile is linear across the polarisation layer of thickness δ. A mass balance across the boundary layer yields equation 2.25.

$$\frac{dC}{dy} = \frac{C_w - C_b}{\delta} = \frac{JC_b}{D} \qquad (2.25)$$

where δ is the boundary layer thickness

The excess solute content in the boundary layer can be estimated using equation 2.26.

$$S = (C_w - C_b)\frac{\delta}{2} \qquad (2.26)$$

where S is the excess solute

Using both equations 2.25 and 2.26, an expression for the boundary layer thickness is obtained.

$$\delta = \left(\frac{2SD}{JC_b}\right)^{0.5} \tag{2.27}$$

The permeate flux rate (J) and the bulk concentration (C_b) are experimental parameters. The excess solute in the boundary layer (S) can be measured by the difference in the bulk solutions. Correlations are available to estimate the diffusion coefficient (D). The wall concentration (C_w) can be estimated by combining equations 2.25 and 2.27.

$$C_w = C_b + \left(\frac{2SJC_b}{D}\right)^{0.5} \tag{2.28}$$

The mass transfer coefficient is defined by equation 2.29.

$$k_m = \frac{D}{\delta} \tag{2.29}$$

According to equation 2.27, the mass transfer coefficient can be estimated using equation 2.30.

$$k_m = \left(\frac{JDC_b}{2S}\right)^{0.5} \tag{2.30}$$

2.5.2 Exponential gradient model

The exponential gradient model assumes the diffusion-convection mass balance remains valid across the boundary layer. A mass balance across the boundary layer yields the following expression.

$$C(y) = C_b e^{\frac{J(\delta-y)}{D}} \tag{2.31}$$

The excess solute in the polarisation layer is estimated using equation 2.32.

$$S = \int_0^{\delta} (C(y) - C_b) dy \tag{2.32}$$

Substituting C(y) in equation 2.32 and integrating yields equation 2.33.

$$S = C_b \left(\frac{D}{J} (e^{\frac{J\delta}{D}} - 1) - \delta \right) \tag{2.33}$$

Equation 2.33 can be solved numerically to obtain the boundary layer thickness. The wall concentration is then calculated using the following equation.

$$C_w = C_b e^{\frac{J\delta}{D}} \tag{2.34}$$

The mass transfer coefficient is calculated using equation 2.29.

2.6 Conclusions

A power law relationship is used to describe flux decline data in this thesis. Although the model gives little insight to the fouling phenomenon, it provides a useful empirical correlation for process design and scale-up (Russotti *et al.*, 1995). The concentration polarisation model is only applicable in the pressure independent region. The resistance model is only applicable in the pressure dependent region. Since all experiments in this thesis have been conducted in the pressure independent region, a concentration polarisation model will be used for predictive purposes in the following chapters.

3 MATERIALS AND METHODS

3.1 Introduction

This chapter provides information on the experimental system studied and the experimental methods employed for investigative and analytical work. Section 3.2 outlines the reasons for the choice of protein for experimental study, the membrane system used and the platform provided for simulation studies. Section 3.3 outlines all experimental methods including assay methods, physical property measurements, yeast homogenate preparation, gel filtration studies and studies on alternative biological systems.

3.2 Experimental system

3.2.1 Choice of protein for experimental study

Yeast alcohol dehydrogenases (ADH) have been used by the research group in the Department of Biochemical Engineering at University College London as a vehicle for the development of a bioprocess simulator. ADH are tetrameric isoenzymes of a molecular mass of ~150 kDa. As intracellular soluble proteins, they provide a suitable system for work involving recovery and purification operations of typical bioprocess unit operations. Packed baker's yeast (DCL Yeast Ltd., Menstrie, Clackmannanshire, U.K.) provides a cheap and reproducible starting source material.

3.2.2 Membrane system

The Bio-Design crossflow filtration apparatus consists of an 8 L holding tank connected to a recirculating gear pump (Model PO811, Bechtech, Chichester, West Sussex, U.K.), pumping process material through a tubular crossflow filtration system. The membranes selected for the system were α-alumina ceramic membranes (Fairey Industrial Ceramics Ltd., Staffordshire, U.K.) with a filtration area of ~0.005 m^2. The single element module allows the use of elements with different nominal pore sizes. Membranes of nominal pore size equivalent to 0.2 μm, 0.8 μm and 1.4 μm were used for filtration experiments. Pressure measurements were obtained from pressure gauges (Wika, U.K.) connected at the inlet and outlet of the membrane module, and the permeate line. Crossflow velocity was measured using a magnetic flowmeter (Type K280/0,

Autometer, Sliedrecht, Holland) and permeate flux rates were measured using an electronic balance (Model BB2400, Metler-Toledo Ltd., Leicester, U.K.). Sample ports were provided on the permeate and retentate line. Operation at constant temperature was possible with the provision of a glycol system cooling the tank contents and the feed line to the membrane system via cooling jackets. The system had backpulsing capabilities with air as the pulsing medium.

3.2.3 Simulation studies

Simulation studies were conducted on an IBM RS6000 (Caplin Cybernetics, Middlesex, U.K.) workstation. The work was performed on SPEEDUP version 5.5 D (AspenTech, Cambridge, U.K.). SPEEDUP (simulation programme for the economic evaluation and design of unsteady-state processes) is a state-of-the-art equation-oriented flowsheeting package capable of steady-state simulation, dynamic simulation, objective function based optimisation, homotopy, parameter estimation and data reconciliation work.

3.3 Experimental methods

To evaluate the condition of the membrane, reverse osmosis (R.O.) water flux measurements as a function of the transmembrane pressure were conducted. Water flux measurements were achieved by filling the tank with R.O. water and adjusting the backpressure valve and the pump speed controller to obtain the required conditions of 0.2 bar transmembrane pressure at a crossflow rate of 0.10 L s^{-1}. The permeate valve was then opened and the average flux for R.O. water was obtained over a 2 minute collection period. Flux measurements were repeated over a range of transmembrane pressures, up to 1.0 bar, at a constant crossflow rate of 0.10 L s^{-1}. The data enabled the calculation of the resistance of the cleaned membrane to permeate flow. The membrane system was then primed with phosphate buffer (100 mM KH_2PO_4, pH 6.5) before the introduction of process feed into the tank. After recirculation of process feed within the membrane system to allow mixing and cooling to 10°C, the required operating conditions were set by adjusting the backpressure valve and the pump speed controller. Filtration was commenced by slowly opening the permeate valve until fully opened, and samples were collected for analysis in 5 mL aliquot fractions.

The membrane was cleaned using a caustic cleaner (1% w/v Ultrasil 41, Henkel Ecolabs Ltd., Swindon, Wiltshire, U.K.). After rinsing the rig with R.O. water to remove particulate material, the solution of Ultrasil was introduced into the rig and recirculated at a crossflow rate of 0.20 L s^{-1} to a temperature of 55°C using a hot rod (BDH, Merck Ltd., Dorset, U.K.). The permeate valve was then partially opened to allow very slow permeation of the hot caustic solution through the membrane for a period of 30 min. The caustic solution was then cooled to room temperature and the rig was rinsed with R.O. water to remove caustic material. Water flux measurements were repeated as described above and the recovered flux was compared to the pre-experimental flux rate to determine the degree of success in cleaning.

3.3.1 Assay methods

Retentate samples collected were pipetted into eppendorf tubes and spun down at 10,500 g for 20 min at room temperature. The recovered supernatants were assayed as described below. All retentate samples and permeate samples collected from homogenate process feeds were assayed for total soluble protein content and alcohol dehydrogenase activity. Assays for glucose-6-phosphate dehydrogenase activity and malate dehydrogenase activity were conducted on selected samples.

3.3.1.1 Total protein determination

Total protein concentrations were determined using the BIO-RAD protein assay (BIO-RAD Laboratories, Hemel Hempstead, Hertfordshire, U.K.). The assay is based on the colour change of a dye (Coomassie Brilliant Blue G-250 in acidic solution) when binding to protein occurs (Bradford, 1976). The dye-binding response to protein concentrations has been found to give an accurate but not entirely linear response.

Bovine serum albumin (BSA, Sigma Chemical Company Ltd., Dorset, U.K.) was used as the protein standard. The dye reagent (BIO-RAD Laboratories, Hemel Hempstead, Hertfordshire, U.K.), provided as a five-fold concentrate, was diluted using de-ionised water. Several solutions of BSA ranging from 0.2 mg mL^{-1} to 1.0 mg mL^{-1} were made and assayed according to the procedure given below. BSA samples, 0.05 mL, were placed in 4 mL cuvettes and 2.5 mL of

diluted dye reagent was added. The sample-reagent solution was mixed by gentle inversion of the cuvettes. After a period of ~10 min, the samples were measured against a reagent blank, containing 0.05 mL of sample buffer, by spectrophotometric analysis at a wavelength of 595 nm. The data obtained was used to provide a standard plot of the optical density reading at 595 nm versus the concentration of protein in sample.

Samples were diluted to produce a response ranging from 0.1 to 0.9 optical density units and assayed in triplicates as described above. Protein concentrations were determined against the BSA standard curve.

3.3.1.2 Alcohol dehydrogenase activity

ADH activity was assayed using the method described by Bergmeyer (1983). The rate of reaction was measured spectrophotometrically by monitoring the change in absorbance of the solution at 340 nm with ethanol as substrate. Nicotinamide-adenine dinucleotide (NAD^+, Sigma Chemical Company Ltd., Dorset, U.K.) is reduced during the reaction.

$$\text{Ethanol} + NAD^+ \leftrightarrow \text{Acetaldehyde} + NADH + H^+$$

The enzymatic activity (E) expressed in units of activity per millilitre of solution is given by equation 3.1.

$$E = \frac{1}{\varepsilon_{340}} \frac{\Delta A}{\Delta t} \qquad (3.1)$$

where $\frac{\Delta A}{\Delta t}$ is the rate of change of absorbance at 340 nm

ε_{340} is the extinction coefficient = 6.22 cm^2 μmol^{-1}.

The assay mix contained 1.8 mM NAD^+, 1.0 mM glutathione (Sigma Chemical Company, Dorset, U.K.), 6.2 mM semicarbazide hydrochloride (Sigma Chemical Company, Dorset, U.K.) and 3.5% v/v ethanol (BDH, Merck Ltd., Dorset, U.K.). Samples were diluted using phosphate buffer (100 mM KH_2PO_4, pH 6.5) so that the maximum absorbance change was

less than 0.7 absorbance units min^{-1}. Sample, 0.05 mL, was added to 3 mL of assay mix, and the reaction was monitored for 60 s and repeated in triplicate for analytical purposes.

3.3.1.3 Glucose-6-phosphate dehydrogenase activity

Glucose-6-phosphate dehydrogenase (G-6-PDH) activity was assayed by the method of Bergmeyer (1983). The rate of increase of absorbance due to the reduction of nicotinamide-adenine dinucleotide phosphate ($NADP^+$, Sigma Chemical Company Ltd., Dorset, U.K.) is a measure of G-6-PDH activity. Glucose-6-phosphate (G-6-P, Sigma Chemical Company Ltd., Dorset, U.K.) was used as the reaction substrate and the reaction was monitored spectrophotometrically at 340 nm.

$$\text{G-6-P} + NADP^+ \leftrightarrow \text{6-phosphogluconolactone} + NADPH + H^+$$

E expressed in units of activity per millilitre of solution is given by equation 3.1.

Sample, 0.05 mL, was added to 3 mL of assay mix containing 86 mM Tris-HCl buffer (pH 7.6) (BDH, Merck Ltd., Dorset, U.K.), 6.9 mM magnesium chloride (BDH, Merck Ltd., U.K.), 1 mM G-6-P and 0.39 mM $NADP^+$. The resulting solution was mixed by inversion of the 4 mL cuvette and the reaction was monitored every 30 s for 5 min. The assays were repeated for analytical purposes.

3.3.1.4 Malate dehydrogenase activity

Malate dehydrogenase activity was determined by measuring the decrease in absorbance due to the oxidation of nicotinamide-adenine dinucleotide reduced form, (β-NADH, Sigma Chemical Company Ltd., Dorset, U.K.). Oxaloacetate (Sigma Chemical Company Ltd., Dorset, U.K.) was used as the reaction substrate and the reaction was monitored spectrophotometrically at 340 nm.

$$\text{Oxaloacetate} + \beta\text{-}NADH + H^+ \leftrightarrow \text{L-malate} + NAD^+$$

E expressed in units of activity per litre of solution is given by equation 3.2

$$E = 4365 \frac{\Delta A}{\Delta t} \qquad (3.2)$$

where $\frac{\Delta A}{\Delta t}$ is the rate of change of absorbance at 340 nm < 0.006 min^{-1}.

The absorbance readings should not exceed one absorbance unit and the reaction was monitored every 5 s for 60 s.

Phosphate buffer, 0.88 mL (100 mM KH_2PO_4, pH 7.4), was pipetted into a 1.5 mL cuvette. Reduced β-NADH, 0.01 mL of a 2% w/v solution, and oxaloacetate, 0.01 mL of a 2% w/v solution, were added to the phosphate buffer in the cuvette. Diluted sample, 0.1 mL, was added to the mixture in the cuvette, and after inversion of the cuvette for gentle mixing, the absorbance was read at 340 nm. The assay was carried out at room temperature and analysed in duplicate.

3.3.1.5 α-amylase activity

The activity of α-amylase was measured in permeate samples and in the soluble fractions of lysed cell and whole cell samples. The assay, based on the method described by Blanchin-Roland *et al.* (1989), is a measure of the breakdown of starch by α-amylase, indicated by the rate of decrease of a coloured starch-iodine complex. Soluble starch, 0.5% w/v, in phosphate buffer (15 mM Na_2HPO_4, pH 5.8) was used as reaction substrate. The starch solution was prepared by heating to boiling point and filtering through a No. 1 Whatman grade filter paper (Whatman International Ltd., Maidstone, U.K.) whilst hot. Fresh iodine reagent was prepared by diluting 100 µL of a 2% w/v potassium iodide solution in 200 mL of an aqueous stock solution containing 2.2% w/v iodine and 4.4% w/v potassium iodide. Samples were diluted to the appropriate concentrations using phosphate buffer (15 mM Na_2HPO_4, pH 5.8) and 150 µL was dispensed into rows of a microtitre plate. The plate containing sample material was incubated at 50°C. Starch solution, 150 µL, was added to the sample row and mixed by repeat pipetting. Reaction mix, 15 µL, was then pipetted into 300 µL of the iodine reagent in a separate microtitre plate to

stop the reaction. The procedure was repeated at several equally spaced time intervals, 2.5 min, up to 15 min. The extent of reaction was measured by reading absorbencies at 620 nm using a plate reader (Model MR7000, Dynatech, Billingshurst, West Sussex, U.K.). The activity of α-amylase was obtained from the gradient of a plot of absorbencies at 620 nm versus time. Samples were assayed in triplicate.

3.3.2 Particle size analysis

Particle size measurements of retentate and selected permeate samples were performed using three different particle sizers depending on the size range of the substance to be measured.

3.3.2.1 Electrical Sensing Zone Method

Particle size analysis of polyethyleneimine flocculated yeast homogenate was carried out using an Elzone (Model 280 PC, Particle Data Ltd., Cheltenham, U.K.). The Elzone consists of a tube with an orifice in its wall which is immersed in an electrolyte solution containing the material to be analysed. A vacuum pump applies a negative pressure across the orifice which causes material and electrolyte solution to flow through it and unbalance a mercury column connected to the system. The system is then isolated from the vacuum source and flow through the orifice continues due to the balancing action of the mercury column. This activates a counter which performs a count on a known volume of material passing through the orifice. The change in electrical resistance across the orifice is monitored by means of immersed electrodes on either side of the tube wall. The resistance is converted to a voltage pulse. The number of particles passing through the orifice is proportional to the number of pulses and the height of a voltage pulse is proportional to the volume of particle.

An 18 μm orifice was used and calibrated using latex particles of sizes 2 μm and 5 μm (Particle Data Ltd., Cheltenham, U.K.). Sodium chloride, 10 % w/v, in phosphate buffer (100 mM KH_2PO_4, pH 6.5) was used as electrolyte solution. The solution was filtered using 0.2 μm cellulose nitrate filters (Whatman, Maidstone, U.K.). Samples, ~ 10 μL, were dispensed into the electrolyte solution and measurements were conducted as described above. Three replicate counts per sample were performed.

3.3.2.2 Laser Diffraction Method

Particle size analysis of whole yeast cells and polyethyleneimine flocculated yeast homogenate was carried out using a Malvern 3600E particle sizer (Malvern Instruments, Malvern, Worcestershire, U.K.). The instrument uses the principle of diffraction as a means of measurement. A low power monochromatic beam of light, incident on particles in a sample cell, is diffracted by the illuminated particles to give a stationary diffraction pattern. The diffraction pattern represents the instantaneous size distribution of particles in the illuminated area. This pattern changes as particles enter and leave the illuminated area. A lens focuses the diffraction pattern onto a photo-electric detector which produces an analogue signal proportional to the incident light intensity. The final measured diffraction pattern, which is representative of the bulk sample, is obtained by integration over a suitable period using a computer directly interfaced to the detector. Having obtained the diffraction pattern, the computer uses non-linear least squares analysis to find the size distribution which gives the most closely fitting diffraction pattern.

A 63 mm lens capable of detecting particle sizes in the range 1.2 μm up to 118 μm was selected and details entered into the computer programme. The sample cell was cleaned with de-ionised water and positioned within the range of the lens. The cell was then filled with 0.2 μm filtered phosphate buffer (100 mM KH_2PO_4, pH 6.5). The tilt (vertical angle) and twist (horizontal angle) adjustment of the cell was performed to ensure that the laser beam reflections from the cell windows were properly directed out of the measurement area. Alignment of the receiver unit was achieved using the X (horizontal adjustment) and Y (vertical adjustment) adjusters until the focused laser spot passed through the main detector, hitting the central detector. Measurements were carried out in two stages. The initial measurement was performed on diluent to eliminate the contribution of non-sample scattering sources. Sample, a pinhead amount, was then added to the cell contents and mixed using a magnetic stirrer. The sample concentration was checked prior to measuring the particle size distribution. Measurements were performed in duplicate for analytical purposes.

Particle size analysis of yeast homogenate, selected permeate samples and *Escherichia coli* whole cells and lysed cells were carried out using a Malvern Series 4700/PCS 100 spectrometer laser sizer (Malvern Instruments, Malvern, Worcestershire, U.K.). The

spectrometer, which operates by photon correlation spectroscopy, consists of a laser transmitter mounted on a turntable which sends a light beam into the sample cell at the centre of the turntable. Scattered light from the sample is recorded in a photon counting device and its intensity and fluctuations in intensity as a function of time are recorded using a digital correlator. The fluctuations in intensity describe the diffusive movement of particles, which is related to the size of the equivalent sphere using Stoke's law. The information from the correlator is passed to a computer for analysis and display. Typical measurements last 5-150 s, during which the sample must remain stable and representative.

The sample viscosity and an assumption of the refractive index of the sample liquid were inputted in the computer programme. The sample cell was cleaned with de-ionised water and filled with 0.2 μm filtered phosphate buffer (100 mM KH_2PO_4, pH 6.5). Sample, ~ 10 μL, was added to the contents in the cell and mixed gently by inversion. The sample cell was held in a glass vat filled with de-ionised water. Temperature of the water in the vat was controlled at 25°C and filtered to remove dust particles using a filter pump. The angle of measurement was set at 90 °. The concentration of sample in the cell was altered until an acceptable count rate of 50,000 to 100,000 counts per s was achieved. Measurements were then conducted in duplicate.

3.3.3 Rheological measurements

The viscosity of process feed-streams was measured using a rotational viscometer (RHEOMAT 115, Contraves AG, Zurich, Switzerland). The concentric cylinder arrangement of the viscometer was used. The measuring cylinder rotates in the substance to be measured and the braking torque exerted on the cylinder by the substance is a measure of its viscosity.

Calibration of the viscometer was done using a standard solution of 5 cp. Approximately 18 mL of solution was transferred into the measuring device using a Gilson pipette. The measuring cylinder was placed into the solution and rotation of the cylinder was commenced by switching on the electromotor. The rotational speed of the measuring cylinder ranges from 5 to 780 min^{-1}. The rotation of the measuring cylinder was increased through the 15 speed steps and the torque recorded. The procedure was repeated in reverse. The shearing speed in the solution is

a function of the rotational speed of the measuring cylinder. The shear stress is a function of the braking torque. These values were used to deduce the viscosity of the glycerol solutions.

The viscosity of feed broths was measured as described above. Samples were analysed in duplicate. All measurements were performed with the temperature of the broth at 10°C.

3.3.4 Dry weight measurements

Dry weights of whole cells in phosphate buffer (100 mM KH_2PO_4, pH 6.5) were determined by pipetting known volumes of sample into pre-weighed eppendorf tubes and drying the sample to a constant weight at 105°C before re-weighing. Samples were analysed in duplicate.

3.3.5 Yeast homogenate preparation

Packed baker's yeast supplied by DCL Yeast Ltd. (Menstrie, Clackmannanshire. U.K.) was suspended in phosphate buffer (100 mM KH_2PO_4, pH 6.5) to give a final wet weight concentration of ~540 g packed weight L^{-1}. The yeast suspension was disrupted using a Manton-Gaulin high pressure homogeniser (Model Lab 60, APV, Crawley, Sussex) at 500 bar for 5 discrete passes, resulting in at least 98% release of intracellular contents. The temperature of the suspension was maintained at 5-10°C using glycol as coolant. The yeast homogenate concentration was then adjusted using phosphate buffer (100 mM KH_2PO_4, pH 6.5) to that required for filtration experiments.

3.3.6 Gel filtration studies

Gel filtration studies were conducted on a Fast Protein Liquid Chromatography (FPLC) system (Amersham-Pharmacia Biotech, Hertfordshire, U.K.). The HR 16/50 column (Amersham-Pharmacia Biotech, Hertfordshire, U.K.) was packed with Superose 12 prep grade media (Amersham-Pharmacia Biotech, Hertfordshire, U.K.) according to the procedure given below.

Superose 12 prep grade in 20 % ethanol was washed three times with de-ionised water to remove all the ethanol. The slurry was transferred to a vacuum flask and degassed before packing. The column was packed at the operating temperature (4°C). All parts of the column

were cleaned with de-ionised water before use. The filters provided with the column were checked for damage before wetting and placement of one filter at the base of the column. A plunger was used to push the bottom filter into place. The packing reservoir was then attached to the other end of the column and the column was mounted vertically on a stand. The degassed slurry was poured down the inside walls of the column with the aid of a metal spatula. After checking the column to ensure no trapped air bubbles, the packing reservoir was filled with de-ionised water and the top of the packing reservoir was screwed on and connected to the pump (P-500, Amersham-Pharmacia Biotech, Hertfordshire, U.K.). The column was packed in two stages. During stage 1, the gel was allowed to settle at the recommended flowrate of 2 mL min^{-1}. This was followed by further packing for 1 h at ~6 mL min^{-1}, not exceeding the pressure limits of the gel. The packing reservoir was then removed and the bed height was adjusted using a rotating plunger. The second filter was placed at the top of the gel bed and the top adapter was adjusted onto the gel surface. With both outlets closed, the column was inverted and reconnected to the pump and the UV monitor. The column was tested for quality of packing using the pulse of a sample of acetone in de-ionised water, 5 mg mL^{-1}, to calculate the number of theoretical plates m^{-1} before eluting with phosphate buffer (100 mM KH_2PO_4, pH 6.5).

Fresh undiluted permeate sample, 1 mL, was loaded onto the column and eluted using phosphate buffer (100 mM KH_2PO_4, pH 6.5) at a flowrate of 0.1 mL min^{-1}. Fractions, 2 mL, were collected after 4 h. Each fraction was assayed for total protein content and alcohol dehydrogenase activity. The assays were performed in duplicate. The procedure was repeated for the soluble fraction of retentate samples.

3.3.7 Polyethyleneimine flocculation

Polyethyleneimine (PEI, Sigma Chemical Company Ltd., Dorset, U.K.), obtained as a 50% w/v aqueous solution, was diluted with de-ionised water to give a 2% w/v aqueous solution. The pH of the resulting solution was adjusted to 6.5 using 4M HCl. Samples of yeast homogenate suspension in eppendorf tubes were dosed with 2% PEI ranging from 5% v/v to 45% v/v. The resulting suspensions were spun down at 10,500 g for 20 min and the recovered supernatants were assayed for alcohol dehydrogenase activity and total protein content. The results were used

to select a suitable dosing ratio for filtration experiments involving PEI flocculated yeast homogenate.

A 2% w/v PEI solution was added to freshly prepared yeast homogenate at the required dosing ratio. The suspension was mixed for 5 min and used as process feed for microfiltration experiments.

3.3.8 *Escherichia coli* fermentation

Escherichia coli cells, strain JM107 with plasmid pQR126, developed by French (1993) were grown in batch mode and used for downstream processing studies investigating the recovery of α-amylase from lysed cells. All chemicals for the fermentation were obtained from Sigma Chemical Company Ltd. (Dorset, U.K.) unless stated otherwise.

An agar solution, 1 L, containing 28 g L^{-1} Oxoid No. 2 (Oxoid Unipath Ltd., Basingstoke, Hampshire, U.K.) in R.O. water and 1% w/v potato starch was autoclaved and cooled to below 42°C. Kanamycin, 0.02 g L^{-1}, was filter sterilised (0.2 μm, Whatman, Maidstone, U.K.) into the cooled sterile agar solution before the plates were poured. The plates were stored at 4°C for use over a two week period. Plates, 4, were inoculated from -70°C stocks using a sterile loop and incubated at 37°C for ~ 24 h.

An inoculum volume, 200 mL, was prepared in two 2L shake flasks. Each flask contained media parts A and B which were prepared separately until fully dissolved in de-ionised water and then mixed together. Part A constituents were 10 g L^{-1} $(NH_4)_2SO_4$, 2.5 g L^{-1} NaCl, 2.16 g L^{-1} Na_2HPO_4, 0.64 g L^{-1} KH_2PO_4 and 1 mL L^{-1} trace element solution. The composition of the trace element solution was 10 g L^{-1} $CaCl_2$, 4 g L^{-1} H_3BO_3, 2 g L^{-1} $MnCl_4.4H_2O$, 0.4 g L^{-1} $CuSO_4.5H_2O$, 0.4 g L^{-1} $CoCl_2.6H_2O$, 0.2 g L^{-1} $NaMoO_4.2H_2O$ and 2 g L^{-1} $ZnSO_4.7H_2O$. Part B constituents were 0.2 g L^{-1} $FeSO_4.7H_2O$ and 0.2 g L^{-1} citric acid. Part D, containing 0.2 g L^{-1} $MgSO_4.7H_2O$ and 4 g L^{-1} glycerol (BDH, Merck Ltd., Dorset, U.K.), was prepared and dispensed into two bijou bottles and autoclaved with the two shake flasks containing media parts A and B. Part C, containing 0.05 g L^{-1} thiamine and 0.01 g L^{-1} kanamycin, was filter sterilised into the shake flasks prior to inoculation from the plates. To inoculate the shake flasks, 3 mL of media from the flasks was pipetted on to the plates and two lines of cells were scraped off and the

media with cells was poured back into the flask. Cells in the shake flasks were grown at 37°C in an orbital incubator at 200 rpm for 23 h.

Fermentations were carried out in 20 L vessels (Model LH20L01, Inceltech, Berkshire, U.K.) with a working volume of 14 L. Parts A and B were made separately and when fully dissolved, added together. Polypropylene glycol, 0.1 mL L^{-1} PPG (BDH, Merck Ltd., Dorset, U.K.), was added to parts A and B. These components of the media were sterilised in situ in the vessel. Part D, ~ 500 mL, was autoclaved in a side arm flask and part C was filter sterilised into part D. This component of the media was added to the fermenter immediately prior to inoculation. Alkali, 4M NaOH, and antifoam, 25 % v/v PPG, were used as control. The sterile medium was then inoculated with the shake flask contents at the appropriate time. The temperature was controlled at 37°C, the pH was controlled at 7, the stirrer speed was set at 500 rpm and airflow was set at 7 L min^{-1}. Optical density of fermenter broth was monitored every 2 h to determine growth rates. After 7 h, the stirrer speed was increased to 1100 rpm and the airflow was increased to 12 L min^{-1}. The fermenter broth was grown to an optical density reading of approximately 30, lasting ~ 24 h. Dissolved oxygen tension levels were maintained above 30% during fermentations.

Fermenter broth, 10 L, was used for downstream processing studies. A tubular bowl centrifuge (Model Sharples 1P, Alfa-Laval Sharples Ltd., Camberley, U.K.) was used to harvest the cells. The cells were resuspended in supernatant to a final volume of 2 L. Lysis solution, 2 L, at room temperature containing 20% w/v sucrose, 1 mM Na_2EDTA and 500 μg mL^{-1} hen egg lysozyme was added to the suspension of cells and the solution was gently mixed at room temperature for 10 min. R.O. water, 2 L, ~ 4°C, was then added to the solution and gently mixed at room temperature for a further 10 min. The resulting suspension was used as feed broth for filtration studies.

Filtration studies were conducted on lysed cells as described in section 3.3. Samples of the soluble fraction of lysed cells and whole cells and permeate samples were assayed for total protein levels as described in section 3.3.1.1 and α-amylase activity as described in section 3.3.1.6. Gel permeation chromatograms were obtained by running samples down a Superose 12 gel filtration column as described in section 3.3.6. Particle size measurements of whole cells and

lysed cells were conducted on the Malvern Series 4700/PCS 100 spectrometer laser sizer as described in section 3.3.2.2. Rheological properties of whole cells and lysed cells were carried out on the RHEOMAT 115 viscometer as described in section 3.3.3.

3.4 Conclusions

The analytical methods described and the models detailed in Chapter 2 will allow the development and experimental verification of bioprocess filtration models. Chapter 4 outlines two approaches to the modelling of filtration systems. The first is based on a statistical approach and requires a high degree of experimentation to develop. The second uses a concentration polarisation model and is based on single experimental measurements of the permeate flux rate for a given membrane pore size. Chapter 5 extends the polarisation modelling approach to a homogenised system. Chapters 6 provides information on an effective strategy for the design and evaluation of membrane filtration systems for use in the bioprocess industries based on experimental and simulation studies.

4 PROCESSING OF WHOLE CELLS

4.1 Introduction

Statistical process models have been used successfully for various applications including fermentation processes (Linko *et al.*, 1992), drying processes (Huang *et al.*, 1993) and chemical processes (Zaldivar *et al.*, 1992). Such studies have been based on artificial neural networks. The network consists of an input layer containing n inputs and an output layer containing m outputs connected by a single hidden layer or multiple hidden layers containing n cells. Each neural cell is a single calculation processor and the neural network consists of an association of neural cells (Dornier *et al.*, 1995). In a typical feed-forward neural network, the input layer simply transmits the input variables without any processing to the next layer (Niemi *et al.*, 1995). Each node in the upper layer (hidden or output layer) receives processed or weighted inputs from each node in the layer below. The weighted parameters are obtained using numerical techniques to provide the best fit to the experimental data. This process is often termed network training and it aims to minimise the differences between the calculated outputs and the experimental outputs. Algorithms available for least-squares optimisation problems often use the steepest descent method or a Taylor-series method. Palosaari *et al.* (1986) used a random search method to simulate the reverse osmosis of ethanol and acetic acid. In the method, the best value was initially found by a random search and subsequent iterations were conducted in a progressively reduced search area. Iterations were continued until the search area was reduced by a given amount. The random search was repeated several times and the most successful random minimisation was accepted as optimal. Once the weighted parameters of the neural network model are determined, simulations of the process can be carried out within the range of variables used in the experiments. Dornier *et al.* (1995), Niemi *et al.* (1995) and Meyer *et al.*, (1998) used neural networks model crossflow microfiltration systems. In their work, the output variables included the permeate flux rate and the membrane rejection characteristics. However, different workers used different inputs to describe their models. Dornier *et al.* (1995) included the transmembrane pressure and the recirculation rate as input variables. Niemi *et al.* (1995) included the aforementioned variables, the feed concentration and the temperature as input variables. Meyer *et al.* (1998) used up to 17 input variables to describe the microfiltration of *Escherichia coli* suspensions including the system hydrodynamics,

the suspension qualities, the membrane qualities, operating parameters and fermentation conditions. The main advantage of using neural networks is the ease of implementation and the accuracy of model predictions. However, the training requirements of the simulator and the specificity of generated models are significant drawbacks.

The concentration polarisation model is often used to describe the permeate flux properties of crossflow filtration systems. However, discrepancies between theoretical and experimental permeate flux rates arise as a result of a lack of understanding of the hydrodynamics of such systems. An alternative approach is to experimentally determine the concentration polarisation model for a given system. Such an approach will involve conducting experiments along with physical property characterisations including rheological measurements. The model parameters are then determined empirically for the given system. The main advantage of such an approach is the ease of implementation and the number of experiments required to model the system. The main drawbacks include the accuracy of model predictions and the model specificity.

This chapter examines the processing of baker's yeast whole cells for a wide range of operating conditions including the effect of broth concentration, the recirculation rate, the transmembrane pressure and the membrane pore size on membrane performance. It sets out to compare two approaches to modelling of filtration systems. The first is based on a statistical approach and uses Pareto charts and normality plots to establish which variables have significant effects on the membrane separation process. A statistical model, based on linear regression, to predict permeate flux rates is developed. The development of this model requires a high degree of experimentation and is quite specific to the system being investigated. The second approach is based on the concentration polarisation model. In contrast to the first approach, single measurements of the permeate flux rate, accompanied with rheological measurements, are required for predictive purposes.

4.2 Experimental methods

Packed baker's yeast was supplied by DCL Yeast Ltd., (Menstrie, Clackmannanshire, U.K). Blocks of packed yeast were suspended in phosphate buffer (100 mM KH_2PO_4, pH 6.5) to

final wet weight concentrations ranging from 50 g packed weight L^{-1} up to 450 g packed weight L^{-1}. The resulting yeast suspensions were used as process feed for microfiltration experiments.

Filtration experiments were conducted on the Bio-Design crossflow filtration rig as described in section 3.2.2 using α-alumina ceramic membranes (Fairey Industrial Ceramics Ltd., Staffordshire, U.K.). Tubular membranes, each with a filtration area of ~ 0.005 m^2, were used with nominal pore sizes equivalent to 0.2 μm, 0.8 μm, and 1.4 μm. Water flux measurements as a function of the transmembrane pressure were performed prior to all experimental runs. Details of experimental procedure can be found in section 3.3 of this thesis.

Physical properties of yeast whole cells including particle size measurements, viscosity measurements and dry weight determinations were performed as described in sections 3.3.2, 3.3.3 and 3.3.4 respectively.

4.3 Properties of yeast whole cells

4.3.1 Particle size distribution of yeast whole cells

The particle size distribution of yeast whole cells (Figure 4.1) was obtained from laser diffraction studies. The distribution was bimodal with peak diameters at ~ 3.0 and ~ 7.0 μm. The presence of a smaller peak may represent daughter cells.

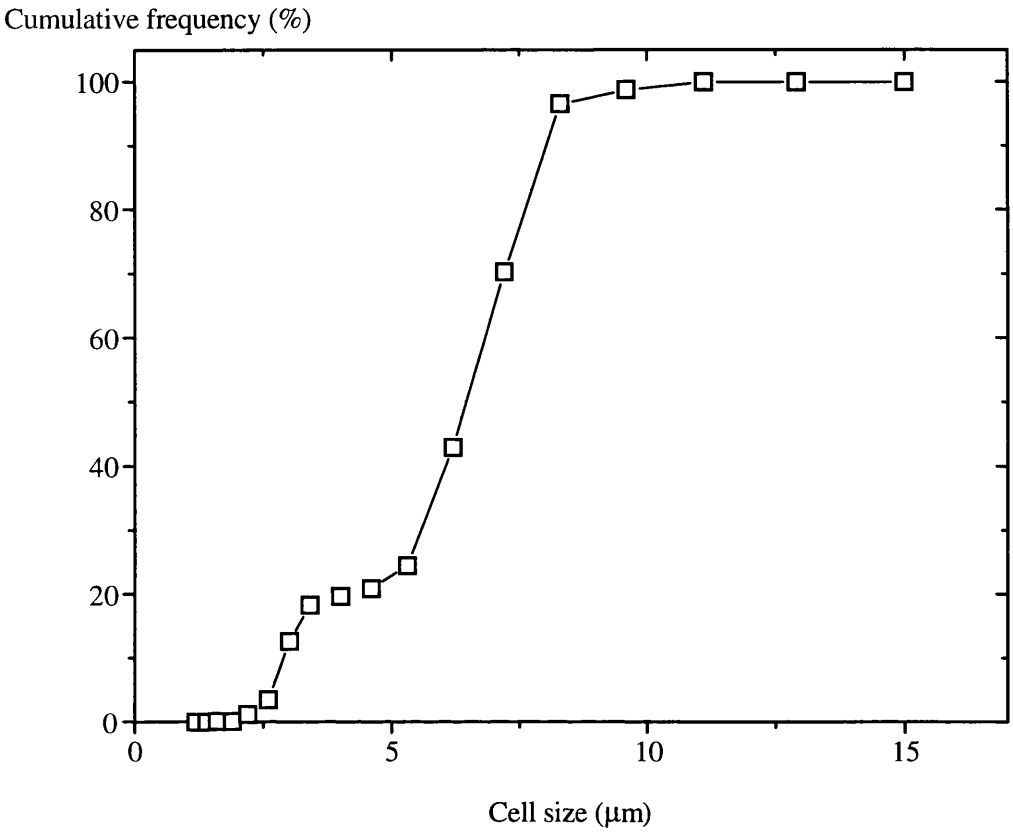

***Figure 4.1**: Particle size distribution of yeast whole cells in phosphate buffer (100 mM KH_2PO_4, pH 6.5) using laser light diffraction.*

An estimate of the density of whole cells from literature is given as 1115 kg m^{-3} (Mosqueira *et al.*, 1981), and the dry-wet weight ratio is estimated at ~ 2:7.

4.3.2 Rheological properties of yeast whole cells

The shear stress-shear rate relationship for yeast whole cells, for the range of yeast concentrations studied, is shown in figure 4.2. The broth exhibits Newtonian behaviour.

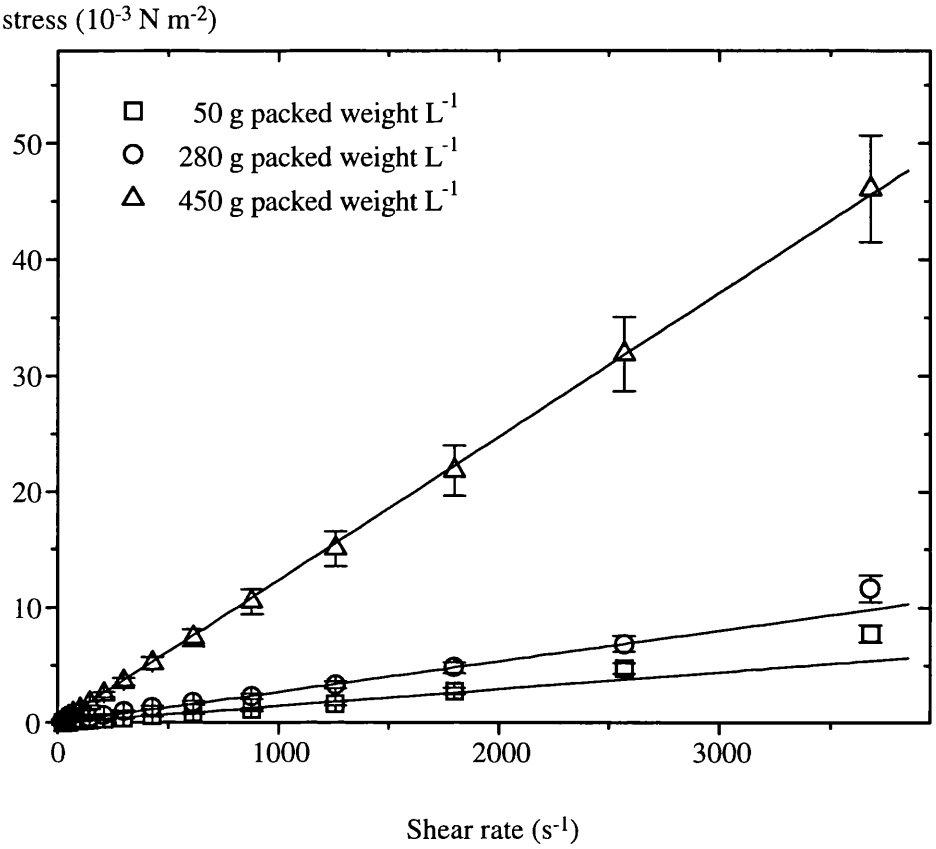

***Figure 4.2**: Shear stress-shear rate relationship for yeast whole cells suspended in phosphate buffer (100 mM KH_2PO_4, pH 6.5).*

The viscosity of yeast whole cells suspended in phosphate buffer as a function of the volumetric solids content of packed whole cells is shown in figure 4.3.

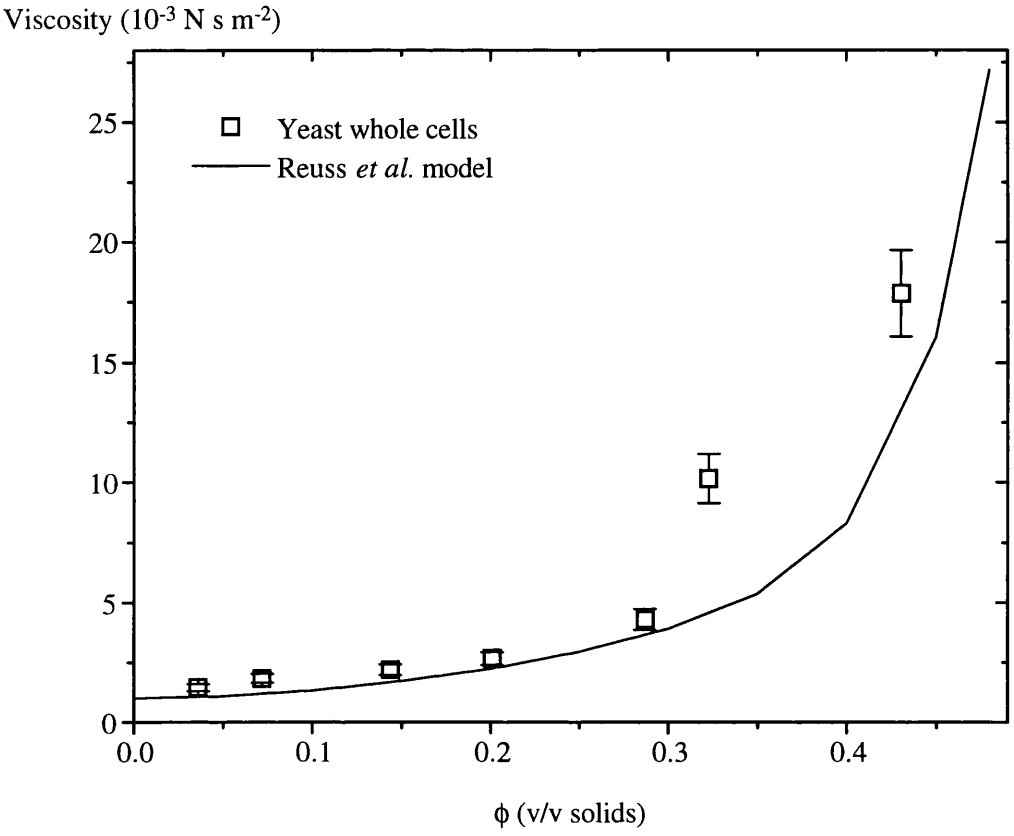

***Figure 4.3**: Viscosity of yeast whole cells in phosphate buffer (100 mM KH_2PO_4, pH 6.5) using a rotational viscometer. The error is estimated at ± 10% and the correlation coefficient (R^2) is calculated as 0.939.*

Several models are available in the literature describing the viscosity of whole cells. The Reuss *et al.* (1979) model gives the closest approximation to our data.

$$\mu_s = \mu_L (1 + a_1 \phi + a_2 \phi^2 + a_3 e^{a_4 \phi}) \qquad (4.1)$$

where μ_s is the viscosity of the suspension

μ_L is the viscosity of the suspending liquid

ϕ is the volume fraction of particles

$a_{i\ (i = 1,...,4)}$ are the Reuss *et al.* model coefficients

4.4 Characteristics of microfiltration systems

Figure 4.4 shows a typical flux decline curve for baker's yeast whole cells suspended in phosphate buffer (100 mM KH_2PO_4, pH 6.5). Initial flux decline is rapid until a pseudo steady-state value is reached. It is this flux rate which is important for long term operation.

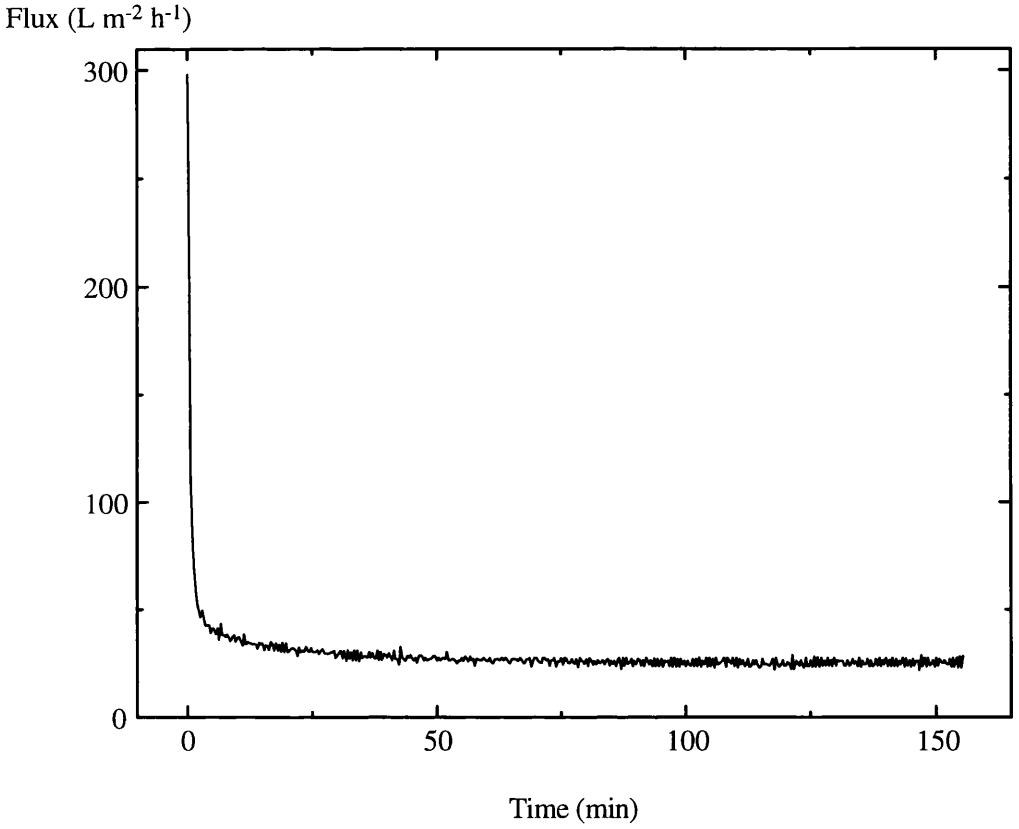

***Figure 4.4**: Typical flux-time profile of microfiltration systems. Experiment was conducted on a ceramic membrane of nominal pore size equivalent to 0.2 μm at the conditions of a cell concentration of 280 g packed weight L^{-1}, a recirculation rate of 1.8 m s^{-1} and a transmembrane pressure of 100 kPa.*

Figure 4.5 shows the flux-pressure profile for yeast whole cells.

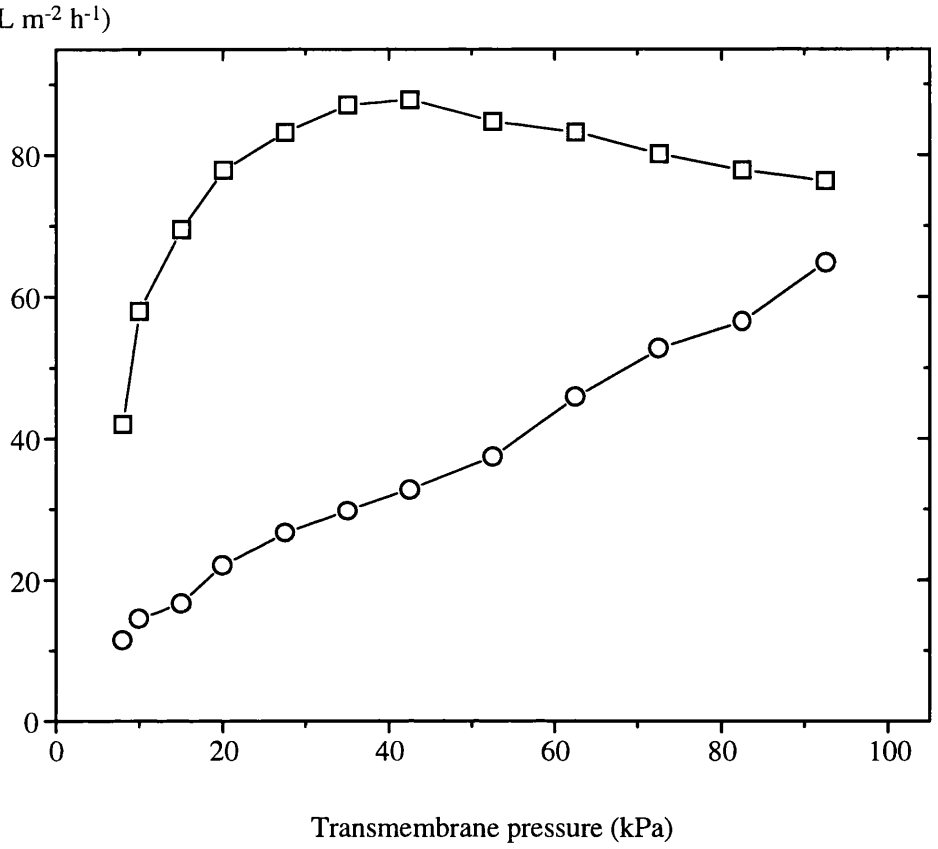

***Figure 4.5**: Flux-pressure profile of yeast whole cells at a concentration of 280 g packed weight L^{-1} and a recirculation rate of 3.5 m s^{-1} using a ceramic membrane of nominal pore size equivalent to 0.2 μm. The squares denote operation in increasing transmembrane pressure and the circles denote operation in decreasing transmembrane pressure.*

The profile obtained is a common feature of biological systems. The critical pressure, the pressure at which an increment in the transmembrane pressure has no effect on the permeate flux rate, is estimated at ~ 40 kPa. There is a high level of hysteresis associated with the membrane system as transmembrane pressures are reduced.

4.5 Results

To establish which process variables have the most significant effect on the performance of our membrane system, a method of experimental design was used. This method allows the abstraction of structured information from physical systems with a minimum of experimentation.

The main features include Pareto charts which identify significant main effects and interactions of process variables and normal probability plots which identify main effects and interactions which are large in comparison to the experimental error.

Experimental design is defined as a combination of statistical techniques for the structured analysis of experimental data (Chadwani, 1995). Haaland (1989) gives a comprehensive guide to experimental design in biotechnology. A typical design for screening physical systems usually takes the following form

- perform experiments in a structured methodical manner
- for each trial determine a value for the response factor
- calculate values for main effects and interactions by manipulation of the response factors
- identify the important main effects and interactions by using Pareto charts
- determine those experimental factors which are not masked by the experimental error by estimating the noise level and the use of normal probability plots
- resolve any interactions between factors by the use of interaction plots

4.5.1 Factorial designs

Full factorial designs are the most commonly used experimental design procedure because they are simple to implement and easy to interpret. In a typical two level design, i.e. a 'high' setting and a 'low' setting for each variable or factor, experiments are performed for each combination of variable settings. The outcome of each experiment is measured by a value determined for the response factor. A full factorial design investigates all of the possible combinations of settings for each variable, allowing the independent estimation of signals associated with each variable and with a combination of variables (Haaland, 1989). The number of experiments which have to be performed in a k-factor, n-level full factorial design is n^k. The number of experiments in the design is the sample size. The sample size for full factorial designs may become large. In such cases, fractional factorial designs are often used for screening physical systems. Such a design approach will inevitably lead to some information loss and possible ambiguity about variable interactions.

To investigate the effect of 4 factors including the membrane pore size, the cell concentration, the recirculation rate and the transmembrane pressure, on the performance of the membrane system, a 3-level fractional factorial design was used. Tables 3.1, 3.2 and 3.3 show values of the flux rate after 1 min (J_1) the fouling index (b) and the flux rate at steady-state (J_{ss}) under various experimental conditions. The values have been determined by fitting the experimental data to the fouling model described by Patel *et al.*, (1987). All experiments have been conducted at 10°C using ceramic membranes described in Appendix A3.

Conc ($g\ L^{-1}$)	Velocity ($m\ s^{-1}$)	ΔP_{tm} (kPa)	J_i ($L\ m^{-2}\ h^{-1}$)	J_{ss} ($L\ m^{-2}\ h^{-1}$)	b	R^2
50	3.5	50	170	61	0.31	0.855
	3.5	100	165	61	0.30	0.835
	1.8	100	152	20	0.62	0.977
	6.0	100	325	66	0.43	0.974
	3.5	200	237	56	0.44	0.877
	3.5	300	302	45	0.58	0.720
280	3.5	50	163	67	0.21	0.826
	3.5	100	150	63	0.22	0.828
	1.8	100	80	26	0.27	0.780
	6.0	100	237	58	0.36	0.981
	3.5	200	166	67	0.24	0.825
	3.5	300	181	65	0.28	0.831
450	3.5	50	73	41	0.14	0.974
	3.5	100	85	45	0.13	0.795
	1.8	100	33	10	0.30	0.962
	6.0	100	151	46	0.28	0.968

***Table 4.1**: Initial and steady-state permeate flux rates observed during the microfiltration of yeast whole cells. Experiments have been conducted on ceramic membranes of nominal pore size equivalent to 0.2 μm for a range of membrane operating conditions. The experimentally determined fouling index (b, equation 2.1, section 2.2) and the correlation coefficient (R^2) are also shown.*

Conc ($g\ L^{-1}$)	Velocity ($m\ s^{-1}$)	ΔP_{tm} (kPa)	J_1 ($L\ m^{-2}\ h^{-1}$)	J_{ss} ($L\ m^{-2}\ h^{-1}$)	b	R^2
50	3.5	50	459	35	0.58	0.972
	3.5	100	569	38	0.57	0.965
	1.8	100	260	16	0.58	0.913
	6.0	100		38		
	3.5	200	356	40	0.53	0.981
280	3.5	50	122	17	0.42	0.994
	3.5	100	151	19	0.44	0.989
	1.8	100	113	12	0.51	0.956
	6.0	100	160	20	0.49	0.973
	3.5	200	179	19	0.55	0.833
450	3.5	50	51	11	0.32	0.867
	3.5	100	53	13	0.33	0.838
	1.8	100	59	10	0.50	0.910
	6.0	100	83	13	0.41	0.936
	3.5	200	69	12	0.44	0.756

***Table 4.2**: Initial and steady-state permeate flux rates observed during the microfiltration of yeast whole cells. Experiments have been conducted on ceramic membranes of nominal pore size equivalent to 0.8 μm for a range of membrane operating conditions. The experimentally determined fouling index (b, equation 2.1, section 2.2) and the correlation coefficient (R^2) are also shown.*

Conc ($g\ L^{-1}$)	Velocity ($m\ s^{-1}$)	ΔP_{tm} (kPa)	J_i ($L\ m^{-2}\ h^{-1}$)	J_{ss} ($L\ m^{-2}\ h^{-1}$)	b	R^2
50	3.5	50	520	22	0.66	0.994
	3.5	100	424	21	0.66	0.990
	1.8	100	354	21	0.60	0.926
	6.0	100	655	28	0.71	0.991
	3.5	200	478	35	0.569	0.977
280	3.5	50	122	12	0.51	0.901
	3.5	100	124	15	0.48	0.981
	1.8	100	105	9	0.53	0.891
	6.0	100	154	12	0.57	0.968
	3.5	200	138	12	0.528	0.941
450	3.5	50	62	9	0.45	0.941
	3.5	100	62	9	0.47	0.926
	1.8	100	55	8	0.40	0.970
	6.0	100	60	9	0.37	0.963
	3.5	200	82	9	0.53	0.951

***Table 4.3**: Initial and steady-state permeate flux rates observed during the microfiltration of yeast whole cells. Experiments have been conducted on ceramic membranes of nominal pore size equivalent to 1.4 μm for a range of membrane operating conditions. The experimentally determined fouling index (b, equation 2.1, section 2.2) and the correlation coefficient (R^2) are also shown.*

4.5.2 Response factors

In the design, there are 81 possible combinations of factor settings, and 80 possible effects and interactions. 44 combinations were selected to estimate the main effects and interactions of the key variables on the performance of the physical system. The response for each

experiment was the steady-state flux rate (J_{ss}). Table 4.4 lists all experiments conducted with associated response factors. Factor A represents the membrane pore size, factor B represents the cell concentration, factor C represents the recirculation rate and factor D represents the transmembrane pressure. Three factor settings were used where -1 represents a 'low' setting, 0 represents an 'intermediate' setting and +1 represents a 'high' setting. Experiment 21 represents the centre point where four trials have been conducted to estimate the experimental error. A summary of the variation in the steady-state flux rate is given below.

Mean	=	17	$L\ m^{-2}\ h^{-1}$
Standard deviation	=	2	
Confidence limits (95%)	=	± 4	
Tolerance limits (95%)	=	± 7	

Experiment	Factor A	Factor B	Factor C	Factor D	Response
1	-1	-1	0	-1	61
2	-1	-1	0	0	61
3	-1	-1	-1	0	20
4	-1	-1	+1	0	66
5	-1	-1	0	+1	56
6	-1	0	0	-1	67
7	-1	0	0	0	63
8	-1	0	-1	0	26
9	-1	0	+1	0	58
10	-1	0	0	+1	67
11	-1	+1	0	-1	41
12	-1	+1	0	0	45
13	-1	+1	-1	0	10
14	-1	+1	+1	0	46

***Table 4.4**: Experimental worksheet for microfiltration runs. Factor A represents the membrane pore size, factor B represents the cell concentration, factor C represents the recirculation rate, and factor D represents the transmembrane pressure. Three factor settings are used where -1 represents a 'low' setting, 0 represents an 'intermediate' setting and +1 represents a 'high' setting.*

Experiment	Factor A	Factor B	Factor C	Factor D	Response
15	0	-1	0	-1	35
16	0	-1	0	0	38
17	0	-1	-1	0	16
18	0	-1	+1	0	38
19	0	-1	0	+1	40
20	0	0	0	-1	17
21(C1)	0	0	0	0	17
22	0	0	-1	0	12
23	0	0	+1	0	20
24	0	0	0	+1	19
25	0	+1	0	-1	11
26	0	+1	0	0	13
27	0	+1	-1	0	10
28	0	+1	+1	0	13
29	0	+1	0	+1	12

***Table 4.4 (contd.)**: Experiment 21 represents the centre point.*

Experiment	Factor A	Factor B	Factor C	Factor D	Response
30	+1	-1	0	-1	22
31	+1	-1	0	0	21
32	+1	-1	-1	0	21
33	+1	-1	+1	0	28
34	+1	-1	0	+1	35
35	+1	0	0	-1	12
36	+1	0	0	0	15
37	+1	0	-1	0	9
38	+1	0	+1	0	12
39	+1	0	0	+1	12
40	+1	+1	0	-1	9
41	+1	+1	0	0	9
42	+1	+1	-1	0	8
43	+1	+1	+1	0	9
44	+1	+1	0	+1	9

Table 4.4 (contd.)

4.5.3 Main effects and interactions

The maximisation of the response was the desired goal and experiments in the top third of table 4.4 gave the best overall results, in particular experiments 1, 2, 4, 6, 7 and 10. Close inspection of the 6 best runs show that the 'low' setting of factor A is the only common feature. Factor B occurs at 'low' and 'intermediate' settings, factor C occurs at 'intermediate' and 'high' settings, and factor D displays all three settings. Estimating the main effects was the difference in average responses between the experiments at the 'high' setting and the 'low' setting for the factor being investigated.

$$E_F = \left(\frac{\sum_i R_{F,i}}{n_i} \right) - \left(\frac{\sum_j R_{F,j}}{n_j} \right) \qquad (4.2)$$

where E_F is the main effect of factor F

$R_{F,i}$ is the response value of factor F at the 'high' setting

$R_{F,j}$ is the response value of factor F at the 'low' setting

n is the number of experiments

To determine the effect of an interaction involving two or more factors, the signs in the relevant column were multiplied together resulting in a new column of either '+1' or '-1'. The effect of the interaction was just the difference in average response between the 'high' settings and the 'low' settings in this new column (Chadwani, 1995). The size of the main effects and interactions for our 4-factor design are best visualised using Pareto charts.

4.5.4 Pareto charts

A Pareto chart is a simple diagrammatic view of the effects and interactions on the response value. It is used to identify the process variable/s which has/have the most significant effect on the response value. Figure 4.6 shows analysis of microfiltration experiments using a Pareto chart.

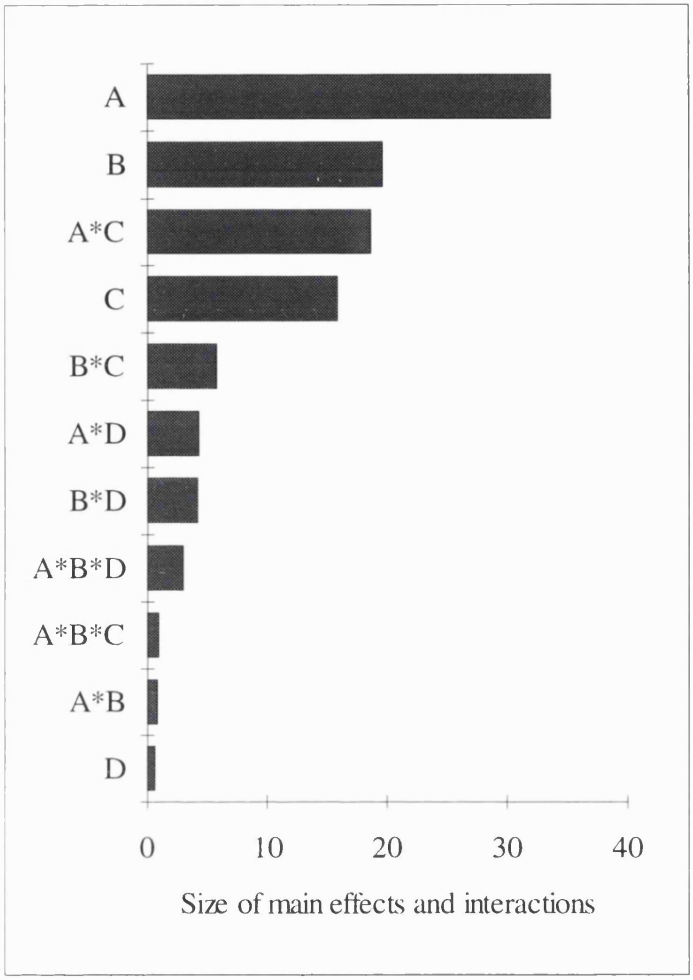

***Figure 4.6**: Pareto chart for microfiltration experiments displaying the most significant effects and interactions on the response value. Factor A represents the membrane pore size, factor B represents the cell concentration, factor C represents the recirculation rate and factor D represents the transmembrane pressure. There are 2^n -1 (n=4) effects and interactions, i.e. 15 effects and interactions. Only 11 effects and interactions are displayed because the interactions between factor C and D have been screened out during the experimental design phase.*

It is clear from the chart that the most significant process variable is factor A, the membrane pore size, which has the biggest effect on the response value. Any process optimisation to improve process performance should begin with this variable. Factors B and C, i.e. the cell concentration and the recirculation rate, and the interaction between the membrane pore size and the recirculation rate are also important with regard to the magnitude of response values. Again,

process optimisation procedures will have to include these factors and interaction. Factor D has little or no significant effect on the response value which implies that the transmembrane pressure is of the least significance with regard to process optimisation. This observation may be indicative of operation above the critical pressure. It is important to note that the interpretation of patterns displayed in the Pareto chart are conditional upon the ranges chosen for the experimental factors. Pareto charts are not useful in determining which effects and interactions are too small and can be ignored. Additional statistical methods are used to determine which effects and interactions rise above the experimental error.

4.5.5 Noise level and normal probability plots

Haaland (1989) proposed the standard deviation of observations for the response factor at the centre point as an estimate of the experimental error or noise for unreplicated designs. This estimate of the noise level can only be used to determine which effects and interactions are significant in comparison with it. A method for separating effects and interactions of factors from the noise level was developed by Daniel (1976), which is an extension of the normality test.

The normality test is a method of determining whether a distribution conforms to a normal distribution. To test if a series of n observations of the variate x are normally distributed, the observations are arranged in order of magnitude as shown below.

$$x_1 \leq x_2 \leq x_3 \leq \ldots \leq x_n \tag{4.3}$$

At each point, the observed cumulative frequency, expressed as a percentage, is calculated.

$$CF(x_i) = 100\left(\frac{i}{n+1}\right) \tag{4.4}$$

where $CF(x_i)$ is the cumulative frequency

x_i is the measured variable

i is the i^{th} observation in the sample (i = 1,2,...,n)

n_i is the number of observations in the sample

If the data are normally distributed, then a graph of the cumulative frequency against the variate x, plotted on normal probability paper should yield a linear curve. The data mean is estimated as the value of the variate x where the cumulative frequency is 50% and the standard deviation is estimated as the difference between the values of the variate at a cumulative frequency of 50% and 84% (Box, 1978). The lines on normal probability plots can be estimated by a method called least median of squared residuals (Rousseeuw *et al.*, 1987). A normal probability plot for the 4-factor design is shown in Figure 4.7.

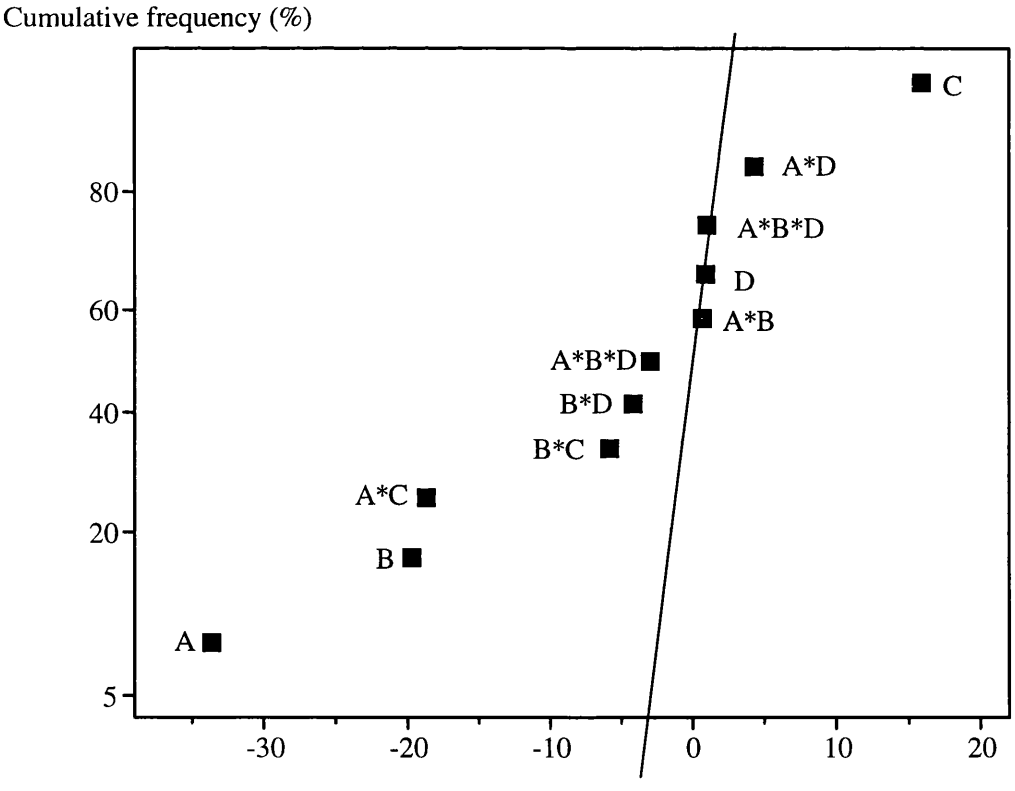

***Figure 4.7**: Normal probability plot for 4 factor experimental design on the microfiltration of whole yeast cells using ceramic membranes. 11 main effects and interactions are displayed, of which 8 effects and interactions are considered to affect microfiltration performance.*

The normal probability plot of the main effects and interactions highlights certain important features. Any effect or interaction which lies on linear curve is simply the result of random variation or noise (Box, 1978). Thus the main effect D, the transmembrane pressure, and interactions A*B and A*B*C had no significant effect on the response value of the physical system. The remaining 8 effects and interactions do not lie on the linear curve and their effects on the physical system cannot be explained by experimental error alone i.e. their effects on the physical system are significant.

The objective of experimental design is to ascertain which factors and interactions have significant effects of the response value, and graphical analysis, such as Pareto charts and normality plots, provide information concerning important effects and interactions. Once the important effects and interactions have been identified, further statistical analysis may be performed.

4.5.6 Detecting curvature

Curvature in the experimental region occurs if there is a non-linear change in the response between the 'high' and the 'low' settings of the experimental factor under investigation. Non-linear behaviour can be detected by adding a middle level for one or more factors. The simplest way to detect curvature is to check if any factors have both 'high' and 'low' settings for the best overall operating regimes. Haaland (1989) recommends the inclusion of centre points for such factors to establish the nature of curvature. The only process variable in the design to display such behaviour is the transmembrane pressure. However, it was noted earlier that the transmembrane pressure had no significant effect on the physical system. Thus, we can ignore the effects of curvature.

4.5.7 Fitting a statistical model

8 significant main effects and interactions have been identified, including main effects A, B, and C, and interactions A*C, B*C, A*D, B*D, and A*B*D. Fitting a statistical model to predict the response value involves constructing a linear model using regression analysis.

$$R = \beta + \beta_1 A + \beta_2 B + \beta_3 C + \beta_4 (A*C) + \beta_5 (B*C) + \beta_6 (A*D) + \beta_7 (B*D) + \beta_8 (A*B*D) + \text{error} \quad (4.5)$$

where R is the residual value

A, B, C, A*C, B*C,... are the significant effects and interactions

β is the intercept term

$\beta_{i\ (i = 1,...,8)}$ are the model coefficients

The coefficients can be obtained directly from the Pareto chart except the intercept term, which is estimated from the experimental data. Thus, the predicted response value is given by equation 4.6.

$$R_{prediction} = 31.7 - 16.84*A - 9.85*B + 7.94*C - 9.33*(A*C) - 2.92*(B*C) + 2.2*(A*D) - 2.1*(B*D) + 1.5*(A*B*D) \quad (4.6)$$

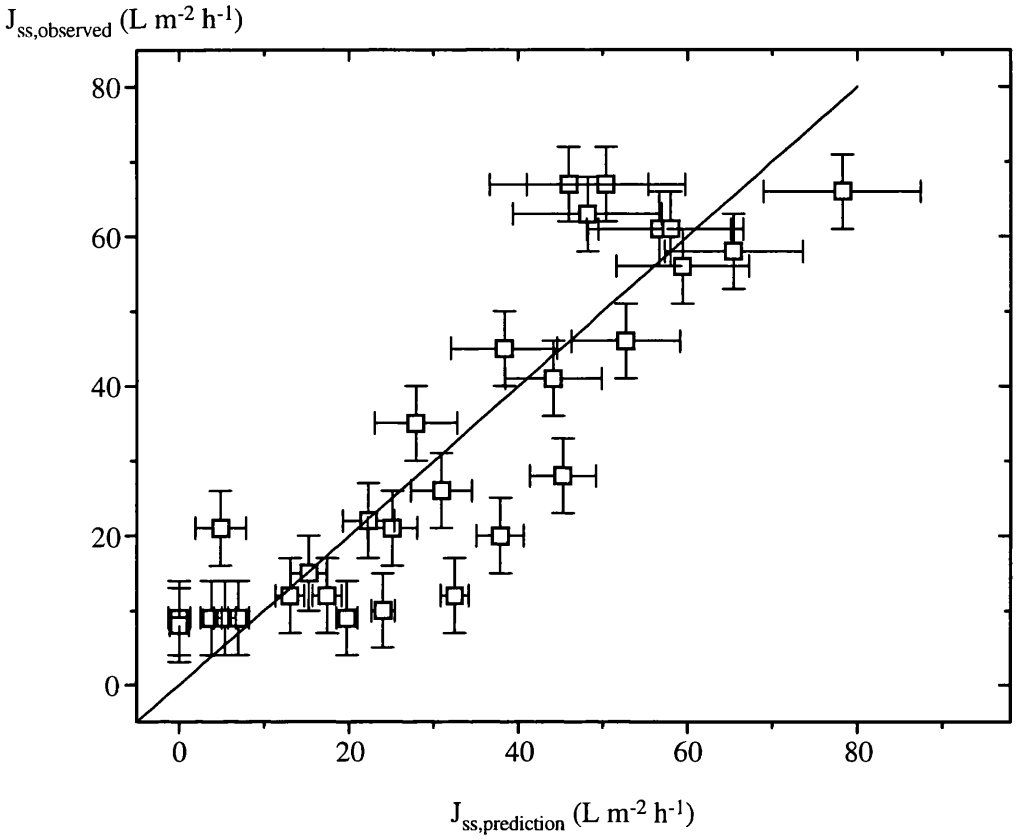

***Figure 4.8**: Observed permeate flux rates of yeast whole cells as a function of the predicted permeate flux rates using ceramic membranes of nominal pore size equivalent to 0.2 μm and 1.4 μm. Experiments have been conducted for a range of yeast whole cell concentrations, 50 g packed weight L^{-1} up to 450 g packed weight L^{-1}, a range of recirculation velocities, 1.8 m s^{-1} up to 6.0 m s^{-1}, and transmembrane pressures ranging from 50 kPa up to 110 kPa. The line graph represents the model predictions, and the error is estimated at ± 14%. The correlation coefficient (R^2) is calculated as 0.76.*

The applicability of such a model to a broader range of membrane pore size, cell concentration and recirculation rate is questionable. As the particle size to the membrane pore size ratio (λ) decreases, the filtration mechanism is altered from a predominant screen filter to a predominant depth filter. Kawakatsu *et al.* (1993) concluded that the relationship between the particle size and the membrane pore size was important for determining the steady-state permeate flux rate. They also concluded that in the filtration of compressible particles such as

Sacchromyces cerevisiae, the steady-state permeate flux rate reached a minimum when $\lambda = 10$. This observation is consistent with our results, within the experimental error, since at $\lambda = 8$, the steady-state permeate flux rate is at a minimum for the experiments conducted. If other biological systems exhibit the same behaviour, it would be interesting to determine whether the significant effects and interactions, for the same range of λ, are identical and also if the ratios of the coefficients in equation 4.6 remain the same.

4.6 Fitting a polarisation model

The steady-state permeate flux rate for a particular set of membrane operating condition was recorded. The condition chosen was that likely to give the highest flux rate so that extrapolation to other data points was by interpolation towards zero. Prediction of permeate flux rates for other membrane operating conditions was achieved by estimating the mass transfer coefficient using information from the single experiment and the Dittus-Boelter correlation for turbulent flow and the assumption of a gel layer of 70% solids by volume. The procedure was repeated for ceramic membranes of different nominal pore size. Figure 4.9 shows the observed permeate flux rates as a function of the predicted flux rates. There is reasonable agreement between the observed values and the predicted values for the membranes of nominal pore size equivalent to 0.8 μm and 1.4 μm. However, for membranes of nominal pore size equivalent to 0.2 μm, there is little agreement. In section 4.6.2, suggestions for model disagreements are given.

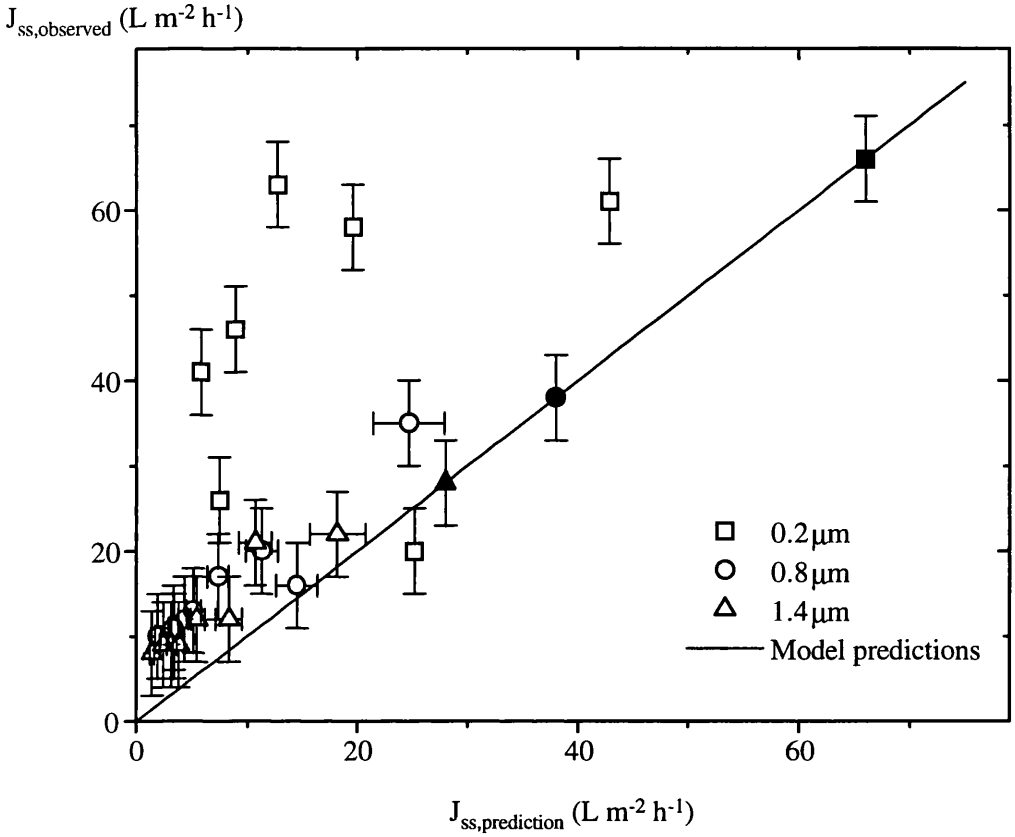

***Figure 4.9**: Observed permeate flux rates of yeast whole cells as a function of the predicted permeate flux rates using ceramic membranes of nominal pore size equivalent to 0.2 μm, 0.8 μ m and 1.4 μm. Experiments have been conducted for a range of yeast whole cell concentrations, 50 g packed weight L^{-1} up to 450 g packed weight L^{-1}, a range of recirculation velocities, 1.8 m s^{-1} up to 6.0 m s^{-1}, and transmembrane pressures ranging from 50 kPa up to 110 kPa. The closed experimental data points have been used to derive expressions of the permeate flux rate as a function of the membrane operating conditions using the concentration polarisation model.*

4.6.1 Effect of membrane pore size on microfiltration performance

For the range of pore sizes examined, there is an increase in the steady-state permeate flux rate as the pore size is reduced. The particle to pore size ratio (λ) increases from a value of ~8 to ~37. Two mechanisms of filtration or a combination of both are possible during filtration namely depth filtration and screen filtration. During depth filtration, which will predominate with

relatively large nominal pore sizes, smaller particles may become entrapped in the pores of the membrane, and removal of such entrapped particles by the feed flow is not possible. This increases the resistance to permeate flow. During screen filtration, which will predominate for relatively small nominal pore sizes, the resistance to permeate flow caused by particles retained in the boundary layer remains on the membrane surface and does not intrude the membrane pores. In reality, a combination of both filtration mechanisms will occur simultaneously because of the pore size distribution of membranes. Thus, we may conclude that the filtration of biological suspensions is better at higher values of λ. However, there must be some optimum λ since the membrane resistance to permeate flow increases with increasing λ.

4.6.2 Effect of cell concentration on microfiltration performance

Cell concentration effects on the performance of microfiltration systems can be monitored by observing the changes in the viscosity of the suspension. The relationship between the cell concentration and the viscosity of the suspension is given by equations 4.1 and 4.2. According to the concentration polarisation model, an increase in the viscosity of the suspension i.e. an increase in the cell concentration, is accompanied by a decrease in the steady-state permeate flux rate. The relationship between the steady-state flux rate and the viscosity of the suspension using the Dittus-Boelter correlation is given below.

$$J_{ss} = A\, \nu^{-0.47} \qquad (4.7)$$

where ν is the kinematic viscosity

A is a constant

Table 4.5 shows the values of the experimentally determined kinematic viscosity exponents for microfiltration experiments conducted. e_i represents the viscosity exponent where i is the recirculation rate.

Nominal pore size (μm)	$\lambda_{estimate}$	$e_{1.8}$ (U = 1.8 m s^{-1})	$e_{3.5}$ (U = 3.5 m s^{-1})	$e_{6.0}$ (U = 6.0 m s^{-1})
0.2	37	-0.34	-0.15	-0.09
0.8	11	-0.43	-0.55	-0.51
1.4	8	-0.58	-0.47	-0.48

***Table 4.5**: Experimentally determined kinematic viscosity exponents for microfiltration experiments conducted on ceramic membranes for a range of operating conditions.*

For ceramic membranes of nominal pore size equivalent to 0.8 μm and 1.4 μm, there is good agreement, within the experimental error, between the experimentally determined exponents and the predicted exponent. There is no significant change in the exponent as recirculation rates are increased. The concentration polarisation model was developed for the filtration of protein solutions using ultrafiltration membranes. The particle to pore size ratio for such systems is very similar to that for the microfiltration of yeast whole cells using the ceramic membranes of nominal pore size equivalent to 0.8 μm and 1.4 μm. This may explain the good agreement between the model predictions and the observed exponents. The same cannot be said for ceramic membranes of nominal pore size equivalent to 0.2 μm. There is little agreement between the predicted exponent and the experimentally determined exponents. Increasing the recirculation rate decreases the kinematic viscosity exponent. Thus, in Figure 4.10, the disagreement between the predicted permeate flux rates and the observed flux rates is directly related to an overestimation of the viscosity exponent. This observation may indicate that as λ increases, concentration effects on the performance of filtration become less significant. Particles resting a on membrane surface with smaller pore sizes are easily dislodged from the membrane surface since the particles are less readily embedded in the pore. In this instance, the membrane is acting as a predominant screen filter, and the effect of increasing the cell concentration is less significant than that observed for membranes acting as predominant depth filters. The recirculation rate has an effect on the viscosity exponent at higher values of λ because particles which are less readily embedded in the

pore are easily swept away into the bulk flow as recirculation rates are increased. This action reduces the boundary layer thickness and thus the concentration of cells in the boundary layer. Hence, the cell concentration effects on permeate flux rates are reduced with increasing recirculation rates.

4.6.3 Effect of recirculation rate on microfiltration performance

Increasing the recirculation rate should increase the permeate flux rate according to the concentration polarisation model. The action of increased recirculation rate is the thinning of the dynamic boundary layer as a result of the increased sweeping action. This increases the back diffusive transport of retained species. At steady-state, the convective transport of retained species to the membrane surface by the suspending liquid equals the back diffusive transport. Thus to maintain equilibrium, the permeate flux rate increases with increasing recirculation rate. There is good agreement between the experimentally determined rate exponents and the predicted exponent. It is likely that the pore density of the membranes will have an effect on the rate exponent, i.e. a higher pore density should favour the steady-state permeate flux rate with increasing recirculation rate.

4.6.4 Effect of transmembrane pressure on microfiltration performance

Many researchers believe that operation at relatively high transmembrane pressures will give rise to high initial fluxes but the pseudo steady-state permeate flux rate will be lower than that for operation at a lower transmembrane pressure. Table 4.6, a subset of Table 4.1, tabulates the initial flux permeate rate (J_1) the steady-state permeate flux rate (J_{ss}) and the fouling index (b, equation 2.1, section 2.2) for 8 microfiltration experiments conducted to test the above hypothesis.

Concentration ($g\ L^{-1}$)	ΔP_{tm} (kPa)	J_i ($L\ m^{-2}\ h^{-1}$)	J_{ss} ($L\ m^{-2}\ h^{-1}$)	b	R^2
50	50	170	61	0.31	0.855
	100	165	61	0.30	0.835
	200	237	56	0.44	0.877
	300	302	45	0.58	0.720
280	50	163	67	0.21	0.826
	100	150	63	0.22	0.828
	200	166	65	0.24	0.825
	300	181	65	0.28	0.831

***Table 4.6**: Initial and steady-state permeate flux rates observed during the microfiltration of yeast whole cells. Experiments have been conducted on ceramic membranes of nominal pore size equivalent to 0.2 μm and a recirculation rate of 3.5 ms^{-1}. The experimentally determined fouling index (b, equation 2.1, section 2.2) and the correlation coefficient (R^2)are also shown.*

Table 4.6 shows that higher transmembrane pressures lead to higher initial permeate flux rates. The prediction that the transmembrane pressure has a negative effect on the steady-state permeate flux rate is also true. The decay rate of the permeate flux rate, denoted by the fouling index, is less significant at the lower cell concentration than at the higher cell concentration.

4.7 Conclusions

The use of fractional factorial experimental design as a methodology for assessing the significant effects and interactions of process variables including the membrane pore size, the cell concentration, the recirculation rate and the transmembrane pressure on the performance of microfiltration has been shown. Analysis of the experimental data using a Pareto chart showed that the membrane pore size had the most significant effect on the performance of the physical

system examined in this thesis. Of the 15 possible main effects and interactions, 8 were found to have a significant effect on the performance of the system. Process optimisation procedures should begin with the most significant effects and interactions.

Using a statistical approach, a linear model for the prediction of the steady-state permeate flux rate was developed. This approach was more accurate than that using a concentration polarisation model characterised by single microfiltration experiments. However, the statistical approach tends to be more specific and requires several experiments to develop. The use of a polarisation model required only one experimental measurement for a given pore size for predictive studies. However, the predictions were unreliable as was shown for ceramic membranes of nominal pore size equivalent to 0.2 μm.

The dominant mechanism of filtration can be changed by altering the membrane pore size. The results have shown that operating the membrane as a predominant screen filter for biological systems favours the steady-state permeate flux rate. Permeate flux rates are also increased with increasing recirculation rate according to the Dittus-Boelter correlation. At lower values of λ, concentration effects on the permeate flux rate were as predicted by the concentration polarisation model. However, an increase in λ resulted in a decrease in the effects of the cell concentration on membrane performance. The transmembrane pressure was shown to have little or no effect on the steady-state permeate flux rate. Higher transmembrane pressures increased the rate of decay of the permeate flux rate.

The following chapter considers the processing of yeast homogenate. A concentration polarisation model is used for predictive purposes and experiments have been conducted to verify the model predictions.

5 PROCESSING OF CELL HOMOGENATE

5.1 Introduction

The recovery of intracellular protein products from cell residuals using crossflow microfiltration is one of the main applications of membrane technology in the bioprocess industries. It is the protein flux rate, the product of the protein transmission and the permeate flux rate, which determines the best membrane operating condition. Chapter 4 highlighted the importance of the particle-to-pore size ratio (λ) and its significance with respect to the predictive capabilities of the concentration polarisation model. For the range of λ studied in this chapter, this type of model should be applicable. This chapter also sets out to explore the hypothesis that single laboratory tests of membrane flux and transmission, accompanied by selected laboratory scale characterisations, may be used to define the operating characteristics of a membrane separation process and allow the evaluation of the effect of a range of operating variables including the recirculation rate and the concentration factor on process performance. Assuming that flux properties do not change significantly, a simple method, based on Ferry's sieving model, has been developed to assess the changes in transmission characteristics with changes in the membrane pore size. The models developed have also been used to estimate the fractionation of protein species during microfiltration. The results have been verified by gel permeation studies. The predicted chromatograms indicate little fractionation of protein species during microfiltration of complex biological feedstocks.

5.2 Experimental methods

Packed baker's yeast supplied by DCL Yeast Ltd. (Menstrie, Clackmannanshire, U.K.), was suspended in phosphate buffer (100 mM KH_2PO_4, pH 6.5) and disrupted in a Manton-Gaulin high pressure homogeniser (Model Lab 60, APV, Crawley, Sussex) according to the method described in section 3.3.5 of this thesis.

Filtration experiments were conducted on the Bio-Design crossflow filtration rig as described in section 3.2.2, using α-alumina ceramic membranes (Fairey Industrial Ceramics Ltd., Staffordshire, U.K.). Tubular membranes, each with a filtration area of ~ 0.005 m^2, were used with nominal pore sizes equivalent to 0.2 μm and 0.8 μm. Water flux measurements, as a

function of the transmembrane pressure, were performed prior to all experimental runs. Details of experimental procedure can be found in section 3.3 of this thesis.

Physical properties of yeast homogenate including particle size measurements and viscosity measurements were performed as described in sections 3.3.2 and 3.3.3 respectively.

5.3 Properties of yeast homogenate

5.3.1 Particle size distribution of yeast homogenate

The particle size distribution of yeast homogenate (Figure 5.1) was obtained using photon correlation spectroscopy. The distribution was bimodal, with peak diameters at ~ 0.25 μm and ~ 1.75 μm. The two peaks may represent the intracellular contents of cells and cellular debris respectively.

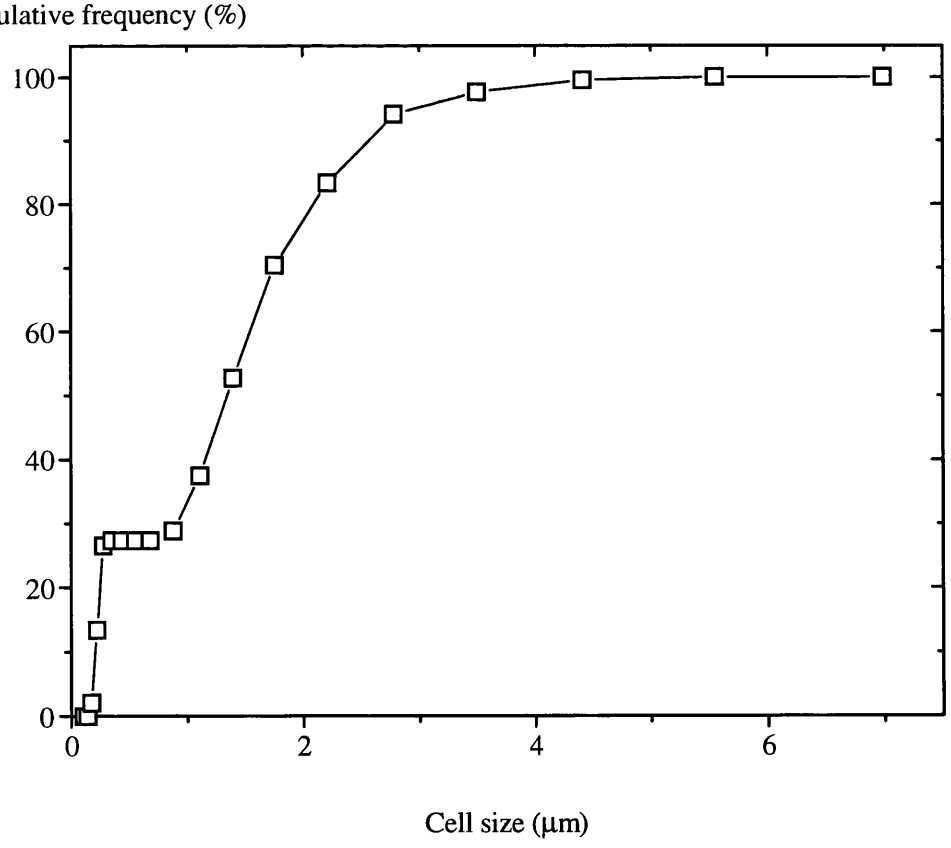

***Figure 5.1**: Particle size distribution of yeast homogenate in phosphate buffer (100 mM KH_2PO_4, pH 6.5) using photon correlation spectroscopy.*

5.3.2 Rheological properties of yeast homogenate

Figure 5.2 shows the shear stress-shear rate relationship for the low concentration yeast homogenate system studied. The sample was prepared by diluting concentrated samples of yeast homogenate, 540 g packed weight L^{-1}, obtained fresh from the high pressure homogeniser with phosphate buffer (100 mM KH_2PO_4, pH 6.5) to the appropriate concentration, i.e. 50 g packed weight L^{-1}.

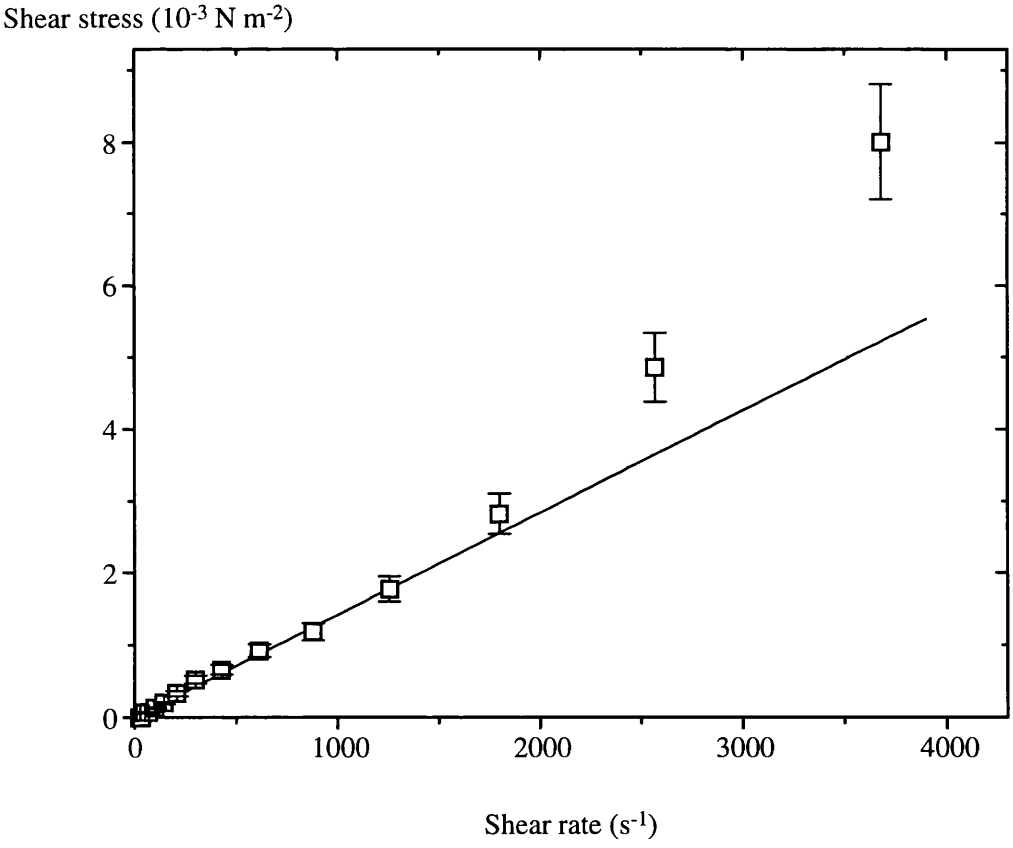

Figure 5.2: Shear stress-shear rate behaviour of yeast homogenate at a cell concentration of 50 g packed weight L^{-1}. The solid line graph represents Newtonian behaviour.

The yeast homogenate suspension exhibits shear thickening behaviour as the shear rate is increased. A power law model is often used to describe shear thickening.

$$\tau = \mu\gamma^p \qquad (5.1)$$

where τ is the shear stress

μ is the suspension viscosity

γ is the shear rate

p is the power law index of the suspension

The power law index (p) is a measure of the degree of non-Newtonian behaviour. The degree of non-Newtonian behaviour displayed by yeast homogenate at the low concentration for the range of shear rate displayed in Figure 5.2 is not very significant, i.e. p = 1.04. However, it is possible that the shift from Newtonian behaviour may be as a result of turbulence in the measuring cylinder.

Figure 5.3 examines the extrapolation of the rheological characteristics to a wider range of concentrations. The change in concentration was effected by diluting freshly prepared yeast homogenate, using phosphate buffer (100 mM KH_2PO_4, pH 6.5), to the appropriate concentrations. This procedure ensured that the solutes to macromolecular component ratio remained constant, a scenario likely to be representative of the retentate composition.

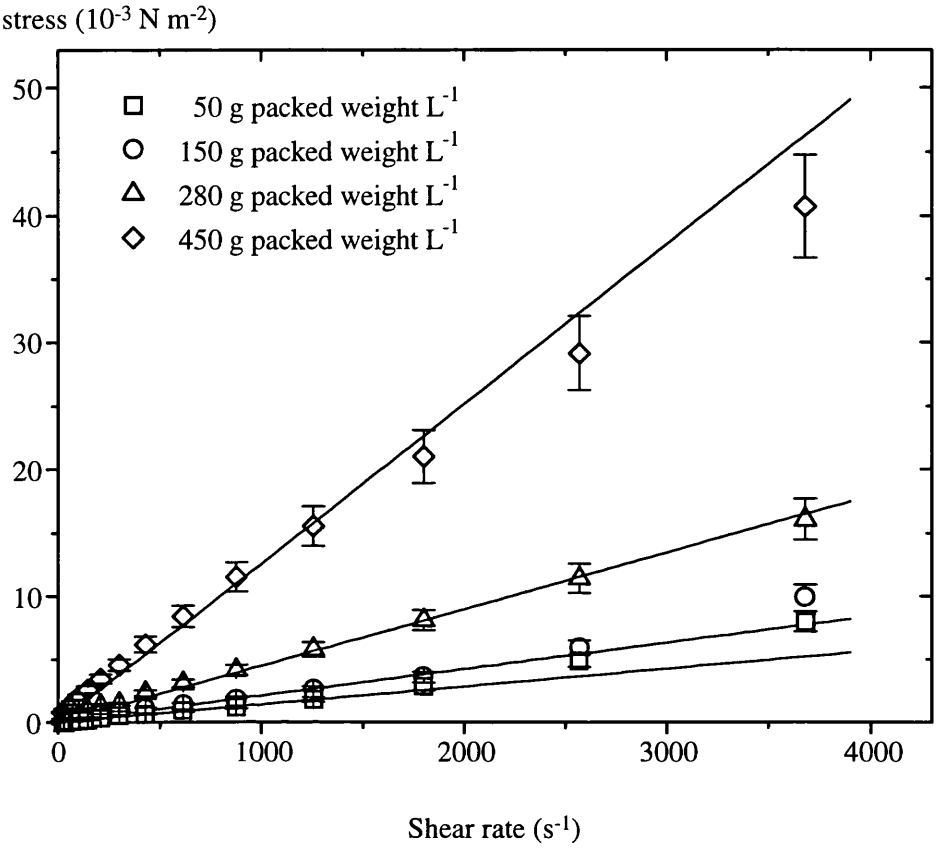

***Figure 5.3**: Shear stress-shear rate behaviour of yeast homogenate for a range of cell concentration. The solid line graphs represent Newtonian behaviour.*

As cell concentrations are increased from 50 g packed weight L^{-1} to 450 g packed weight L^{-1}, the yeast homogenate suspensions move from dilatant suspensions at the low concentrations to pseudoplastic suspensions at the higher concentrations. However, the degree of non-Newtonian behaviour is not significant.

Several models are available in the literature, such as the Vand equation and that given by Reuss *et al.* (1979), which describe the viscosity of yeast whole cells. These models are not applicable to yeast homogenate. However, coupling such models with models describing the viscosity of protein solutions should allow the estimation of the viscosity of yeast homogenate. Pradipasena *et al.* (1977) developed a model for the viscosity of globular protein solutions as a function of the protein concentration using β-lactoglobulin as a model. The apparent viscosity in terms of the wt % concentration of protein is given by equation 5.2.

$$\mu_p = \mu_L (1 + 0.8\ P) \qquad (5.2)$$

where μ_p is the viscosity of protein solution

μ_L is the viscosity of the suspending liquid

P is the wt % concentration of protein

Figure 5.4 shows the viscosity of yeast homogenate as a function of the volume fraction of solids. The viscosity of yeast homogenate was estimated using equation 5.3.

$$\mu_s = \mu_p (1 + a_1 \phi + a_2 \phi^2 + a_3 e^{a_4 \phi}) \qquad (5.3)$$

where μ_s is the viscosity of the suspension

ϕ is the volume fraction of particles

$a_{i\ (i = 1,\ldots,4)}$ are the Reuss *et al.* model coefficients

The agreement between the model predictions and the observed data is good.

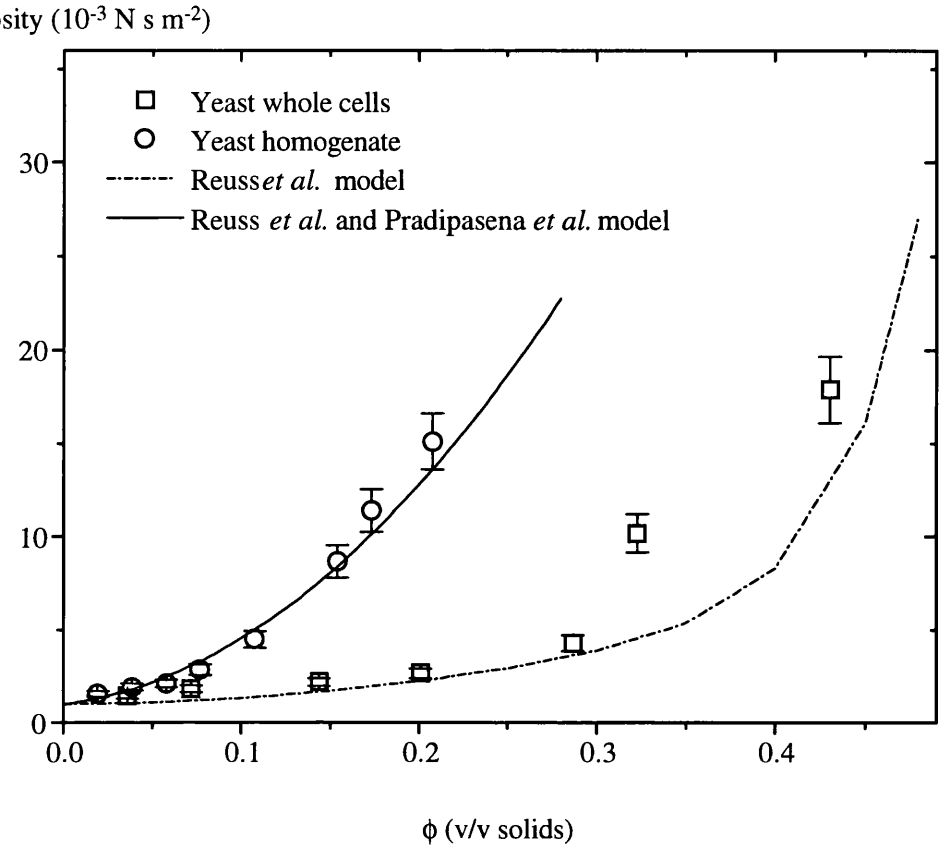

***Figure 5.4**: Viscosity of yeast whole cells and yeast homogenate suspended in phosphate buffer (100 mM KH_2PO_4, pH 6.5). The error in prediction is estimated at ± 10% and the correlation coefficient (R^2) is calculated at 0.98.*

5.4 Results

5.4.1 Flux rates

Table 5.1 shows the values of the permeate flux rate after 1 min (J_1) the quasi steady-state permeate flux rate (J_{ss}) and the fouling index (b, equation 2.1, section 2.2) under various experimental conditions. λ is estimated as ~9 and ~3 for membranes of nominal pore size equivalent to 0.2 μm and 0.8 μm respectively.

Exp	Pore (μm)	Conc ($g\ L^{-1}$)	Vel ($m\ s^{-1}$)	ΔP_{tm} (kPa)	J_1 (LMH)	J_{ss} (LMH)	b	R^2
1	0.2	50	1.8	50	15	11	0.08	0.551
2		50	3.5	50	15	10	0.09	0.565
3		50	7.1	100	65	36	0.14	0.788
4		280	1.8	50	9	5	0.14	0.596
5		280	3.5	50	10	5	0.15	0.537
6		280	7.1	110	30	26	0.02	0.561
7		450	1.8	50	10	5	0.15	0.600
8		450	3.5	50	23	11	0.11	0.595
9		450	7.1	120	30	10	0.25	0.700
10	0.8	50	3.5	50	165	24	0.38	0.987
11		50	7.1	100	376	40	0.45	0.754
12		280	3.5	50	40	12	0.26	0.731
13		280	7.1	110	115	15	0.46	0.989
14		450	7.1	120	110	12	0.73	0.710

***Table 5.1**: Initial and steady-state permeate flux rates observed during the microfiltration of yeast homogenate. Experiments have been conducted on ceramic membranes for a range of membrane operating conditions. The experimentally determined fouling index (b, equation 2.1, section 2.2) and the correlation coefficient (R^2) are also shown. LMH is equivalent to L m^{-2} h^{-1}.*

5.4.1.1 Prediction of permeate flux rates

The flux rate was recorded for a particular set of membrane operating conditions. This was the flux rate after 1 h of operation and was representative of overall operation, i.e. after the initial period of flux decline. The condition chosen was that likely to give a high flux rate so that extrapolation was by interpolation towards zero flux rate.

Using the concentration polarisation model, the permeate flux was predicted, with the assumption of a gel layer of 70% solids by volume, for a range of membrane operating conditions.

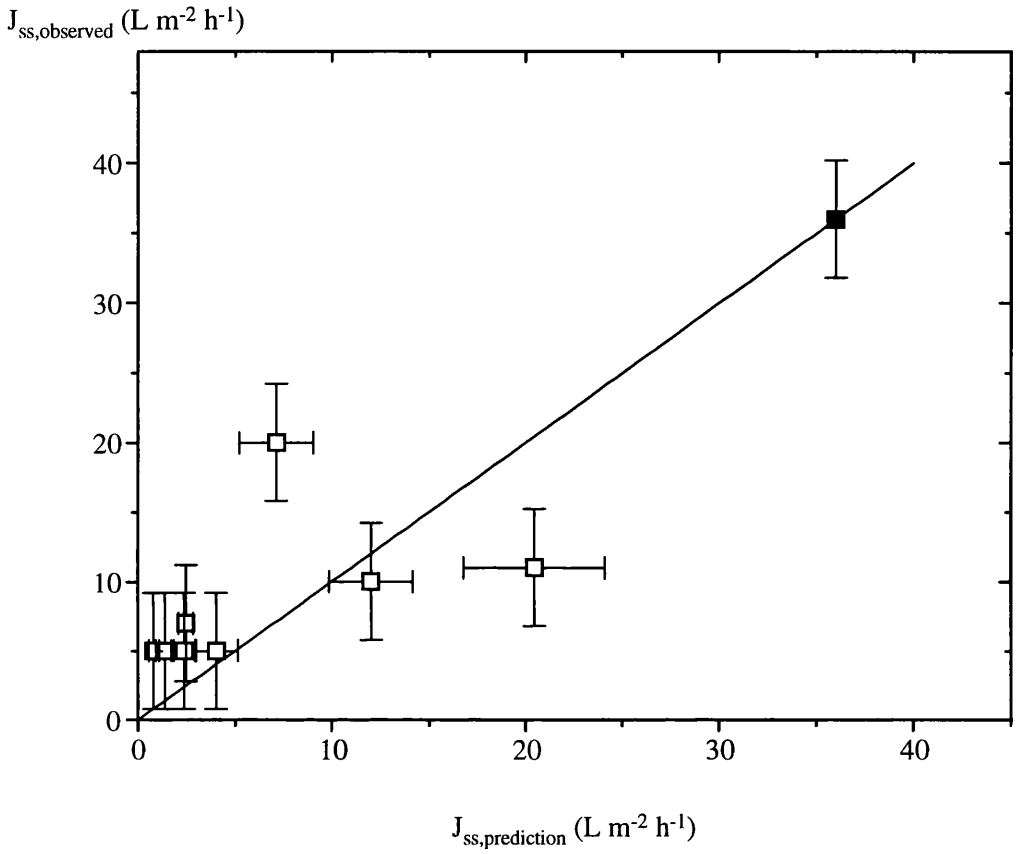

***Figure 5.5**: Observed permeate flux rates of yeast homogenate as a function of the predicted permeate flux rates using ceramic membranes of nominal pore size equivalent to 0.2 μm. J_{ss} represents the quasi steady-state permeate flux rate. Yeast homogenate viscosities are obtained from experimental measurements. Experiments have been conducted for a range of yeast homogenate concentrations, 50 g packed weight L^{-1} up to 450 g packed weight L^{-1}, a range of recirculation rates, 1.8 m s^{-1} up to 7.1 m s^{-1}, and transmembrane pressures ranging from 50 kPa up to 120 kPa. The closed experimental data point, representing conditions of a cell concentration of 50 g packed weight L^{-1}, a recirculation rate of 7.1 m s^{-1} and a transmembrane pressure of 100 kPa, has been used to derive an expression of the permeate flux rate as a function of the membrane operating conditions. The line graph represents the model*

predictions, and the error is estimated at ± 15%. The correlation coefficient (R^2) is calculated as 0.714.

Figures 5.5 shows reasonable agreement between the observed flux rates and the predicted flux rates.

5.4.2 Rejection characteristics

Tables 5.2 shows the values of the transmission of ADH, G-6-PDH, MDH and total protein under various experimental conditions.

Exp	ADH (% trans)	G-6-PDH (% trans)	MDH (% trans)	Protein (% trans)	Solids (% trans)
1	9	10	13	9	-
2	17	19	24	13	-
3	75	78	68	69	-
4	17	22	33	17	-
5	13	16	26	16	-
6	72	75	73	74	-
7	12	13	21	11	-
8	13	14	24	13	-
9	39	41	47	38	-
10	63	-	-	68	3
11	87	-	-	87	3
12	89	-	-	89	2
13	86	-	-	89	3
14	72	-	-	66	2

***Table 5.2**: Transmission of alcohol dehydrogenase, glucose-6-phosphate dehydrogenase, malate dehydrogenase and total protein for microfiltration experiments conducted on ceramic membranes for a range of operating conditions on yeast homogenate.*

5.4.2.1 Prediction of the rejection characteristics of membranes

Prediction of the rejection characteristics of membranes for any given set of membrane operating condition in the polarised region requires a relationship between the mass transfer coefficient and the transmission of protein species. The transmission of ADH, a soluble product of yeast with a molecular weight of 150 kDa, was also recorded for experiment 3 after 1 h of

operation. A sigmoidal model was used to describe the relationship between the mass transfer coefficient and the transmission of the marker protein (ADH).

$$\chi_i = [1-(1-f\,k_i)^2]^2 \qquad (5.4)$$

where χ_i is the sieving coefficient of protein species i

k_i is the mass transfer coefficient of protein species i

f is a constant

Figure 5.6 shows the observed transmission of ADH as a function of the predicted mass transfer coefficient. The model predictions, represented by the line graph, are in reasonable agreement with the observed data.

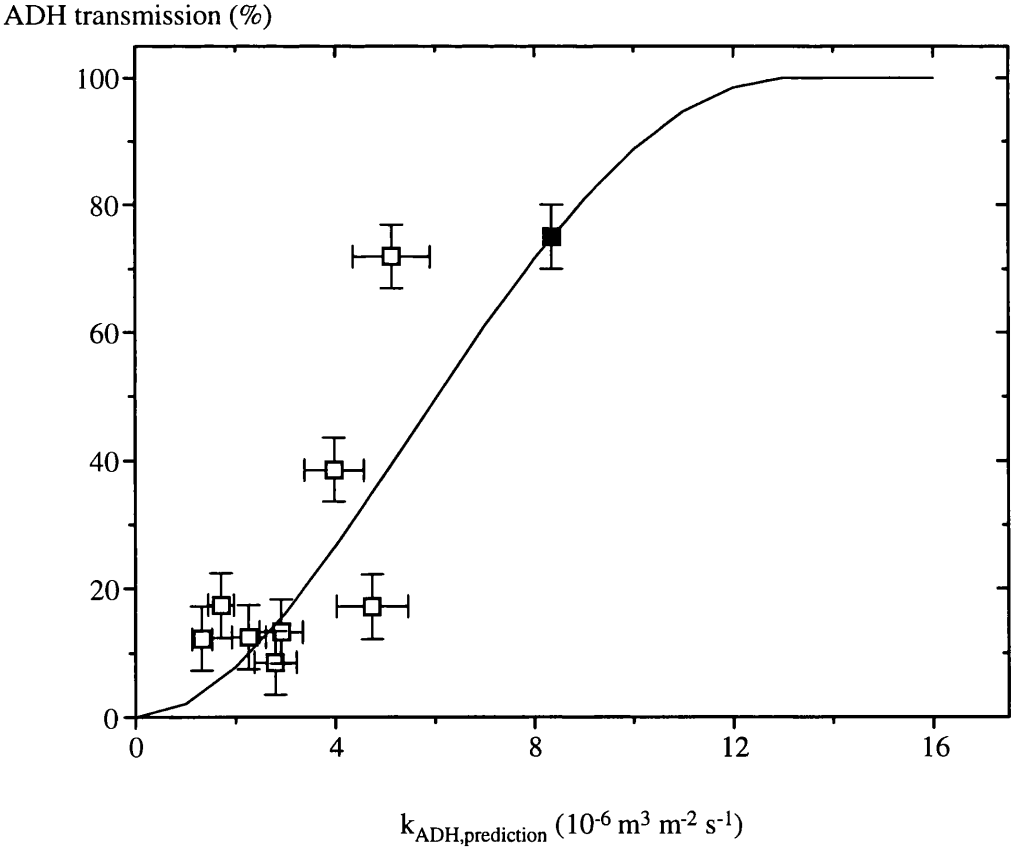

***Figure 5.6**: Observed transmission of alcohol dehydrogenase from yeast homogenate as a function of the predicted mass transfer coefficient. Evaluation of the mass transfer coefficient is*

based on the model prediction of the viscosity of yeast homogenate. The experimental points have been obtained from the same microfiltration experiments shown in Figure 5.5. The line graph represents the model predictions. An estimate of the error is ± 15%, and the correlation coefficient (R^2) is calculated as 0.715.

Figure 5.7 shows the observed ADH transmission as a function of the predicted ADH transmission for the range of membrane operating conditions shown in figure 5.5. The model predictions are in reasonable agreement with the observed transmissions.

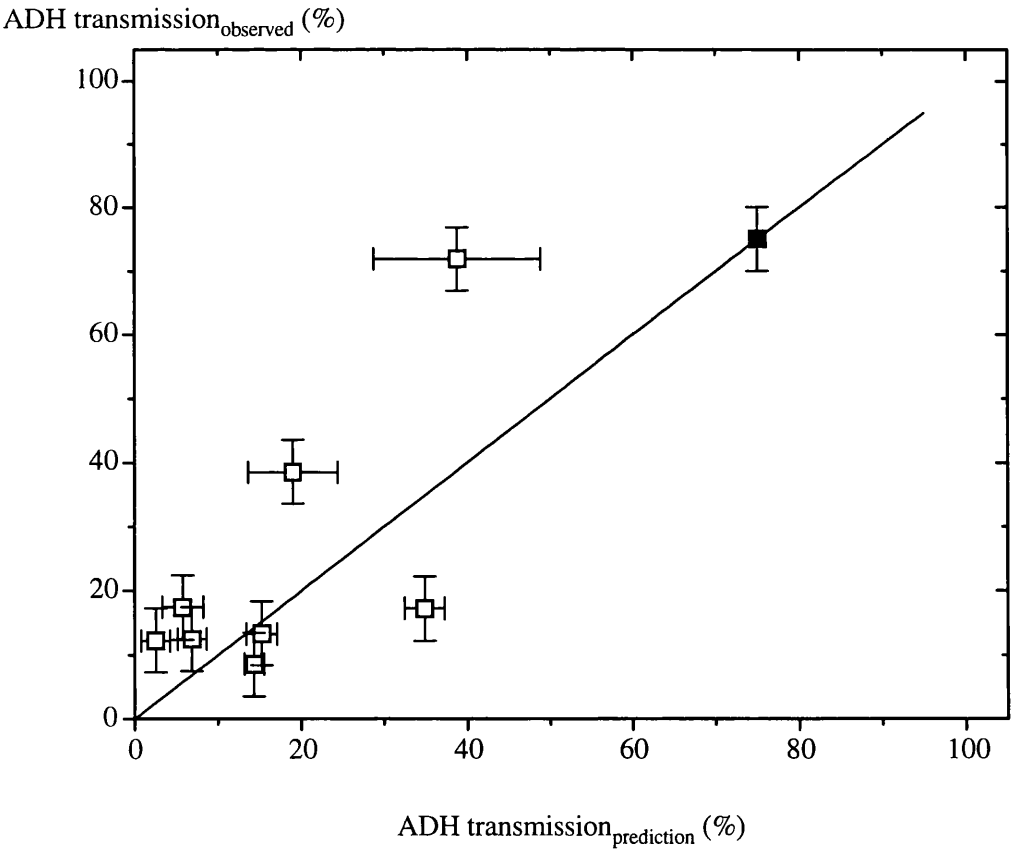

***Figure 5.7**: Observed alcohol dehydrogenase transmission from yeast homogenate as a function of the predicted transmission. The experimental points have been obtained from the same microfiltration experiments shown in Figure 5.5. The model predictions are represented*

by the line graph, with an estimated error of ± 14%. The correlation coefficient (R^2) is estimated as 0.768.

5.4.2.2 Rejection coefficients

In this thesis, the rejection coefficient of protein species i (σ_i) as a function of its molecular weight ($M_{w,i}$) during microfiltration was also described by a sigmoidal model.

$$\sigma_i = \frac{y_{1,i} - y_{0,i}}{1 + \exp\left(-\frac{M_{w,i} - x_0}{dx}\right)} + y_{0,i} \qquad (5.5)$$

where σ_i is the rejection coefficient of species i

$M_{w,i}$ is the molecular weight of species i

$y_{j,i\ (j=0,1)} = f(\sigma_i)$ are model parameters

x_0, dx are constants

The recorded total protein transmission was used to estimate the model constants (x_0, dx) and the model parameters ($y_{j,i}$). Extrapolation of the model predictions requires an estimation of the model parameters. $y_{1,i}$ is a linear function of the total protein transmission passing through the point (1,0) on a ($y_{1,i}$-χ_i) plot. $y_{0,i}$ forces the rejection coefficient-molecular weight relationship to project from the origin and is related to $y_{1,i}$ according to equation 5.6.

$$y_{1,i} = g\, y_{0,i} \qquad (5.6)$$

where g is a constant

Equations 5.4 and 5.5 allow the evaluation of the rejection of protein species as a function of their molecular weight for any given set of membrane operating conditions.

The observed transmission of G-6-PDH, a soluble product of yeast with a molecular weight of 128 kDa, as a function of the predicted transmission of G-6-PDH for a range of

membrane operating conditions is shown in Figure 5.5. Again, the model predictions are in reasonable agreement with the observed transmissions.

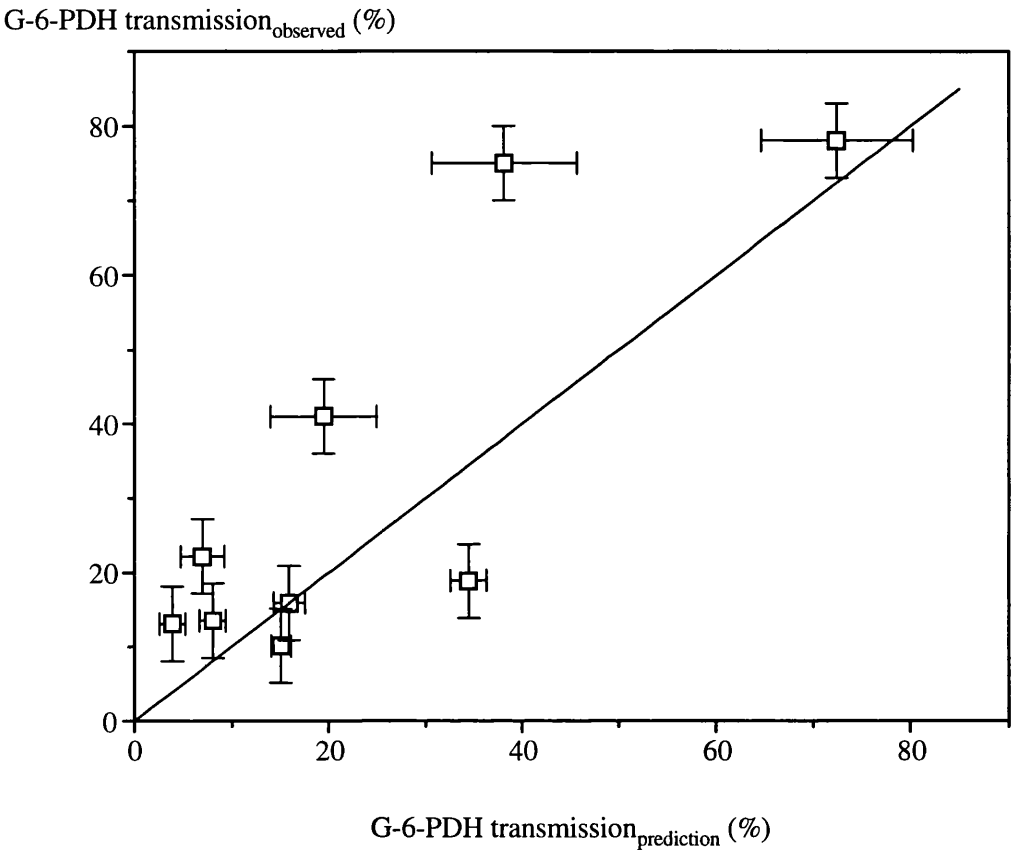

***Figure 5.8**: Observed transmission of glucose-6-phosphate dehydrogenase from yeast homogenate as a function of the predicted transmission. The experimental points have been obtained from the same microfiltration experiments shown in figure 5.5. The model predictions are represented by the line graph, with an estimated error of ± 15%. The correlation coefficient (R^2) is estimated as 0.68.*

Figure 5.9 shows the observed transmission of MDH, a soluble product of yeast with a molecular weight of 70 kDa, as a function of the predicted transmission of MDH for a range of membrane operating conditions. The model predictions are in reasonable agreement with the observed transmission values of MDH.

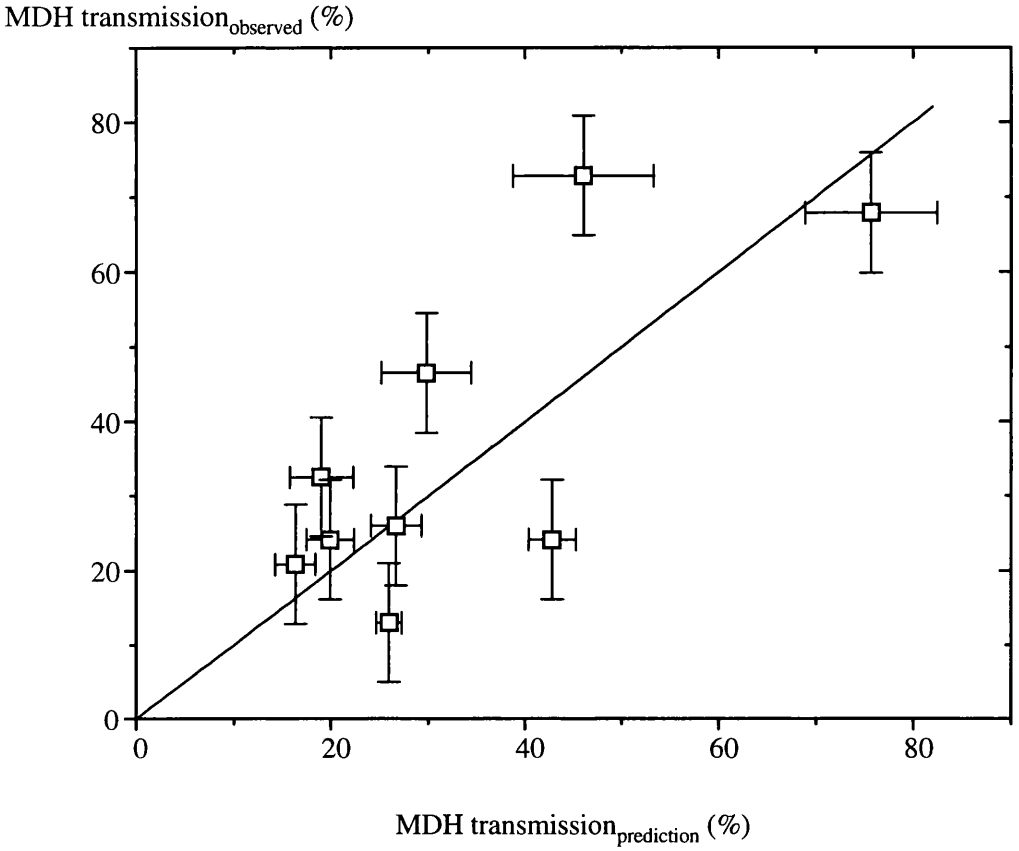

***Figure 5.9**: Observed malate dehydrogenase transmission from yeast homogenate as a function of the predicted transmission. The experimental points have been obtained from the same microfiltration experiments shown in Figure 5.5. The model predictions are represented by the line graph, with an estimated error of ± 15%. The correlation coefficient (R^2) is estimated as 0.73.*

5.4.3 Prediction of the rejection characteristics of 0.8 μm ceramic membranes

A second set of experiments were conducted on 0.8 μm ceramic membranes. A change in the membrane pore size will alter flux and transmission properties of the filtration system. Thus, the mass transfer coefficient of soluble species during microfiltration is also a function of the membrane pore size. Estimation of the mass transfer coefficient for a range of membrane operating conditions in the polarised region can be achieved by conducting a single microfiltration

experiment for a given pore size as shown previously. However, it may be possible to estimate the transmission characteristics of membranes of different pore sizes using Ferry's sieving model. Assuming similar flux rates, the change in transmission of protein species can be modelled by comparing the changes in the sieving characteristics of the different membranes. This change in transmission is given by equation 5.7.

$$\chi_j = \chi_i \left(\frac{2(1-\lambda_j)^2 - (1-\lambda_j)^4}{2(1-\lambda_i)^2 - (1-\lambda_i)^4} \right) \qquad (5.7)$$

The ratio $\lambda_j : \lambda_i$ is the ratio of the effective membrane pore sizes. This was estimated at ~3.4, using the mean pore sizes of the clean membranes. Information from experiment 3, i.e. the transmission of ADH, was used to evaluate λ_i. Figure 5.10 shows the observed ADH transmission as a function of the predicted transmission for 0.8 μm ceramic membranes.

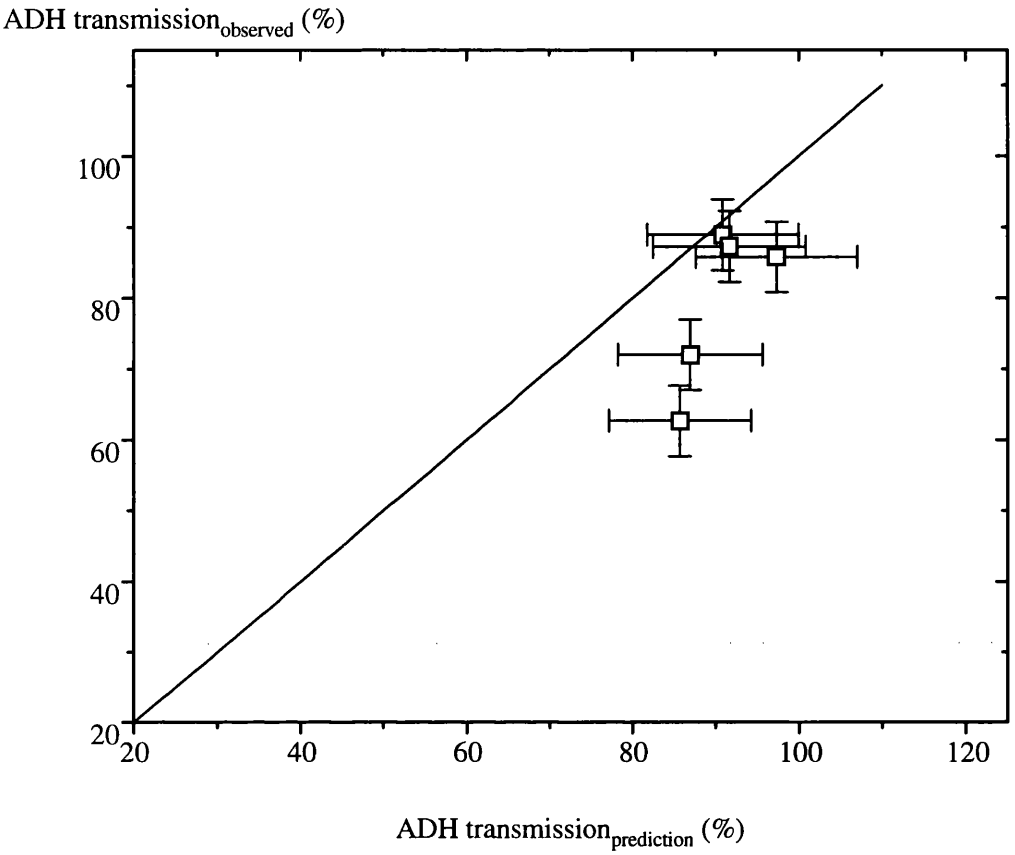

***Figure 5.10**: Observed transmission of alcohol dehydrogenase from yeast homogenate as a function of the predicted transmission using ceramic membranes of nominal pore size equivalent to 0.8 μm. The experiments have been conducted for a range of yeast homogenate concentrations, 50 g packed weight L^{-1} up to 450 g packed weight L^{-1}, a couple of recirculation rates, 1.8 m s^{-1} up to 7.1 m s^{-1}, and a transmembrane pressure of ~100 kPa. The model predictions are represented by the line graph, and the error is estimated at ± 10%. The correlation coefficient (R^2) is calculated as 0.70.*

There is reasonable agreement between the observed alcohol dehydrogenase transmission and the predicted transmission, especially at the higher concentrations.

The ratio λ_j : λ_i should really be based on the effective membrane pore diameters at steady-state. An estimate of the effective pore diameters of the membranes at steady-state is the diameter of the largest particle penetrating the pore. Figures 5.11 and 5.12 shows typical particle

size distributions of the initial and the steady-state permeate samples for the experiments conducted.

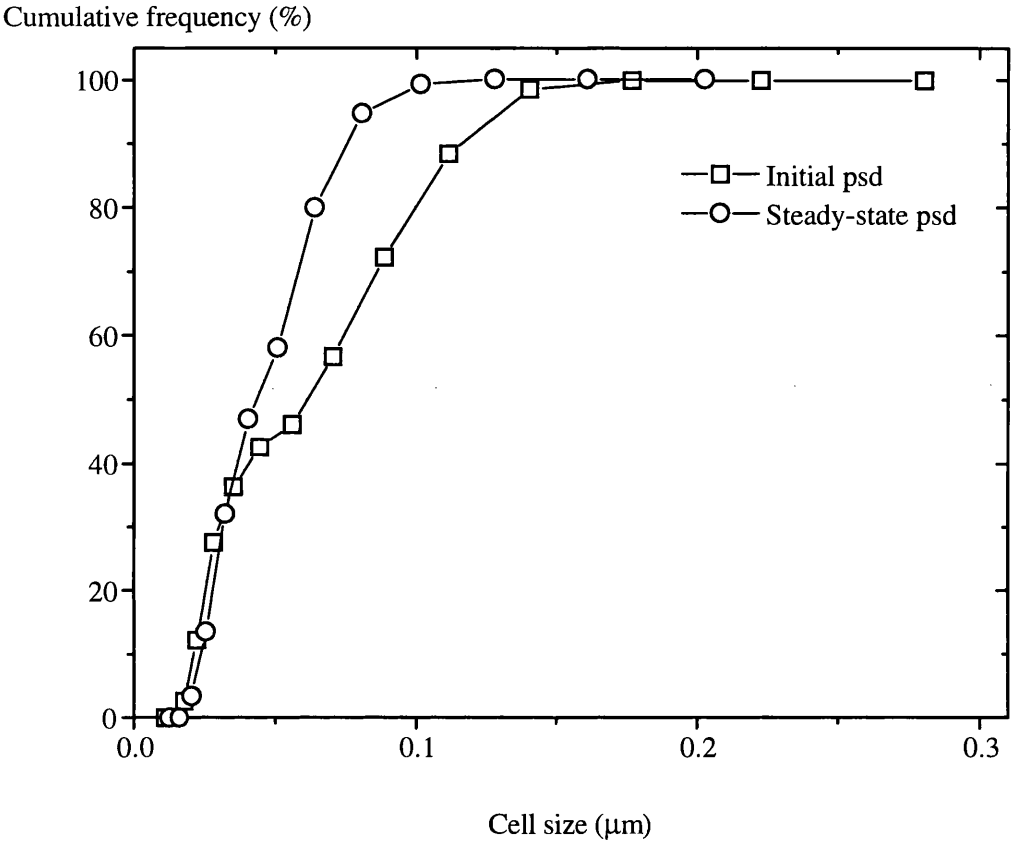

***Figure 5.11**: Particle size distribution of permeate samples, obtained from microfiltration experiments conducted on 0.2 μm ceramic filters, using photon correlation spectroscopy.*

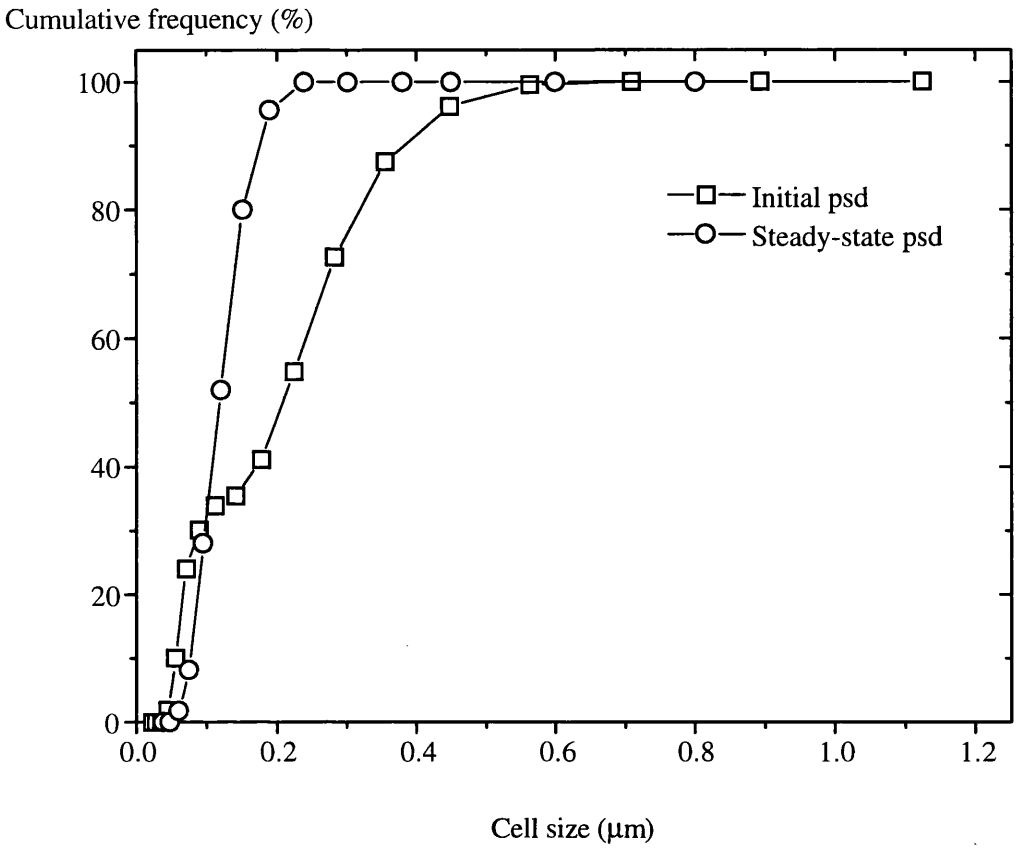

***Figure 5.12**: Particle size distribution of permeate samples, obtained from microfiltration experiments conducted on 0.8 μm ceramic filters, using photon correlation spectroscopy.*

The maximum size of particles penetrating the membranes at steady-state were estimated at ~0.16 μm and ~ 0.35 μm for ceramic membranes of nominal pore size equivalent to 0.2 μm and 0.8 μm respectively. Thus, the experimentally determined ratio, λ_j : λ_i, is ~2.2. Using this value, the predicted transmission of ADH using 0.8 μm membranes was calculated, and Figure 5.13 shows the observed ADH transmission as a function of the predicted transmission.

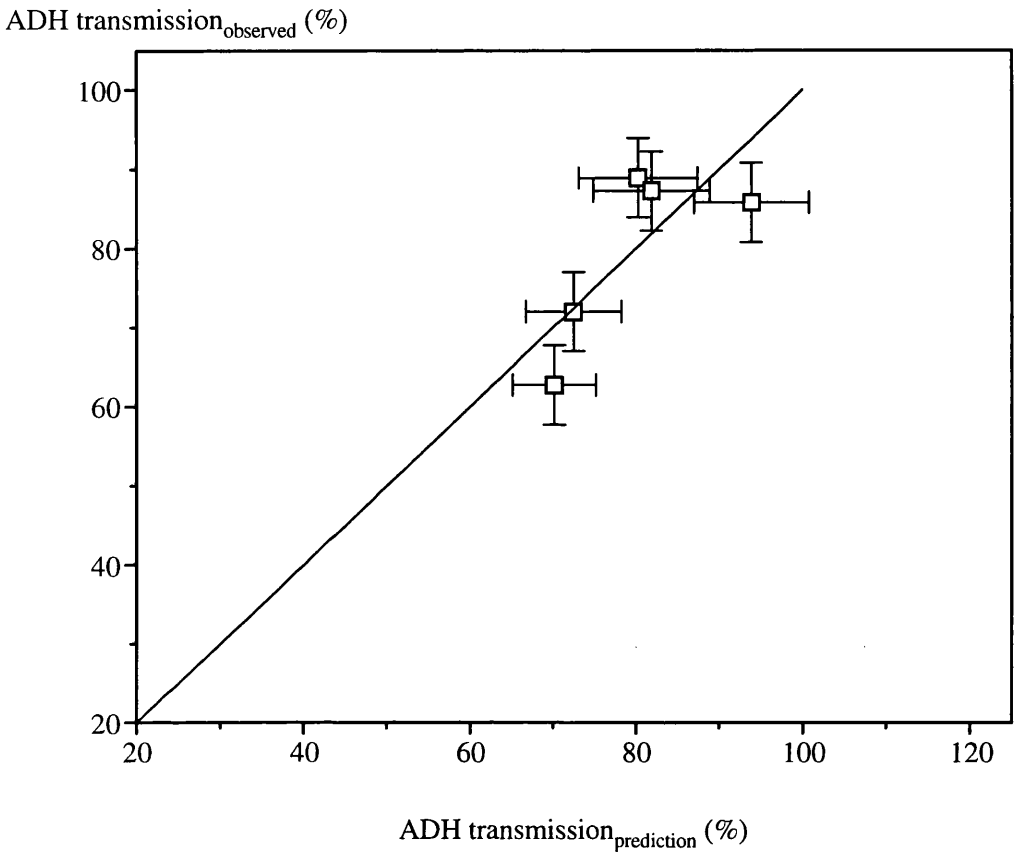

***Figure 5.13**: Observed transmission of alcohol dehydrogenase from yeast homogenate as a function of the predicted transmission using ceramic membranes of nominal pore size equivalent to 0.8 μm. The experiments have been conducted for a range of yeast homogenate concentrations, 50 g packed weight L^{-1} up to 450 g packed weight L^{-1}, a couple of recirculation rates, 1.8 m s^{-1} up to 7.1 m s^{-1}, and a transmembrane pressure of ~100 kPa. The model predictions are represented by the line graph, and the error is estimated at ± 8%. The correlation coefficient (R^2) is calculated as 0.80.*

The agreement between the observed ADH transmissions and the predicted values is very good.

5.4.4 Gel permeation studies

Gel permeation studies were conducted on a Fast Protein Liquid Chromatography system (Amersham-Pharmacia Biotech, Hertfordshire, U.K.). The HR 16/50 column (Amersham-

Pharmacia Biotech, Hertfordshire, U.K.) was packed with Superose 12 prep grade media (Amersham-Pharmacia Biotech, Hertfordshire, U.K.). The column packing was assessed using a sample of acetone in de-ionised water to estimate the number of theoretical plates m^{-1} before eluting with phosphate buffer (100 mM KH_2PO_4, pH 6.5). Samples, 1 mL, were loaded onto the column and eluted using phosphate buffer (100 mM KH_2PO_4, pH 6.5) at a flowrate of 0.1 mL min^{-1}. Fractions, 2 mL, were collected after ~ 4 hr. Each fraction was assayed for total protein content and ADH activity. The assays were performed in duplicate.

5.4.4.1 Column efficiency

The efficiency of chromatographic separation is determined using the concept of the number of theoretical plates m^{-1} (N). N is directly proportional to the degree of resolution of separating species. Figure 5.14 shows the pulse of a sample of acetone in de-ionised water. N is given by equation 5.8.

$$N = 5.54\left(\frac{V_r}{w_n}\right)^2 \frac{1000}{L} \qquad (5.8)$$

where V_r is the retention volume

w_n is the peak width at half peak height

L is the column length

N is calculated at ~ 14,000 plates m^{-1}, which exceeds the value of 10,000 plates m^{-1} needed for satisfactory results.

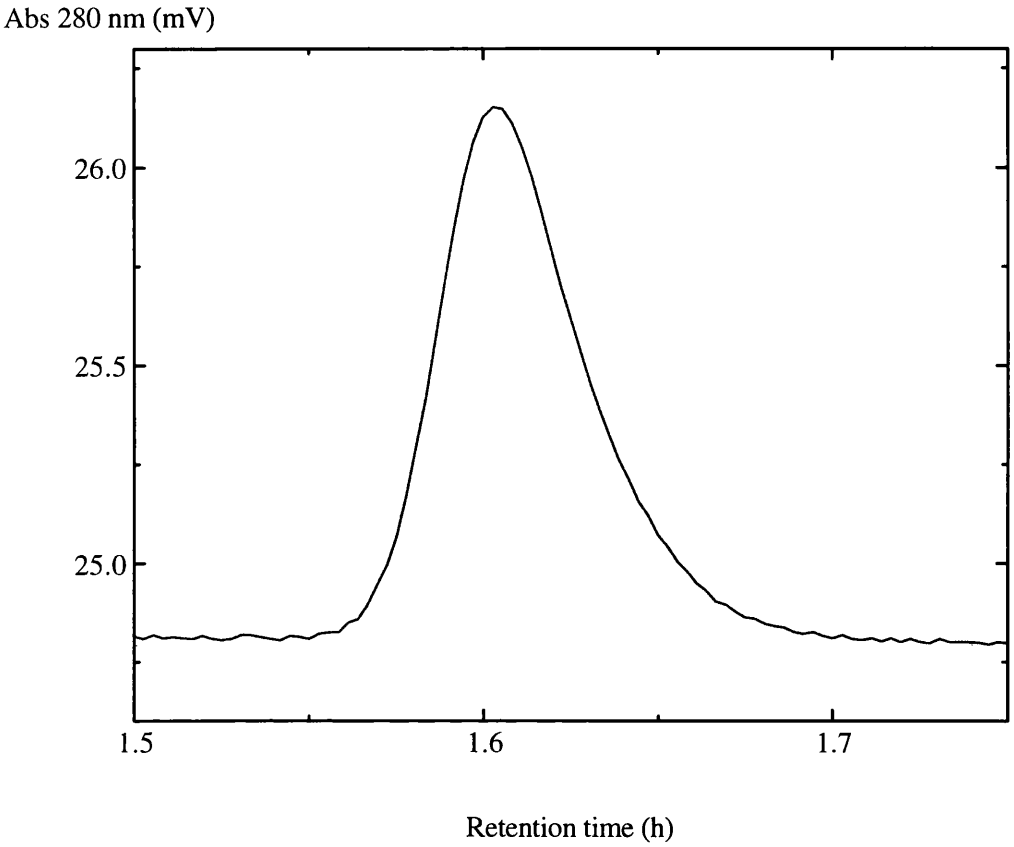

***Figure 5.14**: Acetone pulse (5 mg mL^{-1}) on a Superose 12 prep grade gel permeation column at a flowrate of 1 mL min^{-1}.*

5.4.4.2 Column void volume

A blue dextran pulse (Figure 5.15) was used to estimate the void volume of the column. The void volume was estimated at ~ 39 mL.

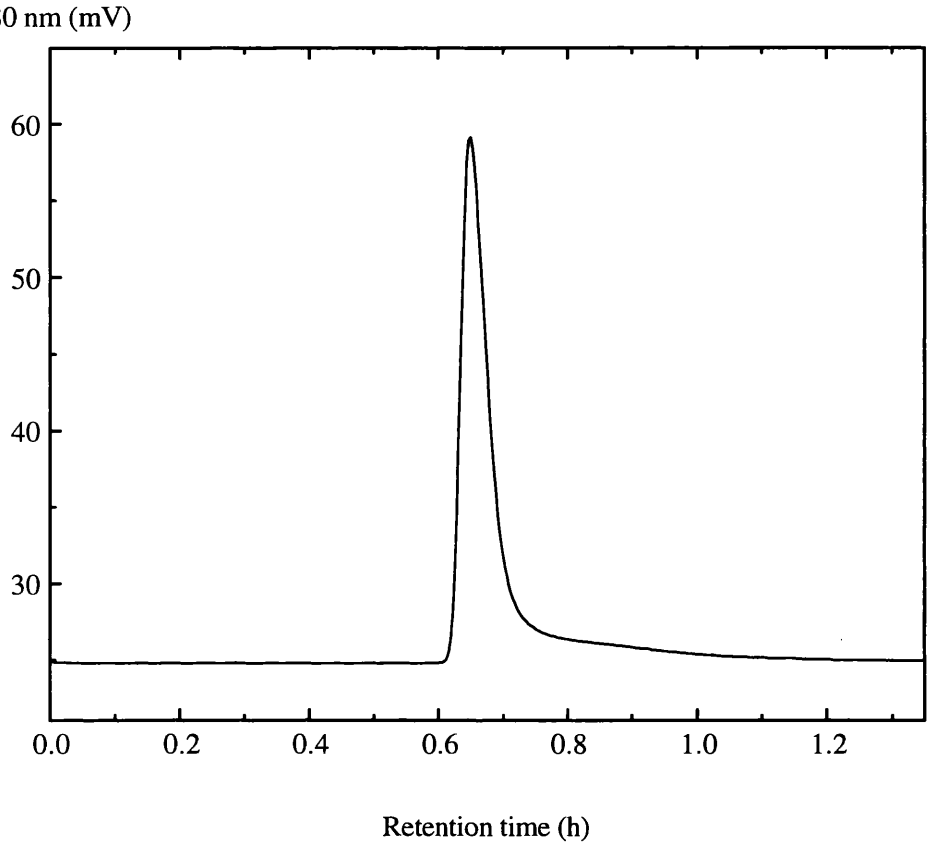

***Figure 5.15**: Blue dextran pulse (1 mg mL^{-1}) on Superose 12 prep grade gel permeation column at a flowrate of 1 mL min^{-1}.*

5.4.4.3 Column resolution

Figure 5.16 shows the resolution of 7 molecular weight markers, each at concentrations of 5 mg mL^{-1} in phosphate buffer (100 mM KH_2PO_4, pH 6.5). The markers include ribonuclease A, 13.7 kDa; chymotrypsinogen, 25 kDa; ovalbumin, 42 kDa; bovine serum albumin, 67 kDa; aldolase, 158 kDa; catalase, 232 kDa; and ferritin, 440 kDa.

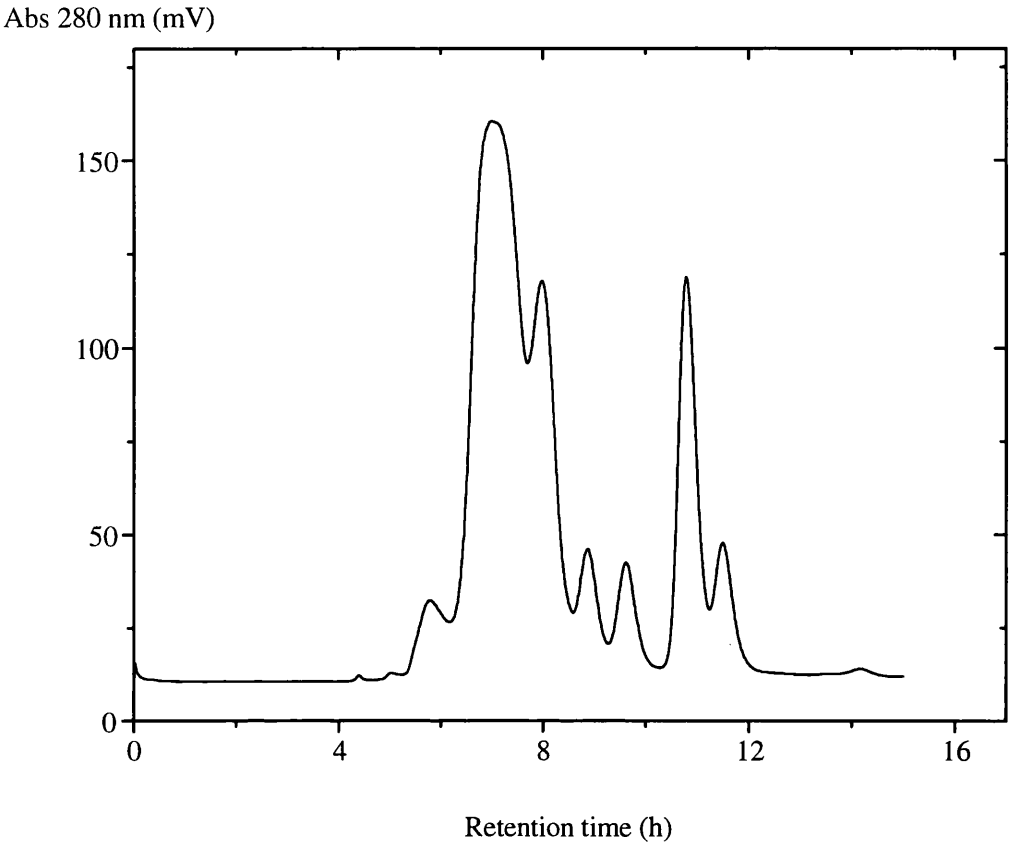

***Figure 5.16**: Molecular weight markers on Superose 12 prep grade gel permeation column at a flowrate of 0.1 mL min^{-1}.*

The peaks from Figure 5.16 have been used to deduce the selectivity curve for Superose 12. Figure 5.17 also shows the selectivity curve for Superose 6 prep grade media (Sigma Chemical Company Ltd., Dorset, U.K.).

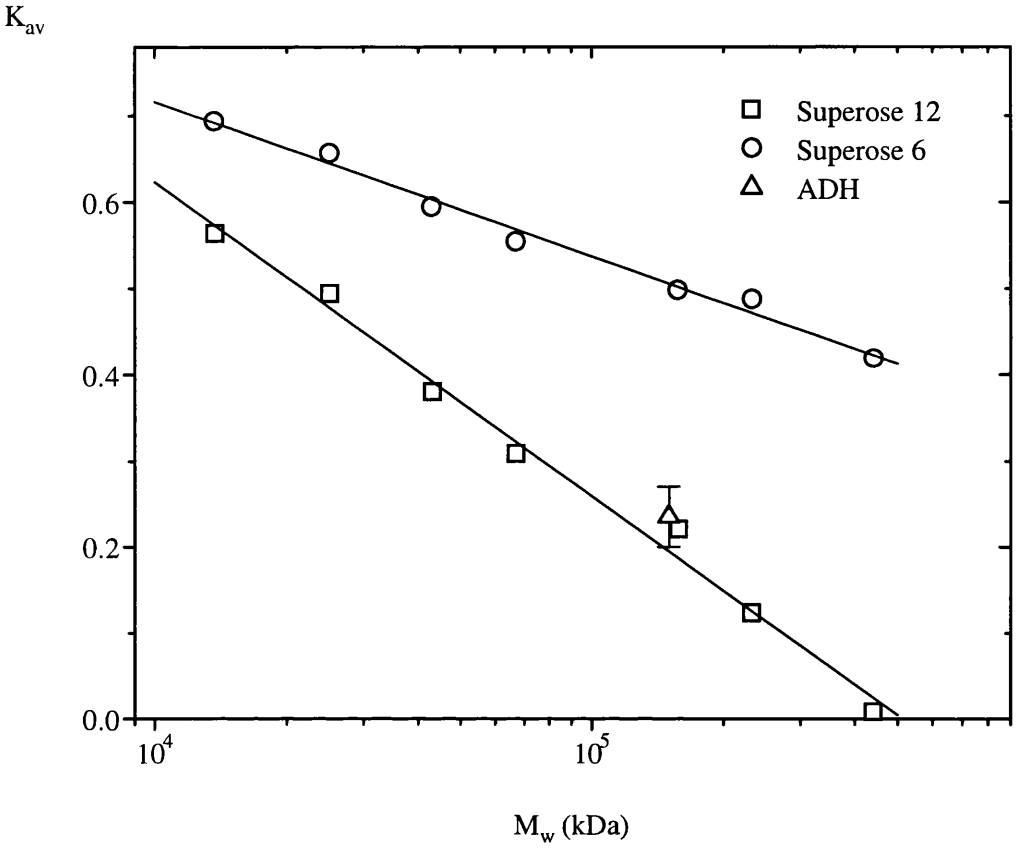

***Figure 5.17**: Selectivity curves for Superose 12 prep grade media and Superose 6 prep grade media.*

Equations 5.9 and 5.10 describe the selectivity curves of Superose 12 prep grade and Superose 6 prep grade respectively.

$$K_{av} = -0.36 \log M_w + 2.08 \quad (5.9)$$

$$K_{av} = -0.18 \log M_w + 1.43 \quad (5.10)$$

where K_{av} is an apparent partition coefficient

M_w is the molecular weight of species

K_{av} can also be evaluated using equation 5.11.

$$K_{av} = \frac{V_e - V_o}{V_t - V_o} \qquad (5.11)$$

where V_e is the elution volume for a given species

V_o is the elution volume of molecules confined to the mobile phase

V_t is the total volume of the packed bed

Superose 12 prep grade was selected for subsequent work as experiments conducted using this media would provide more information on the sieving properties of the membranes.

5.4.4.4 Prediction of gel permeation chromatograms of permeate samples

Figure 5.18 shows the predicted gel permeation chromatogram of the permeate fraction from microfiltration experiments conducted on yeast homogenate at a cell concentration of 50 g packed weight L^{-1}. The plot indicates little fractionation of protein species during microfiltration.

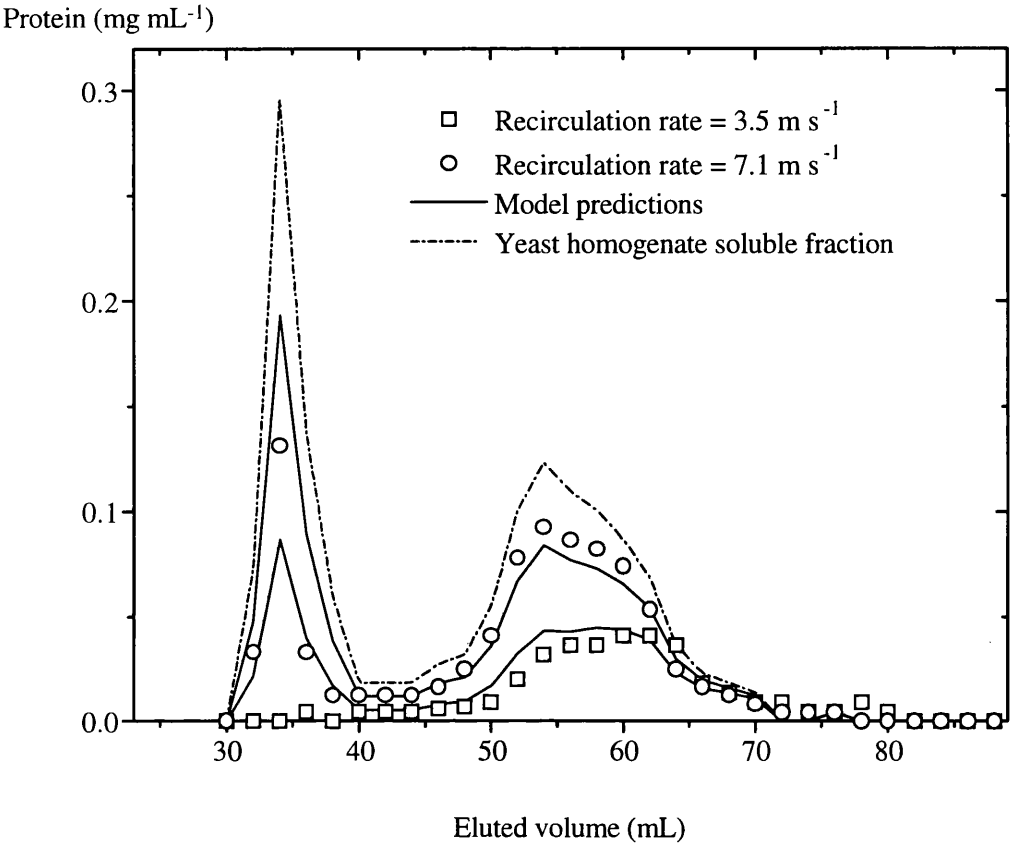

***Figure 5.18**: Prediction of the gel permeation chromatogram of the permeate fraction from microfiltration experiments conducted on a ceramic membrane of nominal pore size equivalent to 0.2 μm at the conditions of a cell concentration of 50 g packed weight L^{-1}.*

Figure 5.19 shows the predicted gel permeation chromatogram of the permeate fraction from microfiltration experiments conducted on yeast homogenate at a cell concentration of 280 g packed weight L^{-1}. Again, the plot indicates little fractionation of protein species.

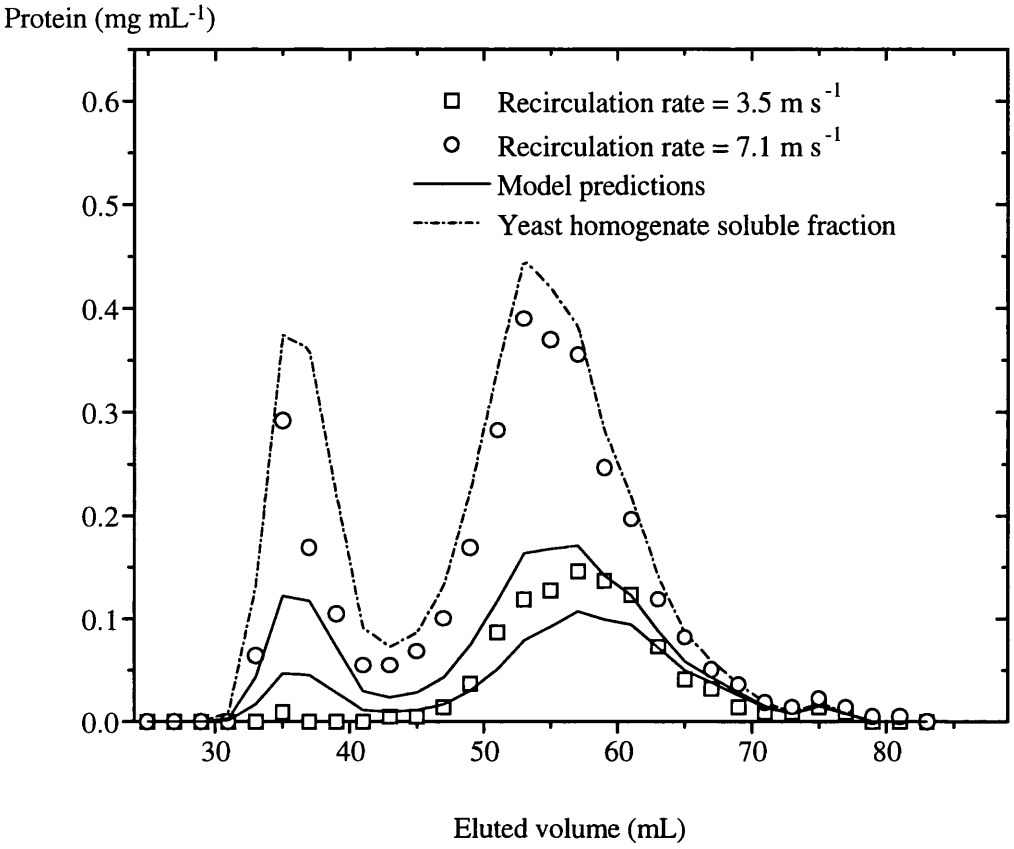

***Figure 5.19**: Prediction of the gel permeation chromatogram of the permeate fraction from microfiltration experiments conducted on a ceramic membrane of nominal pore size equivalent to 0.2 μm at the conditions of a cell concentration of 280 g packed weight L^{-1}.*

Figure 5.20 shows the predicted gel permeation chromatogram of the permeate fraction from microfiltration experiments conducted on yeast homogenate at a cell concentration of 450 g packed weight L^{-1}. Again, the plot indicates little fractionation of protein species .

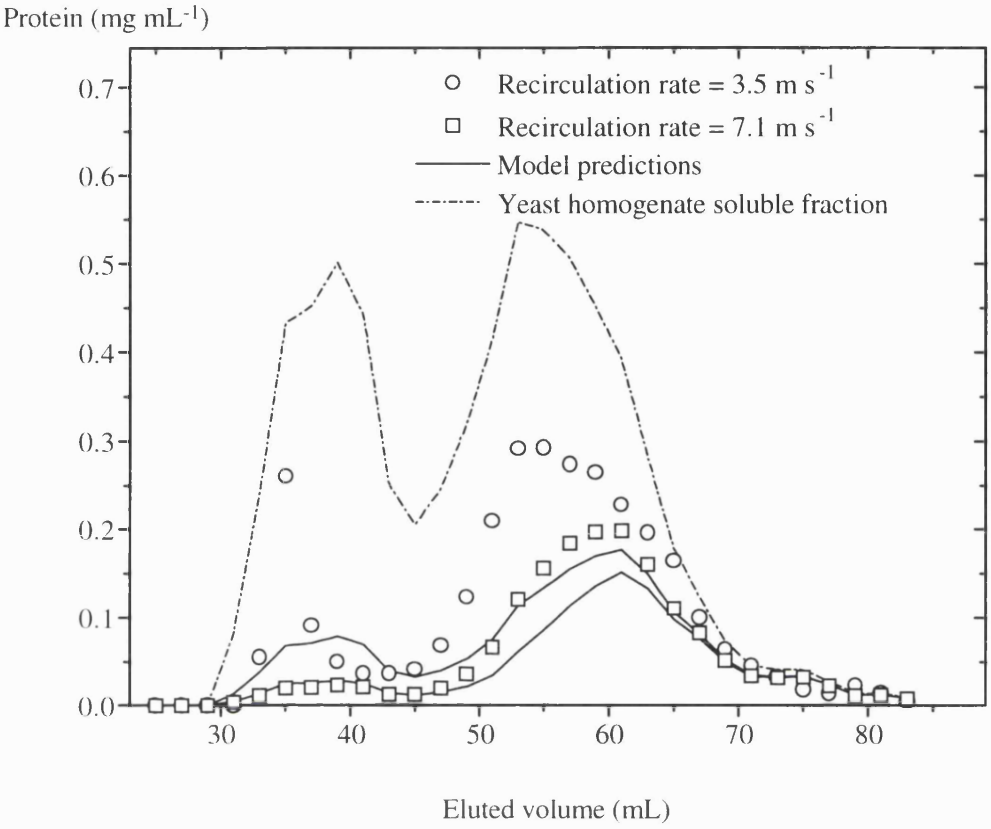

***Figure 5.20**: Prediction of the gel permeation chromatogram of the permeate fraction from microfiltration experiments conducted on a ceramic membrane of nominal pore size equivalent to 0.2 μm at the conditions of a cell concentration of 450 g packed weight L^{-1}.*

A summary of total protein transmission data using gel filtration information is shown in Figure 5.21. The protein transmission is evaluated by comparing the areas under the curves.

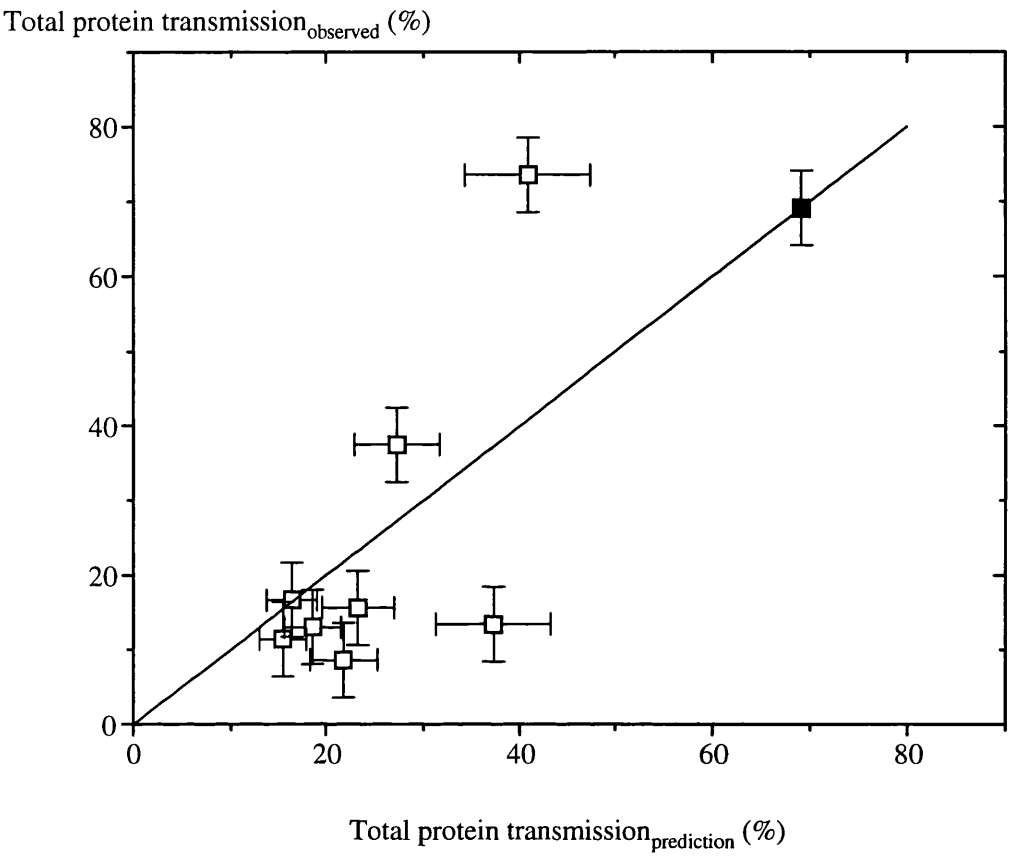

***Figure 5.21**: Observed total protein transmission from yeast homogenate as a function of the predicted transmission. The experimental points have been obtained from the same microfiltration experiments shown in Figure 5.5. The line graph represents the model predictions. An estimate of the error is ± 16%, and the correlation coefficient (R^2) is calculated as 0.67.*

5.5 Conclusions

It has been shown that it is possible to predict the transmission of any soluble protein species from crude biological feedstocks for a wide range of membrane operating conditions in the polarised region by conducting a single microfiltration experiment. The experiment should be conducted at extreme membrane conditions so that extrapolation to other conditions is mainly by interpolation. However, the predictions are based on the accurate determination of the mass transfer coefficient of protein species which is a function of the membrane geometry, the membrane pore size, the membrane operating conditions and the physical properties of the

biological system. The model predictions have been based on the observed transmissions which may exceed 100%. When this occurs, the model predictions, which will equal 100%, may not correlate with the observed transmission data. There may be a maximum possible transmission of protein species with increasing transfer coefficient. Again, the model will be unable to predict such a scenario. Working on the basis of the true transmission of protein species should provide better predictive capabilities when extremes of transmission and mass transfer are reached. The true transmission of protein species requires the estimation of the wall concentration of protein species and Aimar *et al.* (1991) have developed a method for estimating this quantity. A simple method for comparing the rejection characteristics of membranes of different nominal pore sizes using Ferry's sieving model, assuming similar flux characteristics has been also demonstrated. Using the gel permeation chromatogram of the soluble fraction of the retentate, the degree of fractionation of protein species during microfiltration has been demonstrated. The chromatograms also allow the estimation of the total protein transmission data.

Once a mathematical description of a process is available, simulation studies may be conducted to examine the effect of processing variables on process performance. Small-scale studies may be conducted to determine certain solution properties and this information, together with the process model, can be used to predict the performance of larger devices. Chapter 6 uses the information provided in this chapter to develop a systematic approach for the design of membrane separation systems used in the bioprocess industries.

6 SIMULATION OF MEMBRANE SEPARATION PROCESSES

6.1 Introduction

The use of simulation techniques to develop downstream processing routes for biological products is well documented (Petrides *et al.*, 1995). They allow rapid process development with optimal or near optimal process routes, as well as demonstrating process consistency, which may be crucial for regulatory approval. Often, researchers are constrained to using small-scale laboratory processes during initial process development and characterisation but this tends to lead to sub-optimal process routes at production level. As a result, an intermediate process stage often precedes full-scale production. This intermediate level allows the examination of process parameters on the performance of the process flowsheet. Simulation techniques can be applied at this stage to estimate product yields, product purity and the feasibility of potential processing schemes. The characterisation of important process interactions and the optimisation of operating parameters will allow for a reduction in the number of processing trials and hence reduce the overall time required for piloting the bioprocess.

Several platforms are available for simulation-based studies including spreadsheets such as Microsoft Xcel (Microsoft Corp., Seattle, U.S.A.), computer languages such as FORTRAN, BASIC, C and C++, special application packages such as MATLAB (The MathWorks Inc, Massachusetts, U.S.A.), LABVIEW (National Instruments, U.S.A.) and general purpose simulators such as SPEEDUP (AspenTech Ltd., Massachusetts, U.S.A.) and gPROMS (Imperial College, London, U.K.). In this chapter, the application of simulation-based studies for systematic design of membrane separation processes for the bioprocess industries is examined. The process models used in the simulations have been obtained from chapter 5 and literature reviews. The effects of different operating conditions on the performance of the membrane separation system are simulated. The product yield is the key process performance indicator but other variables such as the recovered permeate volume and product purity levels are also considered. The work has been carried out on SPEEDUP (AspenTech Ltd., Massachusetts, U.S.A.). SPEEDUP (AspenTech Ltd., Massachusetts, U.S.A.) is an equation-oriented simulation program designed to model processes as a series of interconnected unit operations. It is designed to solve steady-state process simulation and design problems, simulate dynamic processes,

perform constrained optimisations, perform data reconciliation calculations, perform parameter estimation calculations and sensitivity studies. It may also be interfaced to other packages such as plant control systems for applications such as online optimisation.

6.2 Process selection

Filtration processes are still poorly understood, and the interactions between process streams and membranes leading to low permeate flux rates and poor product transmissions are still quite common. Making the right membrane choices can alleviate some of these common processing problems.

6.2.1 Membrane type

The choice of membrane material will depend on the operating environment. There are membranes which have been specially developed to withstand harsh chemical environments such as pH extremes and organic solvents. Other membranes have been specially formulated to reduce fouling by known foulants such as proteins and anti-foaming agents (Reed, 1996). The membrane material will affect membrane stability and the fouling characteristics.

Crossflow membrane filtration systems are often supplied in four configurations including hollow fibre, spiral wound, flat plate and tubular configurations. Hollow fibre and sipral wound membranes are cheap and compact, but these are not suitable for viscous streams or streams containing suspended solids. Tubular and flat plate modules are bulkier and more expensive but can handle a wide range of feed types including streams containing solids. The choice of membrane configuration will depend on the nature of the process stream.

6.2.2 Membrane pore size

Complete retention of suspended solids is often a requirement when processing streams containing high solids volume fraction. Thus, the maximum membrane pore size is often equivalent to the size of the smallest particle. A large membrane pore size should confer the free passage of macromolecules and achieve high permeate flux rates at low transmembrane pressures. However, for streams containing high levels of suspended solids and macromolecules

such as homogenate streams, the permeate flux rate is independent of membrane permeability. This is so because the membranes are rapidly fouled by proteins and solid material. Consequently, it is probably better to select membranes of smaller pore sizes. Selecting the membrane pore size should be done by conducting single microfiltration experiments at the conditions likely to give the highest permeate flux rate. The membrane chosen should be that which gives the highest product flux rate for the given set of membrane operating conditions.

6.2.3 Literature

Membrane manufacturers will supply information such as water flux rates, rejection data for selected species and chemical compatibility data (Reed, 1996). The rejection data and chemical compatibility data may be helpful and provide some useful indicators on how the membrane may perform. However, water flux measurements are of little use since the operational permeate flux rates will be determined mostly by the properties of the feed and do not often exceed 20% of the water flux rate.

Published literature may provide realistic performance data for a range of applications and membrane types, but these are often conducted on model process streams. The best available performance data will be obtained by conducting unbiased in-house experiments on the process stream of interest.

6.3 Results

The process chosen in this study was the recovery of the intracellular enzyme alcohol dehydrogenase (ADH) from baker's yeast using a 3-stage filtration process including microfiltration and diafiltration. Stage 1 was the first concentration step. Stage 2 involved washing of the concentrated feed-stream with buffer to increase the overall yield of product. Stage 3 represented the final concentration step. To achieve optimal process conditions, the overall rate of product recovery was critical. Other indicators such as the extent of debris removal, the concentration of product in the permeate stream and the volume of product for further purification were also considered.

6.3.1 Input data

6.3.1.1 Process feed and membrane type

The process feed-stream to the membrane was disrupted baker's yeast suspended in phosphate buffer (100 mM KH_2PO_4, pH 6.5). The nature of the feed-stream, i.e. high solids content and high viscosity due to the presence of lipids, nucleic acids, proteins and colloidal material, meant the use of hollow fibre membranes or spiral wound membranes was unsuitable. A tubular membrane system was selected for the study. Although tubular systems have low surface area to volume ratios, they are excellent for handling highly viscous fluids and also suspensions containing solids. Ceramic membranes were also selected for the study because they provide excellent reliability and long lifetime. They are highly resistant to temperature, pressure, organic media, bacterial action and are stable over a wide range of pH. Harsh cleaning regimes can be employed to regenerate the membrane including steam sterilisation and chemical cleaning. They also have the added benefit of tight and consistent pore size distributions.

6.3.1.2 Membrane pore size

Ceramic membranes of nominal pore size equivalent to 0.2 μm, 0.8 μm and 1.4 μm were available for experiments. To select the membrane pore size, single microfiltration experiments were conducted at the membrane conditions likely to the highest permeate flux rates. The solids transmission rate using the membrane of pore size equivalent to 1.4 μm was very high and this membrane was subsequently ignored for selection purposes. Experiments conducted on membranes with pore sizes equivalent to 0.2 μm and 0.8 μm were evaluated for further study. It is the product flux rate, the product of the ADH transmission and the permeate flux rate, which determines the most appropriate membrane pore size. The product flux rate for the condition likely to give the highest permeate flux rate using membranes of nominal pore size equivalent to 0.2 μm and 0.8 μm were estimated at 2.0×10^6 Units (ADH) m^{-2} h^{-1} and 2.6×10^6 Units (ADH) m^{-2} h^{-1} respectively. However, the presence of solids in the permeate stream of the membrane of larger nominal pore size meant it was unsuitable for processing the feed material, according to the selection criterion adopted. This aspect of membrane processing needs to be investigated more thoroughly to establish how the presence of small particles in the process stream interacts with

other unit operations, especially the higher purification stages. However, this will not be discussed in this thesis. Thus, for the purposes of this study, model development was based on data obtained from a single experiment conducted on the membrane of pore size equivalent to 0.2 μm.

6.3.1.3 Model development

The models used in the simulation were the models developed in chapter 5 of this thesis. The concentration polarisation model (section 2.3.1) was used as the basis for steady-state permeate flux rate prediction. The transmission of soluble species in the process feed broth was described by a sigmoidal model (section 5.4.2.1).

6.3.2 Output data

Figure 6.1 illustrates the results of ADH recovery from yeast homogenate using a ceramic membrane of nominal pore size equivalent to 0.2 μm and a membrane area of ~ 0.005 m^2. The graph shows the dependence of the permeate flux and the ADH transmission with time at transmembrane pressures of 20 kPa and 50 kPa.

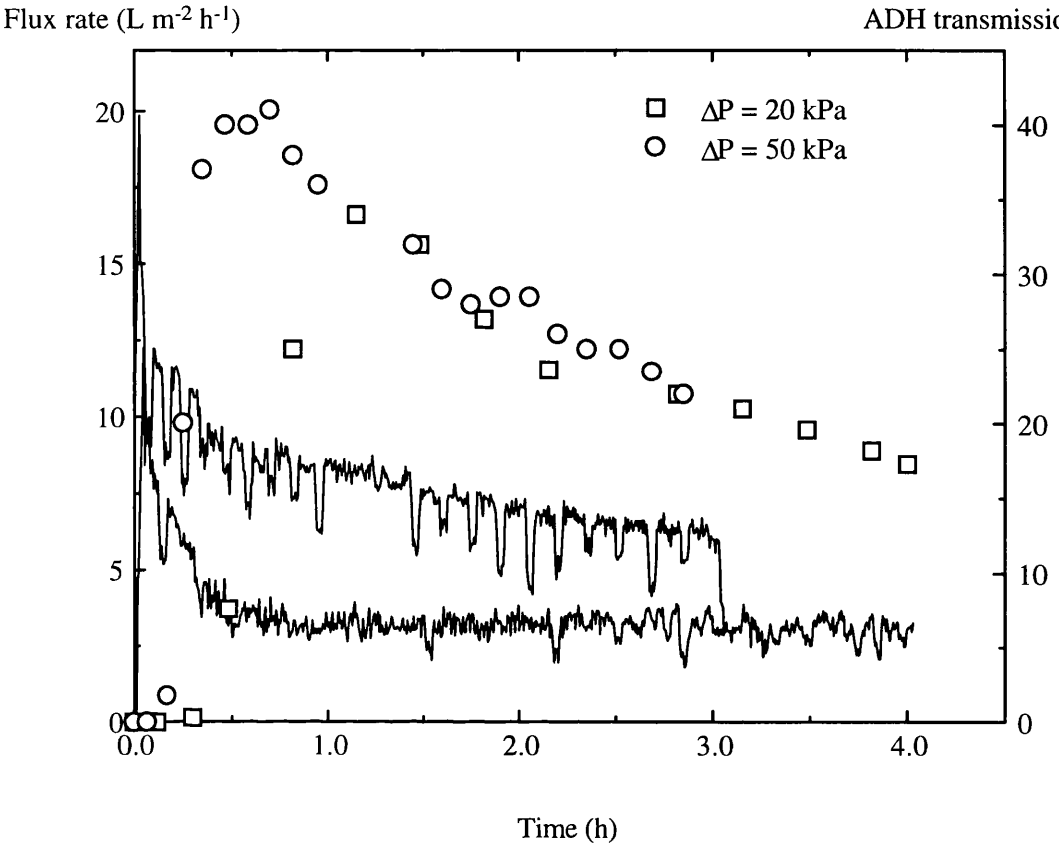

***Figure 6.1**: Permeate flux rate and ADH transmission as a function of the processing time. The experiments have been conducted on yeast homogenate at a cell concentration of 280 g packed weight L^{-1} and a recirculation rate of 3.5 m s^{-1} using microporous membranes of nominal pore size equivalent to 0.2 μm. The solid line graphs represent the permeate flux rates. The lower permeate flux rate occurs at the lower transmembrane pressure.*

The permeate flux rate decreases rapidly during the initial phase of filtration but is stable for several hours following. The line graph ravines represent sample points. The observed permeate flux curve is in agreement with other workers (Kroner *et al.*, 1984, Brown *et al.*, 1987). Kroner *et al.* (1984) and Brown *et al.* (1987) observed sigmoidal flux curves during the concentration of washed and re-suspended *Escherichia coli* cells. They explained their observations qualitatively by separating the curve into three sections. The first phase represented the gel layer build-up phase followed by a constant performance phase over a wide range of cell concentration. The final phase represented the increase in viscosity resulting in a reduction in

membrane performance. The extrapolated final concentration was estimated at ~ 70% wet wt of cells. They concluded that the linear relationship of flux to the logarithm of the cell concentration was not valid for the case of high concentration of microorganisms. The sigmoidal curve for the flux-cell concentration relation is also valid for other microorganisms including *Bacillus* and *Brevibacterium* species (Kroner *et al.*, 1984), baker's yeast (Kroner *et al.*, 1988, Russotti *et al.*, 1995) and *Streptomyces* strains (Russotti *et al.*, 1995). Figure 6.1 also shows the level of ADH transmission decaying with processing time. Other workers (Kroner *et al.*, 1988, Göklen *et al.*, 1994) observed little or no decay of enzyme transmission with processing time. The mechanisms associated with enzyme transmission are little understood and dependent on the specific nature of systems under investigation.

Optimisation of upstream processing often involves maximising the cell mass especially when the product is intracellular (Russotti *et al.*, 1995). This leads to high starting cell concentrations for subsequent downstream processing operations. The effect of the starting cell concentration on the steady-state permeate flux rate and ADH transmission has been studied in chapter 5 and models have been developed to describe such behaviour. Generally, the permeate flux rate decreases with increasing starting cell concentration. Patel *et al.* (1987), Tejayadi *et al.* (1988) and Haarstrick *et al.* (1991) have observed similar results with yeast, bacteria and mycelial cultures respectively. The ADH transmission also decreases with increasing cell concentration.

A base case simulation of the 3-stage filtration process was implemented on SPEEDUP (AspenTech Ltd., Massachusetts, U.S.A.). The initial conditions were set at 100 L of broth at a cell concentration of 50 g packed weight L^{-1} containing 7.5×10^6 Units of ADH. Broth processing was achieved using a tubular membrane with an active area of 0.33 m^2, unless stated otherwise. The results of simulations will now be presented as time series plots. The simulations have been set to run for a maximum processing time of 8 h, reflecting daily operation of a typical bioprocess batch unit, and to a maximum cell concentration of 540 g packed weight L^{-1}, reflecting the confines of rheological studies. The degradation in product transmission with time has been ignored.

6.3.2.1 The effect of the recirculation rate on membrane performance

Figure 6.2 and 6.3 show time series plots of the permeate flux rate and the rejection coefficient of ADH.

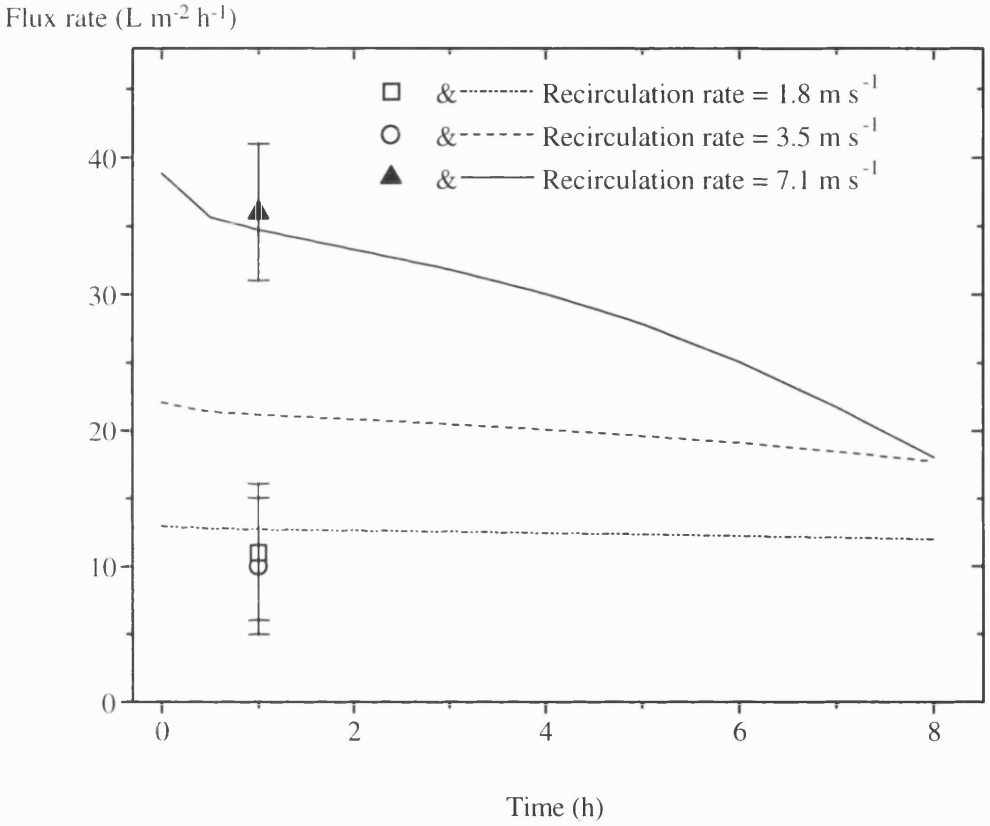

***Figure 6.2**: Simulations of the permeate flux rate as a function of the membrane processing time. The simulations have been conducted assuming an active membrane area of 0.33 m^{-2}. The data points represent the experimental observations. The solid data point has been used to generate the model used for predictive purposes.*

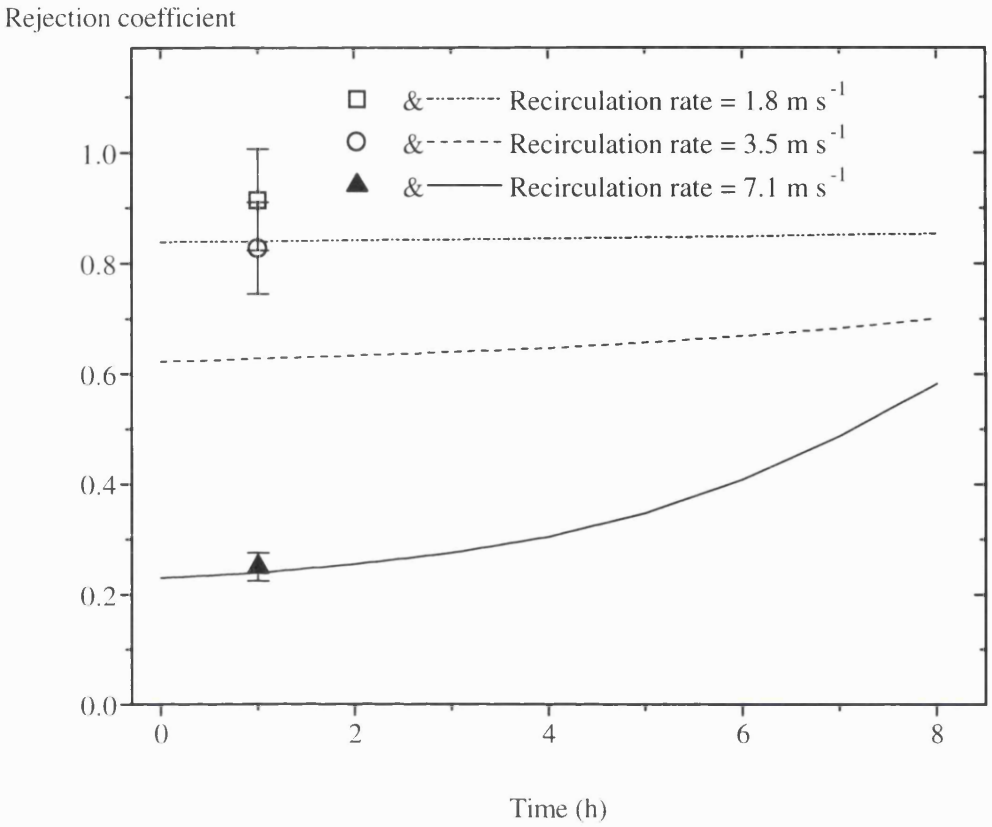

***Figure 6.3**: Simulations of the rejection coefficient of ADH as a function of the membrane processing time. The simulations have been conducted assuming an active membrane area of 0.33 m^{-2}. The data points represent the experimental observations. The solid data point has been used to generate the model used for predictive purposes.*

As demonstrated in previous chapters, higher recirculation rates lead to higher permeate flux rates and consequently higher transmission rates of product. Figure 6.4 shows the product yield as a function of the membrane processing time.

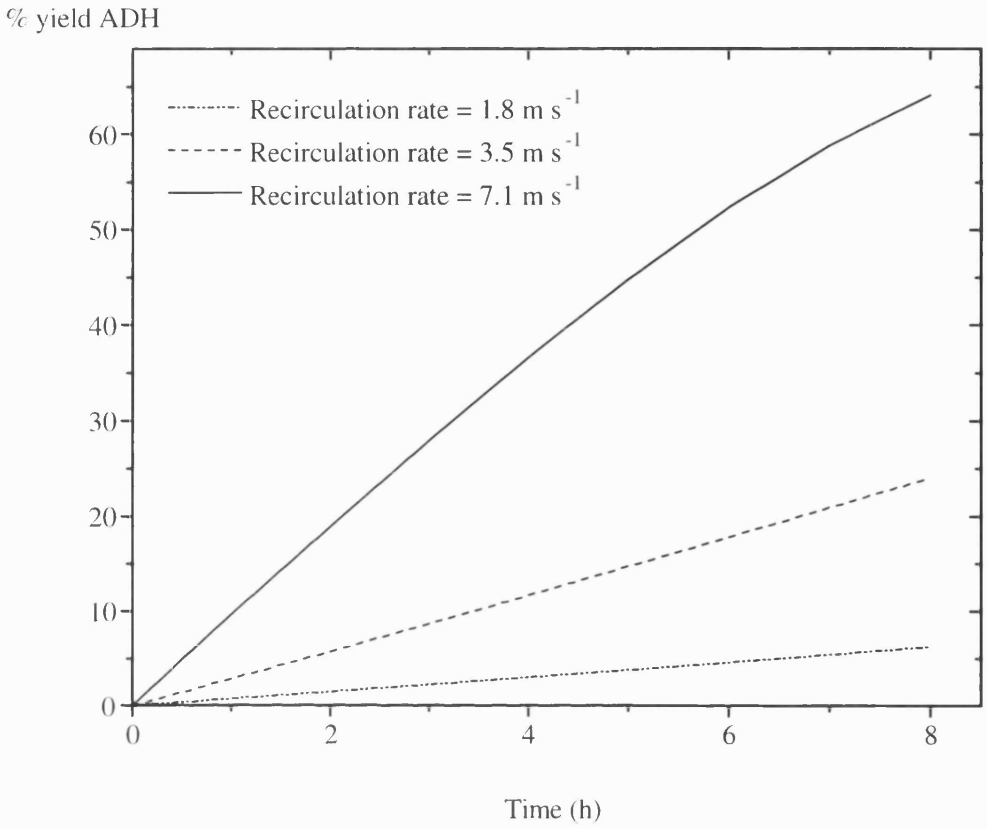

***Figure 6.4**: Simulations of the percentage yield ADH as a function of the membrane processing time. The simulations have been conducted assuming an active membrane area of 0.33 m^{-2}.*

The overall rate of product recovery is increased with increasing recirculation rates. Another important feature of downstream processing, with potential significant economic implications, is the product volume for further purification and the product concentration in the permeate. These are presented in Table 6.1.

U ($m\ s^{-1}$)	V_{perm} (L)	Prod ($U\ mL^{-1}$)
1.8	33	14
3.5	53	34
7.1	77	62

***Table 6.1**: Results of simulations of the product volume and the product concentration in the permeate. The simulations have been conducted assuming an active membrane area of 0.33 m^{-2}. U represents the recirculation rate used during simulation of the membrane process. V_{perm} represents the recovered permeate volume and Prod represents the cumulative product concentration in the permeate measured in enzymatic Units (ADH) mL^{-1} of solution.*

High product concentrations in the permeate and low product volumes favour the economic feasibility of a process. However, attaining such a goal may be at the expense of the overall product yield and a balance needs to be found to maximise the profitability of the process. When the membrane module length is significant, higher recirculation rates will increase the average driving pressure across the module resulting in reduced membrane performance. Such an effect will create an optimum recirculation rate (Datar, 1984, Gabler *et al.*,1985). This effect is illustrated in the next section.

6.3.2.2 The effect of the membrane module length on membrane performance

Increasing the membrane module length will increase the average driving pressure across the module, assuming other operating conditions such as the recirculation rate remain constant. The increase in the transmembrane pressure (ΔP) reduces the efficiency of membrane operation as the steady-state permeate flux rate decreases with ΔP. Figure 6.5 illustrates the effect of the membrane module length on ΔP.

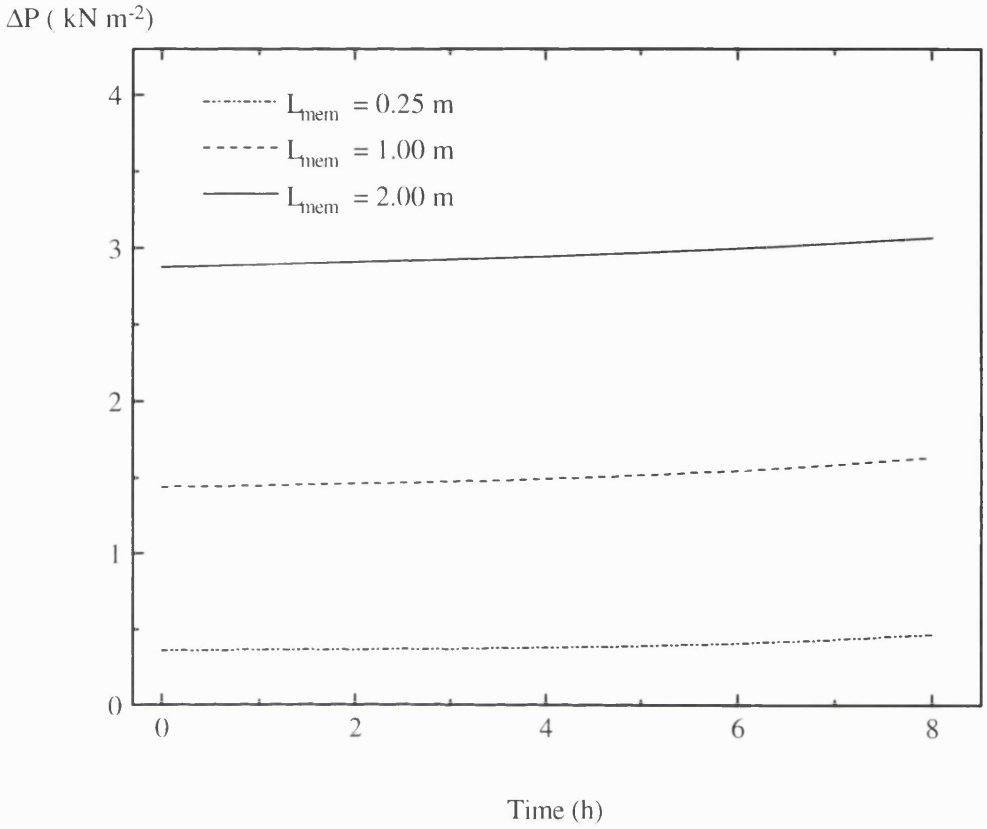

***Figure 6.5**: Simulations of the transmembrane pressure as a function of the membrane processing time.*

The effects of ΔP on the performance of the membrane system are given in Table 6.2. The table demonstrates the benefits of using a shorter module. Product yields are increased as the effect of ΔP on the performance of the membrane system reduces with decreasing module lengths.

L_{mem} (m)	ADH (%)	V_{perm} (L)	Prod (U mL^{-1})	J_{60} (L m^{-2} h^{-1})
0.25	64	77	62	35
1	52	63	63	28
2	40	48	62	22

***Table 6.2**: Results of simulations of the percentage product yield (ADH), the product volume (V_{perm}), the product concentration in the permeate (Prod) and the permeate flux rate after 1 h of processing (J_{60}). The simulations have been conducted at a recirculation rate of 7.1 m s^{-1} and an active membrane area of 0.33 m^2.*

It is interesting to note that the product yield, the product volume and the steady-state permeate flux rate differ significantly when the module length is altered. However, the product concentration in the permeate is little changed. Thus, the results of the simulation suggest that product concentrations in the permeate are predominantly affected by changes in the recirculation rate and not ΔP.

6.3.2.3 The effect of the starting cell concentration on membrane performance

The effect of the initial cell concentration is illustrated in Figure 6.6.

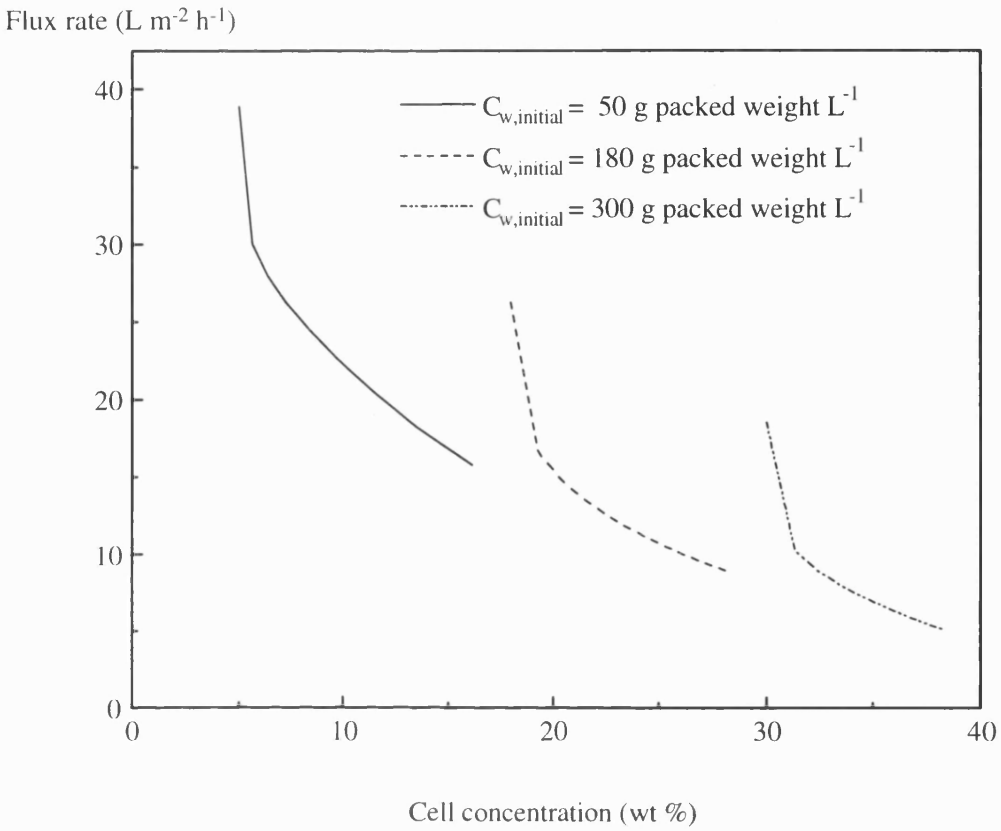

***Figure 6.6**: Simulations of the permeate flux rate as a function of the cell concentration. The simulations have been conducted at a recirculation rate of 7.1 m s^{-1} and an active membrane area of 0.35 m^2.*

Higher initial cell concentrations lead to lower steady-state permeate flux rates as a result of the increase in cell mass deposited per unit filter surface area (Russotti *et al.*, 1995). The membrane performance characteristics as a function of the starting cell concentration are given in Table 6.3.

$C_{w,initial}$ (g L^{-1})	ADH (%)	V_{perm} (L)	Prod (U mL^{-1})	J_{60} (L m^{-2} h^{-1})
50	58	69	63	30
180	20	36	148	17
300	8	22	172	10

***Table 6.3**: Results of simulations of the percentage product yield (ADH), the product volume (V_{perm}), the product concentration in the permeate (Prod) and the permeate flux rate after 1 h of processing (J_{60}). The simulations have been conducted at a recirculation rate of 7.1 m s^{-1}, a membrane module length of 0.75 m and an active membrane area of 0.35 m^2. The product concentration in the retentate stream is a function of the cell concentration and has been estimated at 75 Units (ADH) mL^{-1} of solution, 270 Units (ADH) mL^{-1} of solution and 450 Units (ADH) mL^{-1} of solution for cell concentrations of 50 g packed weight L^{-1}, 180 g packed weight L^{-1} and 300 g packed weight L^{-1} respectively. $C_{w,initial}$ represents the starting cell concentration measured in g packed weight L^{-1}.*

Lower starting cell concentrations lead to higher product yields. However, the recovered volume for subsequent purification is relatively high and the concentration of product in the permeate is relatively low. Thus, selecting the starting conditions for membrane processing will have significant effects on the yield, volume and composition of the product stream for further processing.

6.3.2.4 The effect of the diafiltration volume on membrane performance

Diafiltration is often used for washing and re-suspension of cells. It is also used to increase the overall yield of membrane separation processes. The benefits of diafiltration are offset by the increases in the recovered product volume and the dilution of product in the permeate stream. Thus, it is imperative that excessive volumes of diafiltration buffer are not used

as this will reduce the economic viability of the bioprocess. Table 6.4 illustrates the effect of diafiltration volume on the product yield, product volume and the product concentration in the permeate. Also illustrated in Table 6.4 is the effect of the cell concentration at the start of diafiltration on the performance of membrane processing.

$C_{w,initial}$	$C_{w,d}$	$C_{w,final}$	ADH (%)	V_{perm} (L)	Prod
50	100	235	84	129	48
50	200	200	82	110	56
50	67	277	81	132	46
90	100	181	65	100	87
180	100	360	31	58	143
300	100	457	13	34	170

***Table 6.4**: Results of simulations of the percentage product yield (ADH), the product volume (V_{perm}) and the product concentration in the permeate (Prod). The simulations have been conducted at a recirculation rate of 7.1 m s^{-1}, a membrane module length of 0.75 m, an active membrane area of 0.7 m^2 and a diafiltration volume of 50 L. $C_{w,initial}$ and $C_{w,final}$ represent the starting cell concentration and the final cell concentration measured in g packed weight L^{-1}. $C_{w,d}$ represents the cell concentration at the start of diafiltration and is also measured in g packed weight L^{-1}. Prod is measured in Units of enzymatic activity mL^{-1} of solution.*

From the simulations, the cell concentration at the start of diafiltration impacts significantly the final permeate volume for further processing. This arises because flux rates are higher at lower cell concentrations. Thus, diafiltration beginning at such concentration levels will be completed in reduced time, allowing the membrane separation process to proceed to completion. The cell concentration at the start of membrane processing has a significant effect on

the product yield. The potential effects of the diafiltration volume on the economics of a typical bioprocess have been illustrated in a case study which is presented in the next section.

Ideally, the information obtained from simulation studies should be verified by pilot-scale experimental studies. There was no opportunity for such scale-up studies at the research centre at UCL. However, the benefit of using simulation-based studies can be further illustrated through a realistic membrane case study which is presented in the next section.

6.4 Membrane case study

The case study was initially implemented on SPEEDUP (AspenTech Ltd., Massachusetts, U.S.A.) but recent case studies have been run on LABVIEW (National Instruments, U.S.A.). A summary of the models used in the case study is presented in Appendix A4.

6.4.1 Objective

To specify the design and operating conditions for a membrane separation process which leads to the lowest overall cost for a fermentation-based product manufactured to a specified level.

6.4.2 Introduction

The processing of a fermentation-based product involves a membrane separation stage and further purification stages. The membrane separation stage is critical because it represents the most costly stage in the process in terms of capital investment and operating cost. It is also the stage where the greatest loss of product occurs and the purification achieved in this stage directly determines the performance of subsequent chromatographic separation. To arrive at an optimum design and specification for the membrane separation stage, a computer-based simulation of the process has been developed to generate performance data for pilot-plant trials and the prediction of the resultant overall production costs. The experimental batch-to-batch variation arising from differences in fermentation broth and also changes to the membrane

performance in between trials has been ruled out. The fermentation broth has the following composition

cells	50 g L^{-1} dry weight
product (150 kDa)	10 g L^{-1}
high molecular weight contaminants (> 500 kDa)	0.7 g L^{-1}
medium molecular weight contaminants	1.5 g L^{-1}
low molecular weight contaminants (< 10 kDa)	0.8 g L^{-1}

The membrane stage is operated as a discrete batch unit with the ability to run in both concentration and diafiltration mode.

6.4.3 Input data

The production operation is planned such that the membrane separation is carried out daily and completed in 8 h. 9 input variables determine the process. These are

- the inner membrane diameter (d_m)
- the membrane module length (L_{mem})
- the number of membrane modules
- the desired transmembrane pressure (ΔP)
- the desired crossflow velocity (U)
- the inlet pressure to the module (P_{inlet})
- the extent of concentration during stage 1 (CF_1)
- the extent of diafiltration (DF)
- the overall extent of concentration (CF_2)

6.4.4 Output data

The simulations provide the following output data

- traces of the inlet, outlet and permeate pressures with time
- traces of the retentate flow velocity and permeate flux rate with time
- a trace of the retentate viscosity with time
- traces of the retentate and permeate product concentrations with time

- traces of the retentate and permeate product volumes with time
- analysis of the final cumulative permeate in terms of product (P_d) and contaminant concentrations i.e. high molecular weight contaminants (H_w), medium molecular weight contaminants (M_w) and low molecular weight contaminants (L_w)
- the final product cost (Pr)
- a breakdown of the product cost attributable to the fermentation stage (Ferm), the membrane stage (Mem) and the purification stage (Pur)

6.4.5 Simulation results

Several simulations of the process were conducted and six examples are given in tables 6.5 and 6.6 which illustrate the effect of the input variables on the performance of the membrane separation stage.

INPUTS	1	2	3	4	5	6
d_m (mm)	20	5	20	20	10	20
L_{mem} (m)	2	1	2	1	1	1
modules	20	10	20	20	10	10
ΔP (bar)	7	1	7	1	5	2
U ($m\ s^{-1}$)	8	5	8	10	9	8
P_{inlet}(bar)	10	2	10	2	7	5
CF_1	4	2	4	4	2	3.5
DF	10	1	0.5	0.5	0.5	0.5
CF_2	5	5	5	5	5	5

***Table 6.5**: Input data for membrane simulation case study*

OUTPUTS	1	2	3	4	5	6
P_d (g L^{-1})	2.29	3.92	7.62	7.45	3.75	6.07
H_w (g L^{-1})	0.08	0.04	0.06	0.05	0.05	0.05
M_w (g L^{-1})	0.29	0.18	0.24	0.23	0.20	0.23
L_w (g L^{-1})	0.24	0.73	0.68	0.72	0.65	0.70
Ferm (%)	3.8	33.8	4.5	21.2	30.9	26.7
Mem (%)	78.5	38.7	92.8	63.8	44.0	52.9
Pur (%)	17.7	27.5	2.7	15.0	25.1	20.4
Pr (£ kg^{-1})	345	186	281	69	97	66

***Table 6.6**: Output data for membrane simulation case study*

The effect of the 9 input variables on the performance of the membrane system can be explained in terms of the membrane area, the operating regime and the diafiltration volume. Ignoring pressure drop effects, membrane areas ranging from ~0.15 m^2 - 2.5 m^2 are used in the examples given. In terms of capital investment and operating costs, it is important that the proportion of the final product cost is not heavily weighted in favour of membrane processing. This is apparent in examples 1 and 3 where the product cost attributable to membrane processing exceeds 75%. The reverse is observed with example 2 where the product cost attributable to membrane processing does not exceed 40%. Thus, it would be fair to conclude from the simulations that a membrane area in the range 0.5 m^2 - 1.0 m^2 is suitable for membrane processing. The operating regime will determine the permeate flux rate and transmission characteristics of the membrane. Higher recirculation rates and low transmembrane pressures increase the membrane performance. However, the two effects are opposing and a balance between the recirculation rate and the transmembrane pressure is required to maximise membrane performance. The amount of diafiltration volume used and the cell concentration at the start of diafiltration will affect product recovery levels. Excessive diafiltration volumes will result in huge

volumes for subsequent processing and also very low product concentrations. Example 1 illustrates such a scenario. Excessive diafiltration volumes mean purification costs exceed fermentation costs by a factor of ~ 5 and the final product concentration in the permeate does not exceed 2.5 g L^{-1}. Example 3 demonstrates that using limited diafiltration volumes results in higher product concentrations in the permeate (7.5 g L^{-1}) and reduced product costs attributable to the purification stage. However, some amount of diafiltration is often required to increase product yields. The examples given do not illustrate the effect of the cell concentration at the start of diafiltration on product recovery levels. This effect has already been presented in section 6.3.2.4.

6.5 Conclusions

The use of process simulation in assisting the design of bioprocesses has been demonstrated. The models used in the simulations have been obtained from Chapter 5 and from literature reviews. Pilot-scale verification trials have not been conducted because of a lack of appropriate pilot-scale equipment. The results of the study have shown the potential of using simulations to direct pilot-plant research work and also determine the impact of design and operating parameters on the economics of bioprocesses. Such studies promote the acceleration of bioprocess design and reduce the cost of developing bioprocess recovery routes. They also allow quick evaluation of alternative processing schemes. In the next chapter, the processing of polyethyleneimine flocculated yeast homogenate using membrane separation techniques is presented. The development of new models predicting membrane performance and also the use of some models developed in chapter 5, indicating some degree of generality, will be illustrated.

7 PROCESSING OF FLOCCULATED CELL HOMOGENATE

7.1 Introduction

Successful application of membrane filtration in the bioprocess industries requires a high recovery of the desired product. This is achieved when flux and transmission rates are high. The presence of small particle sizes, a wide particle size distribution and relatively high viscosity due to the presence of proteins, nucleic acids and colloidal material make the processing of cell homogenates difficult. A possible method of enhancing the performance of membrane systems processing cell homogenates is to flocculate selectively certain feed components which are likely to interact with the membrane and hence reduce performance. This chapter examines the membrane processing of polyethyleneimine (PEI) flocculated yeast homogenate for a wide range of membrane operating conditions. The results of single experiments have been used to define the operating characteristics of the membrane system. Comparisons of the performance of membrane systems processing PEI flocculated yeast homogenate to that of untreated yeast homogenate and the implications of the use of PEI in downstream processing schemes will also be addressed in this chapter.

The selective removal of a range of contaminants including nucleic acids, lipids and colloidal proteins from solution of cell homogenates using PEI has been demonstrated by Milburn *et al.* (1990), Bentham (1990) and Cordes *et al.* (1990). The mechanism of flocculation is not clearly understood, but two possible mechanisms have been proposed. The first theory, the 'polymer bridging' theory (Ruehrwein *et al.*, 1952), suggests that particles can be linked together via adsorption onto different segments of the polymer molecule. Such bridging of polymer molecules with other particles results in flocculation. The second theory, the 'electrostatic patch' theory (Gregory, 1969) is relevant to polymers with a high charge density. When oppositely charged patches on different particles and polymer come into contact, an attachment is made resulting in flocculation. The extent of flocculation depends on the physical properties of the polymer including charge density (Lindquist *et al.*, 1976, Mabire *et al.*, 1984) and molecular weight (Gregory, 1976) and on the properties of the solution including pH (Bentham, 1990) and ionic strength (Lindquist *et al.*, 1976, Bentham, 1990).

The presence of non-protein contaminants in cell homogenates hinders enzyme and protein purification because of their high fouling characteristics. Thus, the application of selective flocculation to cell homogenates should facilitate a more effective downstream purification scheme. Milburn *et al.* (1990) conducted centrifugation studies on flocculated yeast homogenate. They selected flocculant dosing rates which enabled optimum clarification and removal of contaminants without entailing excessive loss of product. They concluded that treatment of borax-clarified yeast homogenate with PEI and subsequent removal of flocculated material using centrifugation led to supernatant 90% free of solid material, ~90% free of nucleic acids, 98% free of lipid material and up to 30% free of contaminant protein material. The activity of two target soluble enzymes alcohol dehydrogenase (ADH) and glucose-6-phosphate dehydrogenase (G-6-PDH) was unaffected. However, they also concluded that the processing of flocculated material at high concentrations would be inefficient because of the high solids content. Salt *et al.* (1992) studied the effectiveness of PEI as a specific flocculating agent on several organisms including *Sacchromyces cerevisiae, Escherichia coli* and *Pseudomonas putida.* Their study confirmed the suitability of PEI as a selective flocculant for biological streams. Cordes *et al.* (1990) studied the effect of PEI dosage on particle size, protein loss and the extent of nucleic acid removal in both batch and continuous mode. They achieved more than 95% removal of nucleic acids from yeast homogenates with protein losses of up to 15%. The size of flocculant material ranged from ~ 4 to ~11 μm depending on the mode of operation, the mixing rate and the mean residence time/mixing time. Lower mixing rates favoured the production of bigger particles indicating shear sensitivity of flocculant material.

In the next section, a method for selecting a suitable PEI dosing ratio and the physical properties of PEI flocculated yeast homogenate are presented.

7.2 Experimental methods

7.2.1 Selection of PEI dosing ratio

PEI (Sigma Chemical Company Ltd., Dorset, U.K.), obtained as a 50% w/v aqueous solution, was diluted with de-ionised water to give a 2% w/v aqueous solution. The resulting solution was adjusted to pH 6.5 using 4 M HCl. Samples of freshly prepared yeast homogenate

suspension in Eppendorf tubes were dosed with 2% w/v PEI solution to provide final concentrations ranging from 5% to 45% v/v. The resulting suspensions were spun down at 10,500 g for 20 min and the recovered supernatants were assayed for ADH and total protein content.

PEI selectively flocculates nucleic acids, lipids and colloidal material from solution. However, if dosing ratios are too high then it will begin to flocculate ADH out of solution as well. Figure 7.1 shows the purification factor of ADH, the ratio of ADH concentration to total protein level in solution, as a function of the PEI concentration.

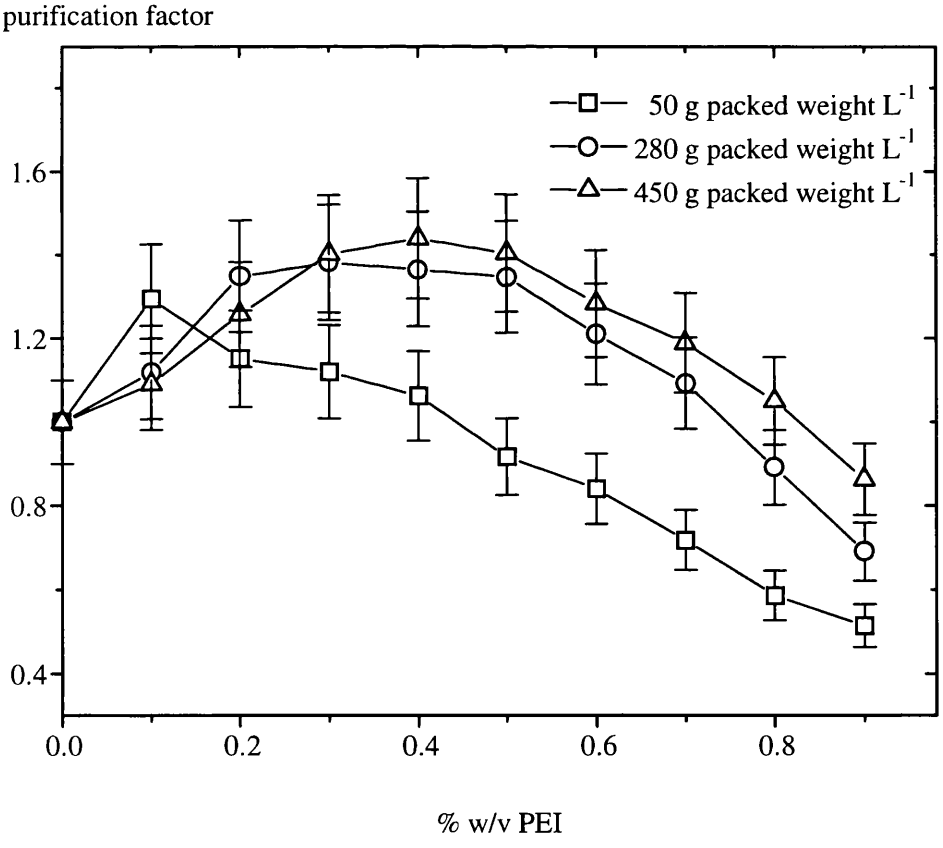

***Figure 7.1**: Purification factor for alcohol dehydrogenase in PEI flocculated yeast homogenate.*

Selection of suitable dosing ratios for subsequent microfiltration experiments was based on a maintenance of ADH activity and the quality of clarified broth samples. At 50 g packed weight L^{-1}, 0.1% w/v PEI solution was selected, at 280 g packed weight L^{-1}, 0.3% w/v PEI solution was selected and at 450 g packed weight L^{-1}, 0.4% w/v PEI solution was selected.

7.2.2 Filtration methods

Packed baker's yeast supplied by DCL Yeast Ltd. (Menstrie, Clackmannanshire, U.K.), was suspended in phosphate buffer (100 mM KH_2PO_4, pH 6.5) and disrupted in a Manton-Gaulin high pressure homogeniser (Model Lab 60, APV, Crawley, Sussex) according to the method described in section 3.3.5 of this thesis. A 2% w/v PEI solution was added to freshly prepared yeast homogenate at the required dosing ratio. The suspension was mixed for 5 min and used as process feed for microfiltration experiments.

7.3 Properties of PEI flocculated yeast homogenate

7.3.1 Particle size distribution of PEI flocculated yeast homogenate

The particle size distribution of PEI flocculated yeast homogenate was obtained from laser diffraction studies (section 3.3.2.2). Figure 7.2 shows distributions with peak diameters of ~ 4.0 μm and ~6.0 μm corresponding to 50 g packed weight L^{-1} and 280 g packed weight L^{-1} respectively.

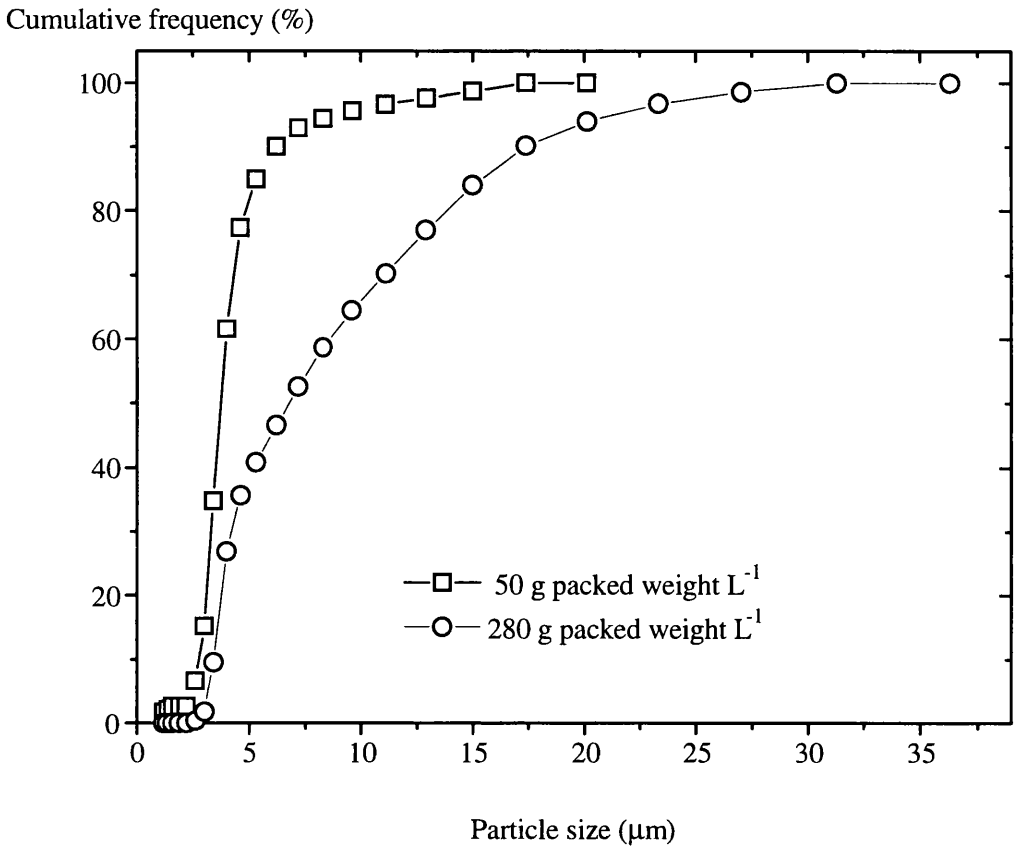

***Figure 7.2**: Particle size distribution of PEI flocculated yeast homogenate suspended in phosphate buffer (100 mM KH_2PO_4, pH 6.5) using laser light diffraction.*

7.3.2 Rheological properties of PEI flocculated yeast homogenate

The viscosity of PEI flocculated yeast homogenate was measured using a rotational viscometer (RHEOMAT 115, Contraves AG, Zurich, Switzerland) as described in section 3.3.3. Using the Reuss *et al.* (1979) and the Pradipasena *et al.* (1977) models for the viscosity of yeast whole cells and globular protein solutions respectively, the solids volume fraction of PEI flocculated yeast homogenate has been estimated. The results are tabulated in Table 7.1.

Conc (g pw L^{-1})	P (wt %)	μ_n (10^{-3} Pa s)	μ_S (10^{-3} Pa s)	ϕ (v/v solids)
50	0.44	1.4	1.9	0.11
280	1.90	2.5	6.5	0.23
450	3.19	3.6	16.6	0.33

***Table 7.1**: Viscosity of PEI flocculated yeast homogenate suspended in phosphate buffer (100 mM KH_2PO_4, pH 6.5). P represents the wt % concentration of soluble proteins, μ_p represents the estimated viscosity of protein solution, μ_s represents the measured viscosity of the suspension and ϕ represents the estimated solids volume fraction. g pw L^{-1} is the concentration measured in g packed weight L^{-1}.*

7.4 Results

7.4.1 Flux rates

Table 7.2 shows the values of the permeate flux rate after 1 min (J_1) the quasi steady-state permeate flux rate (J_{ss}) and the fouling index (b, equation 2.1, section 2.2) under various experimental conditions.

Exp	Pore (μm)	Conc (g L^{-1})	Vel (m s^{-1})	ΔP_{tm} (kPa)	J_i (LMH)	J_{ss} (LMH)	b	R^2
1	0.2	50	7.1	100	150	70	0.15	0.620
2		280	3.5	50	40	18	0.16	0.917
3		280	7.1	100	100	25	0.27	0.744
4		450	7.1	110	60	19	0.25	0.866
5	0.8	50	7.1	100	398	110	0.25	0.958
6		280	3.5	50	50	25	0.14	0.786
7		280	7.1	100	195	40	0.30	0.959
8		450	7.1	110	130	18	0.29	0.866
9	1.4	50	7.1	100	198	33	0.36	0.757
10		280	7.1	100	120	15	0.38	0.839
11		450	7.1	110	55	10	0.34	0.844

***Table 7.2**: Initial and steady-state permeate flux rates observed during the microfiltration of PEI flocculated yeast homogenate. Experiments have been conducted on ceramic membranes for a range of membrane operating conditions. The experimentally determined fouling index (b, equation 2.1, section 2.2), and the correlation coefficient (R^2) are also shown. LMH is equivalent to L m^{-2} h^{-1}.*

7.4.1.1 Prediction of permeate flux rates

Extrapolation of the predicted permeate flux rate by interpolation towards zero has been done for experiments conducted using PEI flocculated yeast homogenate. The concentration polarisation model has been used for flux prediction with the assumption of a gel layer of 70% solids by volume. Figure 7.3 shows the predicted permeate flux rates as a function of the observed flux rates. The closed points represent experiments used for empirical parameter determination of the polarisation model.

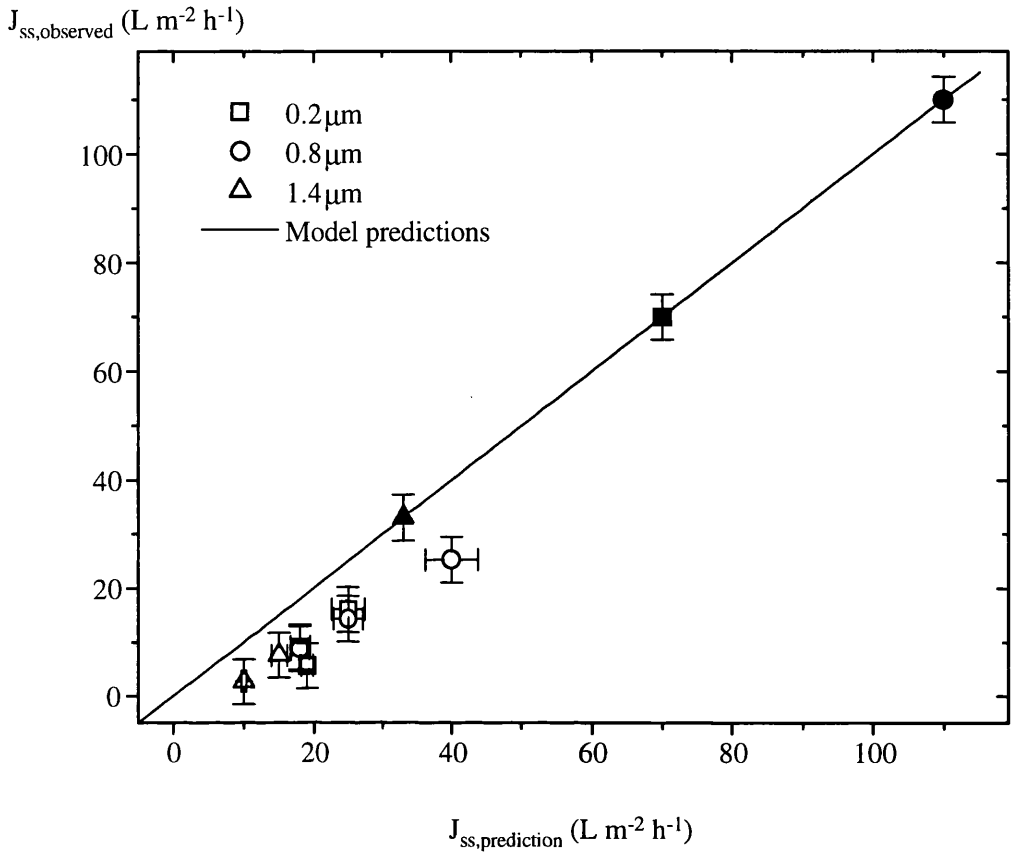

***Figure 7.3**: Observed permeate flux rates of PEI flocculated yeast homogenate as a function of the predicted permeate flux rates using ceramic membranes of nominal pore size equivalent to 0.2 μm, 0.8 μm and 1.4 μm. J_{ss} represents the quasi steady-state permeate flux rate. Viscosities are obtained from model predictions. The line graph represents the model predictions, and the error is estimated at - 10%. The correlation coefficient (R^2) is calculated as 0.985.*

7.4.2 Rejection characteristics

Table 7.2 shows the values of the permeate flux rate after 1 h and the transmission of ADH and total protein under various experimental conditions.

Exp	ADH (% trans)	Protein (% trans)
1	95	91
2	13	17
3	55	54
4	35	39
5	99	100
6	94	86
7	107	100
8	99	98
9	89	85
10	95	91
11	87	85

***Table 7.3**: Observed permeate flux rates and the transmission of alcohol dehydrogenase and total protein for microfiltration experiments conducted on ceramic membranes for a range of operating conditions on PEI flocculated yeast homogenate.*

7.4.2.1 Prediction of the rejection characteristics of membranes

The predicted transmission of ADH has been obtained using the model developed in section 5.4.2.1 of this thesis. Figure 7.4 shows the observed transmission of ADH as a function of the predicted transmission of ADH for a range of membrane operating conditions. The predictions are in good agreement with the observations.

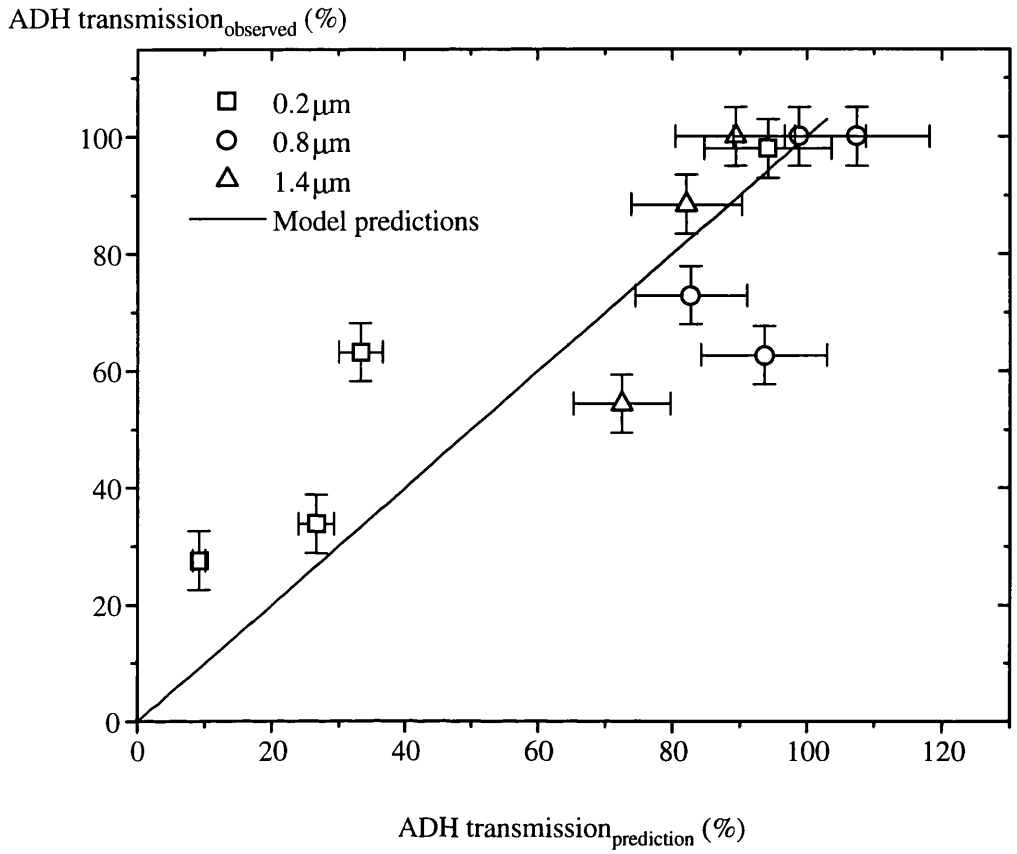

***Figure 7.4**: Observed alcohol dehydrogenase transmission from PEI flocculated yeast homogenate as a function of the predicted transmission using ceramic membranes of nominal pore size equivalent to 0.2 μm, 0.8 μm and 1.4 μm. The experiments have been conducted for a range of yeast homogenate concentrations, 50 g packed weight L^{-1} up to 450 g packed weight L^{-1}, a range of recirculation rates, 1.8 m s^{-1} up to 7.1 m s^{-1}, and transmembrane pressures ranging from 50 kPa up to 120 kPa. The model predictions are represented by the line graph, and the error is estimated at ± 10%. The correlation coefficient (R^2) is calculated as 0.844.*

7.4.4 Gel permeation studies

An example of the predicted gel permeation chromatogram of the permeate fraction from the microfiltration of PEI flocculated yeast homogenate is shown in Figure 7.5. The experiment was conducted at a cell concentration of 280 g packed weight L^{-1}. The model predictions are based on protein transmission data.

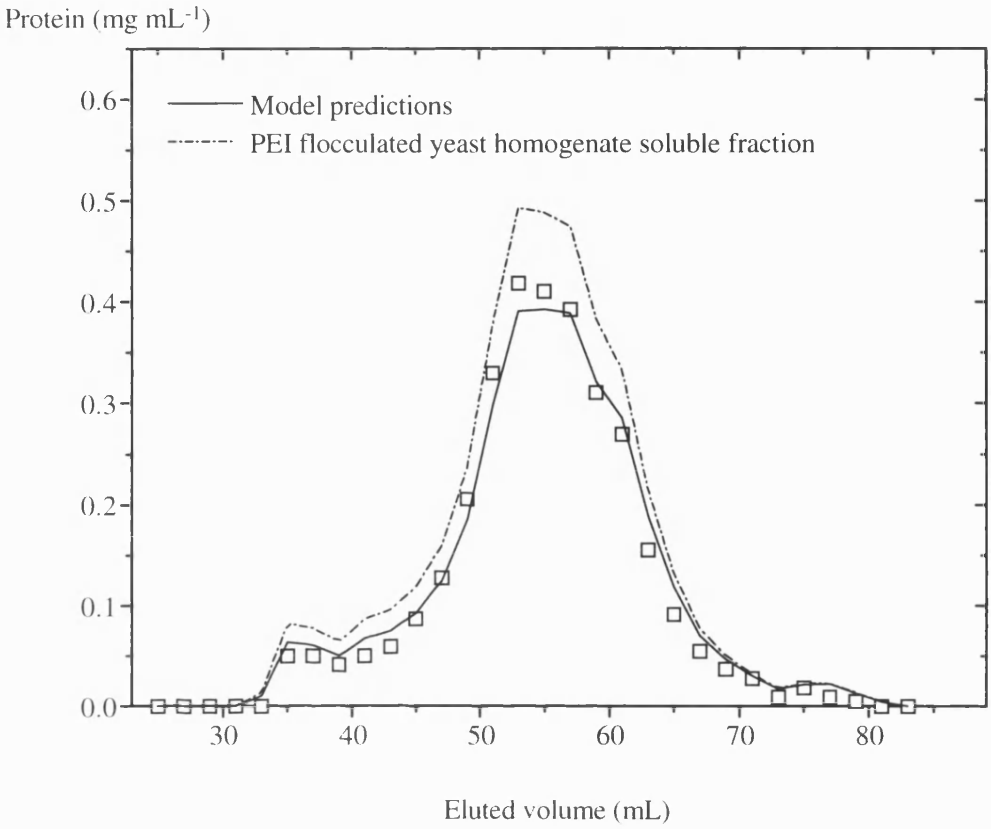

***Figure 7.5**: Prediction of the gel permeation chromatogram of the permeate fraction from a microfiltration experiment conducted on a ceramic membrane of nominal pore size equivalent to 0.8 μm at the conditions of a cell concentration of 280 g packed weight L^{-1}, a recirculation rate of 3.5 m s^{-1}, and a transmembrane pressure of 50 kPa. The error is estimated at ± 8% and the correlation coefficient (R^2) is calculated as 0.991.*

Although the soluble fraction of PEI flocculated yeast homogenate is different from that of yeast homogenate, the prediction of the transmission properties of microfiltration membranes, using the method outlined in section 5.4 of this thesis, is still applicable.

7.5 Conclusions

The prediction of permeate flux rates for a range of membrane operating conditions has been demonstrated using single experimental measurements. The results indicate that the model developed in Chapter 5 of this thesis is applicable to a modified yeast system. Only single

experimental measurements are required to calculate model parameters and constants. The transmission model developed in Chapter 5 has been used to predict the transmission of soluble components of PEI treated yeast homogenate without any modification. The results indicate that such a model may provide a generic basis for the rejection characteristics of ceramic membrane processes employed in the bioprocess industries for primary product recovery involving yeast systems.

The product flux rates for the condition likely to give the highest permeate flux rate are tabulated below.

Nominal membrane pore size (μm)	No pretreatment (Units m^{-2} h^{-1})	PEI pretreatment (Units m^{-2} h^{-1})
0.2	2.0×10^6	4.5×10^6
0.8	2.6×10^6	7.4×10^6
1.4	-	2.0×10^6

***Table 7.4**: Product flux rate for microfiltration experiments conducted at the conditions of a cell concentration of 50 g packed weight L^{-1}, a recirculation rate of 7.1 m s^{-1} and a transmembrane pressure of 100 kPa. The product flux rate is measured in enzymatic units of ADH per unit membrane area per unit time.*

The best product flux rate using PEI treated feed-streams almost trebles that for untreated feed-streams. This result indicates that using PEI pre-treatment methods may enhance microfiltration performance. The use of PEI for large scale operations will depend on a number of factors including the scale of operation, the cost of PEI and the impact of excess soluble PEI on further purification steps. At current vendor prices of ~ £ 50 L^{-1} for a 50% w/v aqueous solution of PEI, the economic implications of using PEI in large scale operations is not severe. As flocculation removes nucleic acids, lipids and colloidal proteins from solution, the permeate

streams of PEI treated feed-streams will exhibit reduced constituent complexity and lower viscosities. This enables further purification stages, often involving chromatographic processes, to be conducted with process streams with reduced fouling potential. Chromatographic processes in a typical bioprocess flowsheet represent a significant proportion of the cost of production. Any improvement in the efficiency of such operations could yield significant economic benefits. The formation of larger particles during flocculation will increase the separation options available to the bioprocess designer. It may also improve the separation performance of individual unit operations. However, the use of pre-treatment methods may be offset by the impact of pre-treatment reagents on the overall process flowsheet. Hall (1996) microfiltered the supernatant of clarified PEI treated yeast homogenate and observed higher fouling characteristics when compared to the supernatant of untreated and clarified yeast homogenate. The loss in membrane performance was attributed to the interaction of excess PEI with the polymeric membrane, and this was supported by the fact that several cleaning regimes were required to restore the pure water flux rate.

The use of pre-treatment methods to enhance downstream bioprocessing schemes has been demonstrated. The application of such methods requires careful consideration of several factors in the context of whole processes. This will inevitable lead to an optimisation problem which can be solved using simulation techniques. In the next chapter, the processing of *Escherichia coli* cell lysate is examined. The use of certain physical property measurements including particle size distributions and rheological measurements to aid model predictions is also examined.

8 PROCESSING OF CELL LYSATE

8.1 Introduction

Recombinant deoxyribonucleic acid (DNA) techniques allow the synthesis of therapeutic and diagnostic protein products in bacterial cells. The large scale growth of recombinant bacteria offers a cheap and reliable way of producing such proteins. The increase in potential products has created a need for robust downstream processing procedures for their recovery and purification (Hoare *et al.*, 1989). The risks to company employees, the general public and the environment when processing recombinant material can be high and strict procedures are needed to contain the material when such scenarios arise. The risk of infection, the use of antibiotics during production and the processing of large liquid volumes have led to strict legislative demands (Fischer, 1996). The use of membrane separation processes to recover recombinant protein products is very attractive because they allow high levels of automation accompanied with complete or near complete material containment. This chapter examines the processing of *Escherichia coli* cell lysate for the recovery of a periplasmic product α-amylase. Periplasmic products exist in the cell compartment situated between the inner cell wall and the outer cell wall. The cells have been grown in batch mode using the method developed by French (1993). A combined lysozyme-osmotic shock treatment of the recovered cells allowed the release of the protein product without entailing full disruption of cells which often complicates subsequent downstream processing operations. Microfiltration experiments have been conducted on lysed cells and the information has been used to develop a model describing the membrane separation performance. The use of physical property measurements including the particle size distribution and rheological studies to predict membrane performance has also been examined. The highly specific nature of biological feed-streams and their interaction with the membrane limits the capability of using such measurements to predict membrane performance. In the next paragraph, a review of the membrane processing of *Escherichia coli* feed-streams is presented.

Escherichia coli is often used as the host organism for plasmid and bacteriophage vectors in manufacturing. These vectors are DNA molecules which provide propagation of a DNA fragment in a growing cell population (Bailey *et al.*, 1986). The vectors often contain selection markers including a gene for antibiotic resistance which allows vector-containing cells

to grow in a medium containing a level of antibiotic which would kill vector-free cells. Bailey *et al.* (1986) give a comprehensive review of cloning technology and include other host organisms such as *Pseudomonas* and *Streptomyces* strains and *Saccharomyces cerevisiae*. Several researchers have investigated the microfiltration of *Escherichia coli* suspensions for the recovery of protein products. Meyer *et al.* (1998) developed a model for the harvesting of *Escherichia coli* whole cells through a shear-enhanced module. The process behaviour was described by a specific artificial neural network based on experimental data and the interactions of 17 parameters were examined. The accuracy of the model predictions and the simplicity of implementation were offset by the number of experiments required to train the simulator. Bailey *et al.* (1997) filtered recombinant *Escherichia coli* cell lysates containing protein inclusion bodies after high pressure homogenisation. The number of passes through the homogeniser increased the broth viscosity and reduced the average particle sizes but this had no effect on the permeate flux rate and the protein transmission for a given membrane. They also studied the effect of the membrane configuration and pore size on the membrane performance and found different levels of permeate flux rate and protein transmission for the various membranes used. Forman *et al.* (1990) and Meagher *et al.* (1994) studied the effect of operational parameters on the performance of crossflow membrane filtration for the recovery of inclusion bodies from *Escherichia coli* cell lysate. These included the effects of the recirculation rate, the transmembrane pressure, the initial concentration, the membrane pore size and the ionic environment. Parnham *et al.* (1995) also investigated protein recovery from *Escherichia coli* cell lysate using microfiltration membranes. They observed little or no enhancement of membrane performance with increasing transmembrane pressure but the performance was improved with increasing shear rate and decreasing solids concentration. The transmission of protein product was highest for dilute suspensions at high shear rates. Parnham *et al.* (1996) used rapid backpulsing as a method to improve membrane performance. At low cell debris concentrations, permeate flux rates were improved by up to 10 times that of unpulsed filtration. However, no flux improvements were observed for higher cell debris concentrations. They also found that rapid backpulsing improved protein transmission for all conditions investigated. Fane *et al.* (1991) studied the effect of membrane surface properties and ionic strength on the filtration of *Escherichia coli* cells suspended in 10^{-4} M NaCl diluent and diluent

containing 0.1 wt % bovine serum albumin. Both factors significantly affected permeate flux rates and protein recovery levels. Smooth hydrophilic membranes returned higher fluxes and recovery levels. Low pressure operation and low ionic strength suspensions performed likewise. Kroner *et al.* (1988) used an axially rotating microfilter to study the influence of a range of operating parameters including the transmembrane pressure, the rotation speed and the broth concentration on cell harvesting, cell debris removal and enzyme recovery. Cell harvesting experiments were performed on a range of organisms including packed baker's yeast suspended in phosphate buffer, fermented batches of *Escherichia coli* cells, *Brevibacterium ammoniagenes* cells and *Bacillus licheniformis* cells. Experiments for the separation of cell debris from enzymes were performed after cell disintegration. They concluded that the improved hydrodynamics of the filter improved the performance of crossflow microfiltration of microbial suspensions. Fischer (1996) conducted microfiltration experiments on *Escherichia coli* cell lysate for a range of membrane operating conditions. Better membrane performance was achieved with ceramic membranes of nominal pore size equivalent to 0.2 μm in comparison to that of an equivalent nominal pore size of 0.8 μm.

In the next sections, details of general techniques used in the fermentation, physical property measurements and downstream processing studies will be presented.

8.2 Experimental methods

Fermentations were carried out in batch mode and a full description is given in section 3.3.8 of this thesis. *Escherichia coli* cells were grown in 20 L vessels at a controlled temperature of 37°C and a controlled pH of 7. The cells were grown on defined media to a dry weight concentration of ~ 10 g L^{-1}. Harvesting of cells was achieved using a tubular bowl centrifuge. The cells were then resuspended in supernatant to a final volume of 2 L. The product release step involved osmotic shock, stripping the cells of their outer walls and releasing the contents of the periplasmic space. Lysis solution at room temperature was added to the suspension of cells and the solution was gently mixed for 10 min. R.O. water was then added to the solution and gently mixed for a further 10 min. The resulting solution was used as feed broth for filtration experiments.

Filtration experiments were conducted on the Bio-Design crossflow filtration rig using ceramic membranes of nominal pore size equivalent to 0.2 μm. Details of experimental procedures can be found in section 3.3 of this thesis.

8.3 Properties of *Escherichia coli* cell lysate

8.3.1 Particle size distribution of *Escherichia coli* cells

The particle size distribution of whole cell broth, lysed cell broth and the soluble fraction of lysed cell broth were obtained from photon correlation spectroscopy (section 3.3.2.2). Whole cell samples displayed a bimodal distribution with peak diameters of ~ 0.8 μm and ~ 2.3 μm. This is represented in Figure 8.1.

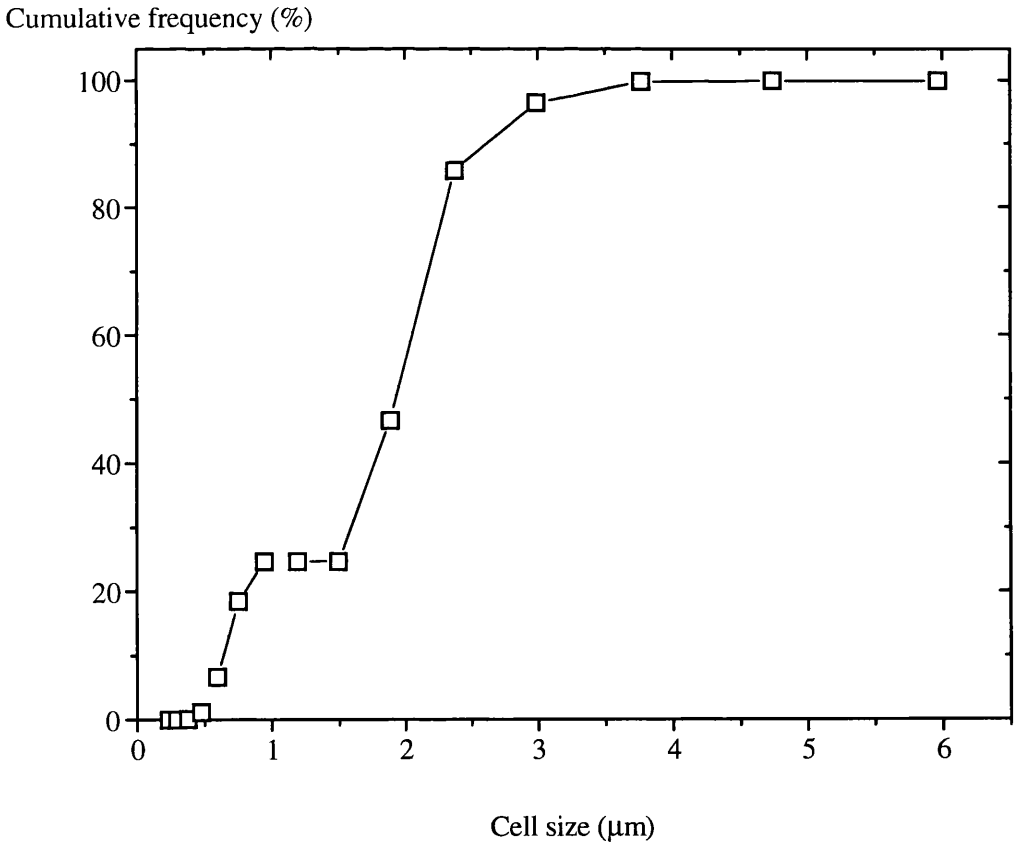

***Figure 8.1**: Particle size distribution of Escherichia coli cells using photon correlation spectroscopy.*

Cell lysate also displayed a bimodal distribution with peak diameters of ~ 0.17 μm and ~ 1.0 μm, which may be attributed to the contents of the periplasmic space and the cells stripped of their outer walls respectively. The size distribution of the soluble fraction of lysed displayed a peak diameter of ~ 0.4 μm and a maximum particle size of ~ 0.75 μm. These distributions are represented in Figure 8.2.

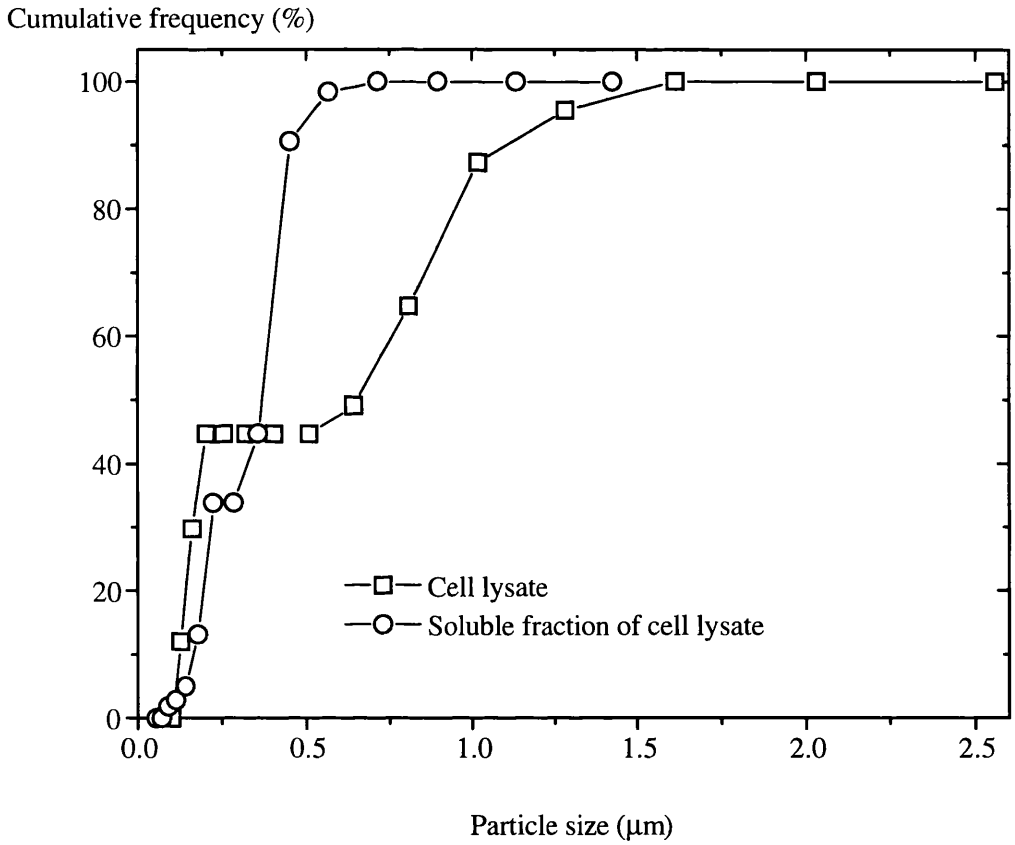

***Figure 8.2**: Particle size distribution of lysed Escherichia coli cells and the soluble fraction of lysed Escherichia coli cells using photon correlation spectroscopy.*

8.3.2 Rheological properties of *Escherichia coli* cells

The viscosity of fermented broth, concentrated fermented broth prior to cell lysis and cell lysate were measured using a rotational viscometer (RHEOMAT 115, Contraves AG, Zurich,

Switzerland) as described in section 3.3.3 of this thesis and estimated at 2.4 mN s m^{-2}, 3.5 mN s m^{-2} and 2.5 mN s m^{-2} respectively.

8.4 Results

Fermentation growth rates were monitored via optical density measurements and on-line measurements of the carbon evolution rate and the dissolved oxygen tension. The former measurements doubled every ~ 2 h indicating no significant lag phase. The level of α-amylase and protein in the soluble fraction of lysed cells were estimated at 2.5 Units mL^{-1} and 0.7 mg mL^{-1} respectively.

8.4.1 Flux rates

Both microfiltration experiments were conducted at the conditions of a recirculation rate of 7.1 m s^{-1} and a transmembrane pressure of 100 kPa. For the given broth concentration, this membrane operating condition represented the condition most likely to yield the highest permeate flux rate. A summary of the membrane performance with respect to the permeate flux rate is given below.

Initial permeate flux rate (J_1)	=	150	L m^{-2} h^{-1}
Steady-state permeate flux rate (J_{ss})	=	30	L m^{-2} h^{-1}
Fouling index (b)	=	- 0.39	

Using an identical approach to that outlined in Chapter 5, it would be possible to predict the membrane performance for a range of membrane operating conditions by extrapolation using a concentration polarisation model.

8.4.2 Rejection characteristics

The transmission of α-amylase and total protein were estimated at 45% and 21% respectively at the start of microfiltration experiments but the levels dropped to ~12% and ~ 7% respectively after ~ 3 hr. The prediction of the rejection characteristics of the membrane for a

range of membrane operating conditions using information from a single microfiltration experiment is obtained using the approach developed in section 5.4.2.1 of this thesis. The model developed is presented below in Figure 8.3.

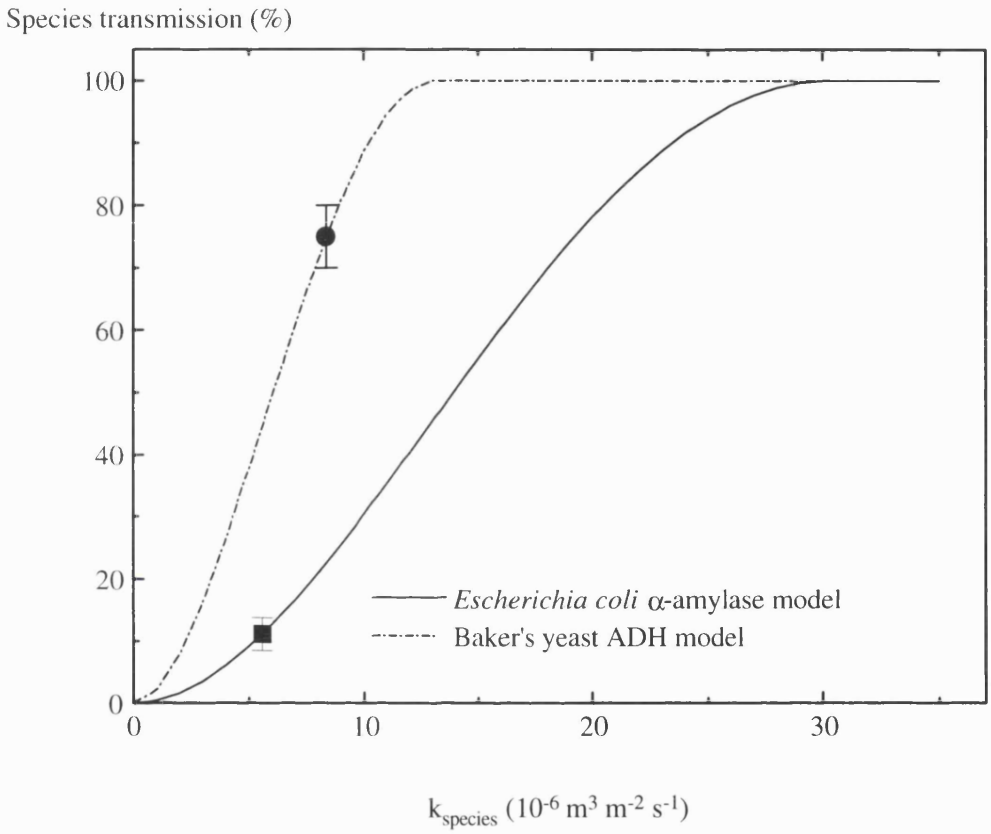

***Figure 8.3**: Models developed for the prediction of the transmission of soluble species as a function of the mass transfer coefficient based on single microfiltration experiments.*

Certain features may provide some insight into membrane performance characteristics. Such information will rely on physical property measurements including particle size measurements and rheological measurements. These properties are presented in Table 8.1. To standardise the solution characteristics but ignoring extracellular soluble protein concentration levels, the viscosity of the process streams have been equalised.

System	Conc (g pw L^{-1})	Pore (μm)	λ	J_{ss}(L m^{-2} h^{-1})
E. coli	50*	0.2	5	30"
Whole cells	250	0.2	37	29
Whole cells	250	0.8	11	17
Whole cells	250	1.4	8	12
Homogenate	175	0.2	9	17
Homogenate	175	0.8	3	19

***Table 8.1**: Predicted permeate flux rates for the microfiltration of an Escherichia coli suspension, yeast whole cells suspended in phosphate buffer (100 mM KH_2PO_4, pH 6.5) and yeast homogenate suspended in phosphate buffer (100 mM KH_2PO_4, pH 6.5). The experimental conditions are set at a recirculation rate of 7.1 m s^{-1}, a transmembrane pressure of 100 kPa and a suspension viscosity of 2.5 mN s m^{-2}. λ represents the particle-to-pore size ratio. * represents the cell concentration in g L^{-1} dry weight. " represents observed permeate flux rates. Pore represents the nominal membrane pore size and g pw L^{-1} represents the cell concentration in g packed weight L^{-1}. J_{ss} represents the steady-state permeate flux rate.*

A comparison of the particle-to-pore size ratio for the *Escherichia coli* based system with that of the baker's yeast system gives no reliable indication of the permeate flux rate. Such a comparison ignores the presence or absence of small particulate species and also the contents of the soluble fraction of the retentate stream which will display very specific interactions with the membrane resulting in different permeate flux rate characteristics.

The transmission characteristics of the two systems are also different. The protein content of the periplasmic space of the *Escherichia coli* cells is inferior to that of yeast homogenate. The presence of lysis solution in the *Escherichia coli* suspension is another difference with respect to the solution characteristics. These are two possible reasons for the differences in rejection properties of membranes.

8.5 Conclusions

The models developed for the *Escherichia coli* system are different to that for baker's yeast. Although the approaches used are identical and therefore generic, the results show that the prediction of the performance of membrane separation processes used in the bioprocess industries will always require some degree of experimentation. The approach used in this thesis is to limit the amount of experiments required to completely model a membrane separation bioprocess. In the next chapter, the main conclusions of this study will be drawn together and suggestions for future work will be presented.

9 CONCLUSIONS

9.1 Introduction

The main focus of this thesis has been the development of robust and predictive models describing the downstream processing of an intracellular protein product using membrane filtration. Verification experiments have been conducted to test the accuracy of model predictions and the models developed have been encoded within SPEEDUP (AspenTech Ltd., Massachusetts, U.S.A.) to demonstrate the application of process simulation within a bioprocess environment. The main conclusions of the studies will now be drawn together.

9.2 Modelling techniques

The initial phase of this study focused on the available approaches to model crossflow membrane filtration for use in a typical bioprocess flowsheet. Most modelling of membrane separation bioprocesses is achieved using a concentration polarisation model or a resistance model. A concentration polarisation model is only applicable in the pressure independent region and a resistance model is only applicable in the pressure dependent region. All experiments conducted in this study reside in the pressure independent region and for this reason a polarisation model was used for predictive purposes. Models based on a polarisation approach were developed by characterising the suspension properties and determining model parameters by conducting single microfiltration experiments for a given membrane pore size. The benefits of using such an approach include a significant reduction in process development time allowing for the rapid piloting of bioprocesses. However, the reliability of the models developed is questionable, as was demonstrated in Chapter 4. This stems from the specific nature of bioprocess feed-streams and their interaction with the membrane. A lack of a true understanding of the prevailing fouling mechanisms means that empirical parameter determination should not be based on single microfiltration experiments. The minimum number of experiments required to develop a robust model will depend on the number of input variables and also the range of variable settings. Such features point the model developer towards a statistical approach to modelling.

Statistical approaches have also been used to model membrane filtration bioprocesses but are less common than polarisation models. Such models use a 'black box' approach by developing an empirical linear or non-linear relationship between n input variables and m output variables. A statistical model based on linear regression was used to describe the permeate flux properties of ceramic membranes during the microfiltration of yeast whole cells. The main benefits of using such an approach include the reliability and accuracy of the model predictions and the ease of implementation. However, statistical models tend to be system specific and require a high degree of experimentation to train the simulator. They also tend to be scale dependent.

In conclusion, it is probably most appropriate to model crossflow membrane filtration systems using a statistical approach. The reasons for using such an approach include

- a high degree of specific interactions between membranes and typical bioprocess feed-streams make the development of theoretical models difficult
- the ease of implementation of statistical models not requiring the estimation of intermolecular forces, particle size distributions, suspension rheological properties and diffusion coefficients which are difficult to measure
- accurate models as a result of continuous updating by including information from all experiments
- the robust nature of models within the confines of variable settings

Statistical models give no indication of possible fouling or separation mechanisms occurring in filtration modules. The behaviour of biological feed-streams in high shearing devices will depend largely on their viscoelastic properties. Newtonian fluids are easier to model in such environments. Non-Newtonian suspensions are less predictable. The benefits of using fluid mechanics to develop rigorous flow models include an understanding of the flow patterns in membrane filtration devices which may explain possible fouling mechanisms. Such models may also explain the interaction between the particle size and the membrane pore size and the importance of hydrodynamic forces in the boundary layer with regard to re-suspended flowing cakes or static non-flowing cakes, the cake thickness and porosity. The development of rigorous flow models will make for models which are scale independent and membrane module geometry independent. Thermodynamic forces such as intermolecular forces and entropic pressure will only

be significant if they match or exceed hydrodynamic forces. Such models may elucidate the effects of certain components such as colloidal proteins, lipids, anti-foam agents and other soluble components on the filterability of biological suspensions.

9.3 Physical property measurements and model development

The possibility of using certain physical property characterisations including particle size measurements and viscosity measurements alongside single microfiltration experiments to determine permeate flux rates and soluble product transmission was examined in Chapters 5, 7 and 8. Using the particle-to-pore size ratio (λ) and information from Chapter 4, it was concluded that an empirically determined concentration polarisation model based on single microfiltration experiments should be applicable to yeast homogenate for the range of λ studied. Verification studies confirmed the applicability of the polarisation model to the yeast homogenate system. Similar results were obtained for polyethyleneimine (PEI) treated yeast homogenate. Yeast whole cells and yeast homogenate displayed an apparent linear response to λ with respect to permeate flux rates and soluble product transmission. However, PEI treated yeast homogenate displayed curvature and the best membrane performance occurred at a value of $\lambda = \sim 10$. This is in complete contradiction to studies conducted in Chapters 4 and 5, and also studies conducted by Kawakatsu *et al.*, (1993) where the worst membrane performance occurred at a value of $\lambda = \sim 10$. Thus, it is erroneous to conclude that compressible systems will display inferior membrane performance at values of $\lambda = \sim 10$ (Kawakatsu *et al.*, 1993). This is a direct consequence of the specific nature of the filtration of biological systems.

Viscosity measurements provide a means of determining the changes in the steady-state permeate flux rate as a function of the cell concentration. However, viscosity measurements give no indication of membrane filtration performance when the host system is changed. This was demonstrated in Chapter 8 where equating the system viscosities but changing the biological system produced vastly different permeate flux rate and transmission properties.

In conclusion, the use of physical property characterisations to predict membrane performance is limited by the highly specific nature of biological feed-streams and their interaction with the membrane.

9.4 Simulation studies

Simulation studies provide a means of studying the effect of a range of design and operating variables on the performance of unit operations. The benefits of using such techniques are enormous and have been highlighted in Chapter 6. Simulations studies were conducted on a 3-stage filtration process for the recovery of alcohol dehydrogenase (ADH) from yeast homogenate. The studies assessed the impact of the recirculation rate, the membrane module length, the starting cell concentration and diafiltration volumes on the product yield and product purity. The models used were those developed in Chapter 5.

To be of real benefit to the bioprocess engineer, process simulation studies should be conducted in conjunction with pilot-scale verification trials. The ability to use simulations to direct pilot-plant research activity is crucial. It is also important that the models developed are scaleable and any sources of inaccuracies quickly found and rooted out. This powerful combination of process simulation and pilot-scale verification will allow for the rapid development of near optimal process routes. Pilot-scale verification of the models developed in this thesis have not been conducted because of a lack of appropriate process-scale equipment.

9.5 Overall conclusions

The development of robust and predictive models for the downstream processing of complex biological feedstocks using membrane filtration has been demonstrated. Such models are empirical in nature because of specific interactions between feed-streams and the membrane which are poorly understood. The unit operation models developed require single experiments to determine empirical parameters. However, the reliability of such an approach is questionable. Statistical models, on the other hand, provide more accurate and reliable predictions but require several experiments to develop and are probable not scaleable. Simulations provide a useful means of understanding fully the implications of design and operating parameters on unit operation performance. The benefits of such techniques in the context of whole processes has been demonstrated by several other workers in the research group (Clarkson, 1994, Zhou *et al.*, 1997, Varga, 1997, Siddiqi, 1998). Other general conclusions are that

- membrane processes allow continuous separations in sterile environments
- membrane operating regimes are less harsh than alternative unit operations such as centrifugation allowing for complete bio-containment
- the product fraction is devoid of any particulate material if membrane pore sizes are selected appropriately simplifying subsequent downstream operations
- feedstock pre-treatment may allow for competitive membrane processes i.e. permeate flux rates in excess of ~ 100 L m^{-2} h^{-1} (Warren *et al.*, 1991)
- simulations of bioprocesses provide a suitable medium for teaching undergraduate students, postgraduate students and industrial delegates.

10 RECOMMENDATIONS FOR FUTURE WORK

The principle areas of this study where work could be expanded and is recommended include

- pilot-scale verification of the models developed using membranes with an active area of ~ 0.5 m^2 capable of processing ~ 50 L of feed broth in a few hours. This will allow process feasibility studies to be conducted.

- simulation studies conducted in the context of whole processes. Bioprocesses are characterised by a high degree of interaction between unit operations. Optimisation of individual unit operations may have detrimental effects on subsequent processing operations. The development of a superstructure of potential processing routes and the optimisation of selected routes will speed up the design of efficient and optimal bioprocesses.

- the filtration of simple model solutions, comprising typical biological feed-stream constituents, to elucidate fouling mechanisms in porous media. Such an approach will allow the testing of more rigorous thermodynamic and hydrodynamic models and establish how significant these forces are during the filtration of increasingly complicated model solutions and complex solutions. The filtration of model systems will also allow for better models describing adhesion and deposition characteristics of solution components onto membrane surfaces.

- the generation of extensive physical property data banks of model and complex biological systems including particle size distributions, rheological properties and electrostatic properties. Incorporation of such databases into simulation software will negate the need for unnecessary repeated experimental determinations and allow for rapid and cost effective piloting of bioprocesses using simulation techniques.

- the generation of computational fluid dynamic (CFD) models describing flow through porous media allowing for better prediction of the hydrodynamic forces in the vicinity of the concentration boundary layer. Understanding the physics of porous systems should provide valuable insight with regard to operating regimes and membrane module construction.

- the development of an artificial neural network to simulate the performance of a typical membrane bioprocess system and include the impact of upstream conditions on membrane performance. Such an approach will allow the examination of a range of factors including the system hydrodynamics, the suspension properties, the membrane properties, the operating parameters and upstream conditions such as fermentation time, the level of anti-foam and final glucose concentrations. Artificial neural networks can be implemented on software packages such as MATLAB (The MathsWorks Inc, Massachusetts, U.S.A.).

APPENDICES

APPENDIX A1 Assays

A1.1 Total protein determination

The BIO-RAD protein assay is based on the differential colour change of a dye, Coomassie Brilliant Blue G-250 in acidic solution, when binding to protein occurs. Bovine serum albumin (BSA, Sigma Chemical Company Ltd., Dorset, U.K.), was used as protein standard, and the change in absorbance at 595 nm with increasing concentrations of BSA is described by equation A1.1 and shown in figure A1.1. Protein assays are subject to errors of ±7 %.

$$\text{Abs 595 nm} = 1.1 \text{ BSA protein units} \qquad \text{(A1.1)}$$

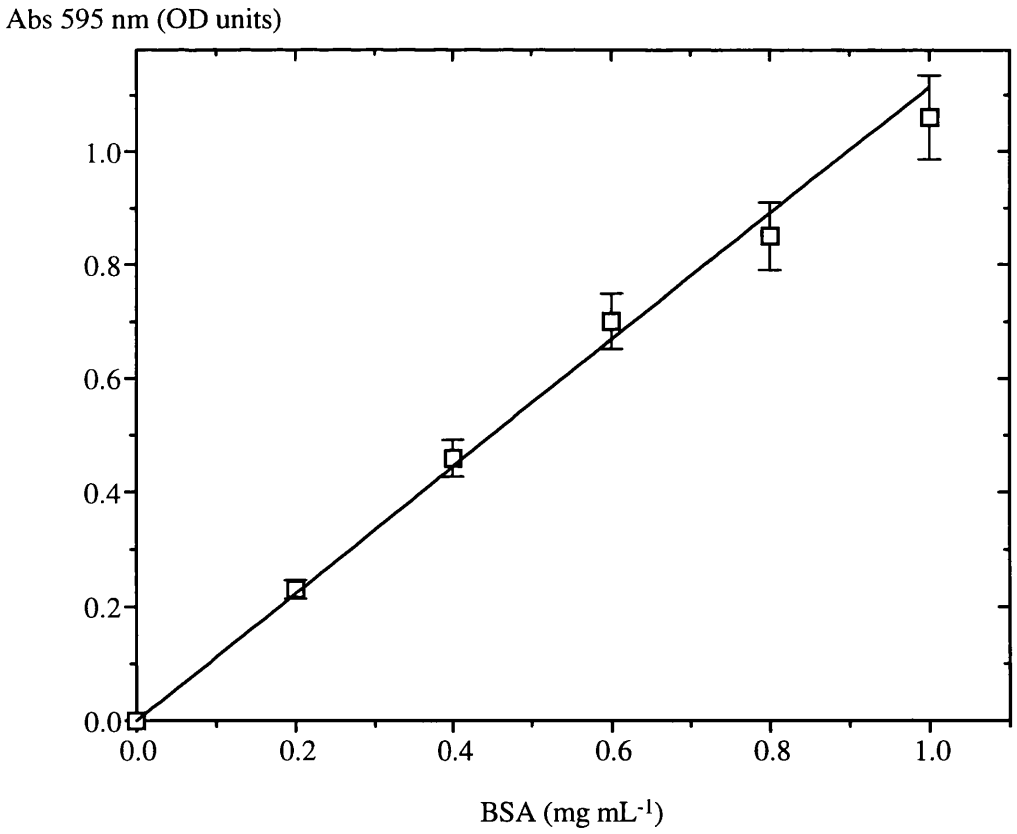

***Figure A1.1**: Protein calibration curve using bovine serum albumin solution as standard.*

Although the protein assay is simple and highly detectable, it does possess some drawbacks. The dye binding response varies with different proteins, and BSA is regarded as a poor standard for most proteins since it gives much higher colour changes. Thus, the protein quantities obtained should be expressed as 'serum albumin units', rather than absolute amounts. When proteins bind to the dye, the absorbance maximum shifts from 465 nm for the dye in acidic solution to 595 nm for the protein-dye complex. This property means the standard curves for most proteins are non-linear as the spectra for the two different dye forms overlap. This problem can be averted by limiting the amount of protein in the sample to that corresponding to the linear part of the standard curve, or plotting the results on log scales, or even measuring the ratio of absorbencies at 595 and 465 nm. Several common laboratory substances are known to have small but detectable effects on the protein assay, but corrections for absorbencies due to colour changes only can be achieved by 'blanking'. All assays were performed in plastic cuvettes.

A1.2 Alcohol dehydrogenase assay

The reduction of NAD^+ to NADH forms the basis of the alcohol dehydrogenase (ADH) activity assay. NADH absorbs light at a wavelength of 340 nm, and the activity of ADH can be monitored by measuring the increase in absorbance at this wavelength. Sigma ADH (Sigma Chemical Company Ltd., Dorset, U.K.) was used as standard for ADH assays. Solutions of Sigma ADH were prepared by dissolving known quantities of lyophilised ADH in phosphate buffer (100 mM KH_2PO_4, pH 6.5). ADH activity assays were performed according to the method of Bergmeyer (1983), as described in section 2.3.1.2. ADH activity measurements are subject to a ± 10 % error.

APPENDIX A2 Stability of yeast alcohol dehydrogenase

A2.1 Introduction

Product stability in biotechnology recovery processes is crucial for high product recovery levels. Several factors may affect product stability including physical and chemical factors such as temperature, pH, chemical additives, and also biological factors such as proteolytic action. This section examines the stability of yeast alcohol dehydrogenases in phosphate buffer (100 mM KH_2PO_4, pH 6.5) stored at 4°C over a period of 3 days.

A2.2 Results

Yeast alcohol dehydrogenases (ADH) are multimeric intracellular isoenzymes located in the cytoplasm and mitochondria of yeast cells. ADH consists of four identical subunits. Each subunit contains a zinc atom at its catalytic site which is necessary for enzyme activity. The isoelectric point of the enzymatically active form of ADH (ADH I) is 5.4. The enzyme is unstable outside the pH range of 6.0-9.0. ADH has a high specificity for ethanol, oxidising the alcohol to an aldehyde in the presence of the coenzyme nicotinamide adenine dinucleotide (NAD^+). Using photon correlation spectroscopy, the diameter of discrete ADH molecules has been estimated as 7.6 nm by Bowen *et al* (1995).

Figure A2.1 shows the stability of ADH in phosphate buffer (100 mM KH_2PO_4, pH 6.5) at 4°C. Yeast homogenate samples were collected and prepared for spectrophotometric analysis as described in section 2.3.1. The prepared samples were stored in a cold cabinet at 4°C, and assays were repeated every 24 h for 3 days. The original undiluted samples were also stored in the cold cabinet, and ADH activity measured over 3 days. At very low concentrations, the decrease in ADH activity is adequately represented by first order decay kinetics.

$$ADH_{activity} = ADH_{initial}\, e^{-k\,t} \qquad \text{(A2.1)}$$

where $ADH_{initial}$ is the initial alcohol dehydrogenase activity

k is the rate constant

t is the time

At higher concentrations, the degradation rate of ADH activity is initially significant but plates out after ~ 20 h.

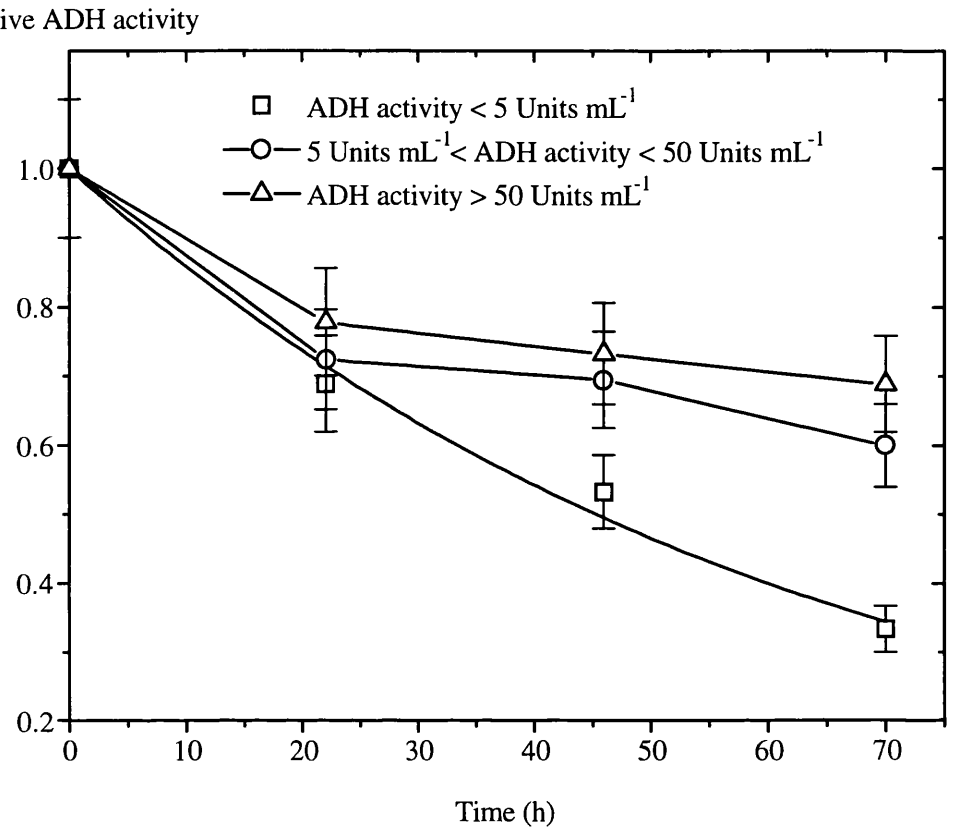

***Figure A2.1**: Stability of yeast alcohol dehydrogenase in phosphate buffer (100 mM KH_2PO_4, pH 6.5).*

A2.3 Discussion

There is a concentration dependence of the degradation rate of ADH in phosphate buffer (100 mM KH_2PO_4, pH 6.5) stored at 4°C. The half life of ADH in phosphate buffer (100 mM KH_2PO_4, pH 6.5) at 4°C is estimated at ~ 45 hr for ADH activity ≤ 5 units mL^{-1}. At higher concentrations, the initial degradation rate is significant but is much reduced after ~ 20 h. This suggests that the degradation rate may be limited by saturation effects at higher concentrations. No mechanism for the degradation of ADH is available in the literature.

The degradation rate of ADH activity will be important for experiments conducted over long periods, particularly gel filtration experiments. Figure A2.2 shows the pulse of Sigma ADH (450 units mL^{-1}) in phosphate buffer (100 mM KH_2PO_4, pH 6.5) on a Fast Protein Liquid Chromatography (FPLC) system using Superose 12 prep grade media (Amersham-Pharmacia Biotech, Hertfordshire, U.K.). Fractions, 2 mL, have been collected and ADH assays performed on each fraction. ADH is eluted after ~ 8 hr. A Gaussian distribution describes the pulse of ADH, and the activity of ADH is represented by the area under the curve.

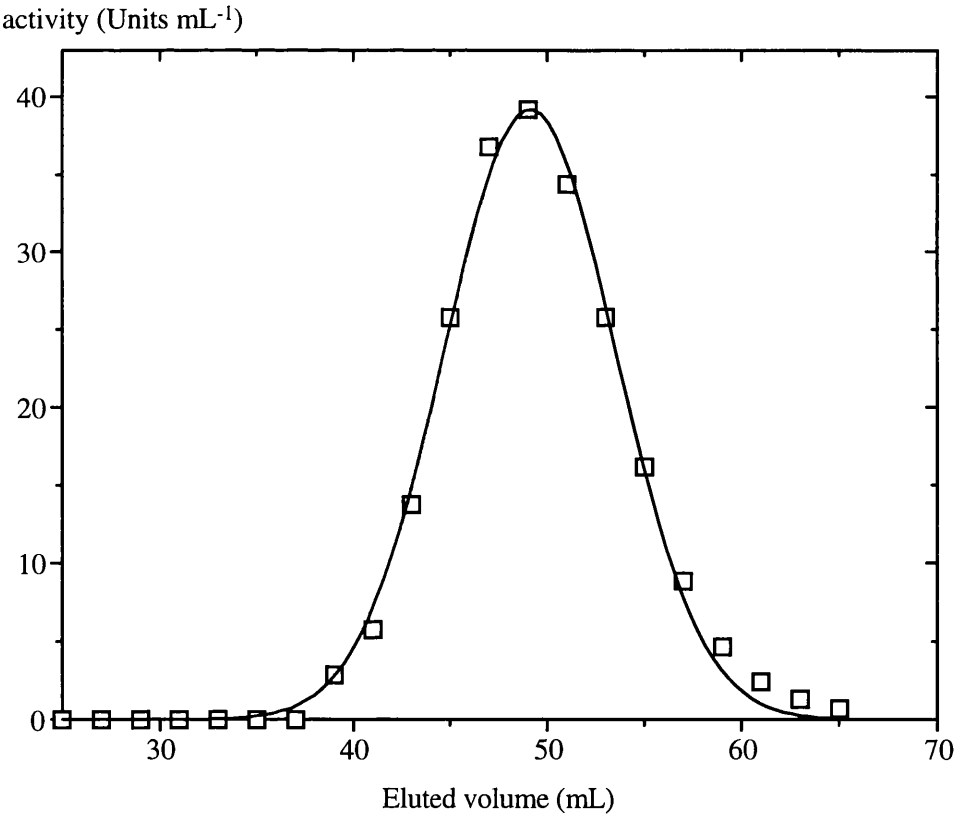

***Figure A2.2**: Sigma ADH pulse on a Superose 12 prep grade gel permeation column*

The activity of ADH, represented by the area under the curve, is estimated at ~ 430 units mL^{-1}.

A2.4 Conclusions

The degradation rate of ADH activity in phosphate buffer (100 mM KH_2PO_4, pH 6.5) stored at 4°C has been measured for a range of ADH concentrations. The rate is significant at very low concentrations of ADH in solution. At higher ADH concentrations, the degradation rate is much reduced and, over a period of ~ 10 h, has limited effect on assay results.

APPENDIX A3 Ceramic membrane elements

A3.1 Introduction

Porous ceramic tubes are currently in use for a wide range of filtration, diffusion and aeration applications. The advantages of ceramic filtration include high resistance to temperature and pressure, high stability in organic solvents and over a wide pH range, insensitivity to bacterial action, and they can be steamed sterilised or chemically sterilised. These properties coupled with consistent pore size distributions and the possibility of processing highly viscous fluids make ceramic filtration attractive for use in the bioprocess industries.

A3.2 Properties of ceramic membrane elements

Ceramic membrane elements of nominal pore sizes equivalent to 0.2 μm, 0.8 μm and 1.4 μm were used for experimental work. Figure A3.1 shows the cumulative pore size distributions of the membrane elements obtained from the manufacturer, Fairey Industrial Ceramics Ltd., Staffordshire, U.K. The membranes consist of a coarse-pore alumina substrate of a mean pore size of ~ 3.5 μm. The substrate is coated with a fine-pore α-alumina layer which acts as the membrane with a porosity of ~ 0.35. The membrane elements were of tubular configuration with 0.006 m internal diameter and 0.25 m length.

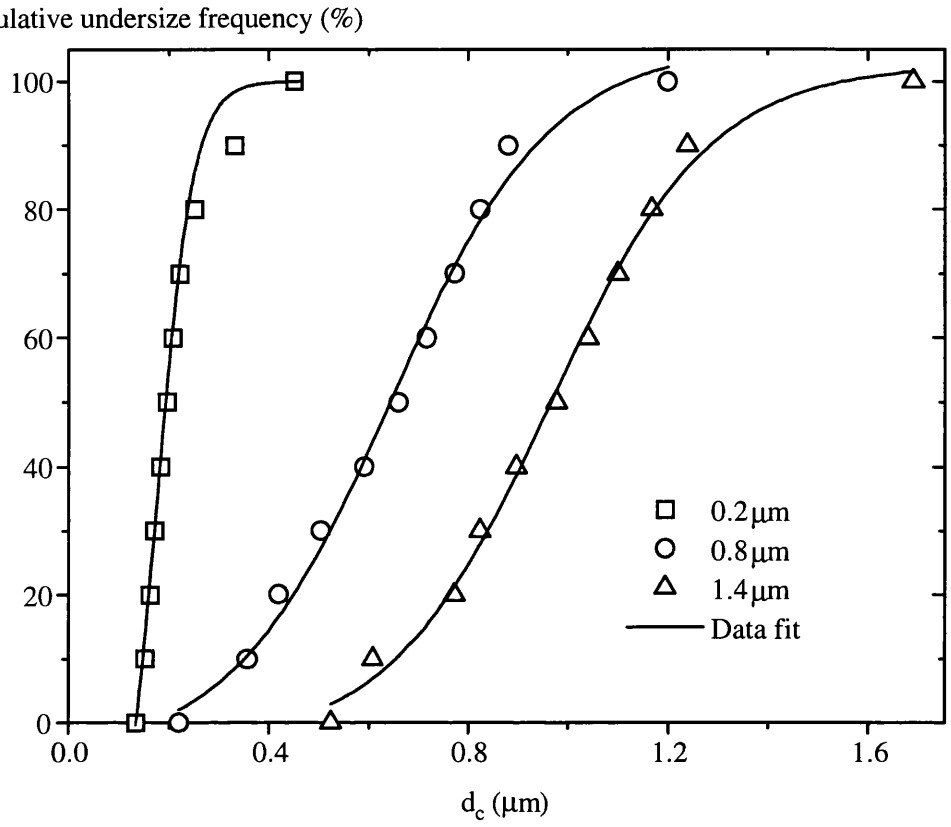

***Figure A3.1**: Ceramic membrane cumulative pore size distributions.*

Using Gaussian fits, the mean pore sizes are estimated at 0.19 μm, 0.65 μm and 0.92 μm (Figure A3.2).

Pore size distribution

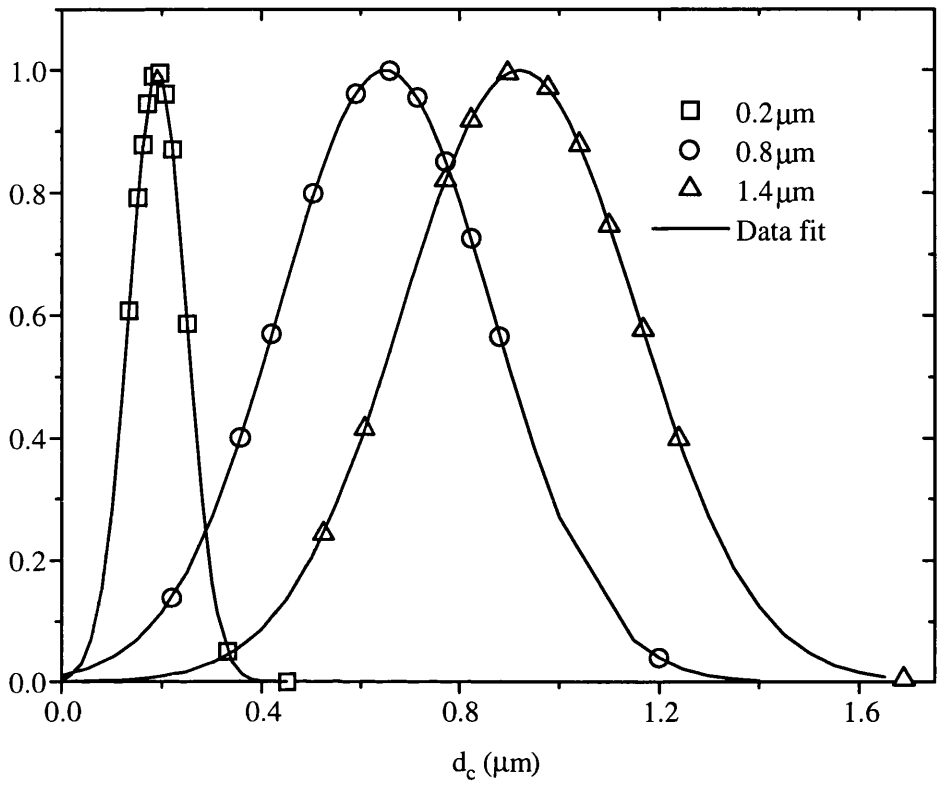

***Figure A3.2**: Ceramic membrane pore size distributions.*

Water flux measurements are also used to characterise membrane systems. Figure A3.3 shows the water flux rates as a function of the transmembrane pressure. There is a proportional increase in flux rates with the transmembrane pressure. The water flux rates are unaffected by the recirculation rate. However, the water flux rate for membranes of nominal pore size equivalent to 0.8 μm marginally exceed those for membranes of a nominal pore size equivalent to 1.4 μm. Assuming the porosity remains constant, as indicated by the manufacturer, the water flux rates are also a function of the the number of pores m^{-2} and the membrane pore size. The number of pores m^{-2} can be computed using the Hagen-Poiseuille equation which describes fluid flow through a cylindrical tube.

$$Q = \frac{\pi n_p r_0^4 \Delta P}{8\mu L} \qquad \text{(A3.1)}$$

where n_p is the number of pores m^{-2}

r_0 is the pore radius

ΔP is the transmembrane pressure

μ is the viscosity of the permeate

L is the pore length

Q is the volumetric filtrate flux

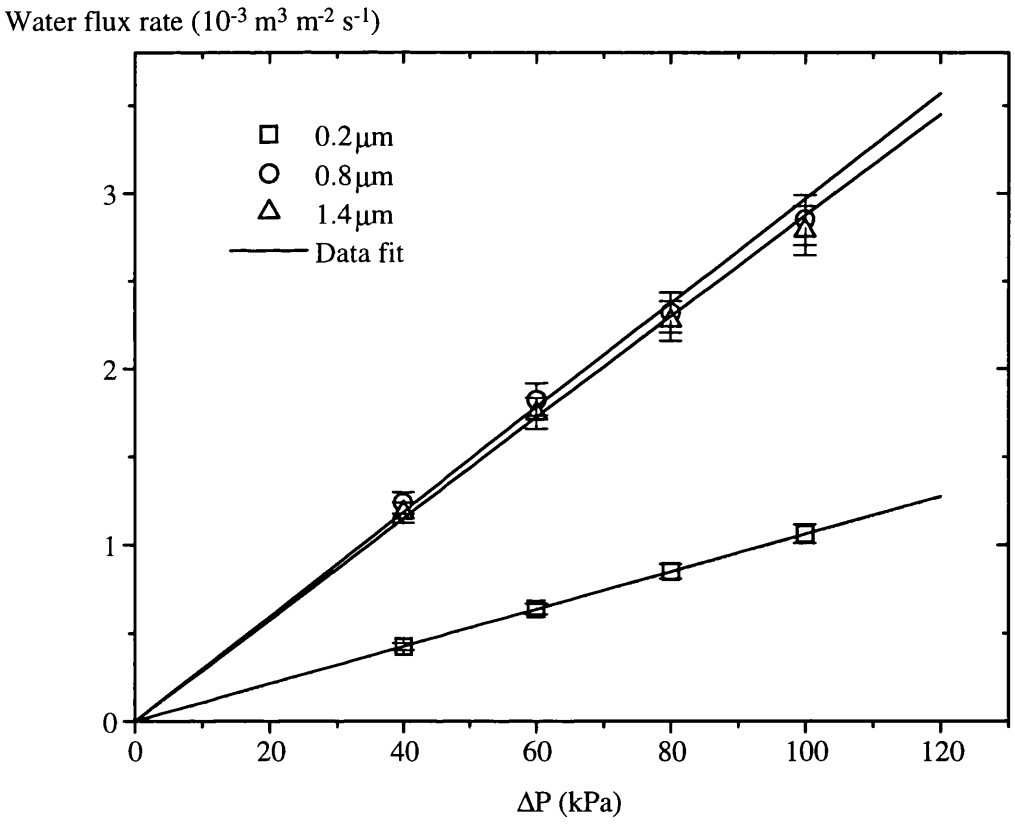

***Figure A3.3**: Water flux rates of ceramic membranes.*

The mean pore size has been used to compute the number of pores m^{-2}. n for membranes of nominal pore size equivalent to 0.2 μm, 0.8 μm and 1.4 μm are estimated as 4.7×10^7 m^{-2},4.0×10^6 m^{-2} and 1.2×10^6 m^{-2} respectively.

APPENDIX A4 Membrane Case study

A4.1 Introduction

Models are an essential component of any simulator. In this appendix, the models used in the case study are presented.

A4.2 Flux model

The Warren *et al* (1991) cake resistance model, describing the permeate flux rate of *Saccharomyces cerevisiae* whole cells as a function of the membrane operating conditions, was used for permeate flux prediction. The model is described by equation A4.1.

$$J = \frac{K_{Warren}\Delta P}{R_{membrane} + R_{cake}} \qquad \text{(A4.1)}$$

where K_{Warren} is the proportionality constant

ΔP is the transmembrane pressure

$R_{membrane}$ is the membrane resistance

R_{cake} is the cake resistance

The cake resistance is a function of the transmembrane pressure, the cell concentration and the shear rate.

$$R_{cake} = K_{cake}\frac{\Delta P^{0.76} C^{0.45}}{\gamma^{0.1}} \qquad \text{(A4.2)}$$

where K_{cake} is the cake resistance proportionality constant

C is the cell concentration

γ is the shear rate

A4.3 Transmission model

The retention coefficient is defined by equation A4.3.

$$\sigma = 1 - \frac{C_p}{C_b} \qquad \text{(A4.3)}$$

where σ is the retention coefficient

C_p is the instantaneous permeate concentration

C_b is the corresponding bulk concentration

A concentration based rejection model was used to describe the transmission characteristics of the membrane.

$$\sigma = \frac{A_0}{t_{decay}} + BC \qquad \text{(A4.4)}$$

where A_0 is the rejection coefficient at time zero and infinite dilution

B is the rejection coefficient constant

t_{decay} is the time decay variable

A4.4 Costing models

The cost correlations used were based on current vendor prices and utility prices. However, some degree of specialisation was adopted for the purposes of the case study.

A4.4.1 Fermentation cost

The fermenter cost was given by equation A4.5.

$$\frac{\text{Fermenter cost}}{\text{annum}} = \frac{C_{ferm} \times S_0}{W_{ferm}} \times V_f \times \left(\frac{V_f}{V_{f,0}}\right)^{\alpha} + (F \times V) \qquad \text{(A4.5)}$$

where C_{ferm} is the unit fermenter cost

W_{ferm} is the fermenter write-off time

S_0 is the scaling factor

V_f is the fermenter volume

F is the annual unit fermenter operating cost

α is a power constant

subscript 0 is the base case value

The fermenter broth cost was given by equation A4.6.

$$\frac{\text{Broth cost}}{\text{annum}} = B \times V_{broth} \qquad \text{(A4.6)}$$

where B is the unit broth cost

V_{broth} is the required broth volume

A4.4.2 Membrane cost

The membrane capital cost was given by equation A4.7.

$$\frac{\text{Capital cost}}{\text{annum}} = \frac{C_{mem} \times S_0}{W_{mem}} \times \left(\frac{L_{mem}}{L_{mem,0}}\right)^{\beta_{mem}} \times A_{mem} \times \left(\frac{A_{mem}}{A_{mem,0}}\right)^{\delta_{mem}} \qquad \text{(A4.7)}$$

where C_{mem} is the unit membrane cost

W_{mem} is the membrane write-off time

L_{mem} is the membrane module length

A_{mem} is the membrane area

β_{mem}, δ_{mem} are power constants

The membrane operating cost was given by equation A4.8.

$$\frac{\text{Operating cost}}{\text{annum}} = M \times \Delta P \times Q \times E_{lec} \times T_{mem} \times \left(\frac{A_{mem}}{A_{mem,0}}\right)^{\varepsilon_{mem}} + LAB \qquad \text{(A4.8)}$$

where M is the operating constant

ΔP is the transmembrane pressure

Q is the flow through the membrane module

E_{lec} is the unit cost of electricity

T_{mem} is the operating time per annum

LAB is the labour cost

ε_{mem} is a power constant

A4.4.3 Purification cost

The cost of purification after the membrane separation stage included the cost of an ultrafiltration step to reduce the product volume to a specified level and the cost of chromatographic separation. These equations are given below.

$$\frac{\text{Concentration cost}}{\text{annum}} = \frac{C_{mem} \times S_0 \times \left(V_{perm} - V_{prod}\right)}{W_{mem} \times UF_{flux}} + \left(U \times T_{conc}\right) \qquad \text{(A4.9)}$$

where V_{perm} is the recovered permeate volume

V_{prod} is the concentrated product volume

UF_{flux} is the permeate flux rate during concentration

U is the operating cost per unit concentration time

T_{conc} is the product concentration time

The purification cost was given by equation A4.10.

$$\frac{\text{Purification cost}}{\text{annum}} = K_{purity} \times V_{prod} \times f\left(P_{initial}\right) \qquad \text{(A4.10)}$$

where K_{purity} is the purification constant

$P_{initial}$ is the product purity to the purification stage

APPENDIX A5 SPEEDUP models

A5.1 Yeast homogenate model

```
TITLE
 Microfiltration for the recovery of soluble proteins

****

OPTIONS
 ROUTINES  SUPERDAE

 EXECUTION
  PRINTLEVEL=0
  TARGET=TERMINAL
  ITERATIONS=2000
  TIME_STEP=0.05
  INTERVALS=180
  RTE=OFF

****

DECLARE
 TYPE
  VOLUME=20:0.0:1500          UNIT="L"
  CONCENTRATION=1:-1E5:10E20   UNIT="g/L"
  VELOCITY=5:0.0:15.0         UNIT="m/s"
  PRESSURE=1:-30:30           UNIT="Bar"
  FLOWRATE=50:0:1000           UNIT="L/hr"
  FLUX=10:0:1000             UNIT="L/m2hr"
  MASS=1000:0:1E20            UNIT="g"
  WV_RATIO=1:0:500            UNIT="g/L"
  VV_RATIO=13:0:500           UNIT="mL/L"
  AREA=1:1E-5:100            UNIT="m2"
  NUMBER=10000:-1E5:4E8
  STRESS=50:0:1E5
  SHEAR=35000:0:1E10
  FRICTION_COEFF=1E-2:-1E5:1E5
  TANK_FACTOR=1:0:20
  VISCOSITY=2E-3:-1E3:1E3
  PERCENTAGE=0:-10:110
  REJECTION=0.6:0:1.2
  PARAMETERS=0.5:-5:5
  RESISTANCE=1:0:10
  DECAY=1:0:2
  TRANSFER=1E-4:-1:1
  LMH_TRANSFER=20:0:1E5
  DIAMETER=0.1:-10:25
  DUMMY=0:-1:100

STREAM MAINSTREAM
 TYPE
```

```
CONCENTRATION,CONCENTRATION,CONCENTRATION,CONCENTRATION,CONCE
NTRATION,FLOWRATE

****

MODEL TANK

 SET
  FEED=100
  CELL_MASS=30
  CELL_DENSITY=1115
  DRY_WET_RATIO=0.3

 TYPE
  TANK_VOL,DI_VOLUME,CELL_VOL  AS    VOLUME
  CELL_CONC                AS    VV_RATIO
  PROD_IN,PROD_OUT,HMW_IN,HMW_OUT,
  MMW_IN,MMW_OUT,LMW_IN,LMW_OUT,
  C_IN,C_OUT               AS    CONCENTRATION
  CONC_FACTOR              AS    TANK_FACTOR
  Q_IN,Q_OUT,Q_FLUX,BUFFER    AS    FLOWRATE

 STREAM
  INPUT      PROD_IN,HMW_IN,MMW_IN,LMW_IN,C_IN,Q_FLUX
  OUTPUT     PROD_OUT,HMW_OUT,MMW_OUT,LMW_OUT,C_OUT,Q_OUT

 EQUATION
  $TANK_VOL=-Q_FLUX+BUFFER;
  CELL_VOL*CELL_DENSITY=1000*CELL_MASS*DRY_WET_RATIO;
  CELL_CONC=CELL_VOL*FEED/TANK_VOL;
  PROD_OUT=PROD_IN/(TANK_VOL-CELL_VOL);
  HMW_OUT=HMW_IN/TANK_VOL;
  MMW_OUT=MMW_IN/TANK_VOL;
  LMW_OUT=LMW_IN/TANK_VOL;
  CONC_FACTOR=FEED/TANK_VOL;
  $DI_VOLUME=BUFFER;
  IF DI_VOLUME>50 OR TANK_VOL>50 THEN
   BUFFER=0
  ELSE
   BUFFER=Q_FLUX
  ENDIF;
  C_OUT=FEED*CELL_MASS/TANK_VOL;
  Q_IN=Q_OUT;

****

MODEL MICROFILTRATION

 SET
  N=50
  TUBE_D=0.006
```

```
TUBE_L=0.75
DENSITY=1115
PI=3.14159
P_MAX=10
D_HOMOG=2.5E-13
D_ADH=3.54E-11
K=430745.93
V=4.413E-4
FEED_VOL=100

TYPE
U                    AS    VELOCITY
P_IN,P_OUT,P_DARCY,TMP     AS    PRESSURE
Q_IN,Q_FLUX              AS    FLOWRATE
FLUX,FLUX_ONE,FLUX_SS      AS    FLUX
TOT_VOL                AS    VOLUME
REYNOLDS               AS    NUMBER
STRESS                 AS    STRESS
SHEAR                  AS    SHEAR
CF                   AS    FRICTION_COEFF
AREA                 AS    AREA
C_IN,C_OUT             AS    CONCENTRATION
PROD_IN,PROD_OUT,PROD_CONC  AS    CONCENTRATION
HMW_IN,HMW_OUT,MMW_IN,MMW_OUT,
LMW_IN,LMW_OUT,HMW_CONC,
MMW_CONC,LMW_CONC          AS    CONCENTRATION
VISCOSITY,KIN_VIS          AS    VISCOSITY
SIGMA_PROD,SIGMA_HMW,
SIGMA_MMW,SIGMA_LMW,PSI_PROD AS    REJECTION
PROD_MASS,HMW_MASS,MMW_MASS,
LMW_MASS,CONT_MASS,PROD_INACT,
PROD_ACT,ACT_PROD,INACT_PROD AS    MASS
YIELD,ACT_YIELD            AS    PERCENTAGE
PROD_LEVEL,CONT_LEVEL,HMW_LEVEL,
MMW_LEVEL,LMW_LEVEL        AS    WV_RATIO
Y0,Y1                  AS    PARAMETERS
J,B                  AS    DECAY
K_PROD                 AS    TRANSFER
KM                   AS    LMH_TRANSFER
X,ABS                  AS    DIAMETER
DUM                  AS    DUMMY

STREAM
INPUT      PROD_IN,HMW_IN,MMW_IN,LMW_IN,C_IN,Q_IN
OUTPUT     PROD_OUT,HMW_OUT,MMW_OUT,LMW_OUT,C_OUT,Q_FLUX

EQUATION
VISCOSITY*1E3=1+V*C_IN'2;
U*AREA=Q_IN;
AREA=N*PI*TUBE_D*TUBE_L;
Q_FLUX=FLUX_SS*AREA;
IF C_IN<100 THEN
```

```
 X=0
ELSE
 X*133.33=C_IN-100
ENDIF;
IF DUM=0 THEN
 FLUX_SS=FLUX_ONE*ABS
ELSE
 FLUX_SS*((DUM*60)'B)=FLUX_ONE*ABS
ENDIF;
ABS=1-(1-(1-X)'2)'2;
$DUM=1;
B=0.00105*((TMP*1E2)'0.823)*((C_IN/10)'0.285);
FLUX_ONE=1.85*FLUX;
C_IN=C_OUT;
REYNOLDS*VISCOSITY=DENSITY*U*TUBE_D;
IF REYNOLDS<2000 THEN
 CF=65.795/REYNOLDS
ELSE
 CF=0.22*(REYNOLDS'-0.25)
ENDIF;
2*STRESS=DENSITY*CF*U'2;
SHEAR*VISCOSITY=STRESS;
P_DARCY*1E5*TUBE_D=2*CF*TUBE_L*DENSITY*U'2;
P_IN=P_OUT+P_DARCY;
IF P_DARCY<P_MAX THEN
 $U=0
ELSE
 P_MAX*1E5*TUBE_D=2*CF*TUBE_L*DENSITY*U'2
ENDIF;
2*TMP=P_IN+P_OUT;
150*EXP(FLUX/KM)=700;
KM*(TUBE_D'0.2)*(KIN_VIS'0.47)=K*(U'0.8)*(D_HOMOG'0.67);
KIN_VIS*DENSITY=VISCOSITY;
K_PROD*(TUBE_D'0.2)*(KIN_VIS'0.47)=0.0109*(U'0.8)*(D_ADH'0.67);
IF K_PROD>1.387E-5 THEN
 PSI_PROD=1
ELSE
 PSI_PROD=(1-(1-72096*K_PROD)'2)'2
ENDIF;
(SIGMA_PROD-Y0)*(1+EXP(-5.6))=Y1-Y0;
SIGMA_PROD=1-PROD_CONC/PROD_IN;
Y1=1-0.94463*PSI_PROD;
Y1=-1.536*Y0;
(SIGMA_HMW-Y0)*(1+EXP(-4.72))=Y1-Y0;
SIGMA_HMW=1-HMW_CONC/HMW_IN;
(SIGMA_MMW-Y0)*(1+EXP(-2.4))=Y1-Y0;
SIGMA_MMW=1-MMW_CONC/MMW_IN;
(SIGMA_LMW-Y0)*(1+EXP(-6))=Y1-Y0;
SIGMA_LMW=1-LMW_CONC/LMW_IN;
$J*1000=-LOG(P_IN/P_MAX+1)*J;
$PROD_MASS=FLUX_SS*AREA*PROD_CONC;
$HMW_MASS=FLUX_SS*AREA*HMW_CONC;
```

```
 $MMW_MASS=FLUX_SS*AREA*MMW_CONC;
 $LMW_MASS=FLUX_SS*AREA*LMW_CONC;
 PROD_OUT=10*FEED_VOL-PROD_MASS;
 PROD_INACT=10*FEED_VOL-PROD_ACT;
 HMW_OUT=0.85*FEED_VOL-HMW_MASS;
 MMW_OUT=0.025*FEED_VOL-MMW_MASS;
 LMW_OUT=0.6*FEED_VOL-LMW_MASS;
 $PROD_ACT*1010=-LOG(2)*PROD_ACT;
 $TOT_VOL=FLUX_SS*AREA;
 ACT_PROD*10*FEED_VOL=PROD_ACT*PROD_MASS;
 YIELD=PROD_MASS*100/(10*FEED_VOL);
 ACT_YIELD=ACT_PROD*100/(10*FEED_VOL);
 INACT_PROD=PROD_MASS-ACT_PROD;
 CONT_MASS=HMW_MASS+MMW_MASS+LMW_MASS+INACT_PROD;
 CONT_LEVEL*TOT_VOL=CONT_MASS;
 PROD_LEVEL*TOT_VOL=ACT_PROD;
 HMW_LEVEL*TOT_VOL=HMW_MASS;
 MMW_LEVEL*TOT_VOL=MMW_MASS;
 LMW_LEVEL*TOT_VOL=LMW_MASS;

****

CONDITIONS
 IF TANK.C_IN>540 OR T>8 THEN PRINT
200,MICROFILTER.AREA,MICROFILTER.Q_IN;
 IF TANK.C_IN>540 OR T>8 THEN PRINT 300,MICROFILTER.TMP;
 IF TANK.C_IN>540 OR T>8 THEN PRINT 400,MICROFILTER.TOT_VOL,
  MICROFILTER.P_DARCY;
 IF TANK.C_IN>540 OR T>8 THEN PRINT 500,MICROFILTER.PROD_MASS,
  MICROFILTER.CONT_MASS;
 IF TANK.C_IN>540 OR T>8 THEN PRINT
600,MICROFILTER.ACT_PROD,TANK.C_IN;
 IF TANK.C_IN>540 OR T>8 THEN PRINT 1000,MICROFILTER.PROD_LEVEL,
  MICROFILTER.PROD_IN,MICROFILTER.VISCOSITY;
 IF TANK.C_IN>540 OR T>8 THEN PRINT 1100,MICROFILTER.HMW_LEVEL,
  MICROFILTER.MMW_LEVEL,MICROFILTER.LMW_LEVEL;
 IF TANK.C_IN>540 OR T>8 OR MICROFILTER.YIELD>99.8 THEN STOP 100,T;

 CODE
C
100  FORMAT(/'RUN TERMINATED AT TIME  ',F4.2,' HOURS'/)
1100 FORMAT(/'[HMW]=',F6.2,' g/L,[MMW]=',F6.2,' g/L,[LMW]=',F6.2,' g/L'/)
500  FORMAT(/'TOTAL PRODUCT MASS = ',F6.2,' g, CONTAMINANT MASS = ',F6.2,'
g'/)
600  FORMAT(/'ACTIVE PRODUCT MASS = ',F6.2,' g, [TANK]=',F6.2,' g/L'/)
200  FORMAT(/'AREA = ',F5.2,' SQ M, VOLUMETRIC FLOWRATE =',F6.2,' L/hr'/)
300  FORMAT(/'TMP = ',F5.2,' Bar'/)
400  FORMAT(/'PERMEATE VOLUME = ',F6.2,' L, PRESSURE DROP = ',F6.2,' Bar'/)
1000 FORMAT(/'[P]=',F6.2,' g/L,[R]=',F6.2,' g/L,VIS =',F5.3,' Ns/m2'/)
C
$ENDCODE
```

```
****

FLOWSHEET
        OUTPUT OF TANK IS INPUT OF MICROFILTER
        OUTPUT OF MICROFILTER IS INPUT OF TANK

****

UNIT TANK IS A TANK

****

UNIT MICROFILTER  IS A MICROFILTRATION

****

OPERATION

 SET
  WITHIN MICROFILTER
   P_OUT=0

 INITIAL
  WITHIN MICROFILTER
   U=7.1
   PROD_MASS=0
   HMW_MASS=0
   MMW_MASS=0
   LMW_MASS=0
   TOT_VOL=0
   PROD_ACT=1000
   J=1
   DUM=0

 INITIAL
  WITHIN TANK
   TANK_VOL=100
   DI_VOLUME=0

 PRESET
  WITHIN TANK
   BUFFER=0.0{:0.0:50.0}
   C_OUT=50{:0:1000}

  WITHIN MICROFILTER
   Q_FLUX=50{:0:1000}

****
REPORT FILTER
 Fields
  &1=MICROFILTER.YIELD;
  &2=MICROFILTER.TOT_VOL;
```

```
 &3=MICROFILTER.FLUX_SS;
 &4=MICROFILTER.C_IN;
 &5=MICROFILTER.SIGMA_PROD;
 &6=MICROFILTER.VISCOSITY;

 Display
 | YIELD = %%%%%%%%  PERCENT    VOLUME = %%%%%%%%  L      |
 | FLUX  = %%%%%%%%  L/m2h      CONC   = %%%%%%%%  g/L    |
 | REJECTION = %%%%%%%%%%       VISCOSITY = %%%%%%%%%%% Pa s|
****
```

A5.2 Membrane case study

A5.2.1 Filtration model

```
TITLE
 Microfiltration for the recovery of soluble proteins

****

OPTIONS
 ROUTINES  SUPERDAE

 EXECUTION
  PRINTLEVEL=0
  TARGET=TERMINAL
  ITERATIONS=2000
  TIME_STEP=0.05
  INTERVALS=180
  RTE=OFF

****

DECLARE
 TYPE
  VOLUME=20:0.0:1500          UNIT="L"
  CONCENTRATION=1:-1:10E10    UNIT="g/L"
  VELOCITY=5:0.0:15.0         UNIT="m/s"
  PRESSURE=1:-30:30           UNIT="Bar"
  FLOWRATE=50:0:1000          UNIT="L/hr"
  FLUX=10:0:1000              UNIT="L/m2hr"
  MASS=100:0:1200             UNIT="g"
  WV_RATIO=1:0:50             UNIT="g/L"
  VV_RATIO=13:0:500           UNIT="mL/L"
  AREA=1:1E-5:100             UNIT="m2"
  NUMBER=10000:0:4E8
  STRESS=50:0:1E5
  SHEAR=35000:0:1E10
  FRICTION_COEFF=1E-2:0:1
  TANK_FACTOR=1:0:20
  VISCOSITY=2E-3:0:1
  PERCENTAGE=0:-10:110
  REJECTION=0.6:0:1.2
  RESISTANCE=1:0:10
  DECAY=1:0:2
  DIAMETER=1:0:25

STREAM MAINSTREAM
 TYPE

CONCENTRATION,CONCENTRATION,CONCENTRATION,CONCENTRATION,CONCE
NTRATION,FLOWRATE
```

```
****

MODEL TANK

 SET
  FEED=100
  CELL_MASS=50
  CELL_DENSITY=1110
  DRY_WET_RATIO=0.3

 TYPE
  TANK_VOL,DI_VOLUME,CELL_VOL  AS    VOLUME
  CELL_CONC                AS    VV_RATIO
  PROD_IN,PROD_OUT,HMW_IN,HMW_OUT,
  MMW_IN,MMW_OUT,LMW_IN,LMW_OUT,
  C_IN,C_OUT               AS    CONCENTRATION
  CONC_FACTOR              AS    TANK_FACTOR
  Q_IN,Q_OUT,Q_FLUX,BUFFER    AS    FLOWRATE

 STREAM
  INPUT      PROD_IN,HMW_IN,MMW_IN,LMW_IN,C_IN,Q_FLUX
  OUTPUT     PROD_OUT,HMW_OUT,MMW_OUT,LMW_OUT,C_OUT,Q_OUT

 EQUATION
  $TANK_VOL=-Q_FLUX+BUFFER;
  CELL_VOL*CELL_DENSITY=1000*CELL_MASS*DRY_WET_RATIO;
  CELL_CONC=CELL_VOL*FEED/TANK_VOL;
  PROD_OUT=PROD_IN/(TANK_VOL-CELL_VOL);
  HMW_OUT=HMW_IN/TANK_VOL;
  MMW_OUT=MMW_IN/TANK_VOL;
  LMW_OUT=LMW_IN/TANK_VOL;
  CONC_FACTOR=FEED/TANK_VOL;
  $DI_VOLUME=BUFFER;
  IF DI_VOLUME>50 OR TANK_VOL>50 THEN
   BUFFER=0
  ELSE
   BUFFER=Q_FLUX
  ENDIF;
  C_OUT=FEED*CELL_MASS/TANK_VOL;
  Q_IN=Q_OUT;

****

MODEL MICROFILTRATION

 SET
  N=10
  TUBE_D=0.02
  TUBE_L=1
  DENSITY=1110
  PI=3.14159
  C_MAX=250
```

```
P_MAX=10
FEED_VOL=100
UF_FLUX=30

TYPE
 U                    AS     VELOCITY
 P_IN,P_OUT,P_DARCY,TMP,P_PERM,
 P_DROP               AS     PRESSURE
 Q_IN,Q_FLUX          AS     FLOWRATE
 FLUX                 AS     FLUX
 TOT_VOL              AS     VOLUME
 REYNOLDS             AS     NUMBER
 STRESS               AS     STRESS
 SHEAR                AS     SHEAR
 CF                   AS     FRICTION_COEFF
 AREA                 AS     AREA
 C_IN,C_OUT           AS     CONCENTRATION
 PROD_IN,PROD_OUT,PROD_CONC   AS     CONCENTRATION
 HMW_IN,HMW_OUT,MMW_IN,MMW_OUT,
 LMW_IN,LMW_OUT,HMW_CONC,
 MMW_CONC,LMW_CONC    AS     CONCENTRATION
 VISCOSITY            AS     VISCOSITY
 SIGMA_PROD,SIGMA_HMW,
 SIGMA_MMW,SIGMA_LMW  AS     REJECTION
 PROD_MASS,HMW_MASS,MMW_MASS,
 LMW_MASS,CONT_MASS,PROD_INACT,
 PROD_ACT,ACT_PROD,INACT_PROD AS     MASS
 YIELD,ACT_YIELD      AS     PERCENTAGE
 PROD_LEVEL,CONT_LEVEL,HMW_LEVEL,
 MMW_LEVEL,LMW_LEVEL  AS     WV_RATIO
 J                    AS     DECAY
 PIPE_D               AS     DIAMETER

STREAM
 INPUT      PROD_IN,HMW_IN,MMW_IN,LMW_IN,C_IN,Q_IN
 OUTPUT     PROD_OUT,HMW_OUT,MMW_OUT,LMW_OUT,C_OUT,Q_FLUX

EQUATION
 VISCOSITY*1E3*1250=C_IN'2;
 U*AREA=Q_IN;
 AREA=N*PI*TUBE_D*TUBE_L;
 Q_FLUX=FLUX*AREA;
 C_IN=C_OUT;
 REYNOLDS*VISCOSITY=DENSITY*U*TUBE_D;
 IF REYNOLDS<800 THEN
  CF=16/REYNOLDS
 ELSE
  IF REYNOLDS<4000 THEN
   CF=0.0078233*REYNOLDS'(108.48/REYNOLDS)
  ELSE
   CF=0.0792*(REYNOLDS'-0.25)
  ENDIF
```

```
ENDIF;
2*STRESS=DENSITY*CF*U'2;
SHEAR*VISCOSITY=STRESS;
P_DARCY*1E5*TUBE_D=2*CF*TUBE_L*DENSITY*U'2;
P_IN=P_OUT+P_DARCY;
(0.5*PIPE_D)'2=4*AREA;
P_DROP*1E5*PIPE_D=2*CF*DENSITY*U'2;
IF P_DARCY+P_DROP<5 THEN
 $P_IN=0
ELSE
 P_OUT=P_DROP
ENDIF;
IF P_DARCY<P_MAX THEN
 $U=0
ELSE
 P_MAX*1E5*TUBE_D=2*CF*TUBE_L*DENSITY*U'2
ENDIF;
2*(TMP+P_PERM)=P_IN+P_OUT;
FLUX*(SHEAR'-0.1)*(C_IN'0.45)=5*J*(TMP*1E5)'0.24;
SIGMA_PROD=0.5/J+0.01*C_IN/C_MAX;
SIGMA_PROD=1-PROD_CONC/PROD_IN;
SIGMA_HMW=0.95+0.03*C_IN/C_MAX;
SIGMA_HMW=1-HMW_CONC/HMW_IN;
SIGMA_MMW=0.9+0.05*C_IN/C_MAX;
SIGMA_MMW=1-MMW_CONC/MMW_IN;
SIGMA_LMW=0.1/J+0.1*C_IN/C_MAX;
SIGMA_LMW=1-LMW_CONC/LMW_IN;
$J*10=-LOG(P_IN/P_MAX+1)*J;
$PROD_MASS=FLUX*AREA*PROD_CONC;
$HMW_MASS=FLUX*AREA*HMW_CONC;
$MMW_MASS=FLUX*AREA*MMW_CONC;
$LMW_MASS=FLUX*AREA*LMW_CONC;
PROD_OUT=10*FEED_VOL-PROD_MASS;
PROD_INACT=10*FEED_VOL-PROD_ACT;
HMW_OUT=0.7*FEED_VOL-HMW_MASS;
MMW_OUT=1.5*FEED_VOL-MMW_MASS;
LMW_OUT=0.8*FEED_VOL-LMW_MASS;
$PROD_ACT*12=-LOG(2)*PROD_ACT;
$TOT_VOL=FLUX*AREA;
ACT_PROD*10*FEED_VOL=PROD_ACT*PROD_MASS;
YIELD=PROD_MASS*100/(10*FEED_VOL);
ACT_YIELD=ACT_PROD*100/(10*FEED_VOL);
INACT_PROD=PROD_MASS-ACT_PROD;
CONT_MASS=HMW_MASS+MMW_MASS+LMW_MASS+INACT_PROD;
CONT_LEVEL*TOT_VOL=CONT_MASS;
PROD_LEVEL*TOT_VOL=ACT_PROD;
HMW_LEVEL*TOT_VOL=HMW_MASS;
MMW_LEVEL*TOT_VOL=MMW_MASS;
LMW_LEVEL*TOT_VOL=LMW_MASS;

****
```

```
CONDITIONS
  IF TANK.C_IN>250 OR T>8 THEN PRINT
200,MICROFILTER.AREA,MICROFILTER.Q_IN;
  IF TANK.C_IN>250 OR T>8 THEN PRINT
300,MICROFILTER.TMP,MICROFILTER.P_PERM;
  IF TANK.C_IN>250 OR T>8 THEN PRINT 400,MICROFILTER.TOT_VOL,
   MICROFILTER.P_DARCY;
  IF TANK.C_IN>250 OR T>8 THEN PRINT 500,MICROFILTER.PROD_MASS,
   MICROFILTER.CONT_MASS;
  IF TANK.C_IN>250 OR T>8 THEN PRINT
600,MICROFILTER.ACT_PROD,TANK.C_IN;
  IF TANK.C_IN>250 OR T>8 THEN PRINT 1000,MICROFILTER.PROD_LEVEL,
   MICROFILTER.PROD_IN,MICROFILTER.VISCOSITY;
  IF TANK.C_IN>250 OR T>8 THEN PRINT 1100,MICROFILTER.HMW_LEVEL,
   MICROFILTER.MMW_LEVEL,MICROFILTER.LMW_LEVEL;
  IF TANK.C_IN>250 OR T>8 THEN STOP 100,T;

  CODE
C
100   FORMAT(/'RUN TERMINATED AT TIME  ',F4.2,' HOURS'/)
200   FORMAT(/'AREA = ',F5.2,' SQ M, VOLUMETRIC FLOWRATE =',F6.2,' L/hr'/)
300   FORMAT(/'TMP = ',F5.2,' Bar, PERMEATE PRESSURE = ',F5.2,' Bar'/)
400   FORMAT(/'PERMEATE VOLUME = ',F6.2,' L, PRESSURE DROP = ',F6.2,' Bar'/)
500   FORMAT(/'TOTAL PRODUCT MASS = ',F6.2,' g, CONTAMINANT MASS = ',F6.2,'
g'/)
600   FORMAT(/'ACTIVE PRODUCT MASS = ',F6.2,' g, [TANK]=',F6.2,' g/L'/)
1000  FORMAT(/'[P]=',F6.2,' g/L,[R]=',F6.2,' g/L,VIS =',F5.3,' Ns/m2'/)
1100  FORMAT(/'[HMW]=',F6.2,' g/L,[MMW]=',F6.2,' g/L,[LMW]=',F6.2,' g/L'/)
C
$ENDCODE

****

FLOWSHEET
              OUTPUT OF TANK IS INPUT OF MICROFILTER
              OUTPUT OF MICROFILTER IS INPUT OF TANK

****

UNIT TANK IS A TANK

****

UNIT MICROFILTER  IS A MICROFILTRATION

****

OPERATION

 SET
  WITHIN MICROFILTER
   TMP=5
```

```
INITIAL
 WITHIN MICROFILTER
  P_IN=6
  U=7.1
  PROD_MASS=0
  HMW_MASS=0
  MMW_MASS=0
  LMW_MASS=0
  TOT_VOL=0
  PROD_ACT=1000
  J=1

INITIAL
 WITHIN TANK
  TANK_VOL=100
  DI_VOLUME=0

PRESET
 WITHIN TANK
  BUFFER=0.0{:0.0:50.0}
  C_OUT=50{:0:1000}

 WITHIN MICROFILTER
  P_DROP=0.1{:0:20}
  Q_FLUX=50{:0:1000}
```

A5.2.2 Costing model

```
TITLE
Costing Membrane Separation Unit

****

OPTIONS
 ROUTINES SUPERDAE

 EXECUTION
  PRINTLEVEL=0
  TARGET=TERMINAL
  ITERATIONS=1000

****

DECLARE
 TYPE
  COST=100:0:1E10
  COST_KG=10:0:1E6
  PUR_FAC=0.6:0:2
  SCALE_FAC=200:0:1E10
  PERCENTAGE=50:0:100

 STREAM MAINSTREAM
  TYPE
   NOTYPE

****

MODEL COST

 SET
  AREA=0.63
  TUBE_L=1
  TMP=2
  Q_IN=5.03
  FEED_VOL=100
  TOT_VOL=92.50
  ACT_PROD=584.17
  CONT_MASS=297.43
  PROD_MASS=789.74
  UF_FLUX=30

 TYPE
  MEM_COST,OP_COST,FERM_COST,BROTH_COST,
  CHROM_COST,UF_COST,TOT_FCOST,TOT_MCOST,
  TOT_CCOST,TOT_COST                AS    COST
  FERM,MEM,CHROM                    AS    PERCENTAGE
  INI_PURITY                  AS    PUR_FAC
  SCALE_FAC                    AS    SCALE_FAC
```

```
 COST_PRICE                    AS    COST_KG
 DUMMY_1,DUMMY_2                     AS    NOTYPE

STREAM
 INPUT       DUMMY_1
 OUTPUT      DUMMY_2

EQUATION
 MEM_COST=18*AREA*TUBE_L'-0.2*AREA'-0.1;
 IF OP_COST<8 THEN
  OP_COST=8
 ELSE
  OP_COST=TMP*Q_IN*AREA'0.2
 ENDIF;
 BROTH_COST=0.05*FEED_VOL;
 FERM_COST=20*FEED_VOL'-0.3;
 INI_PURITY*(CONT_MASS+PROD_MASS)=ACT_PROD;
 CHROM_COST=0.02*FEED_VOL*LOG(100*(1-INI_PURITY));
 IF TOT_VOL<100 THEN
  UF_COST=0
 ELSE
  UF_COST*4*UF_FLUX=20*(TOT_VOL-FEED_VOL)
 ENDIF;
 SCALE_FAC*ACT_PROD=1E5;
 TOT_FCOST=SCALE_FAC*(BROTH_COST+FERM_COST);
 TOT_MCOST=SCALE_FAC*(MEM_COST+OP_COST);
 TOT_CCOST=SCALE_FAC*(CHROM_COST+UF_COST);
 TOT_COST=TOT_FCOST+TOT_MCOST+TOT_CCOST;
 FERM*TOT_COST=TOT_FCOST*100;
 MEM*TOT_COST=TOT_MCOST*100;
 CHROM*TOT_COST=TOT_CCOST*100;
 COST_PRICE*100=TOT_COST;
 DUMMY_1=DUMMY_2;
****

FLOWSHEET
      FEED IS INPUT OF COST_MODEL
           OUTPUT OF COST_MODEL IS PRODUCT

****

UNIT COST_MODEL IS A COST

****

OPERATION

 SET
  WITHIN COST_MODEL
   DUMMY_1=1
```

NOMENCLATURE

Symbols

A	constant (equation 4.7)	-
A_0	rejection coefficient at time zero and infinite dilution	-
$a_{i\ (i = 1,...,4)}$	Reuss *et al.* (1978) model coefficient (equations 4.1, 5.1)	-
A_{mem}	membrane area	m^2
b	experimentally determined fouling index	-
B	unit broth cost	£ L^{-1}
C	concentration of retained species	g L^{-1}
C_b	bulk concentration of retained species	g L^{-1}
C_{ferm}	unit fermentor cost	£ L^{-1}
$CF(x_i)$	cumulative frequency	-
CF_1	extent of concentration during stage 1	-
CF_2	extent of concentration during stage 2	-
C_{mem}	unit membrane cost	£ L^{-1}
C_p	instantaneous permeate concentration	g L^{-1}
C_w	wall concentration of retained species	g L^{-1}
D	diffusion coefficient of retained species	m^2 s^{-1}
d_c	nominal membrane pore size	μm
DF	extent of diafiltration	-
d_m	inner membrane diameter	m
d_p	particle diameter	m
dx	constant (equation 5.5)	-
e	kinematic viscosity exponent	-
E	enzymatic activity	mL^{-1}
E_F	main effect of factor F	-
E_{lec}	unit cost of electricity	£ kWh^{-1}
f	constant (equation 5.4)	-
F	annual unit fermenter operating cost	£ L^{-1} yr^{-1}
Ferm	percent product cost attributable to the fermentation stage	
g	constant (equation 5.6)	-
h	fouling layer thickness	m
H_{mw}	cumulative high molecular weight concentration in the permeate	g L^{-1}
i	i^{th} observation in the sample	-
J_t	permeate flux rate at time t	L m^{-2} h^{-1}
k	constant (equations 2.2, 2.3, 2.4, 2.5)	-
K	proportionality constant (equation 2.11)	-

K_{av}	apparent partition coefficient	-
k_b	Boltzman constant	$J\ K^{-1}$
K_{cake}	cake resistance proportionality constant (equation A4.2)	-
k_f	foulant removal rate constant (equations 2.6, 2.8)	-
k_i	mass transfer coefficient of protein species i (equation 5.4)	$m^3\ m^{-2}\ s^{-1}$
k_m	mass transfer coefficient	$m^3\ m^{-2}\ s^{-1}$
K_{Warren}	proportionality constant (equation A4.1)	-
L	column length	m
LAB	labour cost	£ yr^{-1}
L_{mem}	membrane module length	m
L_{mw}	cumulative low molecular weight concentration in the permeate	$g\ L^{-1}$
M	membrane operating constant (equation A4.8)	-
Mem	percent product cost attributable to the membrane stage	
M_{mw}	cumulative medium molecular weight concentration in permeate	$g\ L^{-1}$
$M_{w,i}$	molecular weight of species i	Da
n	number of experiments	-
N	number of theoretical plates	m^{-1}
n_i	number of observations in sample	-
n_p	number of pores	-
p	power law index of suspension	-
P	wt % concentration of protein	-
P_{inlet}	inlet pressure to membrane module	bar
Pr	product cost	£ kg^{-1}
Prod	cumulative product concentration in the permeate	$g\ L^{-1}$
Pur	percent product cost attributable to the purification stage	
Q	volumetric flowrate	$m^3\ s^{-1}$
r	fouled pore radius	m
R	effective pore radius	m
r_0	unfouled pore radius	m
r_p	radius of diffusing particle	m
R_{cake}	cake resistance to permeate flow	m^{-1}
$R_{F,i}$	response value of factor F at the 'high' setting	-
$R_{fouling}$	resistance to permeate flow due to irreversible fouling	m^{-1}
$R_{F,j}$	response value of factor F at the 'low' setting	-
$R_{membrane}$	membrane resistance to permeate flow	m^{-1}
R_{total}	total resistance to permeate flow	m^{-1}
S	excess solute	$g\ m^{-2}$
S_0	scaling factor	-

t	time	min
T	absolute temperature	K
T_{conc}	product concentration time	h
t_{decay}	time decay variable	-
T_{mem}	total membrane operating time	hr
U	recirculation rate	$m\ s^{-1}$
UF_{flux}	permeate flux rate during concentration	$L\ m^{-2}\ h^{-1}$
u_0	velocity at the centre of the pore	$m\ s^{-1}$
U_{pur}	unit operating cost per unit concentration time	$£\ h^{-1}$
$u(r)$	velocity at a distance r from centre of pore	$m\ s^{-1}$
V	filtrate volume	L
V_{broth}	required broth volume	L
V_e	elution volume for a given species	mL
V_f	fermenter volume	L
V_o	elution volume of molecules confined to the mobile phase	mL
V_p	volume of material entering a pore	L
V_{perm}	recovered permeate volume	L
V_{prod}	concentrated product volume	L
V_t	total volume of the packed bed	mL
W_{ferm}	fermenter write-off time	yr
W_{mem}	membrane write-off time	yr
w_n	peak width at half height (equation 5.8)	m
x_0	constant (equation 5.5)	-
x_i	measured variable	-
y	distance from the membrane surface	m
$y_{j,i\ (j = 0,1)}$	model parameter (equation 5.5)	-
$\frac{\Delta A}{\Delta t}$	rate of change of absorbance	min^{-1}
$\frac{dC}{dy}$	concentration gradient	$g\ L^{-1}\ m^{-1}$

Greek symbols

α	power constant (equation A4.5)	-
β	intercept term	-
$\beta_{i\ (i = 1,...,8)}$	model coefficients (equation 4.5)	-
β_{mem}	power constant (equation A4.7)	-
χ	membrane sieving coefficient	-
χ_i	membrane sieving coefficient of protein species i (equation 5.4)	-
δ	boundary layer thickness	m
δ_{cake}	cake thickness	m
δ_{mem}	power constant	-
$\delta_{membrane}$	membrane thickness	m
ΔP	transmembrane pressure	$N\ m^{-2}$
ε	cake void fraction	-
ε_{mem}	power constant (equation A4.8)	-
ε_{340}	extinction coefficient	$cm^2\ \mu mol^{-1}$
ϕ	volume fraction of particles	-
γ	shear rate	s^{-1}
λ	particle-to-pore size ratio	-
μ	viscosity of the permeate	$N\ s\ m^{-2}$
μ_L	viscosity of the suspending liquid	$N\ s\ m^{-2}$
μ_P	viscosity of protein solution	$N\ s\ m^{-2}$
μ_s	viscosity of suspension	$N\ s\ m^{-2}$
ν	kinematic viscosity	$m^2\ s^{-1}$
ν_D	rate of increase of the deposit layer thickness	$m\ s^{-1}$
σ	retention coefficient	-
σ_i	retention coefficient of protein species i (equation 5.5)	-
τ	shear stress	$N\ m^{-2}$

REFERENCES

Aimar, P, Howell, JA, Concentration polarisation build-up in hollow fibers: a method of measurement and its modelling in ultrafiltration, *Journal of Membrane Science*, 1991, 59, 81-99

Altena, FW, Belfort, G, Otis, J, Fiessinger, F, Rovel, J, Nicoletti, J, Particle motion in a laminar slit flow: a fundamental fouling study, *Desalination*, 1983, 47, 221-232

Asaadi, M, White, DA, A model for determining the steady-state flux of inorganic microfiltration membranes, *The Chemical Engineering Journal*, 1992, 48, 11-16

Atkinson, T, Scawen, MD, Hammond, PM, Biotechnology, Volume 7a, JF Kennedy (ed.), VCH Publishers, Weinheim, Germany, 1987

Attia, H, Bennasar, M, de la Fuente, TB, Study of the fouling of inorganic membranes by acidified milks using scanning electron microscopy and electrophoresis, *Journal of Dairy Research*, 1991, 58, 1, 51-65

Axelsson, HAC, Comprehensive biotechnology, Vol. 2, CL Cooney and AE Humphrey (eds), Pergamon Press, New York, U.S.A., 1985, 325-346

Bailey, SM, Meagher, MM, Crossflow microfiltration of recombinant *Escherichia coli* lysates after high pressure homogenisation, *Biotechnology and Bioengineering*, 1997, 56, 3, 304-310

Bailey, JE, Ollis, DF, Biochemical engineering fundamentals, McGraw-Hill International, Singapore, 2nd edition, 1986

Bailey, FJ, Warf, RT, Maigetter, RZ, Harvesting of recombinant microbial cells using crossflow microfiltration, *Enzyme and Microbial Technology*, 1990, 12, 647-652

Baker, RJ, Fane, AG, Fell, CJD, Yoo, BH, Factors affecting flux in crossflow filtration, *Desalination*, 1985, 53, 81-93

Bashir, I, Reuss, M, Dynamic model for crossflow microfiltration of microbial suspensions in porous tubes, *Chemical Engineering Science*, 1992, 47, 1, 189-203

Belfort, G, Davis, RH, Zydney, AL, The behaviour of suspensions and macromolecular solutions in crossflow microfiltration, *Journal of Membrane Science*, 1994, 96, 1-58

Belfort, G, Nagata, N, Fluid mechanics and crossflow filtration: some thoughts, *Desalination*, 1985, 53, 57-79

Belter, PA, Cussler, EL, Hu, WS, Bioseparations: downstream processing for biotechnology, John Wiley & Sons, New York, U.S.A., 1988

Bentham, AC, The formation, separation and de-watering of aggregated biological materials, *PhD Thesis*, University of London, 1990

Bergmeyer, HU, Methods of enzymatic analysis, Volume 2, 3rd edition, Verlag Chemie, Weinheim, 1983, 139-141, 202-203

Bertram, CD, Hoogland, MR, Li, H, Odell, RA, Fane, AG, Flux enhancement in crossflow microfiltration using a collapsible-tube pulse generator, *Journal of Membrane Science*, 1993, 84, 279-292

Bhattacharya, A, Bioprocess modelling, *American Chemical Society Abstracts*, 1993

Biegler, LT, Chemical process simulation, *Chemical Engineering Progress*, 1989, October, 50-61

Blanchin-Roland, S, Masson, J-M, Protein secretion controlled by a synthetic gene in *Escherichia coli*, *Protein Engineering*, 1989, 2, 473-480

Blake, NJ, Cumming, IW, Streat, M, Prediction of steady-state crossflow filtration using a force balance model, *Journal of Membrane Science*, 1992, 68, 205-216

Bogle, IDL, Middleberg, APG, O'Neill, BK, Modelling for optimisation of biochemical processes involving production and recovery of inclusion bodies, *Chemical and Biochemical Engineering Quarterly*, 1993, 7, 1, 1-5

Bonnerjea, J, Oh, S, Hoare, M, Dunnill, P, Protein purification: the right step at the right time, *Bio/Technology*, 1986, 4, 954-957

Bowen, WR, Gan, Q, Properties of microfiltration membranes: flux loss during constant pressure permeation of BSA, *Biotechnology and Bioengineering*, 1992, 38, 688-696

Bowen, WR, Gan, Q, Properties of microfiltration membranes: the effects of adsorption and shear on recovery of an enzyme, *Biotechnology and Bioengineering*, 1992, 40, 491-497

Bowen, WR, Hall, NJ, Properties of microfiltration membranes: mechanisms of flux loss in the recovery of an enzyme, *Biotechnology and Bioengineering*, 1995, 46, 28-35

Bowen, WR, Williams, PM, Dynamic ultrafiltration model for proteins: a colloidal interaction approach, *Biotechnology and Bioengineering*, 1996, 50, 125-135

Bowen, WR, Xiaowei, Cao, Williams, PM, Predicting performance in biological process engineering-use and elucidation of biochemical information in the membrane separation of biocolloids, (submitted April 1998)

Box, GEP, Hunter, WG, Hunter, JS, Statistics for experimenters, Wiley, New York, U.S.A., 1978

Bradford, M, A rapid and sensitive method for the quantitation of microgram quantities of protein utilising the principle of protein-dye binding, *Analytical Biochemistry*, 1976, 72, 248-254

Brown, DE, Kavanagh, PR, Crossflow separation of cells, *Process Biochemistry*, 1987, 96-101

Brose, D, Dosmar, M, Cates, S, Hutchison, F, Studies on the scale-up of crossflow filtration devices, *PDA Journal of Pharmaceutical Science & Technology*, 1995, 50, 4, 252-260

Campbell, MJ, Walter, RP, McLoughlin, R, Knowles, CJ, Effect of temperature on protein conformation and activity during ultratfiltration, *Journal of Membrane Science*, 1993, 78, 35-43

Carman, PC, Fluid flow through granular beds, *Transactions of the Institution of Chemical Engineers*, 1937, 15, 150-166

Chadwani, R, Matching of bioprocess data records for the rapid diagnosis of chromatographic processes, *PhD Thesis*, University of London, 1995

Charm, SE, Wong, BL, Enzyme inactivation with shearing, *Biotechnology and Bioengineering*, 1970, 12, 1103-1109

Cherkasov, AN, Selective ultrafiltration, *Journal of Membrane Science*, 1990, 50, 109-130

Clarkson, AI, A study of the use of process simulation and pilot-scale verification trials for the design of bioprocesses, *PhD Thesis*, University of London, 1994

Clarkson, AI, Lefervre, P, Titchener-Hooker, NJ, A study of process interactions between cell disruption and debris clarification stages in the recovery of yeast intracellular products, *Biotechnology Progress*, 1993, 9, 462-467

Cooney, CL, Petrides, D, Barrera, M, Evans, L, Computer-aided design of a biochemical process: The Impact of Chemistry on Biotechnology, *American Chemical Society Symposium Series 362,* Washington DC, U.S.A., 1986

Cordes, RM, Sims, WB, Glatz, CE, Precipitation of nucleic acids with poly(ethyleneimine), *Biotechnology Progress*, 1990, 6, 283-285

Creaser, EH, Murali, C, Britt, KA, Protein engineering of alcohol dehydrogenases: effects of amino acid changes at position 93 and 48 of yeast ADH I, *Protein Engineering*, 1990, 3, 6, 523-526

Daniel, C, Applications of statistics to industrial experimentation, Wiley, New York, U.S.A., 1976

Datar, R, Economics of primary separation steps in relation to fermentation and genetic engineering, *Process Biochemistry*, 1986, 21, 1, 19-26

Datar, R, Tangential flow membrane filtration of bacterial cell debris from crude homogenates, *World Biotech Report*, 1984, Vol. 2, A15-A30

Davis, RH, Birdsell, SA, Hydrodynamic model and experiments in crossflow microfiltration, *Chemical Engineering Communications*, 1987, 49, 217-234

Davis, RH, Leighton, DT, Shear-induced transport of a particle along a porous wall, *Chemical Engineering Science*, 1987, 42, 2, 275-281

Davis, RH, Modelling of fouling of crossflow microfiltration membranes, *Separation and Purification Methods*, 1992, 21, 2, 75-126

Davis, RH, Sherwood, JD, A similarity solution for steady-state crossflow microfiltration, *Chemical Engineering Science*, 1990, 45, 11, 3203-3209

Devereux, N, Hoare, M, Dunnill, P, The effect of protein precipitation on the concentration of proteins by ultrafiltration, *Chemical Engineering Communications*, 1986, 45, 255-376

Dornier, M, Decloux, M, Trystram, G, Lebert, A, Dynamic modelling of crossflow microfiltration using neural networks, *Journal of Membrane Science*, 1995, 98, 263-273

Dunnill, P, Speeding bioscience to bioprocesses, *Institution of Chemical Engineers Research Event*, UCL, London, 1994

Eckstein, EC, Bailey, DG, Shapiro, AH, Self-diffusion of particles in shear flow of a suspension, *Journal of Fluid Mechanics*, 1977, 79, 191-208

Elzo, D, Schmitz, P, Houi, D, Joscelyne, S, Measurement of particle/membrane interactions by a hydrodynamic method, *Journal of Membrane Science*, 1996, 109, 43-53

Engler, CR, Comprehensive biotechnology, Vol. 2, CL Cooney and AE Humphrey (eds), Pergamon Press, New York, U.S.A., 1985, 305-324

Ersson, B, Ryden, L, Janson, J-C, Protein purification, J-C Janson and L Ryden (eds), VCH Publishers, New York, U.S.A., 1990, 3-35

Evans, LB, Boston, JF, Britt, HI, Gallier, PW, Gupta, PK, Joseph, B, Mahalec, V, Ng, E, Seider, WD, Yagi, H, ASPEN: an advanced system for process engineering, *Computers and Chemical Engineering*, 1979, 3, 319-327

Evans, LB, Field, RP, Bioprocess simulation: a new tool for process development, *Biotechnology*, 1988, 6, 200-203

Fane, AG, Fell, CJD, A review of fouling and fouling control in ultrafiltration, *Desalination*, 1987, 62, 117-136

Fane, AG, Fell, CJD, Hodgson, PH, Leslie, G, Marshall, KC, Microfiltration of biomass and biofluids: effects of membrane morphology and operating conditions, *Filtration & Separation*, 1991, 332-340

Fane, AG, Fell, CJD, Nor, MT, Ultrafiltration in the presence of suspended matter, *Institution of Chemical Engineers Jubilee Symposium*, 1982, 73, C1-C12

Fane, AG, Fell, CJD, Suki, A, The effect of pH and ionic environment on the ultrafiltration of protein solutions with retentive membranes, *Journal of Membrane Science*, 1983, 16, 195-210

Fane, AG, Fell, CJD, Waters, AC, Ultrafiltration of protein solutions through partially permeable membranes-the effect of adsorption and solution environment, *Journal of Membrane Science*, 1983, 16, 211-224

Ferry, JD, Statistical evaluation of sieve constants in ultrafiltration, *Journal of General Physiology*, 1936, 20, 95-104

Field, RW, Wu, D, Howell, JA, Gupta, BB, Critical flux concept for microfiltration fouling, *Journal of Membrane Science*, 1995, 100, 259-272

Fischer, EJ, Impacts of separation processes on protein recovery from cells and cell spheroplasts, *PhD Thesis*, University of London, 1996

Fish, NM, Lilly, MD, The interactions between fermentation and protein recovery, *Bio/Technology*, 1984, 2, 623-627

Foley, G, MacLoughlin, PF, Malone, DM, Membrane fouling during constant flux microfiltration of dilute suspensions of active dry yeast, *Separation Science and Technology*, 1995, 30, 3, 383-398

Forman, SM, DeBernardez, ER, Feldberg, RS, Swartz, RW, Crossflow filtration for the separation of inclusion bodies from soluble proteins in recombinant *Escherichia coli* cell lysate, *Journal of Membrane Science*, 1990, 8, 2/3, 263-279

Forstrom, RJ, Voss, GO, Blachshear, PL, Fluid dynamics of particle (platelet) deposition for filtering walls: relationship to atherosclerosis, *Journal of Fluids Engineering: Transactions of the American Society of Mechanical Engineers*, 1974, 168-172

French, C, Production and recovery of a recombinant α-amylase enzyme from *Escherichia coli* and *Streptomyces lividans*, *PhD Thesis*, University of London, 1993

Gabler, FR, Comprehensive biotechnology, Vol. 2, CL Cooney and AE Humphrey (eds), Pergamon Press, New York, U.S.A., 1985, 351-366

Gabler, FR, Cell processing using crossflow filtration, *Developments in Industrial Microbiology*, 1983, 25, 381-396

Gabler, FR, Ryan, M, Purification of fermentation products: application to large-scale processes, D LeRoith, T Schilbach and T Leahy (eds.), *American Chemical Society Symposium Series*, 1985, 271, 1-20

Gatenholm, P, Paterson, S, Fane, AG, Fell, CJD, Performance of microfiltration membranes in cell harvesting of *Escherichia coli*, *Process Biochemistry*, 1988, 23, 79-81

Gésan, G, Daufin, G, Merin, U, Labbé, J-P, Quémerais, A, Fouling during constant flux crossflow microfiltration of pretreated whey. Influence of membrane pressure gradient, *Journal of Membrane Science*, 1993, 131-145

Glimenius, R, Microfiltration-state of the art, *Desalination*, 1985, 53, 363-372

Göklen, KE, Thien, M, Ayler, S, Smith, S, Fisher, E, Chartrain, M, Salmon, P, Wilson, J, Andrews, A, Buckland, B, Development of crossflow filtration processes for the commercial isolation of a bacterial lipase, *Bioprocess Engineering*, 1994, 11, 49-56

Green, G, Belfort, G, Fouling of ultrafiltration membranes: lateral migration and the particle trajectory model, *Desalination*, 1980, 36, 129-147

Gregory, J, Flocculation of polystyrene particles with cationic polyelectrolytes, *Transactions of the Faraday Society*, 1969, 65, 2260-2268

Gregory, J, The effect of cationic polymers on the colloidal stability of latex particles, *Journal of Colloid and Interfacial Science*, 1976, 55, 35-44

Gritis, D, Titchener-Hooker, NJ, Biochemical process simulation, *Institution of Chemical Engineers Symposium Series*, 1989, 144, 69-77

Haaland, PD, Experimental design in biotechnology, Marcel Dekker Inc., New York and Basel, 1989

Haarstrick, A, Rau, U, Wagner, F, Crossflow filtration as a method for separating fungal cells and purifying the polysaccharide produced, *Bioprocess Engineering*, 1991, 6, 179-186

Habib, G, *PhD Thesis*, University of London, 1998 (in preparation)

Hall, NJ, The scale-up of protein microfiltration based on laboratory studies of fundamental effects, *PhD Thesis*, University of London, 1998 (in preparation)

Hermia, J, Constant pressure blocking filtration laws- application to power-law non-Newtonian fluids, *Transactions of the Institution of Chemical Engineers*, 1982, 60, 183-187

Hetherington, PJ, Follows, M, Dunnill, P, Lilly, MD, Release of protein from Baker's yeast (*Saccharomyces cerevisiae*) by disruption in an industrial homogeniser, *Transactions of the Institution of Chemical Engineers*, 1971, 49, 142-148

Hildebrandt, JR, Membranes for bioprocessing: design considerations, 1993

Hoare, M, Dunnill, P, Biochemical engineering challenges for purifying useful proteins, *Philosophical Transactions of the Royal Society of London Series B - Biological Sciences*, 1989, 324, 1224, 497-507

Howell, JA, Lojkine, M, Pritchard, M, Cell harvesting using crossflow microfiltration: chromatographic and membrane processes in Biotechnology, CA Costa and JS Cabral (eds.), Kluwer Academic Publishers, Netherlands, 1991, 237-252

Howell, JA, Sub-critical flux operation of microfiltration, *Journal of Membrane Science*, 1995, 107, 165-171

Huang, B, Mujumdar, AS, Use of neural network to predict industrial dryer performance, *Drying Technology*, 1993, 11, 525-541

Hwang, S-J, Chang, D-J, Chen, C-H, Steady-state permeate flux for particle crossflow filtration, *Chemical Engineering Journal*, 1996, 61, 171-178

Jacobsen, C, The control of protein crystallisation, *PhD Thesis*, University of London, 1998

Jörnvall, H, Eklund, H, Brändén, C-I, Sub-unit conformation of yeast alcohol dehydrogenase, *The Journal of Biological Science*, 1978, 253, 23, 8414-8419

Kawakatsu, T, Nakao, S-I, Kimura, S, Effects of size and compressibility of suspended particles and surface pore size of membrane on flux in crossflow filtration, *Journal of Membrane Science*, 1993, 81, 173-190

Kelly, BD, Hatton, TA, The fermentation/downstream processing interface, *Bioseparation*, 1991, 1, 333-349

Kim, KJ, Fane, AG, Fell, CJD, Joy, DC, Fouling mechanisms of membranes during protein ultrafiltration, *Journal of Membrane Science*, 1992, 69, 79-91

Korus, RA, Olson, AC, The use of α-galactosidase and invertase in hollow fibre reactors, *Biotechnology and Bioengineering*, 1977, 19, 1-8

Kroner, KH, Nissinen, V, Dynamic filtration of microbial suspensions using an axially rotating filter, *Journal of Membrane Science*, 1988, 36, 85-100

Kroner, KH, Schütte, H, Hustedt, H, Kula, M-R, Crossflow filtration in downstream processing of enzymes, *Process Biochemistry*, 1984, 19, 2, 67-74

Le, MS, Atkinson, T, Crossflow microfiltration for recovery of intracellular products, *Process Biochemistry*, 1985, 26-31

Le, MS, Spark, LB, Ward, PS, The separation of aryl acrylamidase by crossflow microfiltration and the significance of enzyme/cell debris interaction, *Journal of Membrane Science*, 1984, 21, 219-232

Lee, S-M, The primary stages of protein recovery, *Journal of Biotechnology*, 1989, 11, 103-118

Lee, SS, Burt, A, Russotti, G, Buckland, B, Microfiltration of recombinant yeast cells using a rotating disk dynamic filtration system, *Biotechnology and Bioengineering*, 1995, 48, 386-400

Levesley, JA, Hoare, M, The effect of high frequency backflushing of the microfiltration of yeast homogenate suspensions for the recovery of soluble proteins, *Biotechnology and Bioengineering*, (submitted 1996)

Li, S-L, Chou, K-S, Lin, J-YL, Yen H-W, Chu, I-M, Study on the microfiltration of *Escherichia coli*-containing fermentation broth by a ceramic membrane filter, *Journal of Membrane Science*, 1996, 110, 203-210

Liddell, JM, Engineering processes for bioseparations, LR Weatherley (ed.), Butterworth-Heinemann, Oxford, U.K., 1994

Lindquist, GM, Stratton, RA, The role of polyelectrolyte charge density and molecular weight on the adsorption and flocculation of colloidal silica with polyethyleneimine, *Journal of Colloidal and Interfacial Science*, 1976, 55, 69-72

Linko, P, Zhu, YH, Neural network modelling for real-time variable estimation and prediction in the control of glucoamylase fermentation, *Process Biochemistry*, 1992, 27, 275-283

Lojkine, MH, Field, RW, Howell, JA, Crossflow microfiltration of cell suspensions: a review of models with an emphasis on particle size effects, *Transactions of the Institution of Chemical Engineers*, 1992, 70 (Part C), 149-164

Lu, Y, Clarkson, AI, Titchener-Hooker, NJ, Pantelides, C, Bogle, IDL, Simulation as a tool in the process design and management for production of intracellular enzymes, *Transactions of the Institution of Chemical Engineers*, 1994, 72 (Part A), 371-375

Maa Y-F, Hsu, CC, Membrane fouling in sterile filtration of recombinant human growth hormone, *Biotechnology and Bioengineering*, 1996, 50, 319-328

Magonet, E, Hayen, P, Delforge, D, Delaive, E, Remacle, J, Importance of the structural zinc atom for the stability of yeast alcohol dehydrogenase, *Biochemical Journal*, 1992, 287, 361-365

Mabire, F, Audebert, R, Quivoron, C, Flocculation properties of some water soluble cationic copolymers towards silica suspensions: a semi-quantitative interpretation of the role of molecular weight and cationicity through a 'patchwork' model, *Journal of Colloid and Interfacial Science*, 1984, 97, 120-136

Mannweiler, K, The recovery of biological particles in high-speed continuous centrifuges with special reference to feed-zone break-up effects, *PhD Thesis*, University of London, 1989

Maybury, J, *PhD Thesis*, University of London, 1998 (in preparation)

McDonogh, RM, Bauser, H, Stroh, N, Chmiel, H, Separation efficiency of membranes in biotechnology: an experimental and mathematical study of flux control, *Chemical Engineering Science*, 1992, 47, 271-279

Meagher, MM, Bartlett, RT, Khan, FR, Extraction of riL-2 inclusion bodies from *Escherichia coli* using crossflow filtration, *Biotechnology and Bioengineering*, 1994, 43, 969-977

Meyer, F, Gehmlich, I, Guthke, R, Górak, A, Knorre, WA, Analysis and simulation of complex interactions during dynamic microfiltration of *Escherichia coli* suspensions, *Biotechnology and Bioengineering*, 1998, 59, 2, 189-202

Mikulášek, P, Dolecek, P, Characterisation of ceramic tubular membranes by active pore size distribution, *Separation Science and Technology*, 1994, 29, 9, 1183-1192

Milburn, P, Bonnerjea, J, Hoare, M, Dunnill, P, Selective flocculation of nucleic acids, lipids and colloidal particles from a yeast cell homogenate by polyethyleneimine, and its scale-up, *Enzyme and Microbial Technology*, 1990, 12, 527-532

Mosqueira FG, Higgins JJ, Dunnill P, Lilly MD, Characteristics of mechanically disrupted baker's yeast in relation to its separation in industrial centrifuges, *Biotechnology and Bioengineering*, 1981, Volume 23, 335-343

Narendrannathan, TJ, Dunnill, P, The effect of shear on globular proteins during ultrafiltration: studies on alcohol dehydrogenase, *Biotechnology and Bioengineering*, 1982, 24, 2103-2107

Nagata, N, Herouvis, KJ, Dziewulski, DM, Belfort, G, Crossflow microfiltration of a bacterial fermentation broth, *Biotechnology and Bioengineering*, 1989, 34, 447-466

Nakanishi, K, Tadokoro, T, Matsuno, R, On the specific resistance of cakes of microorganisms, *Chemical Engineering Communications*, 1987, 62, 187-201

Narodoslawsky, M, Friedler, F, Kiraly, L, Altenburger, HJ, SIMBIOS-a new simulation program for biotechnology with novel design, *Chemical and Biochemical Engineering Quarterly*, 1993, 7, 1, 27-30

Niemi, H, Bulsari, A, Palosaari, S, Simulation of membrane separation by neural networks, *Journal of Membrane Science*, 1995, 102, 185-191

Ofsthun, NJ, Colton, CK, Visual evidence of concentration polarisation in crossflow membrane plasmapheresis, *Transactions of the American Society of Artificial Internal Organs*, 1987, 33, 510-517

Ogez, JR, Hodgdon, JC, Beal, MP, Builder, SE, Downstream processing of protein: recent advances, *Biotechnology Advances*, 1989, 7, 489-497

Palosaari, S, Parviainen, S, Hiironen, J, Reunanen, J, Neittaanmäki, A random search algorithm for constrained global optimisation, *Acta Polytechnica Scandinavica CH-Series*, 1986, 172, 1-45

Pantelides, CC, Barton, PI, Equation-orientated dynamic simulation current status and future perspectives, *Computers and Chemical Engineering*, 1993, S17, S263-S285

Parnham, CS, Davis, RH, Protein recovery from cell debris using rotary and tangential crossflow microfiltration, *Biotechnology and Bioengineering*, 1995, 47, 155-164

Parnham, CS, Davis, RH, Protein recovery from bacterial cell debris using crossflow microfiltration with backpulsing, *Journal of Membrane Science*, 1996, 118, 259-268

Petrides, D, BioPro Designer: an advanced computing environment for modelling and design of integrated biochemical processes, *Computers and Chemical Engineering*, 1994, 18, S626-S630

Petrides, D, Cooney, CL, Evans, LB, Field, RP, Snoswell, M, Bioprocess simulation: an integrated approach to process development, *Computers and Chemical Engineering*, 1989, 13, 4/5, 553-561

Petrides, D, Sapidou, E, Calandranis, J, Computer-aided process analysis and economic evaluation of biosynthetic human insulin production - a case study, *Biotechnology and Bioengineering*, 1995, 48, 529-541

Piron, E, René, F, Latrille, E, A crossflow microfiltration model based on integration of the mass transport equation, *Journal of Membrane Science*, 1995, 108, 57-70

Porter, MC, Concentration polarisation with membrane ultrafiltration, *Industrial and Engineering Chemistry: Product Research and Development*, 1972, 11, 3, 234-248

Prádànos, P, Hernández, A, Crossflow ultrafiltration of proteins through asymmetric polysuphonic membranes: retention curves and pore size distributions, *Biotechnology and Bioengineering*, 1995, 47, 617-625

Pradipasena, P, Rha, C, Effect of concentration on apparent viscosity of a globular protein solution, *Polymer Engineering and Science*, 1977, 17, 12, 861-864

Redkar, SG, Davis, RH, Crossflow microfiltration of yeast suspensions in tubular filters, *Biotechnology Progress*, 1993, 9, 625-634

Redkar, SG, Davis, RH, Crossflow microfiltration with high frequency reverse filtration, *American Institution of Chemical Engineers Journal*, 1995, 41, 3, 501-508

Reed, I, Membrane filtration: making the right choices, *Filtration Society Meeting*, UMIST, Manchester, 1996

Reference manuals, Elzone Model 280 PC, Particle Data Ltd., Cheltenham, U.K.

Reference manuals, Malvern 3600E particle sizer, Malvern Instruments, Malvern, Worcestershire, U.K.

Reference manuals, Malvern Series 4700/PCS 100 spectrometer laser sizer, Malvern Instruments, Malvern, Worcestershire, U.K.

Reference manuals, RHEOMAT 115, Contraves AG, Zurich, Switzerland

Reismeier, B, Kroner, K, Kula, M-R, Tangential filtration of microbial suspensions: filtration resistances and model development, *Journal of Biotechnology*, 1989, 12, 153-172

Reuss, M, Josic, D, Popovic, M, Bronn, WK, Viscosity of yeast suspensions, *European Journal of Applied Microbiology and Biotechnology*, 1979, 8, 167-175

Rocek, J, Uchytil, P, Evaluation of selected methods for the characterisation of ceramic membranes, *Journal of Membrane Science*, 1994, 89, 119-129

Romero, CA, Davis, RH, Global model of crossflow microfiltration based on hydrodynamic particle diffusion, *Journal of Membrane Science*, 1988, 39, 157-185

Romero, CA, Davis, RH, Transient model of crossflow microfiltration, *Chemical Engineering Science*, 1990, 45, 1, 12-25

Rousseeuw, PJ, Leroy, AM, Robust regression and outlier detection, Wiley, New York, U.S.A., 1987

Ruehrwein, R, Ward, A, Mechanism of clay aggregation by polyelectrolytes, *Soil Science*, 1952, 73, 485-492

Russotti, G, Osawa, AE, Sitrin, RD, Buckland, BC, Adams, WR, Lee, SS, Pilot-scale harvest of recombinant yeast employing microfiltration: a case study, *Journal of Biotechnology*, 1995, 42, 235-246

Russotti, G, Göklen, KE, Wilson, JJ, Development of a pilot-scale microfiltration harvest for the isolation of physostigmine from *Streptomyces griseofuscus* broth, *Journal of Chemical Technology and Biotechnology*, 1995, 63, 1, 37-47

Salt, DE, Hay, S, Idris, A, Hoare, M, Dunnill, P, Selective flocculation of soluble protein contaminants using polethyleneimine: a broader study of organisms and polymers, 1992

Samsatli, NJ, Shah, N, Optimal integrated design of biochemical processes, *Computers and Chemical Engineering*, 1996, S20, S315-S320

Sargent, RWH, Westerberg, AW, "SPEED-UP" in chemical engineering design, *Transactions of the Institution of Chemical Engineers*, 1964, 42, T190-T197

Scopes, RK, Protein purification: principles and practice, 2nd edition, Springer-Verlag, New York, U.S.A., 1988

Segré, G, Silberberg, A, Behaviour of macroscopic rigid spheres in Poiseuille flow of suspensions: part 2-experimental results and interpretation, *Journal of Fluid Mechanics*, 1962, 14, 136-157

Shamlou, PA, Siddiqi, SF, Titchener-Hooker, NJ, A physical model of high-pressure disruption of baker's yeast cells, *Chemical Engineering Science*, 1995, 50, 9, 1383-1391

Shimizu, Y, Matsushita, K, Watanabe, A, Influence of shear breakage of microbial cells on crossflow microfiltration flux, *Journal of Fermentation and Bioengineering*, 1994, 78, 2, 170-174

Siddiqi, SF, Process simulation and optimisation of high pressure disruption for the release of intracellular proteins, *PhD Thesis*, University of London, 1998

Siddiqi, SF, Clarkson, AI, Keshavarz-Moore, E, Titchener-Hooker, NJ, Modelling of process interactions in biochemical processes, *Institution of Chemical Engineers Research Event*, Cambridge, U.K., 1991

Smith, GJ, Morton, W, Dynamic simulation using an equation-orientated flowsheeting package, *Computers and Chemical Engineering*, 1988, 12, 5, 469-473

Song, L, Elimelech, M, Theory of concentration polarisation in crossflow microfiltration, *Journal Chemical Society Faraday Transactions*, 1995, 91, 19, 3389-3398

Stamatakis, K, Tien, C, A simple model of crossflow filtration based on particle adhesion, *American Institution of Chemical Engineers Journal*, 1993, 39, 8, 1292-1302

Stratton, J, Meagher, MM, Effect of membrane pore size and chemistry on the crossflow filtration of *Escherichia coli* and *Saccharomyces cerevisiae*: simultaneous evaluation of different membranes using a versatile flat-sheet membrane module, *Bioseparation*, 1994, 4, 255-262

Stryer, L, Biochemistry, WH Freeman and Company, New York, 1995, 4th edition

Taddei, C, Aimar, P, Howell, JA, Scott, JA, Yeast harvesting from cider using microfiltration, *Journal of Chemical Technology and Biotechnology*, 1990, 37, 59-66

Taylor, G, Levesley, JA, Hoare, M, Pilot-scale ultrafiltration of concentrated protein precipitate suspensions: the effect of concentration and fluid dynamics, *Chemical Engineering Communications*, 1994, 129, 227-250

Tejayadi, S, Cheryan, M, Downstream processing of lactic acid-whey permeate fermentation broths by hollow fibre ultrafiltration, *Applied Biochemistry and Biotechnology*, 1988, 19, 61-70

Thomas, CR, Nienow, AW, Dunnill, P, Action of shear on enzymes: studies with alcohol dehydrogenase, *Biotechnology and Bioengineering*, 1979, 21, 2263-2278

Thomas, CR, Dunnill, P, Action of shear on enzymes: studies with catalase and urease, *Biotechnology and Bioengineering*, 1979, 21, 2279-2302

Tutunjian, RS, Cell separations with hollow fibre membranes, *Developments in Industrial Microbiology*, 1983, 25, 415-435

Tutunjian, RS, Scale-up considerations for membrane processes, *Bio/Technology*, 1985, 3, July, 616-626

Van der Berg, GB, Smolders, CA, Flux decline in membrane processes, *Filtration and Separation*, 1988, March/April issue, 115-121

Van Reis, R, Industrial-scale harvest of proteins from mammalian cell culture by crossflow microfiltration, *Biotechnology and Bioengineering*, 1991, 38, 413-422

Varga, EG, Modelling of the downstream processing of a recombinant intracellular enzyme, *PhD Thesis*, University of London, 1997

Virkar, PD, Narendranathan, TJ, Hoare, M, Dunnill, P, Studies on the effects of shear on globular proteins: extension to high shear fields and to pumps, *Biotechnology and Bioengineering*, 23, 425-429

Warren, RK, MacDonald, DG, Hill, GA, Crossflow microfiltration of *Saccharomyces cerevisiae*, *Process Biochemistry*, 1991, 26, 337-342

Woodley, JM, Titchener-Hooker, NJ, The use of windows of operation as a bioprocess design tool, *Bioprocess Engineering*, 1996, 14, 263-268

Weijers, SR, Van't Riet, K, Enzyme stability in downstream processing: enzyme inactivation, stability and stabilisation, and quantification of inactivation, *Biotechnology Advances*, 1992, 10, 237-273

Zaldivar, JM, Hernandez, H, Panetsos, Control of batch reactors using neural networks, *Chemical Engineering Proceedings*, 1992, 31, 173-180

Zhou, YH, Holwill, ILJ, Titchener-Hooker, NJ, A study of the use of computer simulations for the design of integrated downstream processes, *Bioprocess Engineering*, 1997, 16, 6, 367-374

Zydney, AL, Colton, CK, Concentration polarisation model for filtrate flux in crossflow microfiltration of particulate suspensions, *Chemical Engineering Communications*, 1986, 47, 1-21